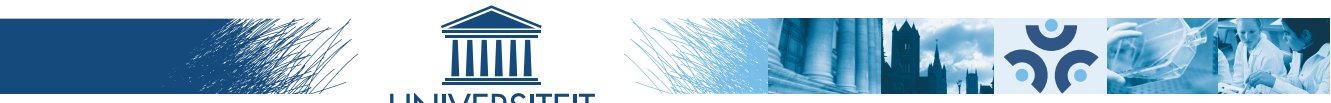

The Multi-Centre Bond Index as a Measure of Aromaticity:

Is Aromaticity a Multidimensional Concept or Not?

Dissertation submitted in fulfilment of the requirements for the degree of
Doctor (Ph.D.) in Sciences: Chemistry
by

Stijn Fias

Department of Inorganic and Physical Chemistry
Faculty of Sciences

Doctoral Supervisor:
Prof. Dr. Patrick Bultinck

March 23th, 2011

ཞེས། །བླ་མ་མཁོན་པོ་འཇམ་དཔལ་དབྱངས་དང་ངོ་བོ་དབྱེར་
མ་མཆིས་པའི་རྗེ་བཙུན་དམ་པ་རྣམས་ལ་ཕྱག་འཚལ་ལོ། །

Abstract

The aim of this work it to examine Multi Centre Bond Indices (MCBI) as a measure of aromaticity by comparing these indices with other energetic, magnetic and electron density criteria for a wide range of different organic and inorganic aromatic molecules. Analysing the results an answer is given to the question whether or not the much debated multi-dimensionality of aromaticity is the cause of some of the contradicting results.

In addition to a revision of the theoretical methods used, the theoretical background (Part I) introduces a method for the fast computation of the Nucleus Independent Chemical Shift (NICS) values, using the so-called pseudo-π-method.

In the second part of the work, the aromaticity and local aromaticity of a large set of polycyclic aromatic hydrocarbons (PAHs) is studied using various aromaticity indices. The Multi Centre Bond Index (MCBI) is compared with an electron density criterion, namely the similarity of a benzenoid ring to benzene. This is done using the Polansky (P) and Number of Overlapping Electrons (NOEL) indices. The Polansky index, introduced in 1967, is based on assessing the similarity between benzenoid rings in polyaromatic hydrocarbons with benzene as a reference system. This approach uses the more approximate Hückel MO theory. By using the quantum similarity theory, a new derivation has been proposed, allowing a generalization of the Polansky index to the *ab initio* level of theory. The similarity is now based on the Number of Overlapping Electrons (NOEL) indices, which is shown to have a good correlation with to the original index. The results obtained for a set of polyaromatic hydrocarbons are found to agree very well with recently published circuit-condensed ring currents and magnetic-energetic aromaticity indices, but no correlation is found with NICS. This is usually seen as a manifestation of the more general multidimensional nature of aromaticity. The sources for the observed correlations are analysed, showing that some indices give conflicting results because they reflect inherently different phenomena.

This comparison of the MCBI with molecular similarity measures is followed by

a detailed study of the aromaticity and local-aromaticity of a large set of polycyclic aromatic hydrocarbons (PAH) using the MCBI and two magnetic indices, namely the Nucleus Independent Chemical Shifts (NICS) and Ring Current Maps (RCM). A detailed examination is made of the multidimensional nature of aromaticity. The lack of a good correlation between the NICS and the Multi Centre Bond Indices is reported and the grounds discussed. It is shown through thorough statistical analysis that the NICS values arise not only from local aromaticity of the benzenoid rings, but also from other circuits. It is shown that the NICS indices do not reveal the individual aromatic nature of a specific ring, contrary to the delocalisation indices. This information allows one to use the Multi Centre Bond Indices to construct the ring current maps of a large set of PAH using this index. These MCBI-RCM are compared with *ab initio* computations of the same maps in the pseudo-π version of the ipsocentric approach. The quality of the comparison indicates that both delocalisation and ring current approaches capture the same information about the aromatic nature of the PAH. Aromaticity as a global property, requires knowledge of more than single circuits, but the present results suggest no need to introduce a multidimensional character for aromaticity. Despite the quality of the comparison there are still rings of which the NICS values are not understood using the previous statistical analysis. Therefore the nonlocal contributions to the NICS are further investigated using a larger set of PAH. To find the source of the contradicting results, the NICS are predicted using the MCBI and compared with *ab initio* results. The NICS of the central rings of perylene- and benzo-[ghi]perylene-like fragments and of coronene appear to have other nonlocal contributions than the ones previously studied. It is shown that a model based on the MCBI-RCM and the inclusion of new circuits proves the existence and shows the nature of these new nonlocal effects on the NICS. This new model leads to a better understanding of the differences between the NICS and delocalisation indices. The results show how the NICS value is not only significantly influenced by the higher order circuits encircling the ring at which it is evaluated but also by the local aromaticity of the surrounding rings. Occasionally, as in the case of coronene, the NICS are even influenced by currents farther away in the molecule.

The final chapter of the second part compares two energy related methodologies, namely the so-called *ef*-value and the topological resonance energy (TRE) with a delocalisation (MCBI) and a magnetic index (NICS). A close relation between the (local) energetic index *ef*-value) and (local) delocalisation indices is found for corresponding conjugated circuits. The reported close correlation between both types of indices implies that no discrepancies between these aromaticity measures exist provided the comparison involves local contributions of individual rings and conjugated circuits. In addition it is also show that the same close parallel can be observed for global aromaticity measures like the TRE or NICS when all the relevant contributions

of conjugated circuits are properly taken into account.

In the third and final part of the thesis the delocalisation and magnetic indices are used to study the aromaticity of some more complex molecules such as the hexaiodobenzene molecule, all-metallic aromatic systems and hydroporphyrins. For the study of hexaiodobenzene (C_6I_6) and its cation ($C_6I_6^{2+}$), two complementary theoretical techniques to study σ-delocalisation and σ-aromaticity are used. The first is capable of displaying the ring current directly and also of disentangling σ and π contributions to it. These current density maps and the orbital contributions to them, as computed in the ipsocentric approach, show that there is indeed a separately identifiable σ ring current in the iodine array of the cation, in addition to the benzenoid π current sustained by the central ring in both the neutral and cationic species. An orbital model for the sense of the current, is provided and the RCM are compared with the multi-centre index, which characterises the underlying cyclic electron delocalisation in both carbon and iodine circuits. Both criteria support the attribution of σ-aromaticity to the iodine array in $C_6I_6^{2+}$. For the PAHs and the relatively simple molecules of hexaiodobenzene and its cation, the relation between the Multi Centre Bond Index and the current density holds, but turning to more complicated molecules such as the metallic Al_4^{2-} and hydroporphyrins,the relation is partially lost. As all-metal aromatic molecules Al_4^{2-} , $LiAl_4^-$ and Li_2Al_4 are studied and it is shown that there is no direct relation between electron delocalisation and the presence of a ring current, other than that a delocalised system is a necessary but not sufficient condition to lead to a ring current. In the case of Al_4^{2-} derived compounds, there is clearly both σ and π electron delocalisation although only the σ system gives rise to a ring current. The analysis of Canonical Molecular Orbitals(CMO)-NICS data is shown to lead to a different conclusion although this method also contains occupied-occupied terms and is not so easily interpretable as ipsocentric ring current maps. Fermi-hole analysis and multicentre indices agree very well among each other in describing electron delocalisation. Concerning the use of the term aromaticity in the present context, one faces the problem of the lack of definition of aromaticity outside the range of benzenoid ring containing molecules. There is no clear cut reason to decide what "benzene like" properties should be conserved most in other molecules to describe them as aromatic. If electron delocalisation suffices, the compounds studied here could be described as both σ and π aromatic. If the presence of a ring current is a requirement for aromaticity, the present molecules are only σ aromatic. It is therefore suggested that one should always narrow down what is meant exactly when using the notion aromaticity. In this context Al_4^{2-} is σ and π aromatic on the account of electron delocalisation but only σ aromatic on the account of presence of a ring current.

Several measures of aromaticity including energetic, magnetic and electron den-

sity criteria are finally employed to show how aromatic stabilisation can explain the stability sequence of hydroporphyrins, ranging from porphin to octahydroporphin, and their preferred hydrogenation paths. The methods employed are topological resonance energies and their circuit energy effects, bond resonance energies, multicenter delocalisation indices, ring current maps, magnetic susceptibilities and nuclear independent chemical shifts. In order to compare the information obtained by the different methods the results have been put on the same scale by using recently proposed approaches. It has been found that all of them provide essentially the same information and lead to similar conclusions. Also, hydrogenation energies along different hydrogenation paths connecting porphin with octahydroporphin have been calculated using Density Functional Theory. It is shown using the methods mentioned above that the relative stability of different hydroporphyrin isomers and the observed inaccessibility of octahydroporphin both synthetically and in nature can be perfectly rationalised in terms of aromaticity.

In general, the results show that, for the PAH, the MCBI correlates well with the similarity of the rings to benzene and with other local aromaticity indices. A good correlation can also be found with global aromaticity indices when the proper combination of conjugated circuits is taken. When looking at molecules where the relation to benzene is lost, things become more complicated. There is no clear cut reason to say which "benzene like" properties should be conserved most in other molecules to describe them as aromatic. Concerning the use of the term aromaticity for these molecules it is therefore suggested that one should always specify exactly what is meant when using the notion aromaticity.

Samenvatting

Het doel van dit werk is het onderzoeken van de waarde van de Multi Centre Delokalisatie Index (MCDI) door deze index te vergelijken met andere energetische, magnetische en elektrondichtheidscriteria voor een breed scala van organische en anorganische moleculen. Tijdens de analyse van de resultaten wordt de vraag beantwoord of de veelbesproken multidimensionaliteit van de aromaticiteit al dan niet de oorzaak is van een aantal van de tegenstrijdige resultaten.

Naast een overzicht van de gebruikte theoretische methoden, introduceert de theoretische achtergrond (Deel I) een methode voor de snelle berekening van de Nucleus Onafhankelijke Chemische Shift (Nucleus Independent Chemical Shift of NICS) door gebruik te maken van de zogenoemde pseudo-π-methode.

In het tweede deel van het werk wordt de aromaticiteit en lokale aromaticiteit van een grote reeks van Polycyclische Aromatische Koolwaterstoffen (PAK) bestudeerd met behulp van verschillende aromaticiteit indices. De MCDI wordt vergeleken met een elektrondichtheids- criterium, namelijk de gelijkenis van een benzenoide ring met benzeen. Dit wordt gedaan met behulp van de Polansky (P) en de Aantal Overlappende Elektronen (Number of Overlapping Electrons of NOEL) indices. De Polansky index, ingevoerd in 1967, is gebaseerd op de gelijkenis tussen de benzenoide ringen in polyaromatische koolwaterstoffen met benzeen als referentiesysteem. Deze aanpak maakt gebruik van de meer benaderende Hückel MO theorie. Door het gebruik van de quantum similariteits theorie, wordt een nieuwe afleiding voorgesteld, waardoor de Polansky index veralgemeend kan worden op *ab initio* niveau. De similariteit is nu gebaseerd op de Aantal Overlappende Elektronen (Number of Overlapping Electrons of NOEL) index, waarvan wordt aangetoond dat deze een hoge mate van gelijkenis vertoont met de oorspronkelijke index. De resultaten verkregen voor een set van PAK komen zeer goed overeen met onlangs gepubliceerde circuit-gecondenseerde kringstromen en magnetisch-energetische aromaticiteitsindices, maar geen correlatie werd gevonden met de NICS waarde. Dit wordt meestal gezien als een manifestatie van het multidimensionele karakter van aromaticiteit. De oorzaken van de

waargenomen correlaties worden geanalyseerd, waaruit blijkt dat sommige indices tegenstrijdige resultaten geven omdat ze inherent verschillende fenomenen weerspiegelen.

Deze vergelijking van de MCDI met indices voor moleculaire similariteit wordt gevolgd door een uitgebreide studie van de aromaticiteit en lokale-aromaticiteit van een grote reeks PAK met behulp van de MCDI en twee magnetische indices, namelijk de NICS en afbeeldingen van de kring stromen (Ring Current Maps of RCM). Een gedetailleerd onderzoek wordt gemaakt van het multidimensionele karakter van aromaticiteit. De oorzaken van het ontbreken van een goede correlatie tussen de NICS en de MCDI worden besproken. Er wordt door middel van een grondige statistische analyse aangetoond dat de NICS waarden niet alleen ontstaan door de lokale aromaticiteit van de benzenoide ringen, maar door bijdragen van andere circuits bevatten. Dit wil zeggen dat de NICS niet het individuele aromatische karakter van een specifieke ring weergeven, in tegenstelling tot de MCDI. Wetende dat de NICS bijdragen van hogere-orde circuits bevatten kan de MCDI gebruikt worden om de kringstromen van een groot aantal PAK te construeren met behulp van deze index. Deze MCDI-RCM worden vergeleken met *ab initio* kringstromen in de pseudo-π versie van de ipsocentrische methode. De kwaliteit van de vergelijking geeft aan dat zowel de delokalisatie indices als de kringstromen dezelfde informatie over het aromatische karakter van de PAK bevatten. Aromaticiteit als een globale eigenschap, vereist dan wel de kennis van meer dan één enkel circuit, maar de huidige resultaten suggereren dat er geen noodzaak om een "multidimensionaal karakter" in te voeren voor aromaticiteit. Ondanks de overeenkomsten tussen de delokalisatie indices en de kringstromen zijn er nog ringen waarvan de NICS waarden niet verklaard kunnen worden met behulp van de voorgaande statistische analyse. Derhalve zijn de niet-lokale bijdragen tot de NICS verder onderzocht met behulp van een grotere set van PAK. Om de oorzaak van de tegenstrijdige resultaten te vinden, worden de NICS voorspeld met behulp van de MCDI en vergeleken met de *ab initio* resultaten. De NICS van de centrale ringen van peryleen- en benzo-[ghi]peryleenachtige fragmenten en van coroneen blijken andere niet-lokale bijdragen te hebben dan diegene die eerder werden bestudeerd. Het wordt aangetoond dat een model gebaseerd op de MCDI-RCM en op het opnemen van nieuwe circuits het bestaan en de aard bewijst van deze nieuwe niet-lokale effecten op de NICS. Dit nieuwe model leidt tot een beter begrip van de verschillen tussen de NICS en de delokalisatie indices. De resultaten tonen aan hoe de NICS waarde niet alleen significant beïnvloed wordt door de hogere orde circuits rondom de ring waar deze wordt berekend, maar ook door de lokale aromaticiteit van de omliggende ringen. In sommige gevallen, zoals in het geval van coroneen, worden de NICS ook beïnvloed door kringstromen verder weg in het molecuul.

Het laatste hoofdstuk van het tweede deel vergelijkt twee energiegerelateerde methoden, de zogenaamde *ef*-waarde en de topologische resonantie energie (TRE), met een delokalisatie (MCDI) en een magnetische index (NICS). Een nauwe relatie tussen de (lokale) energetische index, de *ef*-waarde, en de (lokale) delokalisatie index wordt gevonden voor overeenkomstige geconjugeerde circuits. De gerapporteerde nauwe correlatie tussen beide soorten indices impliceert dat er geen verschillen bestaan tussen deze maatstaven voor aromaticiteit wanneer de vergelijking uitgaat van de lokale bijdragen voor de individuele ringen en geconjugeerde circuits. Daarnaast wordt ook aangetoond dat dezelfde overeenkomst kan worden waargenomen voor globale maatstaven voor de aromaticiteit, zoals de TRE of NICS, wanneer alle relevante bijdragen van geconjugeerde circuits behoorlijk in rekening worden gebracht.

In het derde en laatste deel van het proefschrift worden de delokalisatie en magnetische indices gebruikt voor de studie van de aromaticiteit van meer complexe moleculen zoals de Hexaiodobenzeen molecule, metallische aromatische systemen en de hydroporphyrines. Voor de studie van hexaiodobenzeen (C_6I_6) en zijn kation ($C_6I_6^{2+}$), worden twee complementaire theoretische technieken voor de studie van de σ-delokalisatie en σ-aromaticiteit gebruikt. De eerste is in staat de kringstromen direct weer te geven en de σ en π bijdragen eraan te ontwarren. Deze afbeeldingen van de kringstromen en de orbitaalbijdragen, zoals berekend met de ipsocentrische methode, tonen aan dat er naast de benzenoide π kringstroom in de centrale ring van het neutrale molecule en het kation eveneens een afzonderlijk identificeerbare σ kringstroom aanwezig is in de jood zesring van het kation. Een orbitaalmodel voor de richting van de stroom wordt opgesteld en de RCM worden vergeleken met de Multi Center Delokalisatie Index, die de onderliggende cyclische elektrondelokalisatie in zowel de koolstof- als de joodcircuits aantoont. Beide criteria ondersteunen de toekenning van σ-aromaticiteit aan de joodring in $C_6I_6^{2+}$.

Voor de PAK en relatief eenvoudige moleculen zoals hexaiodobenzeen en zijn kation, houdt de relatie tussen de MCDI en de kringstromen stand, maar bij meer ingewikkelde moleculen, zoals het metallische Al $_4^{2-}$ en de hydroporphyrines, gaat de relatie gedeeltelijk verloren. Bij de studie van de metallische aromatische moleculen Al_4^{2-}, $LiAl_4^-$ en Li_2Al_4 blijkt dat er geen directe relatie bestaat tussen de elektrondelokalisatie en de aanwezigheid van een kringstroom, anders dan dat een gedelokaliseerd systeem een noodzakelijke, maar niet voldoende voorwaarde is om tot een kring stroom te komen. In het geval van de van Al_4^{2-} afgeleide verbindingen, is er duidelijk zowel σ als π elektron delokalisatie hoewel alleen het σ systeem aanleiding geeft tot een kring stroom. De analyse van de canonische moleculaire orbitalen (GMO)-NICS leiden tot een andere conclusie, hoewel deze methode ook bezette-bezette orbitaaltermen bevat en niet zo gemakkelijk te interpreteren valt als de ip-

socentrische kringstromen. De Fermi hole analyse en MCDI komen wel zeer goed overeen wat betreft het beschrijven van de elektrondelokalisatie. Betreffende het gebruik van de term aromaticiteit in de huidige context, stuit men op het probleem van het ontbreken van een definitie van aromaticiteit voor moleculen die geen benzenoide ringen bevatten. Er is geen duidelijke reden om te besluiten welke "benzeenachtige" eigenschappen maximaal moeten worden behouden in andere moleculen om hen te beschrijven als zijnde aromatisch. Als elektrondelokalisatie volstaat, kunnen de verbindingen bestudeerd worden beschreven als zowel σ als π aromatisch. Als de aanwezigheid van een kringstroom een vereiste is voor aromaticiteit, zijn de huidige moleculen enkel σ aromatisch. Daarom wordt voorgesteld om altijd aan the geven wat er precies bedoeld wordt wanneer er gebruik wordt gemaakt van het begrip aromaticiteit. In deze context is Al_4^{2-} σ en π aromatisch als men rekening houdt met de elektrondelokalisatie, maar slechts σ aromatisch als men rekening houdt met de aanwezigheid van een kringstroom.

Verschillende maatstaven voor de aromaticiteit, waaronder energetische, magnetische en elektrondichtheidscriteria zijn uiteindelijk gebruikt om aan te tonen hoe aromaticiteit de volgorde van de stabiliteit van de hydroporphyrines, variërend van porphine tot octahydroporphine, en de preferentiële hydrogeneringspaden tussen hen kan verklaren. De gebruikte methoden zijn topologische resonantie energieën en hun circuit energieeffecten, bindingsresonantieenergieën, MCDI, kringstromen, magnetische susceptibiliteit en de NICS. Om de informatie verkregen met de verschillende methoden te vergelijken zijn de resultaten in dezelfde schaal gezet met behulp van recent voorgestelde methoden. Hieruit blijkt dat ze allen in wezen dezelfde informatie verstrekken en leiden tot soortgelijke conclusies. Ook de hydrogeneringsenergieën langs de verschillende hydrogeneringspaden die porphine met octahydroporphine verbinden zijn berekend met behulp van Density Functional Theory. Met behulp van de hierboven genoemde methoden wordt aangetoond dat de relatieve stabiliteit van de verschillende hydroporphyrine isomeren en de waargenomen ontoegankelijkheid van octahydroporphine zowel synthetisch en in de natuur perfect kan worden gerationaliseerd in functie van de aromaticiteit.

In het algemeen tonen de resultaten dat, voor de PAK, de MCBI goed correleert met de similariteit van de ringen met benzeen en met andere lokale aromaticiteits indices. Een goede correlatie kan ook worden gevonden met de globale aromaticiteits indices wanneer de juiste combinatie van geconjugeerde circuits wordt genomen. Wanneer we kijken naar moleculen, waar er geen relatie met benzeen meer te vinden is, wordt het ingewikkelder. Er is geen duidelijke reden om te zeggen welke " benzeenachtige" eigenschappen maximaal moeten wordenbehouden in andere moleculen om ze te klasseren als aromatisch. Betreffende het gebruik van de term aromaticiteit in deze moleculen wordt daarom gesuggereerd om altijd aan te geven wat precies

bedoeld wordt bij gebruik van het begrip aromaticiteit.

Acknowledgements

Ik wens mijn oprechte dank te betuigen aan iedereen die mij heeft geholpen, in de eerste plaats met het onderzoek en de verhandeling, maar ook allen die mij hebben gesteund de afgelopen zes jaar.

Op de eerste plaats mijn promotor Prof. P. Bultinck voor zijn deskundige begeleiding. Met zijn uitgebreide kennis aan theorie en programmeren stuurde hij het onderzoek steeds in de goede richting. Daarbij liet hij voldoende vrijheid om een eigen weg binnen het onderzoeken te vinden, iets waar ik hem zeer dankbaar voor ben. Ook heeft hij mij het plezier van het programmeren leren ontdekken en stond hij altijd klaar om me te helpen bij het debuggen van mijn code.

I would like to thank Prof. P. W. Fowler for the interesting research-stay in Sheffield. I've also enjoyed his help and the interesting discussions on Ring Currents throughout the past few years. I would also like to thank him for reading and correcting this work and for taking the time to come to Belgium for my defence.

Vervolgens zou ik Prof. C. Van Alsenoy willen danken voor het ter beschikking stellen van de Brabo-code ter berekening van de twee-electron-integralen. Deze code heeft enorm geholpen bij het programmeren van de Ring Currents.

Daarnaast wil ik mijn collega's van S3 danken voor de fijne tijden. In het bijzonder natuurlijk mijn 'kamergenootjes' doorheen de laatste zes jaar: Sofie, Elke en Helen, maar natuurlijk ook de rest: Jonas, Veerle, Els, Matthias, Philip en alle anderen... In het bijzonder zou ik Sofie nogmaals willen danken voor de vele hulp bij de statistische berekeningen.

Dank aan iedereen die mij heeft gesteund de voorbije jaren. In het bijzonder mijn verloofde Amina, voor de steun en geborgenheid die ze mij de laatste zeven jaar steeds heeft geboden. Ik weet dat ik niet altijd de gemakkelijkste persoon ben geweest, ze heeft veel van mij moeten verdragen als mijn code weeral eens niet wilde werken, maar ik zie haar enorm graag en ik wens mij dan ook te verontschuldigen voor de keren dat ik het haar moeilijk heb gemaakt. Vooral koester ik onze vele mooie reizen samen, naar China, India, Egypte, Kenia, Venetië, en vele andere plekken in

de wereld. Met haar heb ik tevens mijn ideale travel buddy gevonden.

Natuurlijk ook dank aan al mijn vrienden, in het bijzonder Ward, Tharphen en Jeroen, maar zeker ook aan Koen, Kim, Erika, Jeanne, Bram, Arne, Bert, Samten, Rebecca en alle anderen die ik nu vergeet. Dank voor de steun, de vriendschap, de ineressante gesprekken en discussies en vooral voor de mooie tijden samen.

ང་ལ་རྒྱབ་སྐྱོར་གནང་མཁན་གྱི་བོད་པའི་གྲོགས་པོ་ཚོ་དང་རྣག་པར་དུ་དའི་དགེ་རྒན་དང་བརྩེ་བའི་གྲོགས་པོ་ཐར་འཕེན་ལ་ཐུགས་རྗེ་ཆེ་ཞུ་ཡིན།

དས་བླ་མ་ཀ་བཀྲ་དང་བླ་མ་བཟོད་པ་དེ་བཞིན་བླ་མ་བཀྲིས་ཉེ་མ་བཙས་ལ་གུས་པ་ཆེན་པོས་ཐུགས་རྗེ་ཆེ་ཞུ་གི་ཡིན།

Contents

Chapter 1

Introduction

Few concepts in chemistry are as widespread as aromaticity[1–4]. Although originally well defined in terms of similarity between benzenoid rings[5], over time it has been used for many different classes of molecules, making it a fuzzy concept. Minkin et al., for example, define eight different classes of aromaticity in their book "Aromaticity and Antiaromaticity, Electronic an Structural Aspects"[2]: Aromaticity, Antiaromaticity, Heteroaromaticity, Homoaromaticity, σ-aromaticity, In-plane aromaticity, Three-dimensional aromaticity and Spherical aromaticity. In addition to the different classes of molecules to which the concept of aromaticity may apply, there is no immediate observable to classify a molecule as aromatic or not. This lack of an immediate observable has resulted in a multiplicity of indices to quantify aromaticity, based on energetic[6], geometric[7], quantum chemical[8] or magnetic considerations[9–13]. The lack of correlation between some of these indices has put forward suggestions that aromaticity is a multidimensional phenomenon[6,14–17].

Recently many authors have started to refer to the local aromaticity of separate rings in molecules, adding even more confusion to the concept of aromaticity. Local aromaticity refers to the degree of aromaticity of a fragment of a molecule, for example, the degree of aromaticity of a specific benzenoid ring in a polyaromatic hydrocarbon. This local aromaticity of a benzenoid ring will then be used to reflect the retention of benzene characteristics. Many works implicitly assume that this local aromaticity is also a multidimensional concept.

A concept closely related to aromaticity is that of electron delocalisation, of which the Multi Centre Bond Indices (MCBI), recently introduced by our group[18–21], has been shown to be a successful measure[22]. The purpose of this work is to examine the correlation between the delocalisation index and other measures of aromatic-

ity, to determine whether there is really a need to invoke the multidimensionality of aromaticity to explain the differences between the measures.

Part I

Theoretical Background

Chapter 2

Aromaticity

There are many definitions for aromaticity, but benzene is considered as the archetype of an aromatic molecule in all of them. Many characteristics of benzene are used to determine the aromaticity in other molecules. The degree of similarity of the characteristic between the molecule under study and benzene is then viewed as a measure of aromaticity. Therefore after a short historical overview (section 2.1) this chapter will discuss the most typical characteristics of benzene (section 2.2) to end with some possible definitions of the concept of aromaticity (section 2.6).

2.1 History

Michael Faraday (1791-1867) was the first to isolate benzene in 1825[23]. In the following years many other scientists discovered different ways to isolate benzene and its related substances. The molecular formula of benzene was at that time surprising since it has an equal number of carbon and hydrogen atoms. Most compounds known until then had a greater proportion of hydrogen atoms. The chemistry of benzene and its related substances gradually became a specific branch of organic chemistry and these substances started to form a chemical family on their own. The first known use of the word "aromatic" as a chemical term is by August Wilhelm Hofmann in 1855[24]. In this paper he refers to a group of acids related to benzoic acid as "aromatic acids", without defining the adjective. Since only some of the acids referred to have notable aromas, the term must refer to their common chemical properties or their structure rather than their smell.

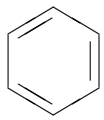

1

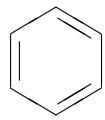

2

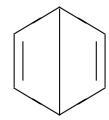

3

For some time, the formula of benzene, C_6H_6, with a 1:1 ratio between the number of hydrogen and the number of carbon atoms, and the known tetravalence of carbon made it hard to determine the structure of benzene. In 1865 the German chemist Friedrich August Kekulé (1829-1896), at that time a professor at Ghent University, was the first to suggest the structure of a six-membered ring of carbon atoms with alternating single and double bonds (compounds **1** and **2**).[25] Only one year later Kekulé published the second volume of his "Lehrbuch der organischen Chemie"[5], with a noteworthy chapter on "Aromatische Substanzen". In this chapter Kekulé defines the aromatic compounds as compounds having a C_6-ring:

> In allen aromatischen Verbindungen kann also, als gemeinschaftlicher Kern, eine aus sechs Kohlenstoffatomen bestehende, geschlossene Kette angenommen werden, die noch sechs freie Verwandtschaftseinheiten besitzt. Man könnte sie durch die Formel: C_6A_6 ausdrücken, in welcher A eine nicht gesättigte Affinität oder Verwandtschaftseinheit bezeichnet.[1] (p. 496)

In 1867, James Dewar (1842-1923) proposed seven possible structures for benzene[26], among which the Kekulé structure, however it is one of these seven which was not advocated by Dewar that is still called the Dewar structure (**3**).[27]

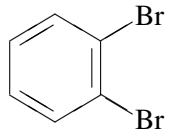

4

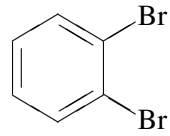

5

The structure proposed by Kekulé was found to be problematic since based on this view of alternating single and double bonds there could be two different 1,2-dibromobenzenes (**4** and **5**), whereas only one form of 1,2-dibromobenzene has ever

[1] Therefore, in all the aromatic compounds one can accept the common core to be a closed chain of six carbon atoms, which has six free connectivity-units. One might express it by the formula: C_6A_6, in which A means a non-saturated affinity or connectivity-unit.

been found. To accommodate this contradiction, Kekulé suggested that the two structures are in equilibrium with each other and are rapidly interchanging. In this way compounds **4** and **5** would also rapidly interconvert. This would explain why only one form has been found.

The cyclic nature of benzene was finally confirmed by the crystallographer Kathleen Lonsdale (1903-1971) in 1929[28].

After the introduction of quantum mechanics, it was Erich Hückel (1896-1980) who in 1930 was the first to separate the bonding electrons of unsaturated molecules into σ- and π-electrons[29]. This separation was then used by him to calculate the π-electron structure of benzene and other cyclo-conjugated hydrocarbons using both valence bond and molecular orbital theory[30–32]. These results explained the stability of benzene quantum mechanically and led to the famous Hückel 4n+2 rule.

2.2 Benzene

Many of the characteristics of benzene are used to determine the degree of aromaticity in other molecules. Among these characteristics are the bond length equalisation, the energetic stability, the presence of a ring current in a magnetic field and the electron delocalisation.

2.2.1 Geometry

Since the work of Lonsdale in 1929 it is known that benzene has a hexagonal, planar structure with C-C bond lengths of 1.39 Å . This bond length lies between the typical bond length for a single C-C bond, which is 1.53 Å and that for a typical C=C double bond, which is 1.34 Å . Later, after the introduction of quantum mechanics, it was found that the highly symmetric D_{6h} structure is the most stable structure on the Potential Energy Surface (PES), with the distorted forms of benzene higher in energy. In contrast to benzene, acyclic polyenes exhibit an alternation of bond lengths and in the case of "anti-aromatic" molecules, the bond length alternation is even more pronounced. For cyclobutadiene for example the symmetric D_{4h} structure is higher in energy than the D_{2h} structure. Here the D_{4h} structure is the transition state between the topomerization of the two rectangular D_{2h} structures. This difference in bond lengths between aromatic, anti-aromatic molecules and acyclic polyenes has served as a basis for the characterisation of a molecule as aromatic or not. The alternation of bond lengths has therefore been used as a measure of aromaticity, for example in the Harmonic Oscillator Model of Aromaticity (HOMA)[2,33,34] where a normalised sum of squared deviations of bond lengths from the optimal value (those for a fully

aromatic system) is used as an aromaticity index:

$$HOMA = 1 - \frac{N}{\#bonds} \sum_{i}^{\#bonds} (d_{opt} - d_i)^2 \tag{2.1}$$

where N is a scaling factor, d_{opt} the optimal bond length (*e.g.* 1.388 Å for the C-C bond in benzene) and d_i the experimental or computed bond length. An aromatic compound has HOMA value close to 1, whereas a non-aromatic compound has value close to 0.

2.2.2 Energetic Stability

The resonance between the two Kekulé structures explained the geometry of benzene, but did not explain its stability, for instance the preference for substitution reactions rather than addition reactions. In addition, the enthalpy of hydrogenation and combustion of benzene is significantly lower than would be expected for the cyclohexatriene structure. The enthalpy of hydrogenation (ΔH) of the double bond in cyclohexene is -120 kJ mol^{-1} and that of the two double bonds of cyclohexa-1,3-diene is a little less than twice this value, -232 kJ mol^{-1}. The hypothetical 1,3,5-cyclohexatriene would thus have a value of approximately -360 kJ mol^{-1} (3 $\times$ -120 kJ mol^{-1}). However, the value of benzene is only -209 kJ mol^{-1}. The difference of 151 kJ mol^{-1} is known as the resonance energy or the aromatic stabilisation energy of benzene (see Fig. 2.1).

A resonance hybrid has a structure that is intermediate between two or more contributing structures. The total energy of the system, however, is lower and therefore more stable than any of the contributing structures. The difference between the energy of the actual molecule and that of the contributing structure with the lowest energy is called the "resonance energy".[36] In the example of benzene, the resonance hybrid is the intermediate between two 1,3,5-cyclohexatriene structures, the contributing structures. The resonance energy is the difference in energy between this structure and that of benzene (see Fig. 2.1). It is important to stress that the resonance energy cannot be measured, but only estimated, since the contributing structures are not observable molecular entities.

Analogous to the reasoning for benzene above, many different approaches have been developed to calculate the resonance energy of other aromatic molecules. The value obtained for the resonance energy, however, greatly depends on the method by which it is calculated.

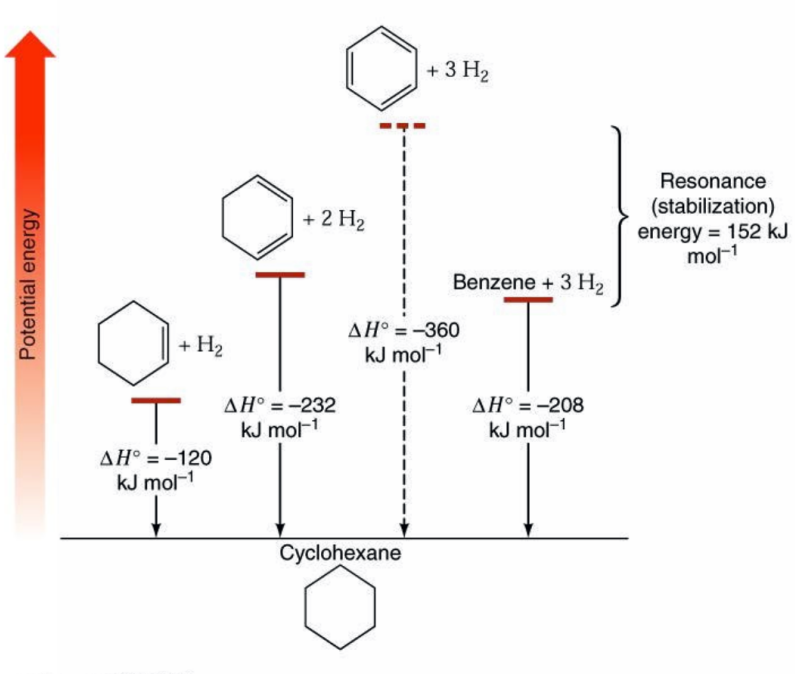

Figure 2.1: The enthalpy of hydrogenation of cyclohexene, cyclohexa-1,3-diene, (hypothetical) 1,3,5-cyclohexatriene, and benzene (Figure from Solomons and Fryhle [35], Fig. 14.1)

2.2.3 Magnetic Considerations

If a magnetic field, $\boldsymbol{H}_0$, is directed perpendicular to the molecular plane of benzene, a diamagnetic ring current is induced in the delocalised π electrons of the aromatic ring. This current in turn generates a magnetic field $\boldsymbol{H}'$, partially cancelling the applied magnetic field, $\boldsymbol{H}_0$. The ring currents themselves can be calculated theoretically[12,37–44] but cannot be measured experimentally, but some of the values derived from this ring current such as the magnetic susceptibility, the ^{1}H and ^{13}C NMR shifts can be compared with experimental values. Since ring currents are also present in Polycyclic Aromatic Hydrocarbons and other aromatic molecules, the ring current itself and the magnetic shielding under the form of the Nucleus Independent Chemical Shift (NICS) grew to be popular tools to access the amount of aromaticity[3,4,9,10].

2.2.4 Electron Delocalisation

The underlying cause to the energetic stability and the ring current of benzene is the presence of six delocalised π electrons. Strictly speaking all the electrons in any molecule are delocalised and in fact one should speak about the delocalisation of the π-type bonds in benzene. IUPAC defines delocalisation as follows:[36]

> A quantum mechanical concept most usually applied in organic chemistry to describe the π-bonding in a conjugated system. This bonding is not localised between two atoms: instead, each link has a 'fractional double bond character' or bond order. There is a corresponding 'delocalisation energy', identifiable with the stabilisation of the system compared with a hypothetical alternative in which formal (localised) single and double bonds are present. Some degree of delocalisation is always present and can be estimated by quantum mechanical calculations. The effects are particularly evident in aromatic systems and in symmetrical molecular entities in which a lone pair of electrons or a vacant p-orbital is conjugated with a double bond (e.g. carboxylate ions, nitro compounds, enamines, the allyl cation). Delocalization in such species may be represented by partial bonds or as resonance (symbolised by a two-headed arrow) between contributing structures.

Since electron (bond) delocalisation is such an important feature of benzene, many indices have been developed to describe the amount of delocalisation within a molecule. These indices have subsequently been used as an index to evaluate the aromaticity in other molecules. Examples are the PDI (Para Delocalisation Index)[8,45], the FLU (fluctuation) index[8,46] and the Multi Centre Bond Index[18–21] used in this work.

2.3 The Hückel 4N+2 Rule

Many other compounds exhibit properties similar to benzene: planarity, bond length equalisation, energetic stability, diamagnetic ring current, electron delocalisation,... Valence bond and molecular orbital theory calculations carried out by Erich Hückel (1896-1980) in the 1930's on benzene and other cycloconjugated hydrocarbons[30–32] showed the stability of molecules containing 2, 6, 10, 14, ... π-electrons. This led to the famous Hückel 4n+2 rule. Planar, cyclic systems with 4n+2 π-electrons will be aromatic, whereas systems with 4n π-electrons are less stable and are called anti-aromatic. Their bond lengths are generally not equalised, break planarity and exhibit a paratropic ring current.

2.4 Polycyclic Aromatic Hydrocarbons (PAH)

By fusing two or more benzene-rings together, one gets aromatic systems with 10, 14, 18, ... π electrons. The simplest example is naphtalene (**6**), formed by two fused benzene rings. The resonance energy is 255 kJ mol^{-1} and thus higher, but not twice that of benzene (151 kJ mol^{-1}). In contrast to benzene, the bond lengths in naphthalene are not all equal.

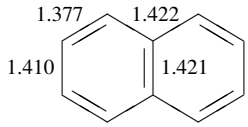

6

When fusing three benzene rings one gets anthracene (linear) and phenanthrene (kinked). The resonance energy of anthracene is 351 kJ mol^{-1}. Examination of the resonance structures indicates that the three rings cannot all have a Kekulé structure at the same time. The central ring of anthracene is more reactive than the outer ones. For example, anthracene is easily oxidised to form anthra-9,10-quinone. Similarly, halogenation of anthracene leads to the addition at the 9,10-positions in the central ring, giving 9,10-dichloro-9,10-dihydroanthracene. In both cases the product contains two fully non-conjugated benzenoid rings. The central ring also acts as a diene in Diels-Alder reactions, for example in the reaction with maleic anhydride.

Phenanthrene has a resonance energy of 351 kJ mol^{-1} and thus is more stable than anthracene. Five resonance structures can be written and in four of them the two outer rings have a Kekulé structure with the 9,10-bond being a double bond. The 9-10 bond is the most reactive bond of phenanthrene. Both reduction and oxidation

of the 9,10-bond are readily accomplished, yielding 9,10-dihydrophenanthrene and phenanthra-9,10-quinone, respectively.

By fusing more benzene rings together, many different Polycyclic Aromatic Hydrocarbons (PAHs) are possible, all possessing considerable aromatic stabilisation energies. Although all PAHs clearly are aromatic compounds, the degree of aromaticity can be different for each ring segment. According to Clar's rule for PAHs (formulated by Erich Clar in 1964) the resonance structure with the most disjoint aromatic π-sextets (i.e. benzene-like moieties) is the most important for the characterization of the properties. For phenanthrene, for example, this is the structure with two aromatic π-sextets in the outer rings and a double bond at the 9,10-position.

2.5 Other Classes of Aromatic molecules

2.5.1 Heterocyclic Aromatic Compounds

Many aromatic molecules have an atom other than carbon as one of the ring atoms. A common example is Pyrrole, a 5-membered ring where an electron-pair of the nitrogen atom forms a delocalised bond with the $p_\perp$-orbitals (perpendicular to the molecular plane) of the carbon atoms. It thus forms an aromatic compound with 6 electrons in delocalised bonds. Other examples are Furan, a 5-membered ring with oxygen, Thiophene, a 5-membered ring with sulphur and Pyridine, a 6-membered ring with nitrogen.

The introduction of heteroatoms changes the aromatic stabilisation, magnetic effect and delocalisation in the molecule, leading to a wide range of aromatic to anti-aromatic molecules for which different indices of aromaticity might come to different conclusions on the degree of aromaticity within the molecule.

2.5.2 All metallic aromatic compounds

In 2001 Li *et al.* published a paper in Science under the title "Observation of All-Metal Aromatic Molecules"[47], where they reported the discovery of an aromatic Al_4^{2-}-cluster. Since this discovery the interest in these compounds has grown enormously[48,49]. As a result, many concepts of aromaticity have been extended to metallic systems: energetic criteria, ring current, electron delocalisation, *etc.*, sometimes leading to contradicting results. Within these studies some discussion has been risen whether or not these molecules are both σ- and π-aromatic, or only σ aromatic. Some all metal aromatic compounds have also been classified as δ-aromatic, in which the delocalised bonds make use of the d-orbitals of the metals[50,51]. In Chapter 11 the

results of some common aromaticity indices on $Li_nAl_4^{n-2}$ molecules are compared with each other.

2.6 Defining Aromaticity

There are many different definitions of aromaticity, with large differences between some of them. The definitions are largely inspired by the research field in which the author is active. Organic chemists tend to highlight the (lack of) reactivity and the stability of aromatic compounds, those studying the magnetic response of molecules will accentuate this criterion whereas those studying delocalisation indices tend to insist on the electron delocalisation. The definition in the IUPAC Gold Book illustrates the problematic character of defining aromaticity since it gives three definitions to define "aromatic"[36,52]:

- In the traditional sense, 'having a chemistry typified by benzene'.
- A cyclically conjugated molecular entity with a stability (due to delocalisation) significantly greater than that of a hypothetical localised structure (e.g. Kekulé structure) is said to possess aromatic character. If the structure is of higher energy (less stable) than such a hypothetical classical structure, the molecular entity is 'antiaromatic'. The most widely used method for determining aromaticity is the observation of diatropicity in the ^{1}H NMR spectrum.
- The terms aromatic and anti-aromatic have been extended to describe the stabilisation or destabilisation of transition states of pericyclic reactions The hypothetical reference structure is here less clearly defined, and use of the term is based on application of the Hückel (4n + 2) rule and on consideration of the topology of orbital overlap in the transition state. Reactions of molecules in the ground state involving anti-aromatic transition states proceed, if at all, much less easily than those involving aromatic transition states.

Emphasis lies here on the (energetic) stability of aromatic structures. Schleyer, the "father" of the Nucleus Independent Chemical Shifts (NICS), a magnetic index, on the other hand, defines aromaticity as[53]:

> Compounds which exhibit significantly exalted diamagnetic susceptibility are aromatic. Cyclic electron delocalisation also may result in

> bond length equalization, abnormal chemical shifts and magnetic anisotropies, as well as chemical and physical properties which reflect energetic stabilisation. Those compound with exalted paramagnetic susceptibility may be anti-aromatic.

As is clear from the definition, emphasis lies on the magnetic criteria and not so much on electron delocalisation. As will be discussed in detail, the results from magnetic criteria and electron delocalisation may contradict.

Chapter 3

Quantum-chemical Background

The electron distribution and therefore the electronic properties of molecules can be calculated using quantum mechanics. For this the non-relativistic, time-independent Schrödinger equation has to be solved:

$$\hat{\mathscr{H}}\Psi = E\Psi \tag{3.1}$$

where the wave function Ψ is the eigenfunction of the Hamiltonian $\hat{\mathscr{H}}$, and E is the total energy of the system.

The simplicity of this formula stands in sharp contrast to the number of difficulties encountered when trying to solve the equation. To enable us to solve the equation for chemically interesting molecules some approximations to both the Hamiltonian and the wave function will need to be introduced. First of all the Hamiltonian will have to be approximated using the Adiabatic and Born-Oppenheimer approximations (Section 3.1), but even with these approximations the Schrödinger equation can only be solved exactly for one-electron systems. To calculate the properties of many-electron systems, the wave function will be approximated using a single or a limited number of Slater Determinants (Section 3.2.1) and using a finite basis-set (Section 3.3). When a single Slater Determinant is used the method is known as the Hartree-Fock method (Section 3.2).

3.1 The Adiabatic and Born-Oppenheimer Approximations

The total Hamiltonian for a system with N electrons and M nuclei can be written as a sum of the kinetic (T) and potential (V) contributions from those electrons and

nuclei. Using atomic units (a.u.), the total Hamiltonian can be written as:

$$\begin{aligned}\hat{\mathscr{H}} &= \hat{T}_{\mathrm{n}} + \hat{T}_{\mathrm{e}} + \hat{V}_{\mathrm{ne}} + \hat{V}_{\mathrm{ee}} + \hat{V}_{\mathrm{nn}} \\ &= -\sum_{i=1}^{N} \frac{1}{2}\nabla_i^2 - \sum_{A=1}^{M} \frac{1}{2M_A}\nabla_A^2 - \sum_{i=1}^{N}\sum_{A=1}^{M} \frac{Z_A}{|\boldsymbol{R}_A - \boldsymbol{r}_i|} \\ &\quad + \sum_{i=1}^{N}\sum_{j>i}^{N} \frac{1}{|\boldsymbol{r}_i - \boldsymbol{r}_j|} + \sum_{A=1}^{M}\sum_{B>A}^{M} \frac{Z_A Z_B}{|\boldsymbol{R}_A - \boldsymbol{R}_B|}\end{aligned} \tag{3.2}$$

with ∇_i^2 and ∇_A^2 the Laplacian operators, M_A and Z_A the mass and atomic number of nucleus A and $\boldsymbol{r}$ and $\boldsymbol{R}$ the position vectors of the electrons and the nuclei respectively. Neglecting the coupling between different electronic surfaces (the adiabatic approximation) and using the fact that the mass of the nuclei is much bigger than that of the electrons[54,55] (the Born-Oppenheimer approximation) the total Hamiltonian reduces to the electronic Hamiltonian, $\hat{\mathscr{H}}_e$:

$$\begin{aligned}\hat{\mathscr{H}}_{\mathrm{e}} &= \hat{T}_{\mathrm{e}} + \hat{V}_{\mathrm{ne}} + \hat{V}_{\mathrm{ee}} \\ &= -\sum_{i=1}^{N} \frac{1}{2}\nabla_i^2 - \sum_{i=1}^{N}\sum_{A=1}^{M} \frac{Z_A}{|\boldsymbol{R}_A - \boldsymbol{r}_i|} + \sum_{i=1}^{N}\sum_{j>i}^{N} \frac{1}{|\boldsymbol{r}_i - \boldsymbol{r}_j|}\end{aligned} \tag{3.3}$$

When looking at the electronic Hamiltonian, we see that both the electronic kinetic energy, $\hat{T}_{\mathrm{e}}$, and the nuclear-electron attraction, $\hat{V}_{\mathrm{ne}}$, are a sum over terms depending on only one electron coordinate, whereas the electron-electron repulsion, $\hat{V}_{\mathrm{ee}}$, depends on two electron coordinates. Collecting the operators according to the number of electron coordinates they depend on, equation 3.3 can be rewritten as:

$$\begin{aligned}\hat{\mathscr{H}}_{\mathrm{e}} &= \sum_{i=1}^{N} \hat{h}_i + \sum_{i=1}^{N}\sum_{j>i}^{N} \hat{g}_{ij} \\ \hat{h}_i &= -\frac{1}{2}\nabla_i^2 - \sum_{A=1}^{M} \frac{Z_A}{|\boldsymbol{R}_A - \boldsymbol{r}_i|} \\ \hat{g}_{ij} &= \frac{1}{|\boldsymbol{r}_i - \boldsymbol{r}_j|}\end{aligned} \tag{3.4}$$

The solution of the Schrödinger equation using this electronic Hamiltonian yields the electronic wave function:

$$\hat{\mathscr{H}}_e \Psi_e = E_e \Psi_e \tag{3.5}$$

The total energy within the given approximations can then be written as the sum of the electronic energy, E_e, and a constant term for the nuclear repulsion energy.

$$E = E_e + \sum_{A=1}^{M} \sum_{B>A}^{M} \frac{Z_A Z_B}{|\boldsymbol{R}_A - \boldsymbol{R}_B|} \tag{3.6}$$

In the Born-Oppenheimer approximation the nuclei can be seen as moving on a potential energy surface, which is the solution of the above electronic Schrödinger equation (equation 3.5). This potential energy surface is independent of the nuclear mass, and thus independent of the atomic isotopes in the molecule. For the majority of the systems the errors introduced by using the Born-Oppenheimer approximation are negligible.

3.2 Hartree-Fock Method

3.2.1 The Single Slater Determinant

The electronic Schrödinger equation can only be solved exactly for one-electron systems. For other systems we have to introduce additional approximations, not to the Hamiltonian, but this time to the wave function. The wave function in equation 3.5 depends on the position and spin of the electrons:

$$\Psi_e = \Psi_e(\boldsymbol{x}_1, \boldsymbol{x}_2, \ldots, \boldsymbol{x}_N) \tag{3.7}$$

where the vectors $\boldsymbol{x}_i$ include the space coordinates, $\boldsymbol{r}_i$, and the spin coordinate, σ_i, of the i-th electron.

To generate approximate solutions for the wave function one uses the variational principle, which states that any approximate wave function has an energy above that of the exact wave function. The energy is equal to the exact solution only if the wave function used is the exact one. By constructing the wave function using a number of parameters, this 'trial' function can be optimised through finding the values of the parameters that minimise the energy. This is done by constructing the electronic wave function from single-electronic wave functions called molecular orbitals (MO, *vide infra*). These molecular orbitals, ϕ_i, are expanded in a set of K basis functions, χ[56,57]:

$$\phi_i^{\alpha}(\boldsymbol{r}) = \sum_{p=1}^{K} c_{pi}^{\alpha} \chi_p(\boldsymbol{r}) \tag{3.8}$$

The molecular orbital coefficients, c_{pi}^{α}, are the parameters which have to be optimised. The spin of the electron is taken into account by using the molecular spinorbitals (MSO):

$$\psi_i(\boldsymbol{x}_1) = \sigma_i(\omega_1)\phi_\mu(\boldsymbol{r}_1) \tag{3.9}$$

where ϕ_μ is the (spinless) molecular orbital associated with the i-th molecular orbital, $\sigma_i(\omega_1)$ is the spin function, which can be $\alpha_i(\omega_1)$ or $\beta_i(\omega_1)$, and ω_1 is the spin variable of the electron.

Electrons are fermions and therefore the electronic wave function must be antisymmetric (change sign) with respect to the interchange of the coordinates of any two electrons. This antisymmetry can be mathematically achieved by using a Slater Determinant. The single-Slater Determinant approximation to the electronic wave function, Φ, is:

$$\Phi = \frac{1}{\sqrt{N!}} \begin{vmatrix} \psi_1(\boldsymbol{x}_1) & \psi_2(\boldsymbol{x}_1) & \dots & \psi_N(\boldsymbol{x}_1) \\ \psi_1(\boldsymbol{x}_2) & \psi_2(\boldsymbol{x}_2) & \dots & \psi_N(\boldsymbol{x}_2) \\ \vdots & \vdots & \ddots & \vdots \\ \psi_1(\boldsymbol{x}_N) & \psi_2(\boldsymbol{x}_N) & \dots & \psi_N(\boldsymbol{x}_N) \end{vmatrix} \tag{3.10}$$

As described above, this approximate wave function can be optimised using the variational principle. The energy,

$$E_e = \frac{\langle \Phi | \hat{\mathscr{H}}_e | \Phi \rangle}{\langle \Phi | \Phi \rangle} \tag{3.11}$$

can be minimised with respect to the molecular orbital coefficients, c_{pi}^{α}:

$$\frac{\partial E_e}{\partial c_{pi}^{\alpha}} = 0 \tag{3.12}$$

3.2.2 The Energy of the Slater Determinant

To facilitate the evaluation of the energy of the Slater determinant, equation 3.10 can be rewritten using the antisymmetrizing operator $\hat{A}$

$$\Phi = \hat{A}\left[\psi_1(\boldsymbol{1})\psi_2(\boldsymbol{2})\dots\psi_N(\boldsymbol{N})\right] = \hat{A}\Pi \tag{3.13}$$

where

$$\hat{A} = \frac{1}{\sqrt{N!}} \sum_{n=0}^{N-1} (-1)^{p_n} \hat{\mathscr{P}}_n = \frac{1}{\sqrt{N!}} \left[\hat{1} - \sum_{ij} \hat{\mathscr{P}}_{ij} + \sum_{ijk} \hat{\mathscr{P}}_{ijk} \dots \right] \tag{3.14}$$

with $\hat{\mathscr{P}}_n$ an operator that generates the nth permutation of the electron labels 1,2, ..., N and p_n the number of transpositions needed to obtain this permutation. $\hat{1}$ is the identity-operator, $\hat{\mathscr{P}}_{ij}$ an operator generating all possible permutations of two electron coordinates, $\hat{\mathscr{P}}_{ijk}$ the permutations of three electron coordinates, *etc*. The antisymmetrising operator $\hat{A}$ commutes with the Hamiltonian ($\hat{A}\hat{\mathscr{H}} = \hat{\mathscr{H}}\hat{A}$) and the antisymmetrising operator acting twice gives the same as the operator acting once, multiplied by $\sqrt{N!}$ ($\hat{A}\hat{A} = \sqrt{N!}\hat{A}$).

The energy may be rewritten in terms of the permutation operator by inserting equation 3.13 in equation 3.11 (and since $\langle\Phi|\Phi\rangle$=1):

$$\begin{aligned} E &= \langle\Phi|\hat{\mathscr{H}}_e|\Phi\rangle \\ &= \langle\hat{A}\Pi|\hat{\mathscr{H}}_e|\hat{A}\Pi\rangle \\ &= \sqrt{N!}\langle\Pi|\hat{\mathscr{H}}_e|\hat{A}\Pi\rangle \\ &= \sum_n (-1)^{p_n}\langle\Pi|\hat{\mathscr{H}}_e|\hat{\mathscr{P}}_n\Pi\rangle \end{aligned} \tag{3.15}$$

It is easily seen that for the one electron operator, $\hat{h}_i$, only the identity operator gives a non-zero contribution to the energy, whereas both the identity operator and $\hat{\mathscr{P}}_{ij}$ give non-zero contributions for the two-electron operator, g_{ij}.

$$\begin{aligned} E_e &= \sum_{i=1}^{N}\langle\Pi|\hat{h}_i|\Pi\rangle + \sum_{i=1}^{N}\sum_{j>i}^{N}\Big(\langle\Pi|\hat{g}_{ij}|\Pi\rangle - \langle\Pi|\hat{g}_{ij}|\hat{\mathscr{P}}_{ij}\Pi\rangle\Big) \\ &= \sum_{i=1}^{N}\langle\psi_i(\boldsymbol{x}_1)|\hat{h}_1|\psi_i(\boldsymbol{x}_1)\rangle + \sum_{i=1}^{N}\sum_{j>i}^{N}\Big(\langle\psi_i(\boldsymbol{x}_1)\psi_j(\boldsymbol{x}_2)|\hat{g}_{12}|\psi_i(\boldsymbol{x}_1)\psi_j(\boldsymbol{x}_2)\rangle \\ &\qquad - \langle\psi_i(\boldsymbol{x}_1)\psi_j(\boldsymbol{x}_2)|\hat{g}_{12}|\psi_i(\boldsymbol{x}_2)\psi_j(\boldsymbol{x}_1)\rangle\Big) \end{aligned} \tag{3.16}$$

Since the two two-electron terms cancel each other when i=j, we can rewrite the double sum without the restriction of j>i ,by introducing a factor $1/2$. Furthermore we will express the energy in terms of Coulomb ($\hat{J}_i$) and Exchange ($\hat{K}_i$) operators:

$$
\begin{aligned}
E_e = &\sum_{i=1}^{N} \langle \psi_i(\boldsymbol{x}_1) | \hat{h}_1 | \psi_i(\boldsymbol{x}_1) \rangle \\
&+ \frac{1}{2} \sum_{i=1}^{N} \sum_{j=1}^{N} \Big(\langle \psi_j(\boldsymbol{x}_2) | \hat{J}_i | \psi_j(\boldsymbol{x}_2) \rangle - \langle \psi_j(\boldsymbol{x}_2) | \hat{K}_i | \psi_j(\boldsymbol{x}_2) \rangle \Big) \\
\hat{J}_i | \psi_j(\boldsymbol{x}_2) \rangle &= \langle \psi_i(\boldsymbol{x}_1) | \hat{g}_{12} | \psi_i(\boldsymbol{x}_1) \rangle | \psi_j(\boldsymbol{x}_2) \rangle \\
\hat{K}_i | \psi_j(\boldsymbol{x}_2) \rangle &= \langle \psi_i(\boldsymbol{x}_1) | \hat{g}_{12} | \psi_j(\boldsymbol{x}_1) \rangle | \psi_i(\boldsymbol{x}_2) \rangle
\end{aligned}
\tag{3.17}
$$

Or in a simpler notation:

$$
E_e = \sum_{i=1}^{N} h_i + \frac{1}{2} \sum_{i=1}^{N} \sum_{j=1}^{N} \Big(J_{ij} - K_{ij} \Big) \tag{3.18}
$$

To determine the set of 'optimal' molecular orbitals, the variation in the energy with respect to the variation in the MSOs, $\partial \psi_i$, has to be zero under the constraint of the MSOs being orthogonal and normalised. This constrained optimization is done by using Lagrange multipliers, λ_{ij}. It can easily be shown (see for instance Roothaan[56] and Hall[58]) that this leads to the famous Hartree-Fock equations:

$$
\hat{F}_i \psi_i = \sum_{j=1}^{N} \lambda_{ij} \psi_j \tag{3.19}
$$

with $\hat{F}$ the Fock operator:

$$
\begin{aligned}
\hat{F}_i &= \hat{h}_i + \sum_{j=1}^{N} \Big(\hat{J}_j - \hat{K}_j \Big) \\
&= \hat{h}_i + \hat{G}_i
\end{aligned}
\tag{3.20}
$$

By means of a unitary transformation, the matrix of Lagrange multipliers can be diagonalised so λ_{ij}=$\delta_{ij}\epsilon_i$:

$$
\hat{F}_i \psi'_i = \epsilon_i \psi'_i \tag{3.21}
$$

The Hartree-Fock equations can be seen as a form of eigenvalue equation, where the Fock operator itself depends on the result of all the MSOs. The Fock operator can thus only be determined when all occupied orbitals are known. This is why

these equations have to be solved iteratively. The Lagrange multipliers ϵ_i are the eigenvalues of the Fock operator in the MSO basis and correspond to MSO energies:

$$\epsilon_i = \langle \psi_i' | \hat{F}_i | \psi_i' \rangle \tag{3.22}$$

The total energy then becomes (dropping the prime notation for the MSOs):

$$E = \sum_{i=1}^{N} \epsilon_i - \frac{1}{2} \sum_{i=1}^{N} \sum_{j=1}^{N} \Big(J_{ij} - K_{ij} \Big) + V_{nn} \tag{3.23}$$

$$\epsilon_i = \langle \psi_i | \hat{F}_i | \psi_i \rangle = h_i + \sum_{j=1}^{N} \Big(J_{ij} - K_{ij} \Big) \tag{3.24}$$

The Hartree Fock Equations are solved using Linear Combinations of Atomic Orbitals (LCAO-approximation, equation 3.8)[56,58]. In this way equation 3.21 may be written as:

$$\hat{F}_i \sum_{p=1}^{K} c_{pi} \chi_p = \epsilon_i \sum_{p=1}^{K} c_{pi} \chi_p \tag{3.25}$$

Multiplying from the left by a basis function χ_q^* and integrating gives:

$$\sum_{p=1}^{K} c_{pi} F_{qp} = \epsilon_i \sum_{p=1}^{K} c_{pi} S_{qp} \tag{3.26}$$

where F_{qp} is the Fock matrix element given as:

$$F_{qp} = \langle \chi_q | \hat{F} | \chi_p \rangle \tag{3.27}$$

$$= H_{qp} + G_{qp} \tag{3.28}$$

and S_{qp} the overlap integral between χ_q and χ_p:

$$S_{qp} = \langle \chi_q | \chi_p \rangle \tag{3.29}$$

In matrix notation the equations are known as the Roothaan-Hall equations[56,58]:

$$\boldsymbol{FC} = \boldsymbol{SC\epsilon} \tag{3.30}$$

To determine the MSO coefficients c_{pi}, the Fock matrix must be diagonalised. However, as has been mentioned before, the Fock operator and thus also the Fock matrix depends on all MO coefficients. The procedure thus starts with an initial guess of the coefficients to form the Fock matrix, to diagonalise it and obtain the first calculated set of MSO coefficients. These are used to form a new Fock matrix which is again diagonalised, *etc*. This procedure is continued until the new set of coefficients equals the previous set within a certain threshold. Solving the equations gives K Molecular Spin Orbitals, all orthogonal to each other. Of these K MSOs, only N are occupied and the remaining $K - N$ are unoccupied and called 'virtual'.

3.2.3 Restricted and Unrestricted Hartree-Fock

So far, the Slater Determinant has been written in terms of Molecular Spin Orbitals. When no restriction is made on the form of the spatial part of the Molecular Spin Orbitals, the procedure is called "Unrestricted Hartree-Fock". In many cases the system to be calculated is a closed shell system (even number of electrons and ground state singlet). For these systems two spin orbitals ψ_i and ψ_j share the same spatial molecular orbital ϕ_i multiplied by an α and a β spin function, and both have the same orbital energy. In these cases the Slater Determinant can be constructed using the (spinless) molecular orbitals alone. When the Slater Determinant is constructed as such, the procedure is called "Restricted Hartree-Fock". Since $\langle\alpha|\alpha\rangle$=$\langle\beta|\beta\rangle$=1 and $\langle\alpha|\beta\rangle$=$\langle\beta|\alpha\rangle$=0, the energy expression of equations 3.17 and 3.18 becomes:

$$E_e = \sum_{i=1}^{N/2} \langle\phi_i(\boldsymbol{x}_1)|\hat{h}_i|\phi_i(\boldsymbol{x}_1)\rangle + \sum_{i=1}^{N/2}\sum_{j=1}^{N/2} \Big(2\langle\phi_j(\boldsymbol{x}_2)|\hat{J}_i|\phi_j(\boldsymbol{x}_2)\rangle \tag{3.31}$$

$$- \langle\phi_j(\boldsymbol{x}_2)|\hat{K}_i|\phi_j(\boldsymbol{x}_2)\rangle\Big) \tag{3.32}$$

$$= 2\sum_{i=1}^{N/2} h_i + \sum_{i=1}^{N/2}\sum_{j=1}^{N/2} \Big(2J_{ij} - K_{ij}\Big)$$

where the summations run over the $N/2$, doubly occupied, (spinless) molecular orbitals.

3.2.4 Electron Correlation

The single Slater determinant is only an approximation to the exact wave function, and thus its energy will always be greater than the exact (non-relativistic) ground state energy (within the Born-Oppenheimer approximation), E_0. The difference between these two energies is called the correlation energy[59]:

$$E_C = E_0 - E_{HF} \tag{3.33}$$

where E_{HF} is the energy in the Hartree-Fock limit (with an infinite basis-set, *vide infra*). This correlation energy will always be negative since the Hartree-Fock energy is always greater than the exact one. The correlation energy can be seen as a measure for the error introduced by using the Hartree-Fock method.

Electron correlation is mainly caused because the electrostatic interaction between electrons is treated only in an average manner within the Hartree-Fock method. This means that the method does not consider the "instantaneous" electrostatic interactions between electrons. The effect of the N-1 electrons on the electron of interest

is treated in an average way. As a consequence, the electron-electron repulsion term is too large resulting in E_{HF} lying above E_0. This part of the electron correlation is usually called dynamical electron correlation because it is related to the actual movements of the individual electrons. A second main contribution to the correlation energy is due to the inadequacy of the single Slater Determinant in describing a given molecular state. This is called the Nondynamical or Static correlation. A typical problem is the dissociation of a bond in the RHF method. The method is a good approximation at equilibrium distance, where the correlation error is small and almost exclusively due to dynamical correlation. However, as the bond is stretched, more than one Slater Determinant is needed to describe the system accurately and the correlation becomes larger. In contrast to the dynamical electron correlation, which is more a short range effect, the Nondynamical contributions are a long range effect and become more important when the bond is stretched.

A large number of methods has been developed to calculate this correlation energy by bringing the wave function closer to the exact solution. A first way of doing this is by making first and higher order corrections to the wave function by mixing in contributions from excited configurations. This method is used in the Configuration Interaction (CI) and Coupled Cluster (CC) approaches. The most common among these methods are CISD and CCSD, where SD means that single and double excitations are used to correct the wave function. Another method to include electron correlation effects is by means of perturbation theory. This can be done by using Møller and Plessets second, third or fourth order perturbation theory (MP2, MP3 and MP4). Finally the electron correlation can be included by using a functional, the method used in Density Functional Theory (DFT).

3.3 Basis Sets

The Roothaan-Hall equations are solved within a certain basis set, which can be chosen as a function of the accuracy needed and the time available for the calculation. The expansion of the unknown molecular orbitals in a set of known functions is not by itself an approximation. If the basis set is complete, the expansion is exact, however this means one has to use an infinite number of basis functions, which is impossible in practice. The approximation in the LCAO-approximation thus lies in the use of a finite number of basis functions. Increasing the number of basis functions for a certain calculation will lower the Hartree-Fock energy, bringing it closer to the true energy of the system. By using an infinite basis set, the best possible energy within the Hartree-Fock approximation would be obtained, this is known as the Hartree-Fock limit. Within a fixed number of basis functions, the accuracy of the

calculation can also be influenced by the shape of the basis functions used. The basis functions can be chosen to have any form as long as their behaviour is physically acceptable. However, the choice of the basis-functions is generally influenced by the computational complexity of their one- and especially two-electron integrals.

3.3.1 Slater-type Functions

The best form for a basis function is one which most closely resembles the form of a true atomic orbital. The Slater-type functions are simple exponentials which mimic the exact solutions for hydrogen-like atoms and take the following analytical form:

$$\chi^{STO}_{n,l,m,\alpha}(\boldsymbol{r},\boldsymbol{\theta},\boldsymbol{\phi}) = N|\boldsymbol{r}|^{n-1}Y_{lm}(\boldsymbol{\theta},\boldsymbol{\phi})e^{-\alpha|\boldsymbol{r}|} \tag{3.34}$$

where n, l and m are the quantum numbers defining the orbital, $\boldsymbol{r}$, $\boldsymbol{\theta}$ and $\boldsymbol{\phi}$ the spherical coordinates, Y_{lm} is a spherical harmonic that describes the angular part of the function, α is the exponent and N is the normalisation factor.

The radial part of this function closely resembles the radial behaviour of atomic orbitals. However, the two-electron integrals are hard to evaluate using these functions, which makes them unattractive for calculating molecular properties.

3.3.2 Gaussian-type Functions

A different function which is more commonly used is the Gaussian-type function, having the following form:

$$\chi^{GTO}_{n,l,m,\alpha}(\boldsymbol{r},\boldsymbol{\theta},\boldsymbol{\phi}) = N|\boldsymbol{r}|^{2n-2-l}Y_{lm}(\boldsymbol{\theta},\boldsymbol{\phi})e^{-\alpha|\boldsymbol{r}|^2} \tag{3.35}$$

or slightly different (with 6 d- and 10 f-functions instead of 5 d and 9 f):

$$\chi^{GTO}_{l_x,l_y,l_z,\alpha}(\boldsymbol{x},\boldsymbol{y},\boldsymbol{z}) = N|\boldsymbol{x}|^{l_x}|\boldsymbol{y}|^{l_y}|\boldsymbol{z}|^{l_z}e^{-\alpha|\boldsymbol{r}|^2} \tag{3.36}$$

with l_x, l_y and l_z positive integers of which the sum determines the type of orbital (l_x+l_y+l_z=l).

In contrast to the Slater-type function, the Gaussian-type function has a r^2 dependence in the exponential. This makes the radial behaviour inferior to the one of the Slater-type function. Slater-type functions have a “cusp” or a discontinuous derivative at the nucleus, whereas Gaussian-type functions do not. This means Gaussian-type functions do not represent the proper behaviour at the nucleus. The r^2 dependence also makes the Gaussian-type function drop too rapidly when going away from the nucleus. These “flaws” are in practice compensated by using a linear combination of Gaussian-type functions, called a contracted Gaussian function,

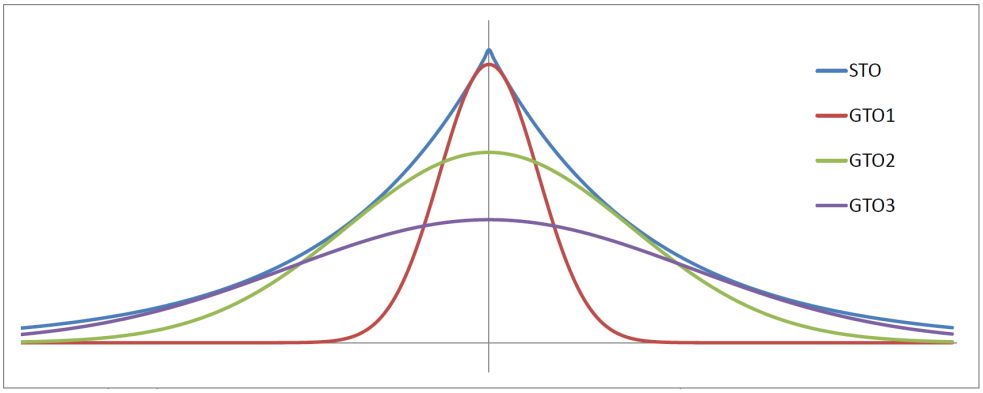

Figure 3.1: Contracted Gaussian functions: approximating a Slater-type orbital with several Gaussian-type orbitals.

to fit the Slater-type function more closely (see Figure 3.1. The need to use more Gaussian-type functions (called primitives) in one basis-functions is more than compensated by the fact that the two-electron integrals can be solved fairly easy in an analytic way, making the contracted Gaussian-type functions less time-consuming.

3.4 Perturbation Theory

Some systems are not completely described by the Hamiltonian in equation 3.2, this is for example the case when the system is in an electric or magnetic field. In these cases extra terms appear in the Hamiltonian, making it more complex. To calculate these systems within the Hartree-Fock approach, there are roughly two ways to handle the problem. First of all, one can include the extra terms of the Hamiltonian into the Fock matrix and run the calculations as such. A second, more widely used method is to calculate the system using the Hamiltonian of equation 3.2 and treating the extra terms as (small) perturbations to the Hamiltonian. This method is called Perturbation Theory.

Using the Hartree-Fock one-electron equivalent of the "unperturbed" Hamiltonian, $\hat{F}^{(0)}$, the eigenfunctions and eigenvalues of a given system can be calculated in absence of the perturbation. Supposing that the solutions for $\hat{F}^{(0)}$ to equation 3.21 are known for a closed-shell system:

$$\hat{F}_i^{(0)}\phi_i^{(0)} = \epsilon_i^{(0)}\phi_i^{(0)} \tag{3.37}$$

When the true $\hat{F}$ differs from $\hat{F}^{(0)}$ to only a small extent, the eigenfunctions and eigenvalues for the true $\hat{F}$ can be calculated using Perturbation Theory. The true $\hat{F}$ can be written as:

$$\hat{F} = \hat{F}^{(0)} + \lambda \hat{F}^{(1)} \tag{3.38}$$

where $\hat{F}^{(1)}$ is a perturbing operator and λ a dimensionless parameter that maps $\hat{F}^{(0)}$ to $\hat{F}$ as it varies from 0 to 1.

For the applications considered in this work, the perturbation will be one to the one-electron part, $\hat{h}_i$, of the Hamiltonian and can be expanded as follows:

$$\hat{h}_i = \hat{h}_i^{(0)} + \lambda \hat{h}_i^{(1)} \tag{3.39}$$

The eigenfunctions and the eigenvalues can be written as a Taylor series in λ:

$$\phi_i = \phi_i^{(0)} + \lambda \left.\frac{\partial \phi_i^{(0)}}{\partial \lambda}\right|_{\lambda=0} + \frac{1}{2!}\lambda^2 \left.\frac{\partial^2 \phi_i^{(0)}}{\partial \lambda^2}\right|_{\lambda=0} + \ldots \tag{3.40}$$

and

$$\epsilon_i = \epsilon_i^{(0)} + \lambda \left.\frac{\partial \epsilon_i^{(0)}}{\partial \lambda}\right|_{\lambda=0} + \frac{1}{2!}\lambda^2 \left.\frac{\partial^2 \epsilon_i^{(0)}}{\partial \lambda^2}\right|_{\lambda=0} + \ldots \tag{3.41}$$

Equations 3.40 and 3.41 are usually written as:

$$\phi_i = \phi_i^{(0)} + \lambda \phi_i^{(1)} + \lambda^2 \phi_i^{(2)} + \ldots \tag{3.42}$$

$$\epsilon_i = \epsilon_i^{(0)} + \lambda \epsilon_i^{(1)} + \lambda^2 \epsilon_i^{(2)} + \ldots \tag{3.43}$$

Inserting equations 3.39, 3.42, 3.43 and 3.20 in equation 3.21 and collecting them according to the order of the perturbation (power of λ) gives the following:

$$\begin{aligned}
&\left\{\hat{h}_i^{(0)}\phi_i^{(0)} + \hat{G}_i\phi_i^{(0)} - \epsilon_i^{(0)}\phi_i^{(0)}\right\} \\
&+\lambda\left\{\hat{h}_i^{(0)}\phi_i^{(1)} + \hat{G}_i\phi_i^{(1)} + \hat{h}_i^{(1)}\phi_i^{(0)} - \epsilon_i^{(0)}\phi_i^{(1)} - \epsilon_i^{(1)}\phi_i^{(0)}\right\} \\
&+\lambda^2\left\{\hat{h}_i^{(0)}\phi_i^{(2)} + \hat{G}_i\phi_i^{(2)} + \hat{h}_i^{(1)}\phi_i^{(1)} - \epsilon_i^{(0)}\phi_i^{(2)} - \epsilon_i^{(1)}\phi_i^{(1)} - \epsilon_i^{(2)}\phi_i^{(0)}\right\} \\
&+\ldots = 0
\end{aligned} \tag{3.44}$$

Using equation 3.42 and the orthonormality-condition $\langle\phi_i|\phi_j\rangle$=$\delta_{ij}$ gives:

$$\begin{aligned}
\langle\phi_i|\phi_j\rangle =& \langle\phi_i^{(0)}|\phi_j^{(0)}\rangle \\
&+ \lambda\left\{\langle\phi_i^{(0)}|\phi_j^{(1)}\rangle + \langle\phi_i^{(1)}|\phi_j^{(0)}\rangle\right\} \\
&+ \lambda^2\left\{\langle\phi_i^{(0)}|\phi_j^{(2)}\rangle + \langle\phi_i^{(1)}|\phi_j^{(1)}\rangle + \langle\phi_i^{(2)}|\phi_j^{(0)}\rangle\right\} = \delta_{ij}
\end{aligned} \tag{3.45}$$

Since $\langle\phi_i^{(0)}|\phi_j^{(0)}\rangle = \delta_{ij}$, the remainder of the terms has to sum to 0.

Although the perturbation is only to the one-electron part, $\hat{h}_i$, of the Hamiltonian, since the two-electron part, $\hat{G}$, depends on all the (perturbed) MOs, this part will also be influenced by the expansion in the following way:

$$\begin{aligned}
\hat{G}_i\phi_i^{(0)} &= \sum_{j=1}^{N/2}\left(2\hat{J}_j\phi_i^{(0)} - \hat{K}_j\phi_i^{(0)}\right) \\
&= \sum_{j=1}^{N/2}\left(2\langle\phi_j|g_{12}|\phi_j\rangle\phi_i^{(0)} - \langle\phi_j|g_{12}|\phi_i^{(0)}\rangle\phi_j\right) \\
&= \left.\sum_{j=1}^{N/2}\left(2\langle\phi_j^{(0)}|g_{12}|\phi_j^{(0)}\rangle\phi_i^{(0)} - \langle\phi_j^{(0)}|g_{12}|\phi_i^{(0)}\rangle\phi_j^{(0)}\right)\right\} \quad \hat{G}_i^{(0)}\phi_i^{(0)} \\
&\quad \left.+\lambda\sum_{j=1}^{N/2}\left(2\langle\phi_j^{(0)}|g_{12}|\phi_j^{(1)}\rangle\phi_i^{(0)} - \langle\phi_j^{(0)}|g_{12}|\phi_i^{(0)}\rangle\phi_j^{(1)}\right.\right. \\
&\qquad \left.\left. + 2\langle\phi_j^{(1)}|g_{12}|\phi_j^{(0)}\rangle\phi_i^{(0)} - \langle\phi_j^{(1)}|g_{12}|\phi_i^{(0)}\rangle\phi_j^{(0)}\right)\right\} \quad \lambda\hat{G}_i^{(1)}\phi_i^{(0)} \\
&\quad \left.+\lambda^2\sum_{j=1}^{N/2}\left(2\langle\phi_j^{(1)}|g_{12}|\phi_j^{(1)}\rangle\phi_i^{(0)} - \langle\phi_j^{(1)}|g_{12}|\phi_i^{(0)}\rangle\phi_j^{(1)}\right)\right\} \quad \lambda^2\hat{G}_i^{(2)}\phi_i^{(0)} \\
&\quad + \ldots \\
&= \hat{G}_i^{(0)}\phi_i^{(0)} + \lambda\hat{G}_i^{(1)}\phi_i^{(0)} + \lambda^2\hat{G}_i^{(2)}\phi_i^{(0)} + \ldots
\end{aligned} \tag{3.46}$$

Thus 3.44 becomes

$$\begin{aligned}
&\left\{\hat{h}_i^{(0)}\phi_i^{(0)} + \hat{G}_i^{(0)}\phi_i^{(0)} - \epsilon_i^{(0)}\phi_i^{(0)}\right\} \\
&+\lambda\left\{\hat{h}_i^{(0)}\phi_i^{(1)} + \hat{G}_i^{(0)}\phi_i^{(1)} + \hat{h}_i^{(1)}\phi_i^{(0)} + \hat{G}_i^{(1)}\phi_i^{(0)} - \epsilon_i^{(0)}\phi_i^{(1)} - \epsilon_i^{(1)}\phi_i^{(0)}\right\} \\
&+\lambda^2\left\{\hat{h}_i^{(0)}\phi_i^{(2)} + \hat{G}_i^{(0)}\phi_i^{(2)} + \hat{h}_i^{(1)}\phi_i^{(1)} + \hat{G}_i^{(1)}\phi_i^{(1)} + \hat{h}_i^{(2)}\phi_i^{(0)} + \hat{G}_i^{(2)}\phi_i^{(0)}\right. \\
&\qquad \left. -\epsilon_i^{(0)}\phi_i^{(2)} - \epsilon_i^{(1)}\phi_i^{(1)} - \epsilon_i^{(2)}\phi_i^{(0)}\right\} \\
&+ \ldots = 0
\end{aligned} \tag{3.47}$$

It is convenient to write the perturbed MOs as a linear combination of the unperturbed $\phi_i^{(0)}$, or in other words use the $\phi_i^{(0)}$ as a orthonormal basis to calculate the perturbed

MOs[60]:

$$\begin{aligned}\phi_i &= \phi_i^{(0)} + \lambda\phi_i^{(1)} + \lambda^2\phi_i^{(2)} + \dots \\ &= \sum_{p=1}^{K} C_{pi}^{(0)}\phi_p^{(0)} + \lambda\sum_{p=1}^{K} C_{pi}^{(1)}\phi_p^{(0)} + \lambda^2\sum_{p=1}^{K} C_{pi}^{(2)}\phi_p^{(0)} + \dots \\ &= \sum_{p=1}^{K}\left[C_{pi}^{(0)} + \lambda C_{pi}^{(1)} + \lambda^2 C_{pi}^{(2)} + \dots\right]\phi_p^{(0)}\end{aligned} \tag{3.48}$$

Using this, the first order equations become:

$$\sum_{l=1}^{K}\left\{\hat{h}_i^{(0)} + \hat{G}_i^{(0)} - \epsilon_i^{(0)}\right\} C_{li}^{(1)}|\phi_l^{(0)}\rangle = -\left\{\hat{h}_i^{(1)} + \hat{G}_i^{(1)} - \epsilon_i^{(1)}\right\}|\phi_i^{(0)}\rangle \tag{3.49}$$

and (from equation 3.45):

$$C_{pi}^{(1)*} + C_{ip}^{(1)} = 0 \tag{3.50}$$

and since $F^{(0)}$=$H^{(0)}$+$G^{(0)}$ (equation 3.28) is a diagonal matrix with elements $\epsilon_p^{(0)}$ and $C_{pi}^{(0)}$ is δ_{pi}, multiplying equation 3.49 from the left by $\langle\phi_p^{(0)}|$ leads to:

$$\left(\epsilon_p^{(0)} - \epsilon_i^{(0)}\right) C_{pi}^{(1)} + H_{pi}^{(1)} + G_{pi}^{(1)} - \epsilon_i^{(1)}\delta_{pi} = 0 \tag{3.51}$$

where $H_{pi}^{(1)} = \langle\phi_p^{(0)}|\hat{h}^{(1)}|\phi_i^{(0)}\rangle$ (*cf.* equations 3.27 and 3.28).

The perturbation mixes a given MO with both occupied and unoccupied MOs, but the mixing of occupied orbitals among themselves does not change the total wave function. This can be shown as follows. Let $\hat{\mathscr{M}}$ be any one electron Hamiltonian:

$$\begin{aligned}\sum_{i=1}^{N/2}\langle\phi_i^{(0)} + \lambda\phi_i^{(1)}|\hat{\mathscr{M}}|\phi_i^{(0)} + \lambda\phi_i^{(1)}\rangle &= \sum_{i=1}^{N/2}\langle\phi_i^{(0)}|\hat{\mathscr{M}}|\phi_i^{(0)}\rangle \\ &+ \lambda\left\{\sum_{i=1}^{N/2}\langle\phi_i^{(1)}|\hat{\mathscr{M}}|\phi_i^{(0)}\rangle + \sum_{i=1}^{N/2}\langle\phi_i^{(0)}|\hat{\mathscr{M}}|\phi_i^{(1)}\rangle\right\} \\ &+ \lambda^2\sum_{i=1}^{N/2}\langle\phi_i^{(1)}|\hat{\mathscr{M}}|\phi_i^{(1)}\rangle\end{aligned} \tag{3.52}$$

For the first order correction, one can write

$$\sum_{i=1}^{N/2}\left(\langle\phi_i^{(1)}|\hat{\mathscr{M}}|\phi_i^{(0)}\rangle+\langle\phi_i^{(0)}|\hat{\mathscr{M}}|\phi_i^{(1)}\rangle\right)=\sum_{i=1}^{N/2}\sum_{p=1}^{N/2}C_{pi}^{(1)*}M_{pi}$$
$$+\sum_{i=1}^{N/2}\sum_{p=1}^{N/2}M_{ip}C_{pi}^{(1)}+\sum_{i=1}^{N/2}\sum_{p=N/2+1}^{K}\left(C_{pi}^{(1)*}M_{pi}+M_{ip}C_{pi}^{(1)}\right) \quad (3.53)$$

where $M_{ip}=\langle\phi_i^{(0)}|\hat{\mathscr{M}}|\phi_p^{(0)}\rangle$. If the indices in the first sum are interchanged and -$C_{pi}^{(1)}$ is substituted for $C_{ip}^{(1)*}$ (equation 3.50), the first sum cancels the second one.

Keeping this in mind, equation 3.51 can be rewritten as (with $1\leq i\leq N/2<p\leq K$)[60]:

$$\left(\epsilon_p^{(0)}-\epsilon_i^{(0)}\right)C_{pi}^{(1)}+H_{pi}^{(1)}$$
$$+\sum_{j=1}^{N/2}\sum_{q=N/2+1}^{K}\left\{\left(2\langle\phi_p^{(0)}\phi_j^{(0)}|g_{12}|\phi_i^{(0)}\phi_q^{(0)}\rangle-\langle\phi_p^{(0)}\phi_j^{(0)}|g_{12}|\phi_q^{(0)}\phi_i^{(0)}\rangle\right)C_{qj}^{(1)}\right.$$
$$\left.+\left(2\langle\phi_p^{(0)}\phi_q^{(0)}|g_{12}|\phi_i^{(0)}\phi_j^{(0)}\rangle-\langle\phi_p^{(0)}\phi_q^{(0)}|g_{12}|\phi_j^{(0)}\phi_i^{(0)}\rangle\right)C_{qj}^{(1)*}\right\}=0 \quad (3.54)$$

If the $C_{pi}^{(1)}$ are real, this becomes:

$$\left(\epsilon_p^{(0)}-\epsilon_i^{(0)}\right)C_{pi}^{(1)}+H_{pi}^{(1)}+\sum_{j=1}^{N/2}\sum_{q=N/2+1}^{K}\left\{\left(4\langle\phi_p^{(0)}\phi_j^{(0)}|g_{12}|\phi_i^{(0)}\phi_q^{(0)}\rangle\right.\right.$$
$$\left.\left.-\langle\phi_p^{(0)}\phi_j^{(0)}|g_{12}|\phi_q^{(0)}\phi_i^{(0)}\rangle-\langle\phi_p^{(0)}\phi_q^{(0)}|g_{12}|\phi_j^{(0)}\phi_i^{(0)}\rangle\right)C_{qj}^{(1)}\right\}=0 \quad (3.55)$$

If they are purely imaginary,

$$\left(\epsilon_p^{(0)}-\epsilon_i^{(0)}\right)C_{pi}^{(1)}+H_{pi}^{(1)}+\sum_{j=1}^{N/2}\sum_{q=N/2+1}^{K}\left\{\left(\langle\phi_p^{(0)}\phi_q^{(0)}|g_{12}|\phi_j^{(0)}\phi_i^{(0)}\rangle\right.\right.$$
$$\left.\left.-\langle\phi_p^{(0)}\phi_j^{(0)}|g_{12}|\phi_q^{(0)}\phi_i^{(0)}\rangle\right)C_{qj}^{(1)}\right\}=0 \quad (3.56)$$

Since the value of the $C_{pi}^{(1)}$ depends on the values of all the $C_{qj}^{(1)}$'s, the equations are coupled and the values have to be found in an iterative way. For this reason these equations are called the coupled perturbed Hartree-Fock equations.

3.5 Electron Density and The Fermi Hole

3.5.1 The Electron Density

The electron density, $\rho(\boldsymbol{r})$, is a function for the probability of finding an electron within a certain volume element $d\boldsymbol{r}$. It is found mathematically as the expectation value of the (Dirac) delta function $\delta(\boldsymbol{r}-\boldsymbol{r}_i)$:

$$\rho(\boldsymbol{r}) = \sum_i^N \int ... \int \Psi^*(\boldsymbol{x}_1, \boldsymbol{x}_2, ..., \boldsymbol{x}_N)\delta(\boldsymbol{r}-\boldsymbol{r}_i)\Psi(\boldsymbol{x}_1, \boldsymbol{x}_2, ..., \boldsymbol{x}_N)d\boldsymbol{x}_1 d\boldsymbol{x}_2 ... d\boldsymbol{x}_N \tag{3.57}$$

Or, since

$$\int_{-\infty}^{\infty} f(\xi)\delta(x-\xi)d\xi = f(x) \tag{3.58}$$

, the electron density can also be found by integrating the square of the wave function over all variables except the spatial coordinates of one electron:

$$\rho(\boldsymbol{r}) = N \int \ldots \int |\Psi(\boldsymbol{x}_1, \boldsymbol{x}_2, \ldots, \boldsymbol{x}_N)|^2 d\boldsymbol{\sigma}_1, d\boldsymbol{x}_2, \ldots, d\boldsymbol{x}_N \tag{3.59}$$

or in a shorter notation:

$$\rho(\boldsymbol{r}) = N \int \Psi\Psi^* d\tau' \tag{3.60}$$

where the integration over $d\tau'$ denotes the integration over all coordinates except the space coordinates of one electron. The electron density itself integrates to the total number of electrons, N, of the molecules:

$$\int \rho(\boldsymbol{r})d\boldsymbol{r} = N \tag{3.61}$$

Another property of the electron density is that it exhibits maxima at the positions of the nuclei ($\boldsymbol{R}_A$). The gradient of the density is discontinuous at these positions (so-called cusps). These cusps are the result of the singularity in the $\hat{V}_{ne}$ ($-\frac{Z_A}{|\boldsymbol{R}_A-\boldsymbol{r}|}$) part in the Hamiltonian when $|\boldsymbol{R}_A-\boldsymbol{r}|$ goes to zero. Furthermore the shape of the cusp is related to the nuclear charge Z_A of the nucleus:

$$\lim_{|\boldsymbol{R}_A-\boldsymbol{r}|\to 0}\left[\frac{\partial}{\partial r} + 2Z_A\right]\overline{\rho}(\boldsymbol{r}) = 0 \tag{3.62}$$

where $\overline{\rho}(\boldsymbol{r})$ is the spherical average of $\rho(\boldsymbol{r})$. Unlike the wave function, the electron density is an observable and can be measured experimentally by X-ray diffraction.

3.5.2 The Pair Density

A quantity related to the electron density is that of the pair density, $\rho_2(\boldsymbol{x}_1, \boldsymbol{x}_2)$, which is the probability of simultaneously finding one electron with spin σ_1 in a certain volume element $d\boldsymbol{r}_1$ and an other electron with spin σ_2 in a certain volume element $d\boldsymbol{r}_2$:

$$\rho_2(\boldsymbol{x}_1, \boldsymbol{x}_2) = N(N-1) \int \dots \int |\Psi(\boldsymbol{x}_1, \boldsymbol{x}_2, \dots, \boldsymbol{x}_N)|^2 d\boldsymbol{x}_3, \dots, d\boldsymbol{x}_N \tag{3.63}$$

The pair density is symmetric in the coordinates and normalised to N(N-1). It is clear that within the (exact) pair density, all information about electron correlation is contained. Related to the pair density is the reduced density matrix for two electrons, γ_2:

$$\begin{aligned}&\gamma_2(\boldsymbol{x}_1, \boldsymbol{x}_2; \boldsymbol{x}_1', \boldsymbol{x}_2') = \\ &N(N-1) \int \dots \int \Psi^*(\boldsymbol{x}_1, \boldsymbol{x}_2, \dots, \boldsymbol{x}_N) \Psi(\boldsymbol{x}_1', \boldsymbol{x}_2', \dots, \boldsymbol{x}_N) d\boldsymbol{x}_3, \dots, d\boldsymbol{x}_N\end{aligned} \tag{3.64}$$

Or written within the basis ψ_i:

$$\gamma_2(\boldsymbol{x}_1, \boldsymbol{x}_2; \boldsymbol{x}_1', \boldsymbol{x}_2') = N(N-1) \sum_{ijkl} \Gamma^{(2)}_{ijkl} \psi_i^*(\boldsymbol{x}_1) \psi_k(\boldsymbol{x}_1') \psi_j^*(\boldsymbol{x}_2) \psi_l(\boldsymbol{x}_2') \tag{3.65}$$

where $\Gamma^{(2)}_{ijkl}$ is the two electron or second order density matrix.

Interchanging the variables $\boldsymbol{x}_1$ and $\boldsymbol{x}_2$ will change the sign of γ_2 because of the antisymmetry of Ψ:

$$\gamma_2(\boldsymbol{x}_1, \boldsymbol{x}_2; \boldsymbol{x}_1', \boldsymbol{x}_2') = -\gamma_2(\boldsymbol{x}_2, \boldsymbol{x}_1; \boldsymbol{x}_1', \boldsymbol{x}_2') \tag{3.66}$$

since $\gamma_2(\boldsymbol{x}_1, \boldsymbol{x}_2; \boldsymbol{x}_1, \boldsymbol{x}_2) = \rho_2(\boldsymbol{x}_1, \boldsymbol{x}_2)$, putting $\boldsymbol{x}_1 = \boldsymbol{x}_1' = \boldsymbol{x}_2 = \boldsymbol{x}_2'$ in equation 3.66 gives:

$$\rho_2(\boldsymbol{x}_1, \boldsymbol{x}_1) = -\rho_2(\boldsymbol{x}_1, \boldsymbol{x}_1) \tag{3.67}$$

which can only be true when $\rho_2(\boldsymbol{x}_1, \boldsymbol{x}_1)$ = 0. This means that the probability of finding two electrons with the same spin at the same point in space has to be zero, which is nothing other than the Pauli principle. This effect is called the exchange or Fermi correlation and does not apply to two electrons having a different spin. Due to the antisymmetry of a Slater determinant this effect is properly included in the Hartree-Fock method and thus has nothing to do with the correlation energy discussed above. The correlation due to repulsion from the charge of the electrons is known as the Coulomb correlation, to distinguish it from the Fermi correlation. Since this repulsion is treated only in an average manner within the Hartree-Fock method, this

Coulomb correlation is completely neglected at the Hartree-Fock level. This can be shown by looking at the expression of the pair density within the Hartree-Fock approximation (using the so-called Löwdin expansion[61]):

$$\rho_2(\boldsymbol{x}_1,\boldsymbol{x}_2) = \sum_{i=1}^{N}\sum_{j=1}^{N}\big\{|\phi_i(\boldsymbol{r}_1)|^2|\phi_j(\boldsymbol{r}_2)|^2|\sigma_i(\omega_1)|^2|\sigma_j(\omega_2)|^2 - \phi_i^*(\boldsymbol{r}_1)\phi_i(\boldsymbol{r}_2)\phi_j^*(\boldsymbol{r}_2)\phi_j(\boldsymbol{r}_1)\sigma_i^*(\omega_1)\sigma_i(\omega_2)\sigma_j^*(\omega_2)\sigma_j(\omega_1)\big\} \tag{3.68}$$

For a two-electron system this becomes:

$$\begin{aligned}\rho_2(\boldsymbol{x}_1,\boldsymbol{x}_2) = {} & |\phi_1(\boldsymbol{r}_1)|^2|\phi_2(\boldsymbol{r}_2)|^2|\sigma_1(\omega_1)|^2|\sigma_2(\omega_2)|^2 \\ & + |\phi_1(\boldsymbol{r}_2)|^2|\phi_2(\boldsymbol{r}_1)|^2|\sigma_1(\omega_2)|^2|\sigma_2(\omega_1)|^2 \\ & - 2\phi_1^*(\boldsymbol{r}_1)\phi_1(\boldsymbol{r}_2)\phi_2^*(\boldsymbol{r}_2)\phi_2(\boldsymbol{r}_1)\sigma_1^*(\omega_1)\sigma_1(\omega_2)\sigma_2^*(\omega_2)\sigma_2(\omega_1)\end{aligned} \tag{3.69}$$

When looking at the probability of finding one electron at $\boldsymbol{r}_1$ and the other with a different spin at $\boldsymbol{r}_2$, the factors σ_1^2 and σ_2^2 in the first two terms are both equal to unity ($\langle\sigma_1|\sigma_1\rangle = 1$). However, since $\sigma_1 \neq \sigma_2$, the last term will vanish due to the orthonormality of the spin functions. Since the electrons are indistinguishable, the first and second term are identical and the final expression becomes $\rho_2(\boldsymbol{x}_1,\boldsymbol{x}_2) = \rho(\boldsymbol{x}_1)\rho(\boldsymbol{x}_2)$ which corresponds to the completely uncorrelated situation.

On the other hand, if the two electrons have the same spin, the last term in equation 3.69 will not reduce to the uncorrelated situation. $\langle\sigma_1|\sigma_1\rangle$ will equal 1 and for $\boldsymbol{r}_1 = \boldsymbol{r}_2$, the third term will cancel the first two and yield $\rho_2(\boldsymbol{x}_1,\boldsymbol{x}_1)= 0$

3.5.3 The Pair Correlation Function and the Exchange Correlation Hole

Since $\rho_2(\boldsymbol{x}_1,\boldsymbol{x}_2)$ reduces to the product of $\rho(\boldsymbol{x}_1)$ and $\rho(\boldsymbol{x}_2)$ in the uncorrelated situation, we can rewrite $\rho_2(\boldsymbol{x}_1,\boldsymbol{x}_2)$ as[62]:

$$\rho_2(\boldsymbol{x}_1,\boldsymbol{x}_2) = \rho(\boldsymbol{x}_1)\rho(\boldsymbol{x}_2)\left[1 + p(\boldsymbol{x}_1,\boldsymbol{x}_2)\right] \tag{3.70}$$

where $p(\boldsymbol{x}_1,\boldsymbol{x}_2)$ is the pair correlation function, a symmetric function that incorporates all non-classical effects. Multiplying the pair correlation function with the electron density and integrating it gives:

$$\int \rho(\boldsymbol{x}_2)p(\boldsymbol{x}_1,\boldsymbol{x}_2)d\boldsymbol{x}_2 = -1 \tag{3.71}$$

which is true for all $\boldsymbol{x}_1$. This has led to the definition of the exchange correlation hole[63], $h(\boldsymbol{x}_1,\boldsymbol{x}_2)$ as:

$$h(\boldsymbol{x}_1, \boldsymbol{x}_2) = \rho(\boldsymbol{x}_2)p(\boldsymbol{x}_1, \boldsymbol{x}_2) \tag{3.72}$$

The exchange correlation hole can be split into the Fermi hole, $f(\boldsymbol{x}_1, \boldsymbol{x}_2)$ and the Coulomb hole $c(\boldsymbol{x}_1, \boldsymbol{x}_2)$. The Fermi hole is the hole caused by the electrons avoiding each other due to the antisymmetry of the wave function and applies only to electrons with the same spin. The Coulomb hole is the hole resulting from the $1/|\boldsymbol{r}_1 - \boldsymbol{r}_2|$ electrostatic interaction and has contributions for electrons of either spin. Within the Hartree-Fock method the Fermi hole is accounted for through the use of a single Slater determinant whereas the Coulomb hole is neglected.

The Fermi Hole

The Fermi hole, caused by the antisymmetry of the wave function, is the most important part of the exchange correlation hole and dominates by far the Coulomb hole. Moreover, the Fermi hole, like the exchange correlation hole itself, integrates to -1.

$$\int f(\boldsymbol{r}_1, \boldsymbol{r}_2) d\boldsymbol{r}_2 = -1 \tag{3.73}$$

The following statements apply to the shape of the Fermi hole:

- Owing to the Pauli principle, two electrons of the same spin cannot be at the same position in space and thus the Fermi hole has to become equal to minus the electron density when $\boldsymbol{r}_1$ approaches the position of the reference electron $\boldsymbol{r}_2$, so $f(\boldsymbol{r}_1 \to \boldsymbol{r}_2, \boldsymbol{r}_2) = -\rho(\boldsymbol{r}_2)$
- It can be shown that $f(\boldsymbol{r}_1, \boldsymbol{r}_2)$ is always negative, so $f(\boldsymbol{r}_1, \boldsymbol{r}_2) < 0$
- Since the exchange correlation hole is the multiplication of the pair correlation function with the electron density, the Fermi hole itself can be seen as the multiplication of a "Fermi correlation function" with the electron density.
- Since the Fermi hole depends on the electron density, the hole will not be spherically symmetric around the reference electron. Usually, the Fermi hole is largest around the reference electron, but there are also situations where the Fermi hole tends to be delocalised.

The Coulomb Hole

Since both the exchange correlation hole and the Fermi hole integrate to -1 (equations 3.71 and 3.73), it follows that the Coulomb hole integrates to zero:

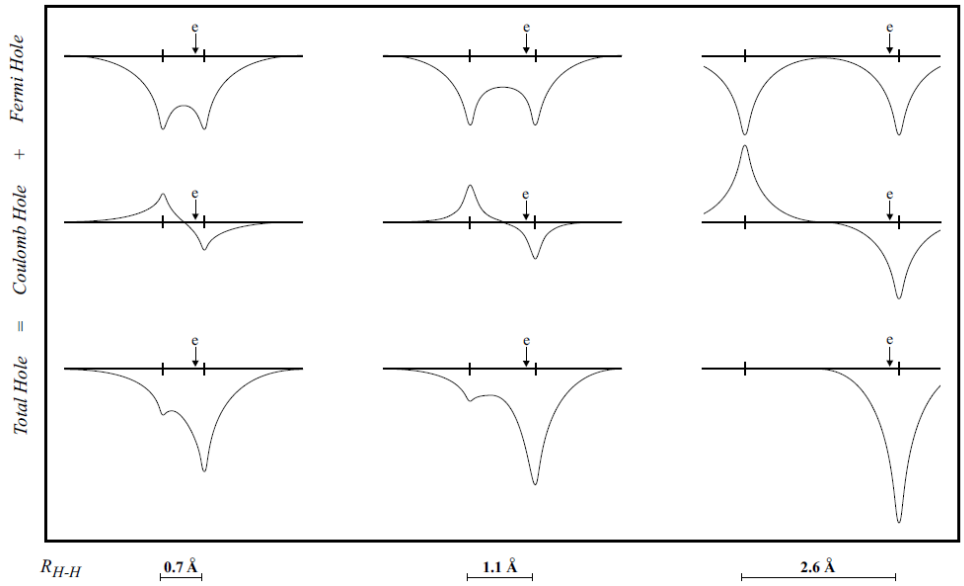

Figure 3.2: The Fermi, Coulomb and the resulting total exchange-correlation holes for H_2 at three different internuclear distances; the position of the reference electron is marked with an arrow (Figure from Koch and Holthausen [64] p. 28 and adapted from Baerends and Gritsenko [65].)

$$\int c(\boldsymbol{r}_1, \boldsymbol{r}_2) d\boldsymbol{r}_2 = 0 \tag{3.74}$$

Because the Coulomb hole is the result of the $1/|\boldsymbol{r}_1 - \boldsymbol{r}_2|$ electrostatic interaction, it is negative and largest at the position of the reference electron and positive farther away from the reference electron (see figure 3.2).

3.6 Population Analysis

Central in chemistry is the idea of a molecule as an arrangement of different atoms held together by bonds. Chemists like dividing the total number of electrons of the molecule amongst the different atoms in the molecule. This is done by assigning certain parts of the electron density to different atoms:

$$\rho_A(\boldsymbol{r}) = w_A(\boldsymbol{r})\rho(\boldsymbol{r}) \tag{3.75}$$

where $\rho_A(\boldsymbol{r})$ is the part of the electron density designated to atom A and $w_A(\boldsymbol{r})$ is a weight function which assigns a part of the electron density, $\rho(\boldsymbol{r})$, at position $\boldsymbol{r}$ to the atom A. Integration of this $\rho_A(\boldsymbol{r})$ gives the number of electrons of atom A in the molecule, N_A:

$$\int \rho_A(\boldsymbol{r}) d\boldsymbol{r} = \int w_A(\boldsymbol{r})\rho(\boldsymbol{r}) d\boldsymbol{r} = N_A \tag{3.76}$$

Subtracting the number of electrons of atom A in the molecule, N_A, from the number of electrons in the neutral, isolated atom, Z_A (the atomic number), gives the charge of the atom in the molecule, q_A:

$$q_A = Z_A - N_A = Z_A - \int \rho_A(\boldsymbol{r}) d\boldsymbol{r} \tag{3.77}$$

There is no unique way for this partitioning of the electron density into different atomic contributions. This has led to a multitude of definitions, which, depending on the molecule, might give very different results.

3.6.1 Mulliken Population Analysis

Due to its simplicity the Mulliken population analysis[66–69] has become one of the most familiar methods for assigning the portion of the electron density to be associated with a given atom.

From equations 3.59 and 3.61 it follows that (within the Hartree-Fock method):

$$N = \int \rho(\boldsymbol{r}) d\boldsymbol{r} = \sum_{i=1}^{N} \int \phi_i^*(\boldsymbol{r}) \phi_i(\boldsymbol{r}) d\boldsymbol{r} \tag{3.78}$$

Expanding the MO in a set of K basis functions, χ (see equation 3.8), equation 3.78 becomes:

$$N = \sum_{i=1}^{N} \sum_{p=1}^{K} \sum_{q=1}^{K} c_{pi}^* c_{qi} \int \chi_p^*(\boldsymbol{r}) \chi_q(\boldsymbol{r}) d\boldsymbol{r} \tag{3.79}$$

and replacing the integral with the overlap matrix S_{pq} (equation 3.29), and defining the density matrix, P_{qp}, as:

$$P_{qp} = \sum_{i=1}^{N} c_{pi}^* c_{qi} \tag{3.80}$$

, the expression can be rewritten as:

$$N = \sum_{p=1}^{K} \sum_{q=1}^{K} P_{qp} S_{pq} \tag{3.81}$$

Since the basis functions are normalised ($S_{pp} = 1$), the expression for N can be written as:

$$N = \sum_{p=1}^{K} P_{pp} + \sum_{p=1}^{K} \sum_{q>p}^{K} 2 P_{pq} S_{pq} \tag{3.82}$$

The Mulliken population analysis aims first to divide N among all the basis functions (in N_p). This is done by taking the diagonal element P_{pp} and dividing the off-diagonal elements equally between the two appropriate basis functions (by taking only the $\sum_{q \neq p}^{K} P_{pq} S_{pq}$ and not the symmetrical $\sum_{q \neq p}^{K} P_{qp} S_{qp}$):

$$N_p = P_{pp} + \sum_{q \neq p}^{K} P_{pq} S_{pq} \tag{3.83}$$

summation over the population of all basis functions (the atomic orbitals) of atom A gives the population N_A:

$$N_A = \sum_{p \in A} N_p \tag{3.84}$$

Despite its wide use, many difficulties arise from using this population analysis[70]. The method is very sensitive to the basis set used and for some molecules the equal division of the overlap-population between the atomic orbitals does not prove to be a good approximation.

3.6.2 Hirshfeld Population Analysis

In the Hirshfeld population analysis[71], the molecular electron density is partitioned among the different atoms based on the weight, $w_A(\boldsymbol{r})$, of the atom in the so-called 'promolecular' density. This promolecular density is constructed by taking the sum of the densities of the isolated atoms, ρ_X^0, in the same geometric arrangement as in the real molecule. The weight function for the atom A in every point in space is simply the share to the promolecular density held by this atom A in this point in space (this is why this method is sometimes called the stockholder method):

$$w_A(\boldsymbol{r}) = \frac{\rho_A^0(\boldsymbol{r})}{\sum_{X=1}^{M} \rho_X^0(\boldsymbol{r})} \tag{3.85}$$

where $\rho_A^0(\boldsymbol{r})$ is the electron density of the isolated atom A and $\sum \rho_X^0(\boldsymbol{r})$ is the promelecular density. The integration of $\rho_A(\boldsymbol{r})$ (equation 3.76) is done numerically. Apart from the electron density, every other three dimensional (molecular) function (e.g. the Fukui function, Fermi hole, ...) can be divided using this method. Despite the fact that the Hirshfeld AIM is quite popular, the model has been shown to have some shortcomings, which have motivated the improvement known as the Iterative Hirshfeld model[72].

3.6.3 Iterative Hirshfeld Population Analysis

Limitations of the Classical Hirshfeld Population Analysis

Even though the Hirshfeld AIM is a popular method, there are some important problems in applying the model. These problems are briefly discussed below and have led to the adaptation of the method by Bultinck et al.[72] to an iterative version of the Hirshfeld model.

(1) Hirshfeld atomic charges tend to be unrealistically small Although there is no unique charge definition, and thus no way to know the exact charge of the atom in a molecule, comparison of the Hirshfeld Population Analysis with other population analysis schemes shows that nearly all other Population Analysis schemes give significantly larger atomic charges than the Hirshfeld scheme[73,74]. Because of this observation, there appears to have grown a consensus that Hirshfeld charges are too small. The reason why Hirshfeld charges are so small can be related to the work

by Ayers who has shown that the Hirshfeld weighting factor aims to make the electron density of the atom in the molecule as similar as possible to that of the isolated atom[75,76]. Therefore it is not surprising that the charges are small.

(2) The Hirshfeld AIM populations depend on the choice of the promolecular density. As has been mentioned above, the promolecular density is obtained from the superposition of atomic densities of neutral atoms. There is however no strict theoretical basis for the choice of the neutral densities to construct the promolecule. A different choice for the promolecular density, for instance with charged atoms, is theoretically possible. For most molecules, neutral atoms are the logical choice for building the promolecule. However, for molecules with significant ionic character such as LiF, a different choice might be justifiable, e.g. with Li^+ and F^-. If one uses the combination of the Li^0 and F^0 densities to construct the promolecule, the atomic charge of Li is $+0.57$. However, considering the combination of the Li^+ and F^- densities, the Li charge becomes $+0.93$. Using the "chemically unreasonable" combination of Li^- and F^+ gives a Li charge of $+0.40$. This sensitivity to the choice of promolecular reference is undesirable since it makes the Population Analysis dependent on the choice of promolecule made.

(3) Hirshfeld charges are available only for neutral molecules. Related to the previous discussion, the ambiguity in how to choose the promolecular density is even more pronounced when a charged molecule is considered. In practical applications, the neutral atomic densities are used to construct the promolecule, but then the promolecule and the charged molecule densities do not integrate to the same number of electrons. This makes it impossible to connect the Hirshfeld charges to information entropy (*vide infra*, next point). As stated by Davidson and Chakravorty, the use of the densities of the neutral atoms to construct the promolecule is an arbitrary choice[73].

(4) Care needs to be taken in connecting Hirshfeld charges to information entropy. Recently, Parr et al. have shown the weighting function for the Hirshfeld AIM to be related to information entropy as the function minimizing the information loss during the formation of the molecule[77–81] However, there is an important requirement for connecting this information theory to the Hirshfeld AIM, the AIM needs to have the same electronic population as the promolecular atom. Failure to meet this condition complicates the exact connection between the Hirshfeld approach and information theory. When constructing the promolecular density by superposition of neutral atoms, this requirement is not fulfilled.

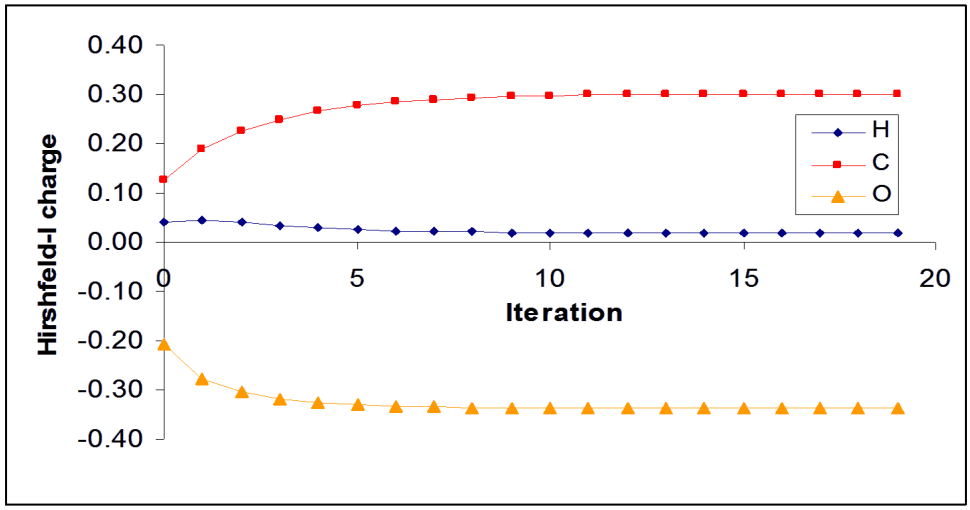

Figure 3.3: The change in the charges of formaldehyde during the iterative proces.

Iterative Hirshfeld Population Analysis

To overcome the difficulties described above, an iterative Hirshfeld method, denoted Hirshfeld-I was proposed by Bultinck et al.[72,74] This method starts from a guess for the initial atomic populations to build up the promolecule (typically the neutral atoms are taken, as in the classical Hirshfeld method). With this initial guess of the promolecule the Hirshfeld populations are computed from the molecular density. Then a new promolecule is constructed using atomic densities that have the same population as the AIM from the previous iteration ($\rho_A^{N_A^{(i-1)}}$). Using that promolecule, the Hirshfeld analysis is again carried out:

$$w_A^{(i)}(N_A^{(i-1)};\boldsymbol{r}) = \frac{\rho_A^{N_A^{(i-1)}}(\boldsymbol{r})}{\sum_{X=1}^{M} \rho_X^{N_A^{(i-1)}}(\boldsymbol{r})} \tag{3.86}$$

This procedure is repeated until the populations of two subsequent iterations are the same to within a certain threshold (see Figure 3.3 for the example of formaldehyde).

To calculate the promolecular atoms with fractional numbers of electrons, the densities of these atoms are computed using standard zero-temperature grand canonical ensemble theory[82,83]:

$$\rho_A^{N_A}(\boldsymbol{r}) = \rho_A^{\lfloor N_A \rfloor}(\boldsymbol{r})\left[\lceil N_A \rceil - N_A\right] + \rho_A^{\lceil N_A \rceil}(\boldsymbol{r})\left[N_A - \lfloor N_A \rfloor\right] \tag{3.87}$$

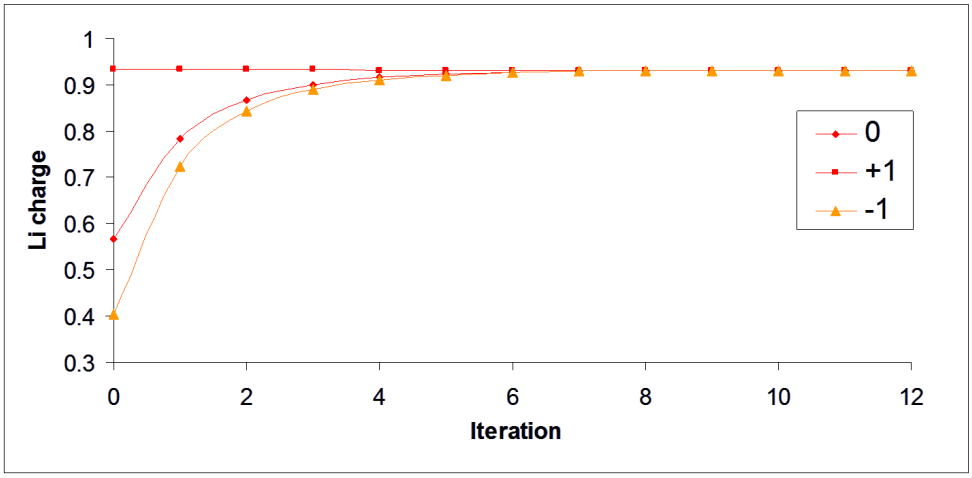

Figure 3.4: The convergence of the charges of LiF, starting from the three possible combinations to construct the promolecule within the classical Hirshfeld method, Li^0-F^0, Li^+-F^- and Li^--F^+.

where $\lfloor N_A \rfloor$ and $\lceil N_A \rceil$ are the lower and upper integer number of the (fractional) N_A.

Using the Iterative Hirshfeld method, the final atomic charges tend to be much larger than in the classical Hirshfeld method[72,74] Secondly, the Hirshfeld-I scheme makes it possible to calculate the population of charged molecules without using promolecular densities that normalise differently from the molecular density. Finally, the Hirshfeld-I scheme strictly adheres to information theory. Also, the basis set dependence has been shown to be very small compared to the classical Hirshfeld method and other atom partitioning methods[72]. When looking at the example of LiF, the Hirshfeld-I procedure yields AIM charges of ± 0.93, which agrees well with the presence of an ionic bond. Figure 3.4 shows how the charges for this molecule, starting from the three possible combinations to construct the promolecule within the classical Hirshfeld method, Li^0-F^0, Li^+-F^- and Li^--F^+, all converge to the same charge within the Iterative Hirshfeld method. This convergence to a single number always takes place, independent of the starting promolecule chosen. The self-consistent Hirshfeld charges are thus independent of the starting promolecule for the iterative process. This important property of the Hirshfeld-I scheme was demonstrated theoretically by Bultinck et al.[72,84].

Introducing self-consistency in the Hirshfeld-I scheme removes most of the arbitrariness in choosing a promolecule. Still, one arbitrary decision remains. Namely the states of the isolated atoms used in constructing the promolecule are chosen arbi-

trarily as the ground state.

3.6.4 Quantum Chemical Topology Analysis

Quantum Chemical Topology Analysis, originally called the "Atoms in Molecules" method[85–87], as developed by the Bader group is based on the topology of the electron density $\rho(\boldsymbol{r})$ and that of the gradient of $\rho(\boldsymbol{r})$. The attractive forces of the nuclei on the electrons create the above mentioned maxima in the electron density at the position of these nuclei ($\boldsymbol{R}_A$)(see 3.5.1). The electron density in the peak around the nucleus can be associated with the central nucleus, and the nucleus with its surrounding electron density constitute the atom in the molecule. The boundaries between the atoms in the molecules can then be determined by the gradient of the electron density. The gradient of a scalar function such as $\rho(\boldsymbol{r})$ at a point in space is a vector pointing in the direction in which the scalar function shows the largest increase:

$$\nabla\rho(\boldsymbol{r}) = \frac{\partial\rho(\boldsymbol{r})}{\partial x}\boldsymbol{i} + \frac{\partial\rho(\boldsymbol{r})}{\partial y}\boldsymbol{j} + \frac{\partial\rho(\boldsymbol{r})}{\partial z}\boldsymbol{k} \tag{3.88}$$

with $\boldsymbol{i}$, $\boldsymbol{j}$ and $\boldsymbol{k}$ the orthogonal unit vectors.

This gradient can be calculated for each point in space, leading to the gradient vector field of the electron density. To associate a point in space with a certain atom, one starts by calculating the gradient at this point and by taking an infinitesimal step in this direction. At this point the gradient can be recalculated to obtain the new direction, in which an other infinitesimal step can be taken. Repeating this method will lead to a trajectory which terminates at a point where the density is at maximum, which (usually) is a nucleus. Within Quantum Chemical Topology Analysis all points along this gradient vector field line belong to the atomic basin of the central nucleus. All points in space which can be connected by a gradient vector field line to a given nucleus form an atomic basin. These basins are mutually exclusive and thus partition the three dimensional space into non-overlapping domains.

The surface bounding an atom in a molecule is one through which there is no flux in the gradient vector field ,$\nabla\rho(\boldsymbol{r})$, called a "zero flux surface". At a point on this surface the gradient of the electron density has no component normal to the surface, meaning that the surface is not crossed by any trajectories of $\nabla\rho(\boldsymbol{r})$:

$$\nabla\rho(\boldsymbol{r}_s)\cdot\boldsymbol{n}(\boldsymbol{r}_s) = 0 \tag{3.89}$$

where $\boldsymbol{n}(\boldsymbol{r}_s)$ is the unit vector normal to the surface at $(\boldsymbol{r}_s)$.

Special points of interest within the molecule are those where the gradient of the electron density vanishes:

$$\nabla\rho(\boldsymbol{r}) = \frac{\partial\rho(\boldsymbol{r})}{\partial x}\boldsymbol{i} + \frac{\partial\rho(\boldsymbol{r})}{\partial y}\boldsymbol{j} + \frac{\partial\rho(\boldsymbol{r})}{\partial z}\boldsymbol{k} = \boldsymbol{0} \tag{3.90}$$

these points are called "critical points" (CP, $\boldsymbol{r}_c$). The maximum at the position of a nucleus is considered as one type of CP, namely, a nuclear critical point. Because of the cusp at the nucleus, the derivative at the nucleus is discontinuous at this point and thus the derivative of the electron density at the position of a nucleus itself is not defined. To distinguish between the local maxima, minima and saddle points in the electron density, the second derivatives of the electron density, namely the elements of the tensor $\nabla\nabla\rho(\boldsymbol{r}_c)$, also known as the "Hessian matrix", are evaluated at the critical point:

$$\nabla\nabla\rho(\boldsymbol{r}_c) = \boldsymbol{A}(\boldsymbol{r}_c) = \begin{pmatrix} \frac{\partial^2\rho(\boldsymbol{r}_c)}{\partial x^2} & \frac{\partial^2\rho(\boldsymbol{r}_c)}{\partial x\partial y} & \frac{\partial^2\rho(\boldsymbol{r}_c)}{\partial x\partial z} \\ \frac{\partial^2\rho(\boldsymbol{r}_c)}{\partial y\partial x} & \frac{\partial^2\rho(\boldsymbol{r}_c)}{\partial y^2} & \frac{\partial^2\rho(\boldsymbol{r}_c)}{\partial y\partial z} \\ \frac{\partial^2\rho(\boldsymbol{r}_c)}{\partial z\partial x} & \frac{\partial^2\rho(\boldsymbol{r}_c)}{\partial z\partial y} & \frac{\partial^2\rho(\boldsymbol{r}_c)}{\partial z^2} \end{pmatrix} \tag{3.91}$$

This Hessian matrix is real and symmetric, so it can be diagonalised using a unitary transformation $\boldsymbol{U}^{-1}\boldsymbol{A}\boldsymbol{U} = \boldsymbol{A}'$. This diagonalisation is equivalent to a rotation of the coordinate system $\boldsymbol{r}(x, y, z) \rightarrow \boldsymbol{r}'(x', y', z')$ (where $\boldsymbol{r}' = \boldsymbol{r}\boldsymbol{U}$) with the "new" axes x', y' and z' aligned with the principal curvature axes of the critical point. The unitary matrix $\boldsymbol{U}$ is constructed from a set of three eigenvalue equations $\boldsymbol{A}\boldsymbol{u}_i = \lambda_i\boldsymbol{u}_i$ (i = 1,2,3) in which $\boldsymbol{u}_i$ is the ith column vector (eigenvector) of $\boldsymbol{U}$. The "new" Hessian matrix $\boldsymbol{A}'$ has the form:

$$\boldsymbol{A}'(\boldsymbol{r}_c) = \begin{pmatrix} \frac{\partial^2\rho(\boldsymbol{r}_c)}{\partial x'^2} & 0 & 0 \\ 0 & \frac{\partial^2\rho(\boldsymbol{r}_c)}{\partial y'^2} & 0 \\ 0 & 0 & \frac{\partial^2\rho(\boldsymbol{r}_c)}{\partial z'^2} \end{pmatrix} = \begin{pmatrix} \lambda_1 & 0 & 0 \\ 0 & \lambda_2 & 0 \\ 0 & 0 & \lambda_3 \end{pmatrix} \tag{3.92}$$

Critical points are classified according to their rank and signature and the nature of the critical point can be denoted as (rank, signature). The rank is the number of non-zero eigenvalues and the signature is the sum of the signs of the Hessian eigenvalues. For example, a maximum in $\rho(\boldsymbol{r}_c)$ has three negative eigenvalues, and hence its signature is $-3 = (-1) + (-1) + (-1)$. The rank is usually 3, which gives rise to four possible signatures, namely:

- (3,-3), a maximum, which can be at the nucleus (*vide supra*), a nuclear critical

point or in rare cases this point will not coincide with a nucleus, this point is then a so-called non-nuclear attractor.

- (3,-1), a saddle point called a bond critical point. This point will always be on the zero flux surface between the atoms involved in the bond.
- (3,1), a saddle point called a ring critical point.
- (3,3), a minimum called a cage critical point.

Chapter 4

Delocalisation Indices

From Hückel-theory it is known that the π-electrons of Polycyclic Aromatic Hydrocarbons are delocalised over the entire molecule. Electron delocalisation is thus intimately connected with the concept of aromaticity. The problem with the quantification of the delocalisation of the electrons in a molecule is in many respects the same as with the quantification of aromaticity itself: "delocalisation" is not directly measurable and there is no single definition for this concept throughout chemistry. The use of delocalisation as a measure of aromaticity thus seems evident, but the problem of ambiguity will remain.

4.1 Delocalisation and the Fermi Hole

As has been mentioned above, the indistinguishability of the electrons demands that the wave function for a many-electron system must be antisymmetric. The result of this antisymmetry is that two electrons with the same spin can not occupy the same point in space. This property can easily been seen in the pair density, since $\rho_2(\boldsymbol{x}_1, \boldsymbol{x}_1) = 0$ (*vide supra*, 3.5.2). As has been shown, the difference between the pair density and the uncorrelated situation can be described by the pair correlation function and the related exchange correlation hole, which in Hartree-Fock is identical to the Fermi hole. The Fermi hole thus describes the manner in which the charge of the reference electron is spread out in space, thereby excluding an identical amount of same-spin density around it. As mentioned above the Fermi hole is usually localised around the reference electron, but when the reference electron is delocalised within the molecule, the Fermi Hole will be too. This means that the extent of localisation or

delocalisation of the density of the electron can be determined by the extent to which the corresponding Fermi hole is spread out within the molecule[88]. From equations 3.70 and 3.72 it follows that the exchange correlation hole, which is the same as the Fermi hole within the Hartree-Fock treatment, can be written as:

$$h(\boldsymbol{x}_1, \boldsymbol{x}_2) = \frac{\rho_2(\boldsymbol{x}_1, \boldsymbol{x}_2)}{\rho(\boldsymbol{x}_1)} - \rho(\boldsymbol{x}_2) \tag{4.1}$$

(where $\boldsymbol{x}_1$ are the coordinates of the reference electron) Or, using closed-shell Hartree-Fock theory, as:

$$h(\boldsymbol{r}_1, \boldsymbol{r}_2) = 2\sum_{i}^{N/2}\sum_{j}^{N/2} \left\{\phi_i^*(\boldsymbol{r}_1)\phi_i(\boldsymbol{r}_2)\phi_j^*(\boldsymbol{r}_2)\phi_j(\boldsymbol{r}_1)\right\} / \rho(\boldsymbol{r}_1) \tag{4.2}$$

Plotting the Fermi hole with a fixed position for the reference electron shows how the density for an electron with coordinate $\boldsymbol{r}_1$ is spread over space and whether it is localised or delocalised within the molecule. Such plots, for the Fermi hole of the π-electrons in benzene at a hight of 0.5 au above the molecular plane are shown in Figures 4.1(a) and 4.1(b). The reference electron is positioned in this plane, directly above the middle of a C-C bond in Figure 4.1(a) and directly above a carbon atom in Figure 4.1(b). Figures 4.1(c) and 4.1(d) show the same Fermi holes for benzene distorted into a Kekulé-like structure with alternating C-C bond lengths. These figures clearly show how the Fermi hole is more localised in the distorted benzene. Notice that the Fermi hole at the "para" position of the reference electron becomes smaller and that the Fermi hole surrounding the reference electron in Figure 4.1(d) is distorted towards the shortened bond, in agreement with the picture of alternating single and double bonds. Figure 4.1(b) also shows how the π-electrons on a carbon atom of benzene are preferentially delocalised onto the para as opposed to a meta carbon atom.

4.2 Domain-average Fermi Hole (DAFH) Analysis

The extent to which an electron is delocalised in a molecule can thus be visualised using the Fermi hole. Although this method works well, as has been shown above, the shape of the Fermi hole depends largely on the choice of the position of the reference electron. To understand fully the delocalisation of the electrons, a large set of Fermi holes with different positions of the reference electron have to be studied, making the method quite inelegant. Furthermore, fixing the position of the reference electron to a single point in space is not compatible with the quantum mechanical

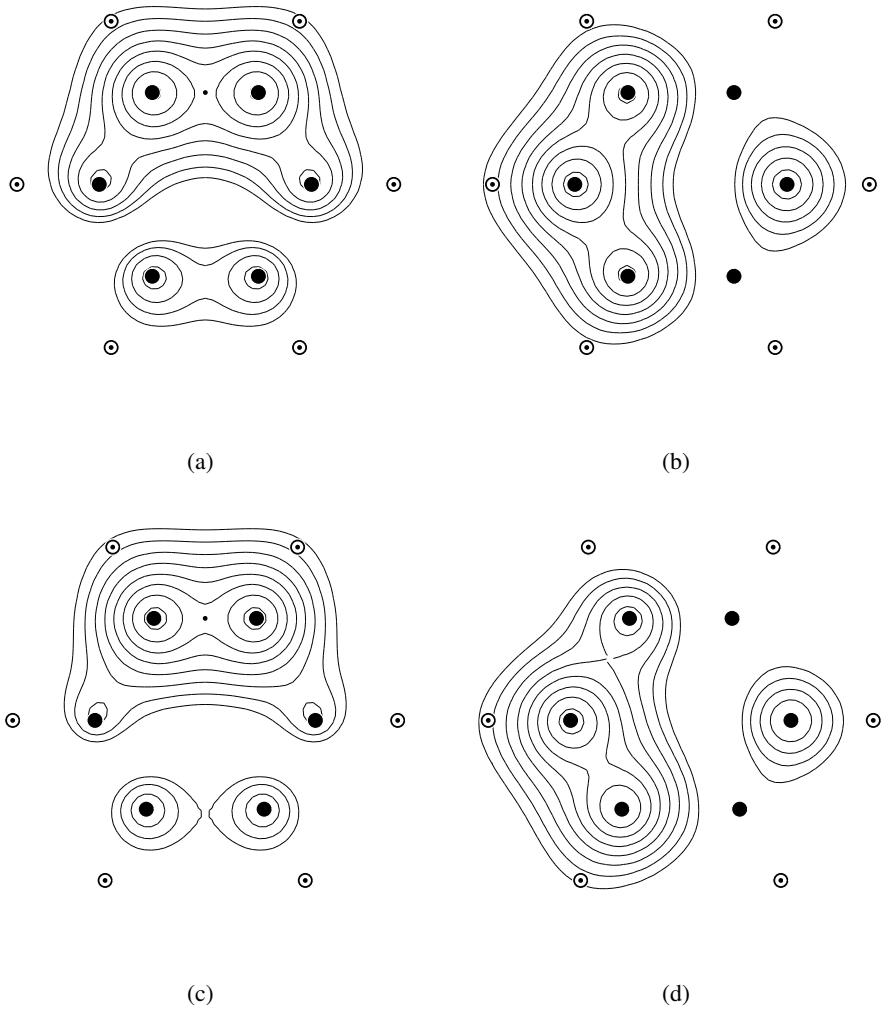

Figure 4.1: Contour maps of the π-electron Fermi hole for the equilibrium geometry of benzene (a,b) and for a distorted geometry with alternating C-C bond lengths of 1.34 and 1.54 Å(c,d), 0.5 au above the molecular plane (where the π density of benzene attains its maximum value). The position of the reference electron is denoted by a dot. (calculated at HF/6-311++G**)

uncertainty principle. Much more sound and realistic would be to allow the position of the reference electron to vary within a certain region Ω of the molecule. Choosing this region as one associated with an individual atom by one of the population analysis methods seems to allow a chemical interpretation of the Fermi hole. In addition to restricting the position of the reference electron into a single atomic region, it might also be useful to investigate the Fermi holes for which Ω is chosen as two neighbouring atomic regions or as some functional group. Ponec[89–91] has shown that the Fermi hole associated with the atomic region of a single atom or a functional group provides valuable information about the valence state of that atom or group in a molecule. This information is not, however, shown by the Fermi hole itself, but was found by introducing the so-called "charge-weighted" Fermi hole, $g_\Omega(\boldsymbol{r}_1)$, obtained by integrating the negative of the product of the Fermi Hole with the electron density over a domain Ω:

$$g_\Omega(\boldsymbol{r}_1) = -\int w_\Omega(\boldsymbol{r}_2) h(\boldsymbol{r}_1, \boldsymbol{r}_2) \rho(\boldsymbol{r}_1) d\boldsymbol{r}_2 \tag{4.3}$$

This "integrated" Fermi hole satisfies the following normalisation:

$$\int g_\Omega(\boldsymbol{r}_1) d\boldsymbol{r}_1 = N_\Omega \tag{4.4}$$

where N_Ω is the number of electrons in the region Ω ($N_\Omega = \int w_\Omega(\boldsymbol{r}_1)\rho(\boldsymbol{r}_1)d\boldsymbol{r}_1$). This is the reason why this is called the "charge-weighted" Fermi hole.

$g_\Omega(\boldsymbol{r}_1)$ has been given the name of domain averaged Fermi hole (DAFH), although in the general definition of equation 4.3, the term domain averaged correlation hole might be more appropriate. This quantity was proposed and first used for a wide range of molecules by Ponec[89–91].

In general, the DAFH, $g_\Omega(\boldsymbol{r}_1)$, is the diagonal element of a DAFH-matrix $g_\Omega(\boldsymbol{r}_1; \boldsymbol{r}'_1)$[92]:

$$g_\Omega(\boldsymbol{r}_1; \boldsymbol{r}'_1) = \int_{\boldsymbol{r}_2 = \boldsymbol{r}'_2} w_\Omega(\boldsymbol{r}_2) \left(\rho(\boldsymbol{r}_1, \boldsymbol{r}'_1)\rho(\boldsymbol{r}_2, \boldsymbol{r}'_2) - \gamma_2(\boldsymbol{r}_1, \boldsymbol{r}_2; \boldsymbol{r}'_1, \boldsymbol{r}'_2) \right) d\boldsymbol{r}_2 \tag{4.5}$$

which can be expressed in terms of a basis with functions ξ_i (which might be natural orbitals):

$$\begin{aligned} g_\Omega(\boldsymbol{r}_1; \boldsymbol{r}'_1) &= N_\Omega \sum_i \eta_i \xi_i^*(\boldsymbol{r}_1)\xi_i(\boldsymbol{r}'_1) - \sum_{ijkl} \Gamma^{(2)}_{ijkl} \xi_i^*(\boldsymbol{r}_1)\xi_k(\boldsymbol{r}'_1) S^\Omega_{jl} \\ &= \sum_{ij} \xi_i^*(\boldsymbol{r}_1) \left[N_\Omega \eta_i \delta_{ik} - \sum_{kl} \Gamma^{(2)}_{ijkl} S^\Omega_{jl} \right] \xi_k(\boldsymbol{r}'_1) \end{aligned} \tag{4.6}$$

where η_i is the occupation number of function ξ_i (which might be non-integer when natural orbitals are used as a basis), $\Gamma^{(2)}_{ijkl}$ is the two electron or second order density matrix (*vide supra*, 3.65) and S^{Ω}_{jl} is the Atomic Overlap Matrix ($S^{\Omega}_{jl} = \int_{\boldsymbol{r}_2=\boldsymbol{r}'_2} w_{\Omega}(\boldsymbol{r}_2)\xi_j(\boldsymbol{r}_2)\xi_l(\boldsymbol{r}_2)d\boldsymbol{r}_2$)

The term between square brackets can be diagonalised such that a set of "domain averaged Fermi hole orbitals" ϑ_i can be obtained:

$$g_{\Omega}(\boldsymbol{r}_1;\boldsymbol{r}'_1) = \sum_i \epsilon_i \vartheta^*_i(\boldsymbol{r}_1)\vartheta_i(\boldsymbol{r}'_1) \tag{4.7}$$

The domain averaged Fermi hole is then obtained by setting $\boldsymbol{r}_1 = \boldsymbol{r}'_1$ in equation 4.7:

$$g_{\Omega}(\boldsymbol{r}_1) = \sum_i \epsilon_i \vartheta^*_i(\boldsymbol{r}_1)\vartheta_i(\boldsymbol{r}_1) \tag{4.8}$$

These functions are then localised using the isopycnic[1] localisation by Cioslowski[93] and can be plotted for any choice of reference domain. The most common choice is to select a domain that corresponds to an atom or a group of atoms. As can be seen in equation 4.6 the calculation of the DAFH requires the so-called atomic overlap matrices S^{Ω}_{kl} for each atom A considered. When working at the Hartree-Fock level of theory where the Löwdin expansion[61] can be used to obtain the second order density from the first order density matrix (Equation 3.68), the DAFH analysis becomes particularly simple (see equation 4.2):

$$\begin{aligned} g_{\Omega}(\boldsymbol{r}_2) &= 2\int \sum_i^{N/2}\sum_j^{N/2} w_{\Omega}(\boldsymbol{r}_1)\left\{\phi^*_i(\boldsymbol{r}_1)\phi_i(\boldsymbol{r}_2)\phi^*_j(\boldsymbol{r}_2)\phi_j(\boldsymbol{r}_1)\right\} d\boldsymbol{r}_1 \\ &= 2\sum_i^{N/2}\sum_j^{N/2} \phi_i(\boldsymbol{r}_2)\phi^*_j(\boldsymbol{r}_2)S^{\Omega}_{ij} \end{aligned} \tag{4.9}$$

where S^{Ω}_{ij} is again the Atomic Overlap Matrix ($S^{\Omega}_{ij} = \int w_{\Omega}(\boldsymbol{r}_1)\phi^*_i(\boldsymbol{r}_1)\phi_j(\boldsymbol{r}_1)d\boldsymbol{r}_1$) Note also that when the entire molecule is considered as a single domain, DAFH eigenvectors are nothing but the localised molecular orbitals themselves.

Domain averaged Fermi hole analysis to large extent reduces to visual inspection of the ϑ_i and evaluation of the numbers ϵ_i. Having chosen a certain domain, the ϑ_i can be contained largely inside this domain. This then corresponds to a core orbital, a lone pair or a chemical bond inside the domain. More interestingly, the ϑ_i can be concentrated outside the domain extending to some other atom, indicating

[1] isopycnic= 'equal density', leaving the total density invariant

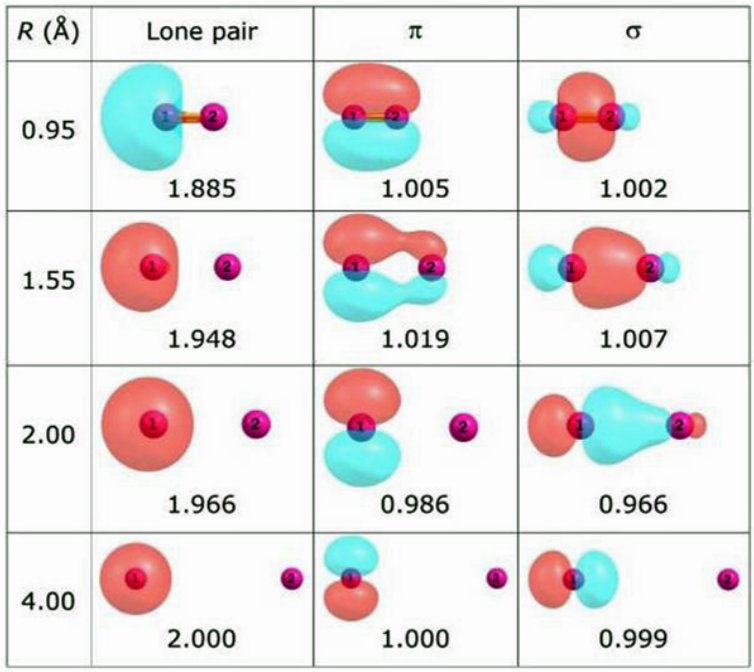

Figure 4.2: N_2 dissociation: Hirshfeld-I DAFH eigenvalues and eigenvectors over the domain of atom N_1 as a function of internuclear distance R. Figure from Bultinck *et al.* [92]

a chemical bond. A delocalised bond is easily recognised realising that the Fermi hole will extend to a set of atoms instead of to only one. The occupation number ϵ_i also reveals interesting information. When one considers splitting the molecule into a set of domains (*e.g.* N separate atomic domains for an N atomic molecule), one can visually inspect the complementary Fermi hole domains and check whether the occupation numbers sum to two in case of a suspected 2-centre 2-electron bond. For a delocalised bond, such as the 4-centre 2-electron bonds, for each of the 4 atomic domains, one expects to find an equivalent kind of Fermi hole with occupation numbers of roughly 0.5 for each domain.

As an example, the DAFH analysis of the N_2 molecule at different interatomic distances is given in Figure 4.2. The atomic overlap matrix, S_{kl}^{Ω}, was constructed using the iterative Hirshfeld method[92]. The calculations were done at full-valence CASSCF with the Cartesian cc-pvdz basis set. The DAFH analysis shows four dominant eigenvectors whose values remain more or less constant with increasing internuclear distance. One of the eigenvalues is close to two and inspection of the associated eigenvector in Figure 4.2 shows that it corresponds to a lone pair on N. The

remaining three eigenvalues remain close to one. The visual inspection of the eigenvectors shows that these are one σ and two π bonds of the NN triple bond at small interatomic distances and their associated free valences at large distances, when the bonds are broken. The figure clearly shows how the π bonds are the first to break, while the stronger σ bond only breaks at a higher interatomic distance

4.3 Two Center Delocalisation Index

The visual inspection of the DAFH is both its strength and its weakness. The visual inspection can show the Lewis-structure of the molecule and its delocalised bonds, such as 4-centre 2-electron bonds, in a clear way. However, comparison of bond strengths and the extend of delocalisation between two bonds or molecules is not always easy. Small changes in the DAFH are not always clearly noticeable. For these comparisons, single values for the bond strength or delocalisation are easier to compare. A single value can be obtaind by integrating the DAFH further over a second domain Ω'. With this value it is possible to determine the extent to which the electrons in a region Ω are delocalised into this another region Ω':

$$k_{\Omega\Omega'} = \int w_{\Omega'}(\boldsymbol{r}_1) g_{\Omega}(\boldsymbol{r}_1) d\boldsymbol{r}_1 \tag{4.10}$$

From equation 4.6 it is clear that this value may be written as:

$$\begin{aligned} k_{\Omega\Omega'} &= N_{\Omega} \sum_i \eta_i S_{ii}^{\Omega'} - \sum_{ijkl} \Gamma^{(2)}_{ijkl} S_{ik}^{\Omega'} S_{jl}^{\Omega} \\ &= N_{\Omega} N_{\Omega'} - \sum_{ijkl} \Gamma^{(2)}_{ijkl} S_{ik}^{\Omega'} S_{jl}^{\Omega} \end{aligned} \tag{4.11}$$

The sum of k_{AB} and k_{BA}, where A and B are atomic domains, gives a bond index called the Shared-Electron Distribution Index (SEDI), Δ_{AB}. This index is sometimes also called the bond order or the (two-centre) Bond index:

$$\Delta_{AB} = k_{AB} + k_{BA} \tag{4.12}$$

The SEDI is the generalization of the Wiberg-Giambiagi-Mayer index [94–96] to the case of three-dimensional partitioning of the molecular density function into atomic domains.

4.4 The Multi Center Bond Index (MCBI)

The "charge-weighted" exchange correlation hole $\rho_X(\boldsymbol{r}_1, \boldsymbol{r}_2)$, used to introduce the DAFH above can be written as:

$$\rho_X(\boldsymbol{r}_1, \boldsymbol{r}_2) = -h(\boldsymbol{r}_1, \boldsymbol{r}_2)\rho(\boldsymbol{r}_1) = 2\sum_{i}^{N/2}\sum_{j}^{N/2} \phi_i^*(\boldsymbol{r}_1)\phi_i(\boldsymbol{r}_2)\phi_j^*(\boldsymbol{r}_2)\phi_j(\boldsymbol{r}_1) \quad (4.13)$$

As a generalisation to this "charge-weighted" 2-electron exchange correlation function any n-electron exchange function (n-EEF) can be defined. For example the 6-electron exchange function (6-EEF) can be defined as:[97]

$$\text{6-EEF}(\boldsymbol{r}_1, \boldsymbol{r}_2, \ldots, \boldsymbol{r}_6) = 2\sum_{i_1}^{N/2}\sum_{i_2}^{N/2}\cdots\sum_{i_6}^{N/2}\prod_{n=1}^{6} \phi_{i_n}(\boldsymbol{r}_n)\phi_{i_{n-1}}^*(\boldsymbol{r}_n) \quad (4.14)$$

where i_0 should be taken as i_6 and $\boldsymbol{r}_0$ as $\boldsymbol{r}_6$. This 6-EEF has successfully been used to evaluate the aromaticity in Polycyclic Aromatic Hydrocarbons by fixing the $\boldsymbol{r}_n$ at the location above the six nuclei where the π electron density reaches its maximum.[97] As the definition implies, the 6-EEF depends on 18 Cartesian coordinates, making it hard to find the maximum of the function for aromatic systems with hetero-atoms, since it will present a global maximum along with several local maxima. This is why the 6-EEF will be integrated over the atomic domains of the six atoms studied. This integration yields the Six Centre Index. It must be noticed that apart from integrating equation 4.14, all possible sequences of integrating $\boldsymbol{r}_1$ to $\boldsymbol{r}_6$ must be taken, including those different to the bonding sequence of the molecule (this is why there are 6! permutations in the definition:[18,19,21,98]

$$\text{SCI}_{AB\ldots F} = \sum_{j}^{N_\alpha}\sum_{k}^{N_\alpha}\cdots\sum_{o}^{N_\alpha}\sum_{i}^{6!} \hat{\mathscr{P}}_i \left[S_{jk}^A S_{kl}^B \ldots S_{oj}^F\right]_\alpha \quad (4.15)$$

$$+ \sum_{j}^{N_\beta}\sum_{k}^{N_\beta}\cdots\sum_{o}^{N_\beta}\sum_{i}^{6!} \hat{\mathscr{P}}_i \left[S_{jk}^A S_{kl}^B \ldots S_{oj}^F\right]_\beta \quad (4.16)$$

The labels A-F refer to the atoms contained in the ring considered and j to o refer to occupied Molecular Orbitals. $\hat{\mathscr{P}}_i$ is a permutation operator that generates 6! terms by interchanging labels j to o . The overlap-matrices S_{jk}^{Ω} can be those of any atom partitioning method desired. In the case of the Mulliken atom partitioning (closed shell), by which the Six Centre Index was originally defined, the SCI can be written as:

$$\mathrm{SCI} = \frac{6}{2^5} \sum_{\nu \in A}^{K} \sum_{\mu \in B}^{K} \cdots \sum_{\xi \in F}^{K} \sum_{i}^{5!} \hat{\mathscr{P}}_i \left[(\mathbf{PS})_{\nu\mu} (\mathbf{PS})_{\mu\lambda} \ldots (\mathbf{PS})_{\psi\xi} (\mathbf{PS})_{\xi\nu} \right] \tag{4.17}$$

Here **P** is the charge and bond order density matrix and **S** is the overlap matrix of the basis functions. The Greek symbols refer to the basis functions, and $\hat{\mathscr{P}}_i$ is a permutation operator that generates 5! terms by interchanging the Greek basis function labels μ to ξ.

Not all aromatic molecules have six-membered rings. Therefore equation 4.15 can be generalised to any number of aroms in a ring, leading to the Multi Centre Bond Indices (MCBI) (also called Multi Centre Delocalisation Index (MCDI) or Multi Centre Index (MCI)):

$$\mathrm{MCBI}_{ABC\ldots K} = \sum_{j}^{N_\alpha} \sum_{k}^{N_\alpha} \sum_{l}^{N_\alpha} \cdots \sum_{o}^{N_\alpha} \sum_{i}^{K!} \hat{\mathscr{P}}_i \left[S^A_{jk} S^B_{kl} S^C_{lm} \ldots S^K_{oj} \right]_\alpha \tag{4.18}$$

$$+ \sum_{j}^{N_\beta} \sum_{k}^{N_\beta} \sum_{l}^{N_\beta} \cdots \sum_{o}^{N_\beta} \sum_{i}^{K!} \hat{\mathscr{P}}_i \left[S^A_{jk} S^B_{kl} S^C_{lm} \ldots S^K_{oj} \right]_\beta \tag{4.19}$$

The MCBI is an extension of the so-called Generalised Population Analysis (GPA).[99–101] The MCBI can be split into orbital contributions[102], for which the closed shell expression becomes:

$$\text{MO-MCBI}_{ABC\ldots K;i} = \sum_{k}^{N/2} \sum_{l}^{N/2} \cdots \sum_{o}^{N/2} \sum_{i}^{(K-1)!} \hat{\mathscr{P}}_i \left[S^A_{jk} S^B_{kl} S^C_{lm} \ldots S^K_{oj} \right] \tag{4.20}$$

4.5 Delocalisation Indices as a Measure of Aromaticity

One of the key features of aromaticity is that there needs to be a delocalised electronic system[2]. Many approaches on ways to measure this extent of electron delocalisation have been published. Among these are those based on higher order density functions. In recent years, several such indices have been developed. Besides the MCBI mentioned above, the most notable are the PDI (Para delocalisation Index)[8,45] and the FLU (fluctuation) indices[8,46]. Both these are based on using only bond indices between two atoms at a time. In the PDI the average bond index between each two atoms in para position is used as an index. In the FLU index, only the bond indices of all couples of covalently bonded atoms is used. In all cases these bond

indices are essentially based on the Wiberg-Giambiagi-Mayer scheme[94–96,103]. Although the Wiberg-Giambiagi-Mayer scheme was originally defined in the Mulliken AIM scheme, all indices can be extended to include other types of population analysis[19,98].

Chapter 5

Magnetic Indices

It is well known that aromatic molecules exhibit strong diamagnetic ring currents induced by an external magnetic field. This property has led to the use of the current density induced by a magnetic field as a measure of aromaticity. In this chapter, first the general expression for the current density is introduced (5.2) and using a suitable vector potential (5.1.1) and perturbation theory (5.1.2), the first-order current density in the presence of a magnetic field can be calculated (5.2.1).

5.1 The Molecule in a Magnetic Field

5.1.1 The Vector Potential

The magnetic flux density can be written in terms of a vector potential, $\boldsymbol{A}$, as (see equation A.9 in Appendix A):

$$\boldsymbol{B} = \nabla \times \boldsymbol{A} \tag{5.1}$$

For the applications in this work, $\boldsymbol{B}$ will be considered uniform, independent of time and along the $\boldsymbol{k}$ (or $\boldsymbol{z}$) axis. Using the Coulomb gauge, the vector potential $\boldsymbol{A}$, can be written as (see equation A.2 in Appendix A):

$$\boldsymbol{A} = \frac{1}{2}\mathscr{B}\boldsymbol{C} = \frac{1}{2}\mathscr{B}(-y\boldsymbol{i} + x\boldsymbol{j}) \tag{5.2}$$

so that

$$\boldsymbol{B} = \frac{1}{2}\mathscr{B}\nabla \times \boldsymbol{C} = \mathscr{B}\boldsymbol{k} \tag{5.3}$$

This corresponds to the description of a uniform magnetic field of induction $\mathscr{B}$ in the $\hat{\boldsymbol{k}}$-direction. Equation 5.2 can also be written as:

$$\boldsymbol{A} = \frac{1}{2}\boldsymbol{B} \times \boldsymbol{r} \tag{5.4}$$

It is easy to show that it is always possible to add a vector function of the form $\nabla\xi$, where ξ is a scalar function, to the vector potential without changing the magnetic field, since $\nabla \times \nabla\xi = 0$. This property is known as the gauge invariance (*vide infra*).

5.1.2 The Perturbation Hamiltonian

As shown in Appendix A, the Hamiltonian in the presence of a magnetic field is (equation A.18):

$$\hat{\mathscr{H}} = \frac{1}{2m_e}\sum_{j}^{N}\left(\hat{\boldsymbol{p}}_j + \frac{e}{c}\hat{\boldsymbol{A}}_j\right)^2 + \hat{V} \tag{5.5}$$

with $\boldsymbol{A}_j$ as

$$\boldsymbol{A}_j = \frac{1}{2}\boldsymbol{B} \times \boldsymbol{r}_j \tag{5.6}$$

and where $\hat{\boldsymbol{p}}_j = -i\hbar\nabla_j$. In this equation, $(\hat{\boldsymbol{p}}_j + \frac{e}{c}\hat{\boldsymbol{A}}_j)^2$ can be expanded as:

$$\left(\hat{\boldsymbol{p}}_j + \frac{e}{c}\hat{\boldsymbol{A}}_j\right)\left(\hat{\boldsymbol{p}}_j + \frac{e}{c}\hat{\boldsymbol{A}}_j\right) = \hat{\boldsymbol{p}}_j^2 + \frac{e}{c}\left(\hat{\boldsymbol{p}}_j \cdot \hat{\boldsymbol{A}}_j + \hat{\boldsymbol{A}}_j \cdot \hat{\boldsymbol{p}}_j\right) + \frac{e^2}{c^2}\hat{\boldsymbol{A}}_j^2 \tag{5.7}$$

When the second term on the right hand side operates on a wave function the term becomes:

$$\begin{aligned}
\frac{e}{c}\left(\hat{\boldsymbol{p}}_j \cdot \hat{\boldsymbol{A}}_j + \hat{\boldsymbol{A}}_j \cdot \hat{\boldsymbol{p}}_j\right)\Psi &= \frac{e}{c}\hat{\boldsymbol{p}}_j \cdot \hat{\boldsymbol{A}}_j\Psi + \frac{e}{c}\hat{\boldsymbol{A}}_j \cdot \hat{\boldsymbol{p}}_j\Psi \\
&= \frac{e}{c}\left(\frac{\hbar}{i}\right)\nabla_j \cdot \hat{\boldsymbol{A}}_j\Psi + \frac{e}{c}\hat{\boldsymbol{A}}_j \cdot \hat{\boldsymbol{p}}_j\Psi \\
&= \frac{e}{c}\left(\frac{\hbar}{i}\right)\left\{(\nabla_j \cdot \hat{\boldsymbol{A}}_j)\Psi + \hat{\boldsymbol{A}}_j \cdot (\nabla_j\psi)\right\} + \frac{e}{c}\hat{\boldsymbol{A}}_j \cdot \hat{\boldsymbol{p}}_j\Psi \\
&= \frac{e}{c}\left(\frac{\hbar}{i}\right)(\nabla_j \cdot \hat{\boldsymbol{A}}_j)\Psi + \frac{e}{c}\hat{\boldsymbol{A}}_j \cdot \hat{\boldsymbol{p}}_j\psi + \frac{e}{c}\hat{\boldsymbol{A}}_j \cdot \hat{\boldsymbol{p}}_j\Psi
\end{aligned}$$

When using the Coulomb gauge (A.2 in Appendix A), $(\nabla_j \cdot \hat{\boldsymbol{A}}_j)$ is zero and 5.7 becomes:

$$\left(\hat{\boldsymbol{p}}_j + \frac{e}{c}\hat{\boldsymbol{A}}_j\right)\left(\hat{\boldsymbol{p}}_j + \frac{e}{c}\hat{\boldsymbol{A}}_j\right) = \hat{\boldsymbol{p}}_j^2 + \frac{2e}{c}\hat{\boldsymbol{A}}_j \cdot \hat{\boldsymbol{p}}_j + \frac{e^2}{c^2}\hat{\boldsymbol{A}}_j^2 \tag{5.8}$$

and the Hamiltonian thus becomes:

$$\hat{\mathscr{H}} = \frac{1}{2m_e}\sum_j^N \hat{\boldsymbol{p}}_j^2 + \hat{V} + \frac{e}{m_e c}\sum_j^N \hat{\boldsymbol{A}}_j \cdot \hat{\boldsymbol{p}}_j + \left(\frac{e^2}{2m_e c^2}\right)\sum_j^N \hat{\boldsymbol{A}}_j^2 \tag{5.9}$$

or in atomic units (and replacing $\hat{\boldsymbol{p}}_j^2$ with the more familiar $-\nabla_j^2$):

$$\hat{\mathscr{H}} = -\frac{1}{2}\sum_j^N \nabla_j^2 + \hat{V} + \frac{1}{c}\sum_j^N \hat{\boldsymbol{A}}_j \cdot \hat{\boldsymbol{p}}_j + \frac{1}{2c^2}\sum_j^N \hat{\boldsymbol{A}}_j^2 \tag{5.10}$$

The first two terms on the right hand side are the Hamiltonian as it would be without the presence of a magnetic field. The other two terms are the first and second order corrections to the Hamiltonian:

$$\hat{\mathscr{H}}^{(1)} = \frac{1}{c}\sum_j^N \hat{\boldsymbol{A}}_j \cdot \hat{\boldsymbol{p}}_j = \frac{1}{2c}\sum_j^N \hat{\boldsymbol{B}} \times \hat{\boldsymbol{r}}_j \cdot \hat{\boldsymbol{p}}_j = \frac{1}{2c}\sum_j^N \hat{\boldsymbol{B}} \cdot \hat{\boldsymbol{r}}_j \times \hat{\boldsymbol{p}}_j \tag{5.11}$$

$$\hat{\mathscr{H}}^{(2)} = \frac{1}{2c^2}\sum_j^N \hat{\boldsymbol{A}}_j^2 = \frac{1}{2c^2}\sum_j^N (\hat{\boldsymbol{B}} \times \hat{\boldsymbol{r}}_j)^2 = \frac{1}{8c^2}\sum_j^N \left\{\mathscr{B}^2 r^2 - (\hat{\boldsymbol{B}}.\hat{\boldsymbol{r}}_j)^2\right\} \tag{5.12}$$

where the vector identities $\boldsymbol{a}\times\boldsymbol{b}\cdot\boldsymbol{c} = \boldsymbol{a}\cdot\boldsymbol{b}\times\boldsymbol{c}$ and $(\boldsymbol{a}\times\boldsymbol{b})\cdot(\boldsymbol{a}\times\boldsymbol{b}) = a^2b^2 - (\boldsymbol{a}.\boldsymbol{b})^2$ are used

5.2 The Current Density

The total number of electrons of the isolated system remains constant regardless of changes within the system itself. This means that the change in electron density, ρ, within a volume element dV has to be equal to the area integral over the current density $\boldsymbol{J}$ through the surface $\boldsymbol{S}$ enclosing the volume element dV (where $\boldsymbol{S}$ is taken outwards).

$$-\frac{\partial}{\partial t}\iiint_{dV} \rho(\boldsymbol{r},t)d\boldsymbol{r} = \oiint_{dV} \boldsymbol{J}(\boldsymbol{r},t)\cdot d\boldsymbol{S} \tag{5.13}$$

Using the divergence theorem (or Gauss-Ostrogradsky theorem), this expression can be written as:

$$-\frac{\partial}{\partial t}\iiint_{dV} \rho(\boldsymbol{r},t)d\boldsymbol{r} = \iiint_{dV} \left(\nabla\cdot\boldsymbol{J}(\boldsymbol{r},t)\right)d\boldsymbol{r} \tag{5.14}$$

which gives the continuity equation (by taking an infinitesimally small dV):

$$\frac{\partial\rho(\boldsymbol{r},t)}{\partial t} = -\nabla\cdot\boldsymbol{J}(\boldsymbol{r},t) \tag{5.15}$$

The change of the electron density in time can also be written as:

$$\begin{aligned}\frac{\partial \rho(\boldsymbol{r},t)}{\partial t} &= \frac{\partial}{\partial t}\sum_i^N \int \Psi^* \delta(\boldsymbol{r}-\boldsymbol{r}_i)\Psi d\tau \\ &= \sum_i^N \int \left\{ \left(\frac{\partial}{\partial t}\Psi^*\right)\delta(\boldsymbol{r}-\boldsymbol{r}_i)\Psi + \Psi^*\delta(\boldsymbol{r}-\boldsymbol{r}_i)\left(\frac{\partial}{\partial t}\Psi\right)\right\} d\tau \\ &= N\int \left\{ \left(\frac{\partial}{\partial t}\Psi^*\right)\Psi + \Psi^*\left(\frac{\partial}{\partial t}\Psi\right)\right\} d\tau' \end{aligned} \tag{5.16}$$

where equation 3.57 has been used and where the integration over $d\tau'$ denotes the integration over all coordinates except the space coordinate $\boldsymbol{r}$ of one electron. Using the time-dependent Schrödinger equation,

$$i\frac{\partial}{\partial t}\Psi(\boldsymbol{r},t) = \hat{\mathscr{H}}\Psi(\boldsymbol{r},t) \tag{5.17}$$

and inserting equation 5.10, $\frac{\partial}{\partial t}\Psi$ can be written as:

$$\frac{\partial}{\partial t}\Psi = -\left[i\sum_j^N \left(-\frac{1}{2}\nabla_j^2 + \frac{1}{2c^2}\hat{\boldsymbol{A}}_j^2 - \frac{i}{c}\hat{\boldsymbol{A}}_j\cdot\nabla_j\right) + i\hat{V}\right]\Psi \tag{5.18}$$

inserting this in equation 5.16 gives:

$$\begin{aligned}\frac{\partial \rho(\boldsymbol{r},t)}{\partial t} =& N\sum_j^N \int \left\{ \left[i\left(-\frac{1}{2}\nabla_j^2 + \frac{1}{2c^2}\hat{\boldsymbol{A}}_j^2 + \frac{i}{c}\hat{\boldsymbol{A}}_j\cdot\nabla_j\right) - i\hat{V}\right]\Psi^*\Psi \right. \\ & \left. - \Psi^*\left[i\left(-\frac{1}{2}\nabla_j^2 + \frac{1}{2c^2}\hat{\boldsymbol{A}}_j^2 - \frac{i}{c}\hat{\boldsymbol{A}}_j\cdot\nabla_j\right) + i\hat{V}\right]\Psi\right\} d\tau' \qquad (5.19) \\ =& N\sum_j^N \left\{ \int \left[-\frac{i}{2}\Psi\nabla_j^2\Psi^* + \frac{i}{2}\Psi^*\nabla_j^2\Psi\right] d\tau' \right. \qquad \text{(a)} \\ & + \int \left[\frac{i}{2c^2}\Psi\left(\hat{\boldsymbol{A}}_j^2\Psi^*\right) - \frac{i}{2c^2}\Psi^*\left(\hat{\boldsymbol{A}}_j^2\Psi\right)\right] d\tau' \qquad \text{(b)} \\ & - \int \frac{1}{c}\left[\Psi\left(\hat{\boldsymbol{A}}_j\cdot\nabla_j\Psi^*\right) + \Psi^*\left(\hat{\boldsymbol{A}}_j\cdot\nabla_j\Psi\right)\right] d\tau' \qquad \text{(c)} \\ & \left. - \int \left[i\Psi\hat{V}\Psi^* - i\Psi^*\hat{V}\Psi\right] d\tau'\right\} \qquad \text{(d)} \end{aligned}$$

of which integrals (b) and (d) are zero. By writing

$$\sum_j^N \int -\frac{i}{2}\Psi\nabla_j^2\Psi^* d\tau = \sum_j^N \int -\frac{i}{2}\nabla_j \cdot (\Psi\nabla_j\Psi^*)\, d\tau' + \sum_j^N \int \frac{i}{2}\left\{\frac{\partial\Psi}{\partial x}\frac{\partial\Psi^*}{\partial x} + \frac{\partial\Psi}{\partial y}\frac{\partial\Psi^*}{\partial y} + \frac{\partial\Psi}{\partial z}\frac{\partial\Psi^*}{\partial z}\right\} d\tau' \quad (5.20)$$

and recognising that

$$\frac{1}{c}\sum_j^N \int \nabla_j \cdot \left(\Psi^*\hat{\boldsymbol{A}}_j\Psi\right) d\tau' = \frac{1}{c}\sum_j^N \int \left[\Psi\left(\hat{\boldsymbol{A}}_j \cdot \nabla_j\Psi^*\right) + \Psi^*\left(\hat{\boldsymbol{A}}_j \cdot \nabla_j\Psi\right)\right] d\tau' \quad (5.21)$$

expression 5.19 can then be rewritten as

$$\frac{\partial\rho(\boldsymbol{r},t)}{\partial t} = N\sum_j^N \int \nabla_j \cdot \left\{-\frac{i}{2}\left[\Psi\nabla_j\Psi^* - \Psi^*\nabla_j\Psi\right]\right\} d\tau' - \frac{N}{c}\sum_j^N \int \nabla_j \cdot \left(\Psi^*\hat{\boldsymbol{A}}_j\Psi\right) d\tau' \quad (5.22)$$

Comparing equations 5.15 and 5.22 leads to the following expression for $\boldsymbol{J}(\boldsymbol{r},t)$:

$$\begin{aligned}\boldsymbol{J}(\boldsymbol{r},t) &= N\sum_j^N -\frac{i}{2}\int (\Psi\nabla_j\Psi^* - \Psi^*\nabla_j\Psi)\, d\tau' - \frac{N}{c}\sum_j^N \hat{\boldsymbol{A}}_j \int (\Psi^*\Psi)\, d\tau' \\ &= \frac{N}{2i}\int (\Psi^*\nabla\Psi - \Psi\nabla\Psi^*)\, d\tau' - \frac{N}{c}\hat{\boldsymbol{A}}\int \Psi\Psi^* d\tau' \end{aligned} \quad (5.23)$$

or

$$\boldsymbol{J}(\boldsymbol{r},t) = -\frac{N}{2}\int \{\Psi^*\hat{\boldsymbol{p}}\Psi - \Psi\hat{\boldsymbol{p}}\Psi^*\}\, d\tau' - \frac{N}{c}\hat{\boldsymbol{A}}\int \Psi\Psi^* d\tau' \quad (5.24)$$

where the integration over $d\tau'$ denotes the integration over all coordinates except the space coordinates of one electron.

5.2.1 The First-order Current Density

When writing the wave function in terms of the unperturbed wave function (without the magnetic field) and the first-order correction, $\Psi = \Psi^{(0)} + \Psi^{(1)}$ and inserting this in equation 5.24 gives:

$$\boldsymbol{J}(\boldsymbol{r},t) = -\frac{N}{2}\int\left\{\Psi^{(0)*}\hat{\boldsymbol{p}}\Psi^{(0)} - \Psi^{(0)}\hat{\boldsymbol{p}}\Psi^{(0)*}\right\}d\tau' \quad \text{(a)}$$

$$-\frac{N}{2}\int\left\{\Psi^{(0)*}\hat{\boldsymbol{p}}\Psi^{(1)} - \Psi^{(0)}\hat{\boldsymbol{p}}\Psi^{(1)*} + \Psi^{(1)*}\hat{\boldsymbol{p}}\Psi^{(0)} - \Psi^{(1)}\hat{\boldsymbol{p}}\Psi^{(0)*}\right\}d\tau' \quad \text{(b)}$$

$$-\frac{N}{c}\hat{\boldsymbol{A}}\int\Psi^{(0)}\Psi^{(0)*}d\tau' \quad \text{(c)}$$

$$-\frac{N}{2}\int\left\{\Psi^{(1)*}\hat{\boldsymbol{p}}\Psi^{(1)} - \Psi^{(1)}\hat{\boldsymbol{p}}\Psi^{(1)*}\right\}d\tau' \quad \text{(d)}$$

$$-\frac{N}{c}\hat{\boldsymbol{A}}\int\Psi^{(1)}\Psi^{(0)*}d\tau' - \frac{N}{c}\hat{\boldsymbol{A}}\int\Psi^{(0)}\Psi^{(1)*}d\tau' \quad \text{(e)}$$

$$-\frac{N}{c}\hat{\boldsymbol{A}}\int\Psi^{(1)}\Psi^{(1)*}d\tau' \quad \text{(f)}$$

In the above equation line (a) is the current density without the presence of a magnetic field. When $\Psi^{(0)}$ is real (as is the case throughout this work) this term will be zero since $\Psi^{(0)*} = \Psi^{(0)}$. Lines (b) and (c) are the first order current density. Notice that line (c) is first order in $\boldsymbol{B}$ through $\hat{\boldsymbol{A}}$. Lines (d) and (e) are second order terms and (f) is third order. The first order current density, $\boldsymbol{J}^{(1)}(\boldsymbol{r},t)$, can thus be written as:

$$\boldsymbol{J}^{(1)}(\boldsymbol{r},t) = -\frac{N}{2}\int\left\{\Psi^{(0)*}\hat{\boldsymbol{p}}\Psi^{(1)} - \Psi^{(0)}\hat{\boldsymbol{p}}\Psi^{(1)*} + \Psi^{(1)*}\hat{\boldsymbol{p}}\Psi^{(0)} - \Psi^{(1)}\hat{\boldsymbol{p}}\Psi^{(0)*}\right\}d\tau' - \frac{1}{c}\hat{\boldsymbol{A}}\rho^{(0)}(\boldsymbol{r},t) \quad (5.25)$$

The first-order correction to the molecular wave function $\Psi^{(1)}$ due to the magnetic field perturbation is purely imaginary, leading to the expression for the first-order current density as:

$$\boldsymbol{J}^{(1)}(\boldsymbol{r},t) = -N\int\left\{\Psi^{(0)*}\hat{\boldsymbol{p}}\Psi^{(1)} + \Psi^{(1)*}\hat{\boldsymbol{p}}\Psi^{(0)}\right\}d\tau' - \frac{1}{c}\hat{\boldsymbol{A}}\rho^{(0)}(\boldsymbol{r},t) \quad (5.26)$$

Within the Hartree-Fock Approximation, and in a magnetic field which is independent of time, the first-order current density can be written as:

$$\boldsymbol{J}^{(1)}(\boldsymbol{r}) = -2\sum_{i=1}^{N/2}\left\{\phi_i^{(0)*}\hat{\boldsymbol{p}}\phi_i^{(1)} + \phi_i^{(1)*}\hat{\boldsymbol{p}}\phi_i^{(0)}\right\} - \frac{1}{c}\hat{\boldsymbol{A}}(\boldsymbol{r})\rho^{(0)}(\boldsymbol{r}) \quad (5.27)$$

The first term of this equation is normally called the 'paramagnetic' contribution, while the second is called the 'diamagnetic' contribution to the current density. The first-order corrections to the Molecular Orbitals, $\phi^{(1)}$, are expanded in the unperturbed virtual orbitals as (equation 3.48):

$$\phi_i^{(1)} = \sum_{p=N/2+1}^{K} C_{pi}^{(1)} \phi_p^{(0)} \tag{5.28}$$

where the expansion coefficients $C_{pi}^{(1)}$ are the solutions to the equations 3.56:

$$\left(\epsilon_p^{(0)} - \epsilon_i^{(0)}\right) C_{pi}^{(1)} + \langle \phi_p^{(0)} | \hat{\mathscr{H}}^{(1)} | \phi_i^{(0)} \rangle + \sum_{j=1}^{N/2} \sum_{q=N/2+1}^{K} \left\{ \left(\langle \phi_q^{(0)} \phi_p^{(0)} | g_{ij} | \phi_j^{(0)} \phi_i^{(0)} \rangle \right.\right. \\ \left.\left. - \langle \phi_p^{(0)} \phi_j^{(0)} | g_{ij} | \phi_q^{(0)} \phi_i^{(0)} \rangle \right) C_{qj}^{(1)} \right\} = 0 \tag{5.29}$$

where $\hat{\mathscr{H}}^{(1)}$ is given by equation 5.11:

$$\hat{\mathscr{H}}^{(1)} = \frac{1}{c} \sum_{j}^{N} \hat{\boldsymbol{A}}_j \cdot \hat{\boldsymbol{p}}_j = \frac{1}{2c} \sum_{j}^{N} \boldsymbol{B} \cdot [(\boldsymbol{r}_j - \boldsymbol{r}_0) \times \hat{\boldsymbol{p}}_j] = \frac{1}{2c} \sum_{j}^{N} \boldsymbol{B} \cdot \hat{\boldsymbol{L}}_j \tag{5.30}$$

where $\boldsymbol{r}_0$ is the origin or centre of the vector-potential (the gauge origin) and $\hat{\boldsymbol{L}}$ the angular momentum operator. As mentioned before, it is always possible to change the vector function $\hat{\boldsymbol{A}}_j$ to $\hat{\boldsymbol{A}}_j'$ without changing the magnetic field by adding the gradient of any scalar function ξ to $\hat{\boldsymbol{A}}_j$ (*vide supra*):

$$\hat{\boldsymbol{A}}_j' = \hat{\boldsymbol{A}}_j + \nabla \xi(\boldsymbol{r}_j) \tag{5.31}$$

For a given magnetic field $\boldsymbol{B}$, one is free to choose any gauge $\hat{\boldsymbol{A}}_j$ that correctly describes $\boldsymbol{B}$. A change of $\hat{\boldsymbol{A}}_j$ as in equation 5.31 is called a gauge transformation. Since properties as the current density and the related magnetic susceptibility and the nuclear shielding are determined by the magnetic field $\boldsymbol{B}$, they should only depend on this magnetic field and not on the particular gauge chosen to describe this magnetic field. The properties should thus be gauge invariant. An example of a gauge transformation as in equation 5.31 is a shift in the gauge origin $\boldsymbol{r}_0$ by a vector $\boldsymbol{d}$[37]. The scalar function, ξ, and the resulting vector function $\hat{\boldsymbol{A}}_j'$ are:

$$\xi = -\frac{1}{2}(\hat{\boldsymbol{B}} \times \boldsymbol{d}) \cdot \boldsymbol{r}_j \tag{5.32}$$

$$\hat{\boldsymbol{A}}'_j = \frac{1}{2}\hat{\boldsymbol{B}} \times (\boldsymbol{r}_j - \boldsymbol{r}_0 - \boldsymbol{d}) \tag{5.33}$$

Notice that the Coulomb gauge is only shifted by a constant ($-y\boldsymbol{i} + x\boldsymbol{j} \rightarrow -(y - y_d)\boldsymbol{i} + (x - x_d)\boldsymbol{j}$), so $\nabla \cdot \hat{\boldsymbol{A}}'_j$ is still zero and 5.8 still holds. While this change in origin does not affect the description of the magnetic field $\boldsymbol{B}$, it does change $\hat{\mathscr{H}}^{(1)}$ into

$$\begin{aligned}\hat{\mathscr{H}}^{(1)\prime} &= \frac{1}{c}\sum_j^N \hat{\boldsymbol{A}}'_j \cdot \hat{\boldsymbol{p}}_j = \frac{1}{2c}\sum_j^N \boldsymbol{B} \cdot \left[(\boldsymbol{r}_j - \boldsymbol{r}_0 - \boldsymbol{d}) \times \hat{\boldsymbol{p}}_j\right] \\ &= \hat{\mathscr{H}}^{(1)} - \frac{1}{2c}\sum_j^N \boldsymbol{B} \cdot \boldsymbol{d} \times \hat{\boldsymbol{p}}_j = \hat{\mathscr{H}}^{(1)} + \delta\hat{\mathscr{H}}^{(1)}\end{aligned} \tag{5.34}$$

and the first order corrections to the wave function change by $\delta\phi_i^{(1)}$:

$$\begin{aligned}\phi^{(1)\prime} &= \phi^{(1)} + \delta\phi_i^{(1)} \\ &= \phi_i^{(1)} + \sum_{p=N/2+1}^{K} \delta C_{pi}^{(1)} \phi_p^{(0)}\end{aligned} \tag{5.35}$$

The change in the first order corrections to the wave function, $\delta\phi_i^{(1)}$, can be found by inserting equations 5.34 and 5.35 in equation 5.29. The resulting equations for $\delta C_{pi}^{(1)}$ have the same form as the coupled perturbed Hartree-Fock equations:

$$\begin{aligned}\left(\epsilon_p^{(0)} - \epsilon_i^{(0)}\right)\delta C_{pi}^{(1)} + \langle\phi_p^{(0)}|\delta\hat{\mathscr{H}}^{(1)}|\phi_i^{(0)}\rangle + \sum_{j=1}^{N/2}\sum_{q=N/2+1}^{K}\Big\{\Big(\langle\phi_q^{(0)}\phi_p^{(0)}|g_{ij}|\phi_j^{(0)}\phi_i^{(0)}\rangle \\ - \langle\phi_p^{(0)}\phi_j^{(0)}|g_{ij}|\phi_q^{(0)}\phi_i^{(0)}\rangle\Big)\delta C_{qj}^{(1)}\Big\} = 0\end{aligned} \tag{5.36}$$

The first order coupled perturbed Hartree-Fock wave function for any gauge origin and any field $\boldsymbol{B}$ can be found by independently solving six coupled perturbed Hartree-Fock equations, for $\hat{\mathscr{H}}^{(1)}$ (or $\delta\hat{\mathscr{H}}^{(1)}$) being $\hat{\boldsymbol{L}}_x$, $\hat{\boldsymbol{L}}_y$, $\hat{\boldsymbol{L}}_z$, $\hat{\boldsymbol{p}}_x$, $\hat{\boldsymbol{p}}_y$ and $\hat{\boldsymbol{p}}_z$ resulting in $\phi_i^{(1)\hat{\boldsymbol{L}}_x}$, $\phi_i^{(1)\hat{\boldsymbol{L}}_y}$, $\phi_i^{(1)\hat{\boldsymbol{L}}_z}$, $\phi_i^{(1)\hat{\boldsymbol{p}}_x}$, $\phi_i^{(1)\hat{\boldsymbol{p}}_y}$ and $\phi_i^{(1)\hat{\boldsymbol{p}}_z}$ respectively. For a magnetic field applied along the z-axis ($\boldsymbol{B} = \mathscr{B}\boldsymbol{1}_z$, with $\boldsymbol{1}_z$ the unit vector along the

z-axis, *cf.* equation 5.3), the total first order correction to the Hamiltonian (with $\boldsymbol{r}_0$ been put to $\mathbf{0}$ and $\boldsymbol{d}$ as the gauge origin) is:

$$\hat{\mathscr{H}}^{(1)} = \frac{\mathscr{B}}{2c}\sum_j^N \mathbf{1}_z \cdot \hat{\boldsymbol{L}}_{\boldsymbol{j}} - \frac{\mathscr{B}}{2c}\sum_j^N \mathbf{1}_z \cdot \boldsymbol{d} \times \hat{\boldsymbol{p}}_j = \frac{\mathscr{B}}{2c}\sum_j^N \left(\hat{\boldsymbol{L}}_z - d_x\hat{\boldsymbol{p}}_y + d_y\hat{\boldsymbol{p}}_x\right) \quad (5.37)$$

and the total first order correction to the i-th molecular orbital $\phi_i^{(1)}$ can be expressed in terms of these components:

$$\phi_i^{(1)} = \frac{\mathscr{B}}{2c}\left(\phi_i^{(1)\hat{\boldsymbol{L}}_z} - d_x\phi_i^{(1)\hat{\boldsymbol{p}}_y} + d_y\phi_i^{(1)\hat{\boldsymbol{p}}_x}\right) \quad (5.38)$$

Inserting this expression in equation 5.27 leads to the following equation for $\boldsymbol{J}^{(1)}(\boldsymbol{r})$:

$$\begin{aligned}\boldsymbol{J}^{(1)}(\boldsymbol{r}) = -\frac{\mathscr{B}}{c}\sum_{i=1}^{N/2}\Big\{&\phi_i^{(0)*}\hat{\boldsymbol{p}}\phi_i^{(1)\hat{\boldsymbol{L}}_z} + \phi_i^{(1)\hat{\boldsymbol{L}}_z*}\hat{\boldsymbol{p}}\phi^{(0)} \\ &- d_x\left(\phi_i^{(0)*}\hat{\boldsymbol{p}}\phi_i^{(1)\hat{\boldsymbol{p}}_y} + \phi_i^{(1)\hat{\boldsymbol{p}}_y*}\hat{\boldsymbol{p}}\phi^{(0)}\right) \\ &+ d_y\left(\phi_i^{(0)*}\hat{\boldsymbol{p}}\phi_i^{(1)\hat{\boldsymbol{p}}_x} + \phi_i^{(1)\hat{\boldsymbol{p}}_x*}\hat{\boldsymbol{p}}\phi^{(0)}\right)\Big\} \\ &- \frac{1}{2c}\hat{\boldsymbol{B}} \times (\boldsymbol{r} - \boldsymbol{d})\rho^{(0)}(\boldsymbol{r})\end{aligned} \quad (5.39)$$

The first order current density $\boldsymbol{J}^{(1)}$ is independent of the gauge origin. Because of this gauge independence, $\boldsymbol{J}^{(1)}(\boldsymbol{r})$, at any given point $\boldsymbol{r}$ can be calculated by choosing the origin of the gauge at this point $\boldsymbol{r}$ (so $\boldsymbol{d} = \boldsymbol{r}$). By doing so, one preforms a 'separate gauge transformation for each point in real space' [37]. Notice that by doing so, the diamagnetic term vanishes since $(\boldsymbol{r} - \boldsymbol{d}) = 0$. This is why this method is called the 'continuous transformation of origin of current density -diamagnetic zero' (CTOCD-DZ)[12,38–40], which is equivalent to the CGST method by Keith and Bader[37] and is also labelled as the ipsocentric method[41,42].

5.3 Ring Current Maps as a measure of aromaticity

The first order current density (5.27) is traditionally understood to be composed of a diamagnetic and a paramagnetic term:

$$\begin{aligned}\boldsymbol{J}^{(1)}(\boldsymbol{r}) &= -2\sum_{i=1}^{N/2}\left\{\phi_i^{(0)*}\hat{\boldsymbol{p}}\phi_i^{(1)} + \phi_i^{(1)*}\hat{\boldsymbol{p}}\phi_i^{(0)}\right\} - \hat{\boldsymbol{A}}(\boldsymbol{r})\rho^{(0)}(\boldsymbol{r}) \\ &= \boldsymbol{J}^{(d)}(\boldsymbol{r}) + \boldsymbol{J}^{(p)}(\boldsymbol{r}) \end{aligned} \tag{5.40}$$

The exact total current density $\boldsymbol{J}^{(1)}$ is independent of the gauge origin of $\hat{\boldsymbol{A}}$, but the partitioning between $\boldsymbol{J}^{(d)}$ and $\boldsymbol{J}^{(p)}$ is not. Despite its frequent use, it has long been recognised that this distinction between diamagnetic and paramagnetic terms has no real physical meaning.[104]

By using the CTOCD-DZ formulation, the diamagnetic component $\boldsymbol{J}^{(d)}$ vanishes and both the diamagnetic and the paramagnetic 'contribution' to the total current density are described by a single term which depends on the accessibility of excited states through translation ($\hat{\boldsymbol{p}}$) and rotational ($\hat{\boldsymbol{L}}$) transitions:

$$\boldsymbol{J}^{(1)}(\boldsymbol{r}) = -2\sum_{i=1}^{N/2}\left\{\phi_i^{(0)*}\hat{\boldsymbol{p}}\phi_i^{(1)} + \phi_i^{(1)*}\hat{\boldsymbol{p}}\phi_i^{(0)}\right\}_{\boldsymbol{d}=\boldsymbol{r}} \tag{5.41}$$

A distinction between diamagnetic and paramagnetic terms can however be made, writing $\phi_i^{(1)}$ as:

$$\begin{aligned}\phi_i^{(1)} &= \phi_i^{(1)\boldsymbol{B}\cdot\hat{\boldsymbol{L}}(\boldsymbol{0})} - \phi_i^{(1)\boldsymbol{B}\cdot\boldsymbol{d}\times\hat{\boldsymbol{p}}} \\ &= \left(\phi_i^{(1)\hat{\boldsymbol{L}}(\boldsymbol{0})}\right)\cdot\boldsymbol{B} - \left(\boldsymbol{d}\times\phi_i^{(1)\hat{\boldsymbol{p}}}\right)\cdot\boldsymbol{B} \\ &= \left(\sum_{p=N/2+1}^{K} C_{pi}^{(1)\hat{\boldsymbol{L}}(\boldsymbol{0})}\phi_p^{(0)}\right)\cdot\boldsymbol{B} - \left(\boldsymbol{d}\times\sum_{p=N/2+1}^{K} C_{pi}^{(1)\hat{\boldsymbol{p}}}\phi_p^{(0)}\right)\cdot\boldsymbol{B} \\ &= \phi_i^{(p)} + \phi_i^{(d)} \end{aligned} \tag{5.42}$$

The term $\phi_i^{(p)}$ gives rise to a paramagnetic contribution $\boldsymbol{J}^{(p')}$ and is determined by the accessibility of excited states via rotational ($\hat{\boldsymbol{L}}$) transitions. $\phi_i^{(d)}$ gives rise to a diamagnetic contribution $\boldsymbol{J}^{(d')}$ and is determined by the accessibility of excited states via translational ($\hat{\boldsymbol{p}}$) transitions.

From equation 5.41 it can be seen that the first order current density $\boldsymbol{J}^{(1)}$ can be written as a sum of orbital contributions:

$$\boldsymbol{J}^{(1)}(\boldsymbol{r}) = -2\sum_{i=1}^{N/2}\boldsymbol{J}_i^{(1)}(\boldsymbol{r}) \tag{5.43}$$

Where the 'orbital current densities' $\boldsymbol{J}_i^{(1)}$ are:

$$\boldsymbol{J}_i^{(1)}(\boldsymbol{r}) = \left\{ \phi_i^{(0)*} \hat{\boldsymbol{p}} \phi_i^{(1)} + \phi_i^{(1)*} \hat{\boldsymbol{p}} \phi_i^{(0)} \right\}_{\boldsymbol{d}=\boldsymbol{r}} \tag{5.44}$$

The ring currents can now be analysed using this information. For a magnetic field applied along the z-axis, the relevant operators are the rotation about the field direction, $\hat{\boldsymbol{L}}_z$, and the two translations within the molecular plane, $\hat{\boldsymbol{p}}_x$ and $\hat{\boldsymbol{p}}_y$ (*cf.* equation 5.39). Three factors will determine the existence and the strength of the contribution by one of these operators: symmetry, spatial distribution and energy.[12]

Symmetry: The symmetry of the occupied and virtual orbital involved in the transition will determine whether or not a rotational or translational transition is possible. Let $\Gamma(\phi_i^{(0)})$ and $\Gamma(\phi_p^{(0)})$ be the irreducible representations of the occupied and the virtual orbital respectively. A transition $\phi_i^{(0)} \rightarrow \phi_p^{(0)}$ then has (see sections 8-3 and 8-4 in Bishop[105]):

- a diamagnetic contribution to $\boldsymbol{J}_i^{(1)}$ when the direct product of the representations $\Gamma(\phi_i^{(0)}) \otimes \Gamma(\hat{\boldsymbol{p}}_x) \otimes \Gamma(\phi_p^{(0)})$ or $\Gamma(\phi_i^{(0)}) \otimes \Gamma(\hat{\boldsymbol{p}}_y) \otimes \Gamma(\phi_p^{(0)})$ contains the totally symmetric representation Γ^1
- a paramagnetic contribution to $\boldsymbol{J}_i^{(1)}$ when the direct product of the representations $\Gamma(\phi_i^{(0)}) \otimes \Gamma(\hat{\boldsymbol{L}}_z) \otimes \Gamma(\phi_p^{(0)})$ contains the totally symmetric representation Γ^1

Spatial distribution: When a transition is symmetry-allowed, the magnitude of the contribution will depend on the spatial distribution of the occupied and virtual orbitals. Both orbitals should occupy the same region in space and both $\phi_i^{(0)}$ and $\hat{\boldsymbol{p}}_x \phi_p^{(0)}$, $\hat{\boldsymbol{p}}_y \phi_p^{(0)}$ or $\hat{\boldsymbol{L}}_z \phi_p^{(0)}$ should have similar nodal structures for the transition to be significant. This criterion leads to the following rule of thumb: two orbitals with a similar nodal structure, related by a rotation tend to give a significant paramagnetic contribution. When the virtual orbital is the result of the bisection of the occupied orbital by a nodal plane perpendicular to the molecular surface, the transition tends to give a significant diamagnetic contribution.

Energy: Due to the $1/(\epsilon_p^{(0)} - \epsilon_i^{(0)})$ dependence of $C_{pi}^{(1)}$, the energy differences should be small. This $1/\Delta\epsilon$ dependence implies that, when symmetry-allowed, the HOMO-LUMO transition will contribute the most to the ring-current, and generally the total current will be dominated by transitions from the higher occupied orbitals to the lower virtual orbitals.

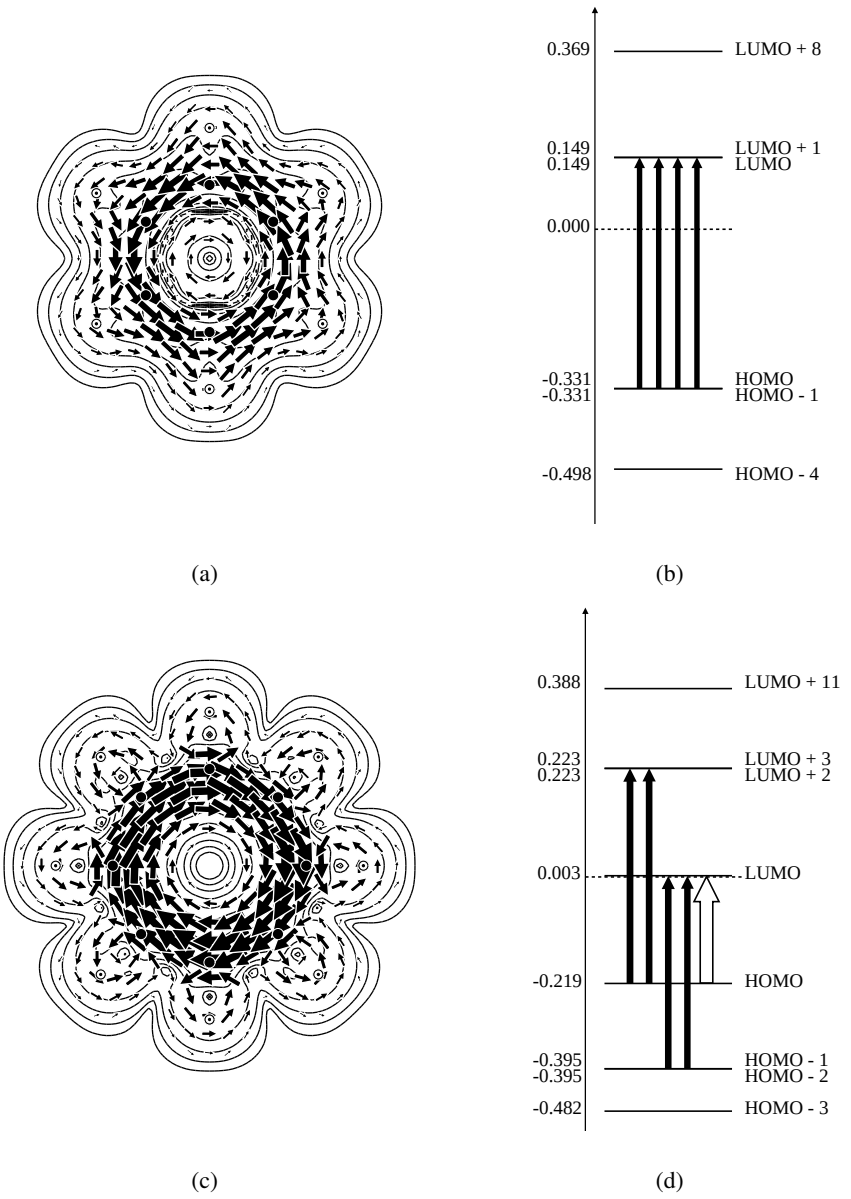

Figure 5.1: The current density maps for benzene (a) and flattened cyclooctatetraene (c) 1 Bohr above the molecular plane and the translational (diatropic, black arrows) and rotational (paratropic, arrows without filling) transitions between individual pairs of an occupied and virtual orbital (b, d). Only significant contributions based on the value $C_{pi}^{(1)\hat{\boldsymbol{L}}_z}$, $C_{pi}^{(1)\hat{\boldsymbol{p}}_x}$ and $C_{pi}^{(1)\hat{\boldsymbol{p}}_y}$ are shown and the width of the arrow reflects the magnitude of the contribution to the total current. The vertical axis denotes orbital energies (in au). (calculated at HF/6-31G**)

These rules are a useful tool for analysing and explaining the origin and strength of the current density in a wide range of molecules. As an example the ring current an the most important transitions of benzene and cyclooctatetraene are given in figure 5.1. The ring current maps clearly show the diatropic, aromatic character of benzene and the paratropic, anti-aromatic character of cyclooctatetraene. The diatropic ring current in benzene is caused by HOMO-LUMO translational transitions, for the LUMOs of benzene are related to the HOMOs through the bisection of the HOMOs by a nodal plane. For cyclooctaterraene the D_{8h} geometry leads to an open singlet configuration, of which the degenerate HOMO is lifted by adopting a D_{4h} geometry for which the Ring Current Map (RCM) is shown in figure 5.1(c). The paratropic ring current is caused by a HOMO-LUMO rotational transition, since the HOMO and LUMO have virtually the same shape (and thus the same nodal structure), differing from each other only by a 90° rotation.

5.4 The Nucleus Independent Chemical Shift

The presence of a magnetic field $\boldsymbol{H}_0$ induces electric currents in the molecule. These electric currents in their turn generate a magnetic field $\boldsymbol{H}'$. From the ring current ($\boldsymbol{J}^{(1)}(\boldsymbol{r})$), $\boldsymbol{H}'$ can be calculated at any position $\boldsymbol{r}_X$ using the Biot-Savart law:

$$\boldsymbol{H}'(\boldsymbol{r}_X) = -\int \left\{(\boldsymbol{r}-\boldsymbol{r}_X)\times \boldsymbol{J}^{(1)}(\boldsymbol{r})\right\}/|\boldsymbol{r}-\boldsymbol{r}_X|^3 d\boldsymbol{r} \tag{5.45}$$

The induced field $\boldsymbol{H}'$ can strengthen the applied magnetic field ($\boldsymbol{H}_0$) when the molecule is paramagnetic or weaken $\boldsymbol{H}_0$ when the molecule is diamagnetic. The induced field $\boldsymbol{H}'$ can be expressed in terms of the magnetic field strength by means of the magnetic shielding tensor σ:

$$\boldsymbol{H}'(\boldsymbol{r}) = -\sigma(\boldsymbol{r})\boldsymbol{H}_0(\boldsymbol{r}) \tag{5.46}$$

The nuclear shielding tensor σ is thus the negative proportionality factor between the electronically induced magnetic field, taken at the atomic position, and the externally applied one[106]. The Nucleus Independent Chemical Shift (NICS) corresponds to the negative of either the trace or some component, depending on the version of NICS used, of this tensor computed at some point in space. NICS are nucleus independent since these points usually do not coincide with any nucleus. Over time, different kinds of NICS indices have appeared[10,107,108]. Originally, they were computed at the centre of the rings and the trace of the chemical shift tensor was used as an index (the so called NICS(0)). In a later stage, it was suggested that NICS should be computed at 1 Å above the centre of the ring to reflect better the π component of

the NICS[107] (NICS(1)). Fowler et al. pointed out the tensor character of the chemical shift and consequently that only the σ_{zz} should be used[13,109]. This has led to the introduction of the NICS(0)$_{zz}$ and NICS(1)$_{zz}$. More recently, it is advised to use yet another NICS approach, where the σ_{zz} is computed for only the π orbitals[13,110].

Most often the NICS are computed at the centre of an aromatic ring or 1Å above the centre of the ring, assuming that the NICS value in this single point is a measure of the size of the ring current in this ring. This means that all information of the ring current in the entire molecule is somehow considered reflected in a single point, an approach which has been heavily criticised[11,13,109,111]. As mentioned above, over time, the schemes for the calculation of NICS have been refined to cope with different criticisms, but clearly reduction of the rich information of a RCM to a single number remains questionable, as completely different RCM could give rise to nearly indistinguishable NICS values. Although criticised on several occasions[19,109,111,112], the practice of computing NICS values in the centre of an aromatic ring as an index of the degree of aromaticity remains a common method among computational chemists. In many cases, NICS and RCM lead to similar conclusions, but for many polycyclic aromatic hydrocarbons (PAH) NICS can give unexpected results. One well known class of problematic cases is when bifurcated circuits arise[112–114]. (*vide infra*, Chapter 8)

Chapter 6

The Pseudo-π approach

6.1 Introduction

The interest in calculating the aromatic properties of larger systems and bigger molecular sets has recently brought back the 1937 idea of London who modelled the current density of the π-system of some aromatic hydrocarbons using systems built up by hydrogen atoms replacing the carbon atoms[115]. This method has been revived in aromaticity studies by Fowler *et al.* to allow for a substantial reduction in the computational cost of ring current calculations[116]. This so called pseudo-π method has proven to be surprisingly accurate in describing the ring currents[116] and in calculating the Multi Centre Bond Indices[117] and Nucleus Independent Chemical Shift[118] of Polycyclic Aromatic Hydrocarbons (PAH). Using this Pseudo-π-method it is possible to reduce the computer time drastically, allowing the calculation of the properties of increasingly larger systems[119].

The calculations using the pseudo-π method can (until now) only be done on hydrocarbons. The effect of heteroatoms have not been described using this method. The calculation is done in the following way:

- If needed, the geometry of the PAH is optimised at some desired level of theory, considering all C and H atoms but constraining the geometry to planarity.

- After this optimization all hydrogen atoms are removed from the previous structure. The carbon atoms of the molecular skeleton are subsequently replaced by hydrogen atoms at the same coordinates.

- The hydrogen atoms are each given a single 1s (STO-3G) basis function and a single point ab initio calculation is performed using HF/STO-3G calculations for this hydrogen network.

- The desired information (MCBI, current density, NICS, ...) can then be calculated using this hydrogen system.

In case of frozen geometries, of course one can skip the first step and proceed immediately to the second step. As discussed in detail by Fowler *et al.*, there is a one-to-one relationship between the π-MO's obtained from the ab initio calculation with the entire molecule and the σ-ones from the hydrogen network calculation. In this chapter, the use of the pseudo-π method for the calculation of current density maps, MCBI and NICS will be discussed.

6.2 The Ring currents

As Fowler and Steiner argue, there is a one-to-one correspondence between the Hückel molecular orbitals of a π system of the Hydrocarbon (C_N) and the σ-orbitals of an array of hydrogen atoms (H_N) with the same geometry. The symmetries of the orbitals are also related. In a planar system, each π molecular orbital of symmetry $\Gamma(\pi)$ is converted to a related σ molecular orbital of symmetry $\Gamma(\sigma)$ by the replacing the p_π-type AOs by s-type AOs. $\Gamma(\pi)$ and $\Gamma(\sigma)$ are related by the symmetry of a translation perpendicular to the plane, Γ_z :

$$\Gamma(\sigma) = \Gamma(\pi) \otimes \Gamma_z \tag{6.1}$$

In the same study Fowler and Steiner found that if the STO-3G hydrogens are placed at the same positions as the carbon atoms, the two systems C_N and H_N show a close numerical match between the energies of the occupied π-orbitals of the full C_N system and those of the σ orbitals of the H_N model.

Because of this correspondence in symmetry, spatial distribution and energy between the full C_N system and the H_N model (*vide supra*) the pseudo-π model gives a close numerical match to the π current density of the original carbon system at a height of 1 Bohr.

6.3 The MCBI

For multicentre indices, the pseudo-π approach has been shown to allow a very fast and accurate calculation of both the PDI and SCI indices[117]. For the SCI indices the

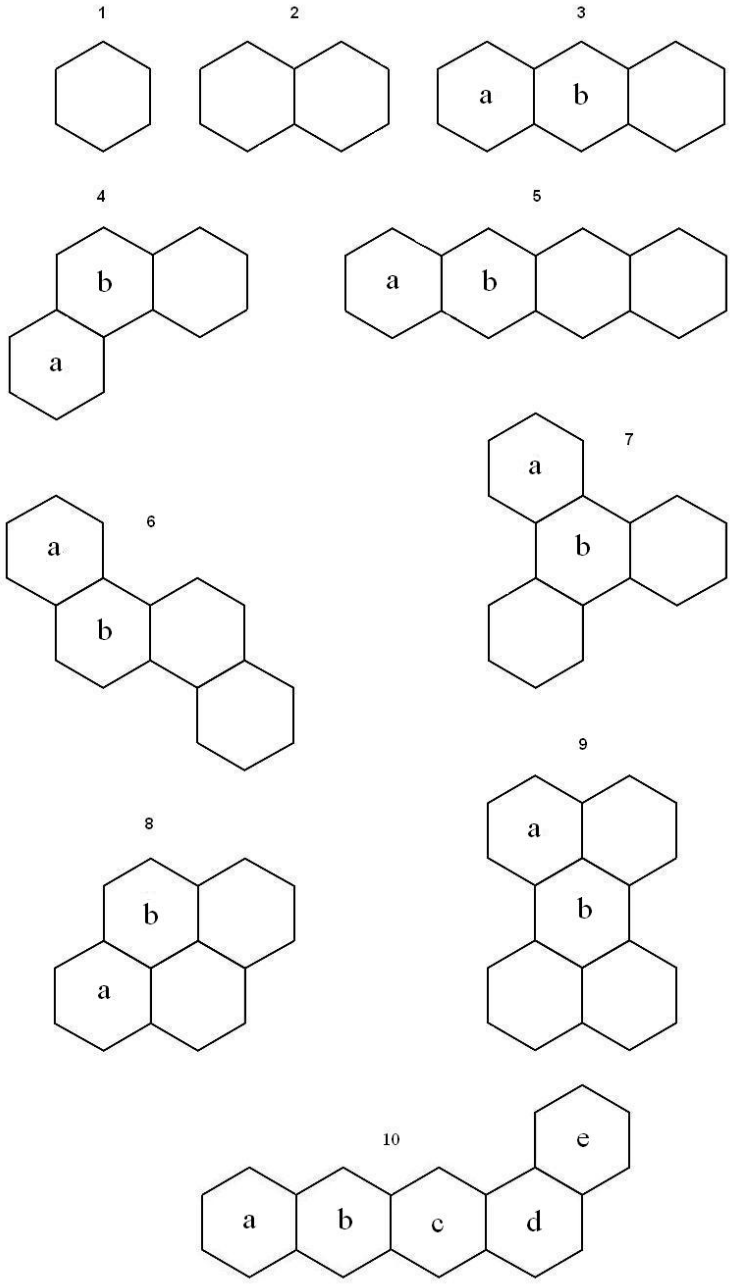

Figure 6.1: Some common PAH, included in this study. Only the σ-framework is shown.

Table 6.1: The different QCTA-SCI and Pseudo-π-SCI (PP-SCI) values of PAH 1 to 9 in Fig 6.1. Both the numerical value and the value expressed as a percentage of the value for benzene are given. (QCTA calculated using optimised geometry at B3LYP/6-311G**, PP calculated at HF/STO-3G)

Molecule	Ring	QCTA-SCI	QCTA-SCI(%)	PP-SCI	PP-SCI (%)
1		0.0817	100	0.0494	100
2		0.0439	54	0.0270	55
3	a	0.0331	40	0.0208	42
	b	0.0302	37	0.0189	38
4	a	0.0525	64	0.0324	66
	b	0.0202	25	0.0123	25
5	a	0.0284	35	0.0184	37
	b	0.0251	31	0.0159	32
6	a	0.0499	61	0.0308	62
	b	0.0253	31	0.0155	31
7	a	0.0580	71	0.0359	73
	b	0.0094	12	0.0056	11
8	a	0.0407	50	0.0258	52
	b	0.0210	26	0.0122	25
9	a	0.0395	48	0.0244	49
	b	0.0068	8	0.0038	8

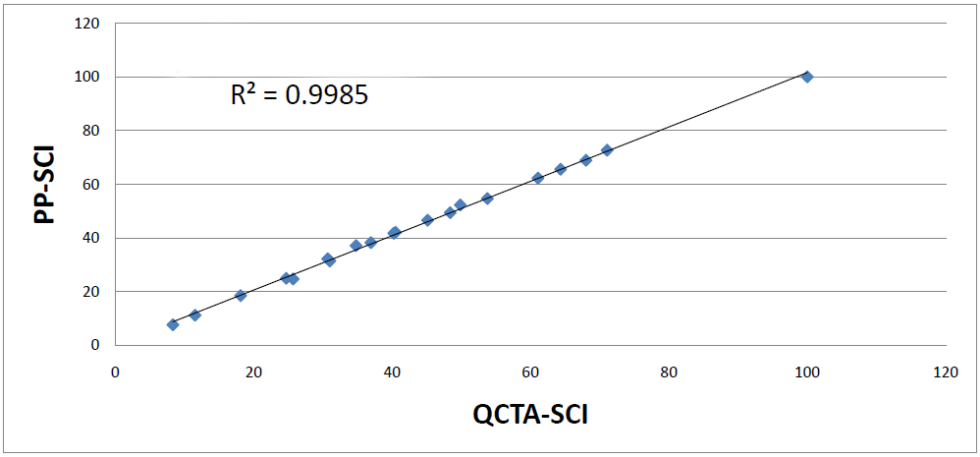

Figure 6.2: Plot of the QCTA-SCI and PP-SCI values of table 6.1 in benzene-% .

correlation coefficient between the full molecular indices and the pseudo-π indices amounts nearly 99%. Also, it was found that the effect on the SCI of clamping benzenoid rings is the same, independent of using the full molecular calculation or the pseudo-π approach[117].

As an example the values of the SCI calculated using the QCTA-partitioning on the normal molecule and the SCI calculated using the Mulliken-partitioning on the pseudo-π-model of some common PAH's (Fig 6.1) are given in table 6.1. The excellent correlation between the Full-SCI and Pseudo-π-SCI (PP-SCI) can be seen in figure 6.2. Moreover Bultinck *et al.* found that the values obtained with the real molecular calculation using Mulliken partitioning are both qualitatively and quantitatively reproduced within the pseudo-π method. As the number of basis functions in a pseudo-π calculation is much smaller than in a complete molecular calculation, it becomes tractable to compute delocalisation indices for larger rings. The applicability of the pseudo-π scheme thus allows to extend the range of multicentre index calculations that can be performed, for instance allowing to computing also Ten-Centre-Indices as well as Fourteen-Centre-Indices (*vide infra*).

6.4 The NICS

Recently, the validity of the pseudo-π method for the computation of NICS was established by Fias *et al.*[118]. Although the Nucleus Independent Chemical Shift has been a popular tool for describing the aromaticity of Polycyclic Aromatic Hydrocar-

Table 6.2: The different NICS and PP-NICS-values of some common PAH (Fig 8.3). The SCI value is the Pseudo-π-value expressed as a percentage of the value for benzene.

Molecule	Ring	NICS(0)	NICS(1)	$NICS_{zz}(0)$	$NICS_{zz}(1)$	PP-NICS	PP-$NICS_{zz}$	SCI
1		-8.73	-10.98	-14.17	-28.91	-17.49	-41.21	100
2		-9.23	-11.55	-13.79	-29.76	-17.14	-40.34	55
3	a	-8.52	-11.02	-11.48	-27.95	-15.95	-36.90	42
	b	-11.34	-13.37	-17.98	-34.43	-19.34	-46.99	38
4	a	-8.91	-11.33	-12.27	-28.85	-17.49	-41.07	66
	b	-6.64	-9.69	-3.97	-23.09	-13.31	-29.11	25
5	a	-7.92	-10.53	-9.58	-26.38	-15.02	-34.16	37
	b	-11.37	-13.45	-17.90	-34.49	-19.25	-46.83	32
6	a	-8.86	-11.30	-12.03	-28.67	-17.40	-40.82	62
	b	-7.00	-10.04	-4.47	-23.90	-14.54	-32.47	31
7	a	-7.64	-10.32	-8.00	-25.57	-16.86	-38.94	73
	b	-2.95	-6.99	9.29	-13.89	-8.53	-15.10	11
8	a	-11.65	-13.77	-19.73	-35.81	-20.20	-49.27	52
	b	-4.65	-8.22	1.96	-18.60	-10.69	-20.98	25
9	a	-5.10	-8.23	0.17	-19.04	-14.95	-33.41	49
	b	8.19	2.15	42.68	13.75	3.37	20.64	8
10	a	-8.25	-10.86	-10.59	-27.23	-15.50	-35.55	39
	b	-11.34	-13.48	-17.72	-34.31	-19.43	-47.28	34
	c	-10.05	-12.48	-13.47	-31.06	-18.12	-43.17	34
	d	-3.78	-7.40	4.94	-15.72	-9.67	-18.43	16
	e	-8.31	-10.83	-10.29	-27.06	-17.13	-39.87	70

Table 6.3: The correlations between the different types of NICS values.

R^2	PP-NICS	PP-$NICS_{zz}$
NICS(0)	0.929	0.932
NICS(1)	0.938	0.942
$NICS_{zz}(0)$	0.952	0.958
$NICS_{zz}(1)$	0.947	0.952

bons for more than ten years, no test had yet been performed on the applicability of the pseudo-π method for the computation of the NICS indices.

In order to have a sufficiently large dataset, 113 polycyclic aromatic hydrocarbons (PAH) have been used. This set of PAHs include benzene, naphthalene, anthracene, phenanthrene, 104 benzenoids with four, five and six rings together with the cyclopentadienyl anion, the tropylium ion, azulene and the fluorene anion to incorporate some five- and seven-membered rings. The molecular set contains a total of 499 symmetry-unique rings. All molecular geometries were constructed from Z-matrices with C-C bond lengths equal to 1.4 Å and C-H bond lengths equal to 1.1 Å . Bond angles and dihedral angles were frozen to standard values, so that the molecules are considered planar and the highest symmetry is obtained for all PAHs. The molecules were thus constrained to their "frozen ideal geometry". The NICS(0), NICS(1), and their zz-components were evaluated at the centres of the aromatic rings and 1 Å above the rings using the B3LYP functional and the 6-311G** basis set using Gaussian-03[120]. The Pseudo-π NICS (PP-NICS) were only calculated at the centres of the rings using HF/STO-3G.

First the correlation between the NICS and pseudo-π-NICS (PP-NICS) is discussed. The different values of the NICS and PP-NICS of some common PAH's (Fig 6.1) are presented in table 6.2. From this data it is seen that the PP-NICS mimic the trends in the NICS values. The correlations between the different types of NICS are summarised in table 6.3. These are the correlations for all 499 symmetry unique rings of the 113 molecules. From this data it is clear that all NICS and PP-NICS-values are significantly correlated, with the R^2-values above 0.9. Since the Pseudo-π method mimics the π-system of the molecules, one would expect the NICS(1) to show a better correlation with the PP-NICS than the NICS(0). This is indeed confirmed by our calculations, for which the R^2-values are slightly bigger. From these correlations it is also seen that the more aromatic-sensitive NICS(1) and the $NICS_{zz}$ give slightly better correlations with the PP-$NICS_{zz}$. These findings clearly show that the PP-NICS are a worthy alternative to the complete NICS-calculations.

Part II

The Aromaticity of Polycyclic Aromatic Hydrocarbons

Chapter 7

Correlation between delocalisation indices and Generalised Polansky Index

7.1 Introduction

In the present chapter[121], the electron density itself (or more precise the Density Matrix) is used as a natural way to investigate aromaticity, rather than using structural features or quantities derived from it. To that end, molecular quantum similarity theory is used as a technique to investigate how different benzenoid rings are compared to benzene itself in different polycyclic aromatic hydrocarbons. The use of electron density, and a fortiori molecular quantum similarity theory, to assess the degree of aromaticity was previously proposed by Giambiagi et al., who suggested its use to "open up new insights into the concept of aromaticity, with solid chemical and mathematical foundations"[122]. Although suggested several years ago, no in-depth report has yet been published on the application of the molecular quantum similarity theory in the context of aromaticity. This was the motivation for the present study[121].

7.1.1 Theoretical Development

The natural starting point for the present study is the important work by Polansky and Derflinger published in 1967[123]. Based on the Clar postulate[124] that individual benzenoid rings in polycyclic aromatic hydrocarbons (PAH) can be regarded as local benzene-like regions, Polansky and Derflinger proposed to characterise the aromaticity of these rings in PAH by the "similarity" to benzene itself. This similarity was characterised by the value of a certain index derived from the charge-density bond order matrix. This approach was, however, formulated only at the level of the Hückel Molecular Orbital theory (HMO). Nowadays the HMO theory is sometimes considered outdated and despite the attractiveness of the Polansky index, no attempt has so far been reported to incorporate this aromaticity measure as such into the framework of more sophisticated contemporary computational tools. Our aim in this study is to fill this gap and to attempt a generalization of the Polansky approach so as to be applicable at the *ab initio* level of theory. Prior to describing the basic idea of our generalization, it is worthwhile to describe briefly the original approach[123]. For this purpose, let us consider a polycyclic aromatic hydrocarbon consisting of K fused benzenoid rings and let us characterise the π-electron structure of this hydrocarbon by the set of Hückel molecular orbitals ϕ_i expressed as a linear combination of atomic p_π orbitals χ_μ (*cf.* equation 3.8).

$$\phi_i(\boldsymbol{r}) = \sum_{\mu=1}^{K} c_{\mu i}\chi_\mu(\boldsymbol{r}) \tag{7.1}$$

where the summation runs over all M atoms in the molecule.

Based on these orbitals, it is straightforward to introduce the charge density-bond order matrix (Equation 3.80)

$$P_{\nu\mu} = \sum_{i=1}^{N} c^*_{\mu i}c_{\nu i} \tag{7.2}$$

This matrix, whose dimension is $N \times N$, characterises the distribution of electron density in the whole molecule. In addition to this global information, the matrix also allows one to get information on the electron structure of any particular benzenoid ring within the molecule. Such information about the particular ring L is inherently contained in the fragment of the whole density matrix (7.2), involving only the atoms contributing to this ring. The basic idea of the Polansky-Derflinger approach to the classification of aromaticity of such a ring is based on the ingenious comparison of the fragment density matrices characterizing the benzenoid ring L in the polycyclic molecule A with the density matrix of benzene, B. Such a comparison is quantitatively expressed by the index:

$$p_{L,B} = \frac{1}{2N_L} \sum_{\mu \in L}^{M} \sum_{\substack{\nu > \mu \\ \nu \in L}}^{M} P^A_{\mu\nu} P^B_{\mu\nu} \tag{7.3}$$

where N_L is the number of atoms involved in the ring considered (6 in the case of a benzenoid ring). The reason for including this parameter is to ensure proper normalization of the index so as to provide maximum similarity (identity) for the comparison of benzene with itself. In all other cases, the values will be smaller than 1 and the more the index deviates from its idealised value 1, the less similar is a given ring L to benzene and, consequently, the smaller will be its aromaticity. In this way, a simple Hückel Molecular Orbital program can be used to compute very quickly the necessary similarity measures for all benzenoid rings that will be considered in the present work. After being reminded of the basic idea of the original Polansky approach, let us now address the problem of its generalization beyond the scope of the HMO theory. As already said above, the basic idea of the Polansky approach was to gauge the aromaticity of a given ring in PAH by its similarity to benzene itself. While in the original HMO-like approach this similarity is straightforwardly given by the index (7.3), the same approach cannot be straightforwardly extended to more sophisticated levels of theory. To overcome the drawback of the original approach, we found it useful to benefit from our experience with molecular quantum similarity and to attempt a generalization of the index 7.3 in a way that would resemble as much as possible the original approach by Polansky.

For a detailed account of molecular quantum similarity, the reader is referred to recent reviews.[125,126] For the present goals, it suffices that the similarity between two molecules, A and B, is expressed via the Molecular Quantum Similarity Measure (MQSM) as:

$$Z_{A,B} = \int \left[\rho_A(\boldsymbol{r}_1) \Omega(\boldsymbol{r}_1, \boldsymbol{r}_2) \rho_B(\boldsymbol{r}_2)\right] d\boldsymbol{r}_1 d\boldsymbol{r}_2 \tag{7.4}$$

where $\Omega(\boldsymbol{r}_1, \boldsymbol{r}_2)$ is a positive definite operator, and $\rho_A(\boldsymbol{r}_1)$ is the one electron density for molecule A at $\boldsymbol{r}_1$. Another quantity that describes the degree of similarity between the two molecules is the Euclidean distance:

$$d^2_{A,B} = Z_{A,A} + Z_{B,B} - 2Z_{A,B} \tag{7.5}$$

Working within a single determinant method, and using the Dirac delta function as operator in 7.4 , it is immediately seen that computation of the MQSM will require computing overlap integrals over four basis functions as:

$$Z_{A,B} = \int \rho_A(\boldsymbol{r}_1) \rho_B(\boldsymbol{r}_1) d\boldsymbol{r}_1 = \sum_{\nu \in A} \sum_{\mu \in B} \sum_{\sigma \in C} \sum_{\kappa \in D} P^A_{\nu\sigma} P^B_{\mu\kappa} S_{\mu\kappa\nu\sigma} \tag{7.6}$$

Computing all these four centre overlap integrals ($S_{\mu\kappa\nu\sigma}$), especially for larger numbers of basis functions, becomes a very limiting step. This inspired Cioslowski *et al.*[127] to introduce a slightly different approach where the comparison of the molecules is not based on the electron densities but on first order density matrices[128].In this Number of Overlapping Electrons (NOEL) approach, the integral 7.7 is introduced, which represents the similarity measure between the first order density matrix $\rho_A(\boldsymbol{r}, \boldsymbol{r}')$ of molecule A, with the first order density matrix of molecule B $\rho_B(\boldsymbol{r}, \boldsymbol{r}')$.

$$Z_{A,B} = \int \rho_A(\boldsymbol{r}, \boldsymbol{r}')\rho_B(\boldsymbol{r}, \boldsymbol{r}')d\boldsymbol{r}d\boldsymbol{r}' \tag{7.7}$$

As a result, the NOEL index between the two molecules A and B is given by:

$$\text{NOEL}_{A,B} = Z_{A,B} = \sum_{IJ} n_{AI}n_{BJ} \left|\langle\chi_{AI}|\chi_{BJ}\rangle\right|^2 \tag{7.8}$$

where n_{AI} is the occupation number of Molecular Orbital (MO) I in molecule A and is the natural spin orbital J of molecule B. It is immediately seen that at the Hartree-Fock level of theory, the self-similarity NOEL index Z_{AA} is equal to the number of electrons in a molecule. Computing the NOEL indices as in equation 7.8 is naturally very quick, since one needs only the MO overlap matrix between the molecules involved. This gives the NOEL index an important computational advantage over the MQSM in Equation 7.6. Up to now, the NOEL index has been mainly used to study the similarity between benzene and a small number of substituted benzene molecules, such as Aniline, Nitrobenzene, *etc.* and to study GammaAminoButyric Acid (GABA) agonists[127,129]. Cioslowski *et al.* also noted the apparent similarity between the NOEL index and the Polansky approach, but no in-depth analysis of the performance of the NOEL index for aromaticity has been performed thus far.

Our aim in this study is to explore the above close parallel of both approaches and to demonstrate that the appropriately defined NOEL index can indeed be used as a measure of aromaticity of individual benzenoid rings of a given PAH, in a similar way to the original Polansky index. For this purpose, it is necessary to modify the definition of the NOEL index to make it correspond as much as possible to the intended application. This requires, first of all, specifying how to characterise the density matrix of the fragment L in a PAH.

Several techniques could be proposed to do this, for example the Hirshfeld[71] procedure or the Atoms-In-Molecules (QCTA) approaches[85–87]. Although both are attractive schemes, they require substantial computational effort and are quite hard to use for the molecules that are presently used. Instead, we introduce an efficient procedure in which the fragment densities are obtained using Mulliken projection operators[130,131] Using this approach, the carbon C_6 (denoted L) backbone fragment

density matrices for a benzenoid ring in a molecule M can be obtained through the following projection operator:

$$\Pi_L = \sum_{\nu \in L} \sum_{\mu} S^{-1}_{\nu\mu} |\nu\rangle\langle\mu| \tag{7.9}$$

The summation, on the one hand, runs only over the basis functions on the benzenoid ring L and, on the other hand, all basis functions μ, located everywhere in the molecule. This allows us, within a single determinant wave function, as in Hartree-Fock and formally DFT, to obtain fragment density matrices in the molecule M, expressed as:

$$\rho^M_L(\boldsymbol{r}, \boldsymbol{r}') = \Pi_L \rho^M(\boldsymbol{r}, \boldsymbol{r}') = \left[\sum_{\nu \in L} \sum_{\mu} S^{-1}_{\nu\mu} |\nu(\boldsymbol{r})\rangle\langle\mu(\boldsymbol{r}')| \right] \sum_{\sigma\lambda} D^M_{\lambda\sigma} |\lambda(\boldsymbol{r})\rangle\langle\sigma(\boldsymbol{r}')| \tag{7.10}$$

where D^M is the charge and bond order matrix of molecule M. The fragment density matrix then becomes:

$$\rho^M_L(\boldsymbol{r}, \boldsymbol{r}') = \sum_{\nu \in L} \sum_{\sigma} D^M_{\nu\sigma} |\nu(\boldsymbol{r})\rangle\langle\sigma(\boldsymbol{r}')| \tag{7.11}$$

Using the above projection for both benzenoid ring fragments L and for the benzene carbon ring itself, the NOEL index $Z_{L,B}$ between two fragments can be obtained by the application of projector Π_L on the density matrix of the first molecule and Π_B for the C_6 ring in benzene. It then becomes clear that the similarity between the C_6 ring in the benzenoid ring L in molecule A, and that in benzene, B, is given by:

$$\text{NOEL}_{L,B} = Z_{L,B} = \sum_{IJ} n_{AI} n_{BJ} \langle \Pi_L \chi_{AI} | \Pi_B \chi_{BJ} \rangle \langle \chi_{AI} | \chi_{BJ} \rangle \tag{7.12}$$

Equation 7.12 allows a very efficient calculation of the similarity between the benzenoid ring L in the PAH and the pure benzene ring and it is also worth noting that it can be straightforwardly used also at the correlated post-Hartree-Fock level of theory. In connection with Equation 7.12, it is also interesting to note that for planar molecules considered in the present work, we can also distinguish between the σ and π density of the rings, so that separate σ and π components of the NOEL indices can be calculated as well. Such an additional partitioning can be especially useful just in our case, since it is widely recognised that the phenomenon of aromaticity is closely linked to the existence of delocalised π bonding.

7.1.2 Application to Polycyclic Aromatic Benzenoid Hydrocarbons

The algorithm described above was applied to a set of polycyclic aromatic benzenoid ring containing hydrocarbons (Table 7.1). This set comprises molecules from previous studies of Giambiagi *et al.*[122] and Polansky *et al.*[127] and adds several more molecules.

Table 7.1: Molecules contained in the studied set of PAHs. Roman numbers refer to the different symmetry-unique rings in the molecules.

	**1**	benzene
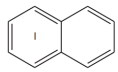	**2**	naphthalene
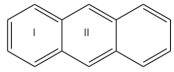	**3**	anthracene
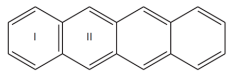	**4**	tetracene
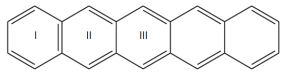	**5**	pentacene
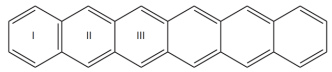	**6**	hexacene
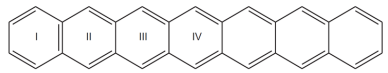	**7**	heptacene
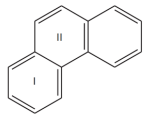	**8**	phenanthrene
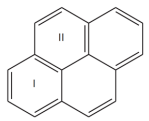	**9**	pyrene
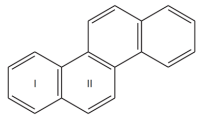	**10**	chrysene

Table 7.1 continued

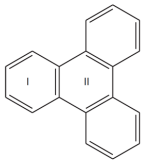	**11**	triphenylene
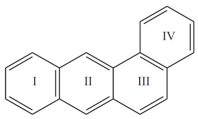	**12**	1,2-benzoanthracene
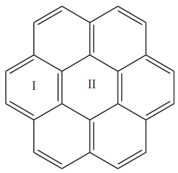	**13**	coronene
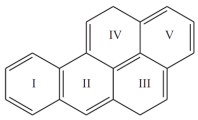	**14**	3,4-benzopyrene
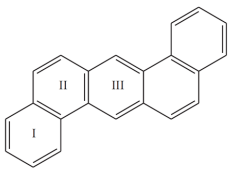	**15**	1,2,5,6-dibenzoanthracene
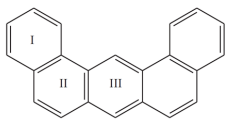	**16**	1,2,7,8-dibenzoanthracene
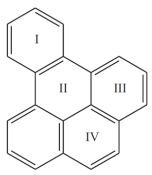	**17**	1,2-benzopyrene
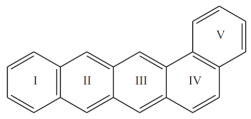	**18**	1,2-benzotetracene

Table 7.1 continued

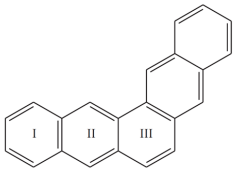

19 pentaphene

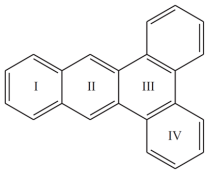

20 1,2,3,4-dibenzoanthracene

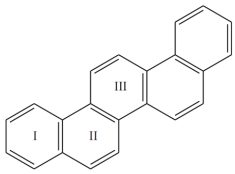

21 picene

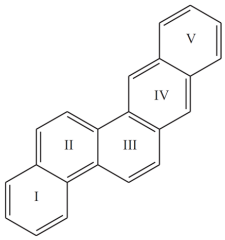

22 2,3,7,8-Dibenzophenanthrene

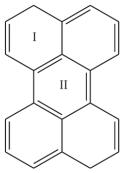

23 perylene

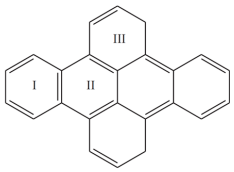

24 1,2-6,7-dibenzopyrene

Table 7.1 continued

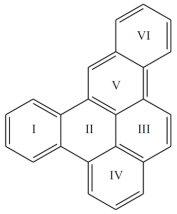

25 1,2-4,5-dibenzopyrene

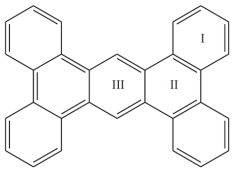

26 1,2-3,4-5,6-7,8-tetrabenzoanthracene

The symmetry unique rings in every molecule are labelled by Roman numerals for easy reference. For all molecules, the idealised carbon skeleton geometry was constructed first by combining the carbon rings of B3LYP/ 6-31G* optimised benzene. After having constructed the carbon skeleton of the PAH, the hydrogens were added as appropriate using idealised CH bond distances and assuming idealised CCH bond angles. In this approach, no geometry optimization was performed in order to retain as much correspondence to the classical Hückel approach as possible. The Hückel approach does not explicitly use a molecular geometry, but rather a topological matrix reflecting only the carbon-carbon primary bonding pattern. Yet, the assumption of equality of all α and β integrals in the Hückel method can be viewed as equivalent to using ideal benzene ring geometries. Once these geometries were constructed, Gaussian03[120] was used for calculation of charge and bond order matrices using the B3LYP[132–134] hybrid density functional and the 6-31G* basis set[135,136]. NOEL indices between a benzenoid ring in molecule M and the benzenoid ring of benzene were obtained using in-house written software, fully interfaced to Gaussian03. In addition to NOEL values and its components, Table 7.2 also presents the values of another recently proposed aromaticity measure, namely the Six-Centre Bond Index (SCI)[18]. This index is based on Generalised Population Analysis (GPA)[99], which allows quantification of multicentre bonding, even in difficult cases such as multicentre bonding in homoaromatic systems[137].

7.2 Results and Discussion

As said above, the main goal of this study is to demonstrate the applicability of the NOEL index (Equation 7.12) to the quantitative characterization of the aromaticity of individual benzenoid rings in PAHs. The calculated values of the NOEL index as well as its σ and π components are summarised in Table 7.2. The same table also contains the values of the original Polansky HMO similarity index and the values of Six-Centre Bond Indices (SCI)[18], which were recently proposed as a new measure of aromaticity[18].

Table 7.2: Aromaticity indices computed for the entire PAH set shown in Table 7.1

Comp. No.	Ring label	SCI	$P_{LB}.10^3$	Z_{LB}^{total}	Z_{LB}^{σ}	Z_{LB}^{π}
1	I	0.048	1000	35.082	29.082	6.000
2	I	0.026	912	34.404	28.692	5.712
3	I	0.022	893	34.339	28.695	5.644
3	II	0.017	840	33.778	28.287	5.491
4	I	0.020	888	34.314	28.697	5.617
4	II	0.015	825	33.731	28.287	5.443
5	I	0.020	886	34.302	28.697	5.605
5	II	0.014	821	33.713	28.289	5.423
5	III	0.013	811	33.689	28.287	5.402
6	I	0.019	888	34.297	28.697	5.600
6	II	0.014	824	33.704	28.289	5.415
6	III	0.013	816	33.674	28.289	5.385
7	I	0.019	885	34.295	28.697	5.598
7	II	0.014	819	33.700	28.289	5.411
7	III	0.012	806	33.667	28.289	5.377
7	IV	0.012	804	33.660	28.291	5.368
8	I	0.030	928	34.497	28.725	5.772
8	II	0.013	813	33.713	28.310	5.403

Comp. No.	Ring label	SCI	$P_{LB}.10^3$	Z_{LB}^{total}	Z_{LB}^{σ}	Z_{LB}^{π}
9	I	0.022	882	34.174	28.547	5.628
9	II	0.013	818	33.771	28.351	5.420
10	I	0.029	923	34.485	28.728	5.757
10	II	0.014	832	33.806	28.338	5.468
11	I	0.033	940	34.589	28.773	5.815
11	II	0.006	714	33.002	27.899	5.104
12	I	0.023	899	34.357	28.693	5.664
12	II	0.018	850	33.846	28.315	5.531
12	III	0.010	793	33.642	28.314	5.328
12	IV	0.031	930	34.516	28.730	5.785
13	I	0.016	837	33.884	28.403	5.481
13	II	0.007	753	33.232	27.987	5.245
14	I	0.026	913	34.447	28.726	5.721
14	II	0.011	795	33.501	28.139	5.361
14	III	0.011	802	33.714	28.355	5.359
14	IV	0.015	838	33.875	28.387	5.489
14	V	0.022	880	34.178	28.553	5.625
15	I	0.031	929	34.511	28.732	5.780
15	II	0.011	800	33.661	28.311	5.349
15	III	0.021	863	33.919	28.342	5.577
16	I	0.031	929	34.510	28.730	5.780
16	II	0.011	800	33.669	28.320	5.349
16	III	0.020	863	33.916	28.340	5.576
17	I	0.033	940	34.589	28.775	5.814
17	II	0.006	720	33.048	27.925	5.122
17	III	0.025	894	34.267	28.597	5.671
17	IV	0.013	818	33.769	28.359	5.410
18	I	0.021	890	34.325	28.697	5.628

Comp. No.	Ring label	SCI	$P_{LB}.10^3$	Z_{LB}^{total}	Z_{LB}^{σ}	Z_{LB}^{π}
18	II	0.016	829	33.740	28.285	5.455
18	III	0.016	834	33.790	28.314	5.475
18	IV	0.009	787	33.614	28.316	5.298
18	V	0.031	931	34.520	28.731	5.789
19	I	0.024	901	34.366	28.695	5.671
19	II	0.019	851	33.854	28.318	5.535
19	III	0.008	772	33.570	28.319	5.251
20	I	0.024	903	34.364	28.691	5.672
20	II	0.020	859	33.918	28.355	5.563
20	III	0.004	694	32.936	27.903	5.033
20	IV	0.034	942	34.603	28.780	5.823
21	I	0.029	924	34.490	28.730	5.760
21	II	0.014	827	33.793	28.341	5.452
21	III	0.017	850	33.897	28.365	5.532
22	I	0.028	922	34.478	28.728	5.750
22	II	0.015	836	33.828	28.343	5.486
22	III	0.011	812	33.736	28.342	5.394
22	IV	0.018	848	33.839	28.317	5.522
22	V	0.023	897	34.352	28.694	5.658
23	I	0.023	885	34.215	28.574	5.641
23	II	0.004	698	32.940	27.915	5.024
24	I	0.033	940	34.588	28.775	5.813
24	II	0.005	719	33.041	27.928	5.113
24	III	0.027	906	34.364	28.650	5.713
25	I	0.034	941	34.603	28.782	5.822
25	II	0.004	704	32.993	27.928	5.065
25	III	0.015	838	33.878	28.400	5.478
25	IV	0.024	891	34.268	28.605	5.663

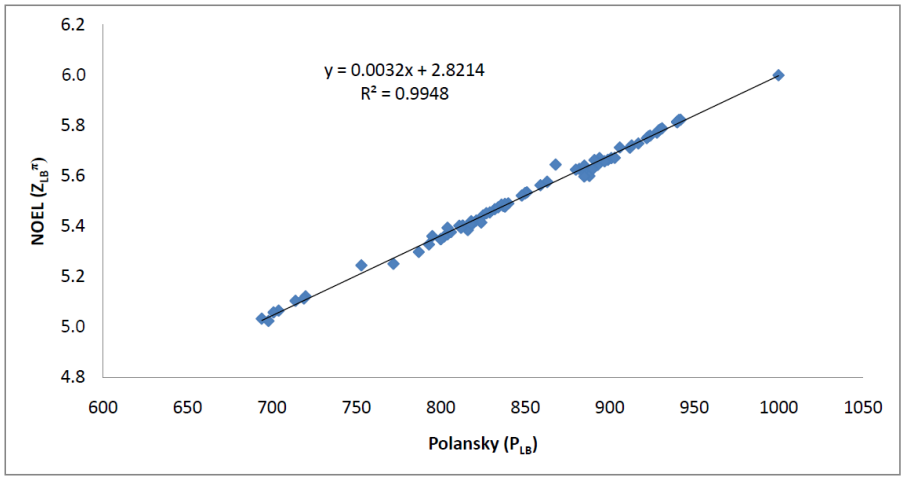

Figure 7.1: Correlation between the HMO Polansky index P_{LB} and the π component of NOEL Z_{LB}^{π} for the set of studied molecules.

Comp. No.	Ring label	SCI	$P_{LB}.10^3$	Z_{LB}^{total}	Z_{LB}^{σ}	Z_{LB}^{π}
25	V	0.012	804	33.574	28.180	5.394
25	VI	0.027	917	34.452	28.723	5.729
26	I	0.033	940	34.598	28.783	5.816
26	II	0.005	701	32.966	27.908	5.058
26	III	0.024	868	34.049	28.404	5.645

To demonstrate the applicability of the NOEL index as an aromaticity index, it is first shown that there is indeed a close parallel between the NOEL index and the similarity index previously introduced by Polansky and Derflinger[123] As the aromaticity of PAH is evidently due to the presence of an extended delocalised π system, it seems reasonable to assume that such a parallel can be best expected between the original HMO index (Equation 7.3), which is inherently based only on the π electron approximation, and the π component of the NOEL index Z_{LB}^{π}. The correlation between the corresponding quantities is displayed in Figure 7.1.

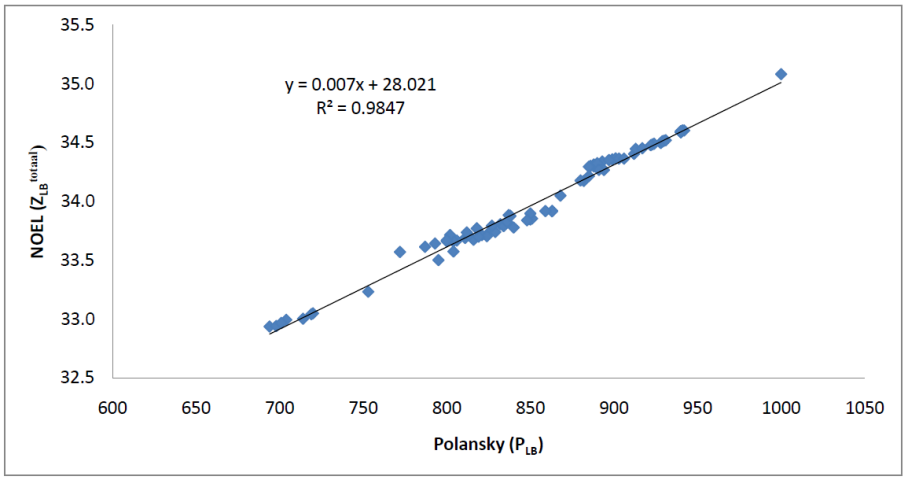

Figure 7.2: Correlation between Polansky indices P_{LB} and the NOEL index Z_{LB}^{total} total for the set of studied molecules.

As Figure 7.1 shows, the correlation is indeed very good. This result is very important since the existence of the correlation clearly implies that the parallel between both types of indices is indeed very deep. This is especially noteworthy since two quite different quantum chemical theories are used to calculate them, namely the HMO and DFT methods. This proves that the agreement between Equations 7.3 and 7.12 bears more than a conceptual similarity. In fact, the application of the Zero Differential Overlap approximation to equation 7.12 immediately leads to virtually the same expression as in equation 7.3. The existence of the nearly perfect correlation between both types of indices also implies that the present quantum similarity approach can indeed be considered as a generalization of the original Polansky approach beyond the scope of the HMO approximation. The only difference between the two types of indices is in the scaling. While the similarity of benzene to itself is characterised by the maximum value of the Polansky index 1, the NOEL index Z_{LB}^{π} is in this case equal to 6 (the number of overlapping π electrons between two benzene molecules). In all other cases, the values of both indices are smaller than the above limits and, in fact, the deviations of the actual values from these limits are just a measure of the extent of aromaticity of a given benzenoid ring in any particular case.

Although the existence of the nearly perfect correlation between the original Polansky index and the π component of NOEL is indeed encouraging, it was also interesting to see to what extent the parallel between both indices can be affected by

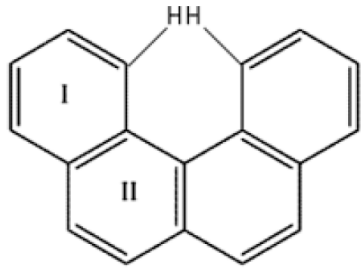

Figure 7.3: 3,4-benzophenanthrene with the two hydrogen atoms causing high steric strain.

also taking the σ component of NOEL into account. Intuitively, one can expect that because the aromaticity is primarily connected with π electrons, inclusion of electron densities of the σ carbon backbone will probably result in deterioration of the correlation. An example of the correlation of original Polansky indices with the NOEL index Z_{LB}^{total} is shown in Figure 7.2.

Although the existence of the parallel between Polansky and NOEL indices is still clearly evident, the quality of the correlation is indeed slightly lower than in the previous case. This result is, in fact, not too surprising since the σ component of the electron density considered in the NOEL can undoubtedly be affected by the steric strain, which in some molecules can result from the close approach of hydrogen atoms. An example of such a strained system can be, *e.g.*, the 3,4-benzophenanthrene (Figure 7.3) and indeed the point corresponding to ring I of this molecule represents an outlier in the correlation.

The extent of this strain is, of course, slightly overestimated in our case where the geometry of the carbon skeleton was forced to be planar; in a real molecule, the geometry optimization would release a part of this strain by allowing the system to deviate from the planarity. Besides the above discussed results, another interesting trend lies in the correlation between Z_{LB}^{π} and the Six Center Index (SCI). It was found previously[18] that there is a very good agreement between the SCI and the Polansky index. The same good agreement exists between the SCI and Z_{LB}^{π} . The latter correlation is depicted in Figure 7.4 with a logarithmic relationship. Such a logarithmic relationship is reminiscent of the Polansky-SCI correlation reported previously[18].

After having demonstrated the close parallel between the Polansky and NOEL indices, let us discuss the relation of the new index to the existing aromaticity measures and indices. For this purpose, we report the results of the statistical analysis aimed at revealing the eventual existence of the mutual correlation between various aromaticity measures and indices. In this study, such a comparison is performed between

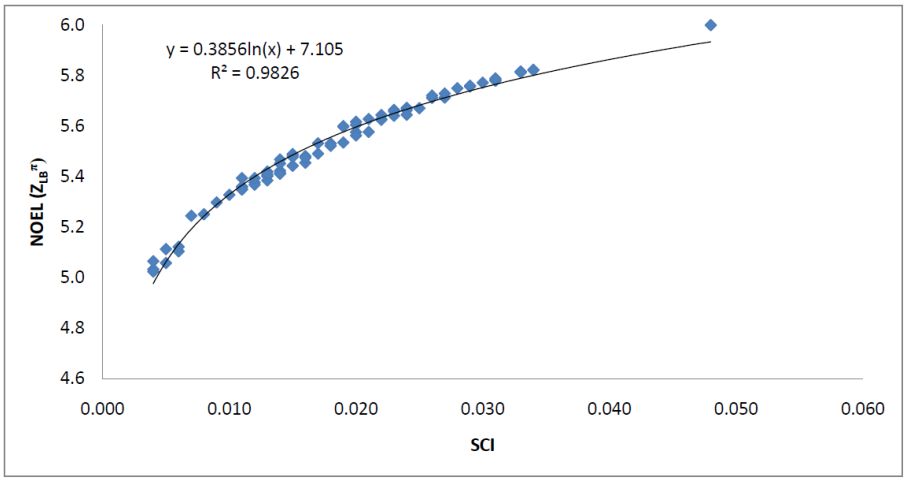

Figure 7.4: Correlation between Polansky indices P_{LB} and the NOEL index Z_{LB}^{total} total for the set of studied molecules.

NOEL and/or SCI and other aromaticity indices such as NICS, Average Two-centre Indices (ATI) and the Bond Order Index of Aromaticity (BOIA), whose values were calculated in the same way as described previously[18]. The Harmonic Oscillator Model of Aromaticity (HOMA), a structural criterion[2,33,34], was not considered in the present study since the use of fixed geometries would yield no differences between the different benzenoid rings.

Results of the mutual correlations of various aromaticity indices are summarised in Table 7.3, which shows the values of the corresponding correlation coefficients R^2.

As can be seen, very satisfactory correlations are observed not only between the NOEL index Z_{LB}^{π}, Polansky index P_{LB} and/or SCI, but a correlation of similar quality exists also with another structural aromaticity index BOIA (R^2 = 0.94). Slightly poorer is the correlation with ATI, which is an index related to another aromaticity index, namely the Para delocalisation Index (PDI)[45]. On the other hand, there is practically no correlation between Z_{LB}^{π} and NICS. This result is not too surprising. These indices represent, namely, two different types of aromaticity measures (structural *vs.* magnetic, *vide infra*). Summarizing the above results, it is possible to conclude that the correlation between Z_{LB}^{π} and the Polansky index clearly demonstrates that the quantum similarity based index serves as an *ab initio* generalization of the HMO based Polansky index. It also shows that the quantum similarity theory can be used as the method to quantify concepts such as aromaticity, as it was suggested by Giambiagi et al. in their earlier work[122].

Table 7.3: Correlation coefficients R^2 between different aromaticity indices for the PAH set. The values above the diagonal are calculated on the frozen geometries, while the values under the diagonal are for optimised geometries.

	SCI	P_{LB}	Z_{LB}^{total}	Z_{LB}^{σ}	Z_{LB}^{π}	NICS	ATI	BOIA
SCI	1.00	0.92	0.90	0.84	0.94	0.22	0.77	0.86
P_{LB}		1.00	0.98	0.93	0.99	0.33	0.77	0.92
Z_{LB}^{total}			1.00	0.98	0.97	0.27	0.70	0.85
Z_{LB}^{σ}				1.00	0.91	0.22	0.62	0.75
Z_{LB}^{π}					1.00	0.33	0.77	0.94
NICS						1.00	0.51	0.46
ATI						0.33	1.00	0.81
BOIA						0.46	0.81	1.00

7.3 Conclusions

The Polansky index, introduced in 1967, is based on assessing the similarity between benzenoid rings in polyaromatic hydrocarbons with benzene itself as a reference system. This approach applied the Hückel MO theory, which is nowadays considered to be less accurate. By using the quantum similarity theory, a new derivation has been proposed, allowing a generalization of the Polansky index to *ab initio* levels of theory. The similarity is now based on NOEL indices, which are shown to bear a high degree of similarity to the original index. The approach was applied to a set of polyaromatic hydrocarbons, for which the new NOEL indices were used to assess aromaticity. Excellent correlation is found with the Polansky index, especially when only the p electron density matrix is considered in the NOEL index. The NOEL index of aromaticity can be regarded as a novel quantum similarity based approach to aromaticity. NOEL indices can be computed very efficiently, since they only require the density matrices of two molecules and the overlap matrix between the basis functions of both molecules.

Chapter 8

Correlation between Delocalisation Indices and Magnetic Indices

8.1 Introduction

In the present chapter, the correlation is examined between two magnetic indices of aromaticity, namely the Nucleus Independent Chemical Shift (NICS) index[9,10] and ring current maps (RCM)[12,13], and an index based on the extent of electron delocalisation, the Multi Centre Bond Indices (MCBI). It is well-known that aromatic compounds exhibit special magnetic properties[2]. The most prominent effect is the occurrence of diatropic ring currents in aromatic molecules. These ring currents lie at the basis of the so-called Nucleus Independent Chemical Shift (NICS) index[9,10,107,108] (*vide supra*), used often to quantify (local) aromaticity. Ring currents arise under the presence of an external magnetic field and in turn cause an induced magnetic field. The nuclear shielding tensor σ is the negative proportionality factor between the electronically induced magnetic field, taken at the atomic position, and the externally applied one[106]. The NICS correspond to the negative of either the trace or some component, depending on the version of NICS used, of this tensor computed at some point in space (*vide supra*). In many cases, NICS and RCM lead

to similar conclusions, but for many polycyclic aromatic hydrocarbons (PAH) NICS can give unexpected results. One well known class of problematic cases is when bifurcated circuits arise[112–114].

One of the key features of aromaticity is that there needs to be a delocalised electronic system[2]. Many approaches have been published before on ways to measure this extent of electron delocalisation. Among these are the MCBI, the PDI (Para delocalisation Index)[8,45] and the FLU (fluctuation) indices[8,46]. In fact, the MCBI, PDI and FLU were all originally introduced as aromaticity indices, but there is an important distinction that should be kept in mind when using a delocalisation index to quantify aromaticity.

The distinction emerges when we examine the magnetic properties of an aromatic system. It has long been known that aromatic and antiaromatic systems sustain ring currents in the presence of a magnetic field. This forms the basis of the use of ring current (RC) maps[12,13] as an indicator of aromaticity and antiaromaticity. Both aromaticity and antiaromaticity imply a delocalised electronic structure, but a molecule could have a delocalised system, and still not show a ring current when exposed to a magnetic field. In a perturbation theory approach, the distribution and intensity of ring currents depends on the availability of virtual orbitals of appropriate symmetry[12,41,138]. In this sense, significant delocalisation is a necessary but not a sufficient condition for a ring current. Moreover, if a ring current does appear, the delocalisation index does not reveal information on its sense: diatropic aromatic and paratropic antiaromatic currents are both associated with delocalisation.

As mentioned above, aromaticity is often considered a multidimensional property[6,14–16]. This means that indices could, in principle, reflect the same general concept and still not correlate well mutually. Before accepting claims of multidimensionality, one needs to examine in detail the grounds for poor correlation between indices of aromaticity.

This chapter will investigate whether or not the multicentre indices and NICS and ring current maps can be reconciled. To do this, a large number of polycyclic aromatic hydrocarbons (PAH) are used. The reason for using these molecules is that they are known to be aromatic compounds, but the many different structures notably change the aromaticity of the individual rings, depending on their place in the molecule. There has already been quite some discussion of the performance of NICS for the quantification of local aromaticity in the PAHs, especially for the central rings of anthracene and other linear acenes[19,111,139–143]. NICS consistently make the central rings of linear acenes more aromatic than those on the outer edges of the acenes, and often make them more aromatic than benzene itself. Nevertheless, linear polyacenes are commonly known to become more reactive with an increasing number of rings and are known to be more reactive towards the inner rings, suggest-

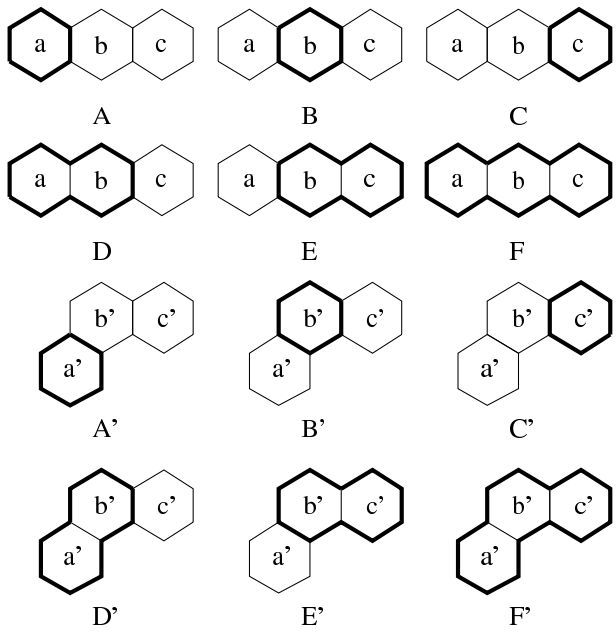

Figure 8.1: The different six-, ten-, and fourteen-centre circuits in anthracene and phenanthrene.

ing a decrease of aromatic character. The NICS-values, however, increase towards the inner rings, suggesting an increase in aromaticity, contradicting the experiment. Because of this contradiction the NICS data for the linear acenes have been met with scepticism[19,111,139,140], although according to Schleyer et al., one should not use chemical reactivity as an aromaticity criterion[143]. The SCI predicts a reverse trend in the local aromaticity of these rings[18,19,137]. This contradiction can be explained be due to the influence of different higher-order circuits on the NICS rather than the local (benzenoid) aromaticity alone[20]. In anthracene, for example, there are 3 of these higher-order aromatic circuits (D to F in figure 1) which could contribute to the NICS-value. The SCI on the other hand only describes the benzenoid aromaticity. In this chapter it will be shown that using the Multi Centre Bond Indices the NICS values can be broken up into the different six-, ten- and fourteen-centre contributions.

The problem of separating the contributions of different current paths has already been handled by some other research-groups. Anusooya et al. calculated the ring currents for polyacenes along different circulation paths, using the Pariser-Parr-Pople π-electron model[140]. Aihara et al. used topological resonance energies and bond resonance energies built on graph theory to calculate current density maps and the

contribution for different circuits in linear polyacenes[139]. In a different study, the same author presented the graph theoretical circuit resonance energies for all circuits of 10 PAHs and the current density maps obtained by superposing the currents of the individual circuits[144].

8.2 Computational Methods

In order to have a sufficiently wide set of data, 394 PAH molecules ranging from benzene, naphthalene, anthracene, phenanthrene to 104 benzenoids with four, five and six rings and 286 PAH built from seven and eight benzenoid rings were used. The molecular set contains a total of 2640 symmetry-unique rings. For practical reasons the set was divided in two subsets, one "smaller" set of 108 PAH molecules with one to six rings containing 493 symmetry-unique rings and a second, larger set of 286 PAH built from seven and eight benzenoid rings, containing 2147 symmetry unique rings.

For all PAH, the molecular geometries were constructed from Z-matrices with C-C bond lengths equal to 1.4 Å and C-H bond lengths equal to 1.1 Å . Bond angles and dihedral angles were frozen to standard values, so that the molecules are considered planar and the highest symmetry is obtained for all PAHs. For all 394 molecules the MCBI, NICS and RCM were computed using the pseudo-π method.

For the first set, the molecules were also optimised with the constraint of planarity. All optimizations were carried out at the B3LYP/6-311G** level using Gaussian-03.[120] For these molecules, NICS were evaluated for both the "frozen" and optimised geometries at the centres of the aromatic rings and 1 Å above the rings using B3LYP/6-311G**. For comparison the NICS were also computed using the pseudo-π method starting from the optimised geometry.

To determine the connection between MCBI and NICS, the smaller set of 108 PAH was used to study the correlation. To test the results, the correlation was subsequently evaluated using the remaining 286 PAH built from seven and eight benzenoid rings.

Multicentre indices were computed using the in home developed Kekule program which is linked to Gaussian-03[120] via the formatted checkpoint file of the latter. As will be shown below, multicentre indices were computed for the benzenoid circuits containing six atoms (SCI), naphthalene like circuits containing 10 atoms (TCI) and 14-membered circuits either with all three rings in a linear sequence (FCI-a) or in an angular sequence (FCI-b) (Fig 8.1).

For the study of correlations between the NICS and multicentre indices, the ARTE-QSAR program was used[145]. This program allows deriving regressions and

correlations with main focus on the statistical validity and allows to establish the domain of applicability of the regressions found.

The MCBI-current maps and full ring current maps were calculated and compared for all 394 PAH. As mentioned, the molecules were taken to be in ideal geometries, with a uniform C-C bond length of 1.4 Å. Previous studies have shown that optimization of the molecular structure has only a minor influence on calculated values of ring current and MCBI. Calculation of RCMs used the SYSMO program[146].

To summarise:

	108 PAH	286 PAH
Pseudo-π-MCBI/FRO	X	X
Pseudo-π-MCBI/OPT	X	-
Pseudo-π-RCM/FRO	X	X
Pseudo-π-RCM/OPT	-	-
Pseudo-π-NICS/FRO	X	X
Pseudo-π-NICS/OPT	X	-
NICS/FRO	X	-
NICS/OPT	X	-

8.3 Multidimensionality of delocalisation indices and Nucleus Independent Chemical Shifts

The purpose of the work in the present section is to examine the correlation between General Population Analysis (GPA) based multicentre indices on the one hand and NICS on the other hand. As will be reported below, there is no significant correlation. The second aim is then to study in detail the correlation and to examine whether there exists also a local version of the above mentioned mulidimensionality. The lack of correlation is then explained by purely chemical reasoning. After the hypothesis has been developed, an in-depth statistical study is made to see whether the hypothesis is supported quantitatively.

8.3.1 Non-local contributions to the NICS

Having calculated the NICS and multicentre aromaticity indices for all molecules, it is worth examining the correlation between both sets of indices. The correlation coefficiënt amounts only 38 %. Figure 8.2 shows the predicted NICS, based on the SCI alone on the one hand and the actual, computed NICS on the other. The predicted NICS are obtained by the regression equation between the actual NICS and the SCI. This may be seen as a confirmation of the multidimensional nature of aromaticity.

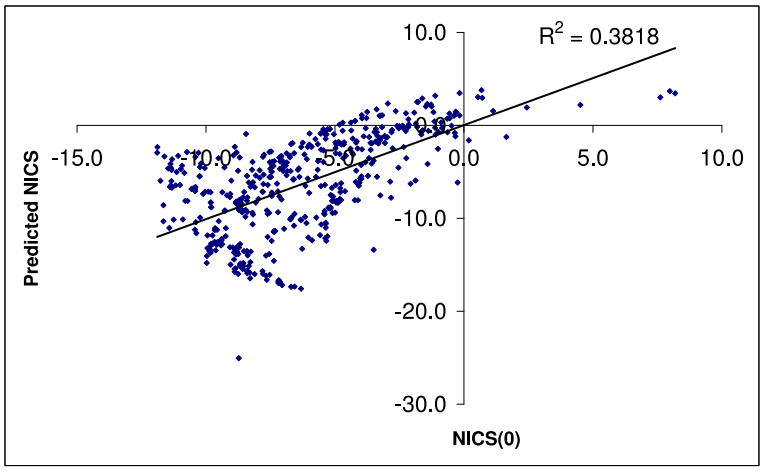

Figure 8.2: The regression between the NICS(0) and the NICS(0) predicted by the SCI-values.

Yet, merely observing this fact is not sufficient as such a poor correlation can indicate nothing but a total failure of the aromaticity concept.

The situation, however, is not so drastic. It has been reported before that in some cases there is no divergence between the NICS and MCBI. As an example, Bultinck et al. found that for homo-aromatic systems, there is a good correlation between NICS and multicentre indices and that these regressions are equally valid for classical five membered aromatic molecules such as thiophene, pyrrole,... [137] The lack of correlation thus apparently appears when molecules contain several aromatic rings[18]. This is in line with observations by Stanger et al.[111] or Solà and co-workers[17,147,148].

Turning back to ring currents, it is well-known that one can consider different circuits as contributors to the total ring current[139,144]. As an example, anthracene contains 6 different aromatic circuits (Figure 8.1). Three of them correspond to benzenoid circuits, two to naphthalene like circuits and one circuit that follows the edge of the entire molecule. The ring current $j(\mathbf{r})$in every point in the molecule can be considered as arising from the different circuits[11]. In anthracene, using the notation used in figure 8.1, one can write:

$$\begin{aligned} j(\mathbf{r}) &= j_A(\mathbf{r}) + j_B(\mathbf{r}) + j_C(\mathbf{r}) + \\ & \quad j_D(\mathbf{r}) + j_E(\mathbf{r}) + \\ & \quad j_F(\mathbf{r}) \end{aligned} \tag{8.1}$$

The proposed use of NICS as a local aromaticity criterion for a specific benzenoid

ring would rely implicitly on the assumption that for example on the centre of the ring A, the contributions from circuits B-F would be zero or cancel completely. Such cancellation is not guaranteed at all. As has been stated before by Bultinck et al., the more negative NICS value in the centre of the inner ring may very well be due to the fact that this point is encircled by more aromatic circuits, rather than that $j_B(\mathbf{r}_B) > j_A(\mathbf{r}_A)$[20].

Analogous to equation 8.1, one could suggest also that the NICS computed at a certain point originates from all circuits in a molecule, or:

$$\begin{aligned} \text{NICS}(\mathbf{r}) &= \text{NICS}_A(\mathbf{r}) + \text{NICS}_B(\mathbf{r}) + \text{NICS}_C(\mathbf{r}) + \\ &\quad \text{NICS}_D(\mathbf{r}) + \text{NICS}_E(\mathbf{r}) + \\ &\quad \text{NICS}_F(\mathbf{r}) \end{aligned} \tag{8.2}$$

Given the fact that the NICS indices for single ring molecules seem to usually correlate quite well with the multicentre index for the ring involved[137], one could suggest the following hypothesis. Suppose that for each circuit one has a similar correlation between the NICS contribution and the multicentre index for that circuit. For example in anthracene (Figure 8.1), this supposes :

$$\text{NICS}_A(\mathbf{r}) \sim \text{SCI}_A \tag{8.3}$$
$$\text{NICS}_D(\mathbf{r}) \sim \text{TCI}_D \tag{8.4}$$
$$\text{NICS}_F(\mathbf{r}) \sim (\text{FCI-a})_F \tag{8.5}$$

Then the total NICS at the centre of some ring X could be written in terms of the SCI, TCI, FCI-a and FCI-b encircling this ring via a linear relationship:

$$\text{NICS}(\mathbf{r}_\text{X}) = a\text{SCI} + b\sum_j \text{TCI}_j + c\sum_k \text{FCI-a}_k + d\sum_l \text{FCI-b}_l + \text{C}^{\text{te}} \tag{8.6}$$

In this regression line, the summations are limited to only those rings that effectively encircle the centre of the ring X. This means that contributions from other circuits more distant from the ring centre are not considered. As Schleyer et al. have shown, these are indeed quite small and thus can be neglected in the regression above[143][1].

FCI-a and FCI-b are the 14-centre indices in the linear sequence and the angular sequence respectively (F and F' in Fig 8.1). One might, however, postulate that since the linear and angular FCI are both indices for 14-centre-delocalisations, they should have an equal contribution to the NICS. Separating the anthracene and the phenanthrene circuit might then just be an unnecessary degree of freedom in the

[1]The effect of other circuits will, however, be the subject of further study later in this Chapter

model. In this line of thought one could take the sum of the FCI-a and FCI-b and treat it as a total FCI.Using this approach, equation 8.6 can be rewritten as:

$$\mathrm{NICS}(\mathbf{r}_\mathrm{x}) = a\mathrm{SCI} + b\sum_j \mathrm{TCI}_j + c\sum_k (\mathrm{FCI\text{-}a}_k + \mathrm{FCI\text{-}b}_k) + \mathrm{C}^{\mathrm{te}} \tag{8.7}$$

Both approaches will be studied throughout the following section.

8.3.2 Statistical verification

Using the NICS and multicentre index data obtained from the pseudo-π calculations, the linear regression from equation 8.6 was performed. In a first step, frozen geometries were used. This constraint will be released later in the study.

For any statistical model, first it should be checked what is the Topliss ratio of the regression[149], this is the ratio of the number of molecules over the number of selected descriptors. In the present application, 3 or 4 regression coefficients are used. This gives a very favourable Topliss ratio as there are 496 data points. This means that for every coefficient there are more than 100 data points. As a reference for the quality of this ratio, one can mention that the European Union guidelines for good QSAR practice recommend Topliss ratios of at least 5 and preferably 8[150].

The NICS were fitted to the SCI, TCI and FCI using equation 8.6, and the constants a, b, c and d were calculated. This was done for the NICS(0), NICS(1), the $\mathrm{NICS_{zz}}(0)$, the $\mathrm{NICS_{zz}}(1)$, the PP-NICS and the PP-$\mathrm{NICS_{zz}}$ on the ideal frozen geometries, and for the PP-NICS and the PP-$\mathrm{NICS_{zz}}$ on the optimised planar geometries. The R^2 values between the different NICS-values and the NICS predicted by the models are presented in Table 8.1. All values show a significant correlation coefficient around 0.84 and above. When comparing the two methods there is only a slight improvement seen when taking the FCI-a and FCI-b as separate descriptors. Apparently in each model the NICS values and the PP-$\mathrm{NICS_{zz}}$ values are equally well correlated with the values obtained by the linear relation of the multicentre-indices. The pseudo-π-values seem to be better predictable than the classical NICS. This might be due to a better one-to-one correspondence with the actual π-electron delocalisation, by elimination of the σ-framework. The PP-$\mathrm{NICS_{zz}}$ values predicted by both models, compared to the actual value for some common PAH's (Fig 8.3) are shown in Table 8.2 and 8.3.

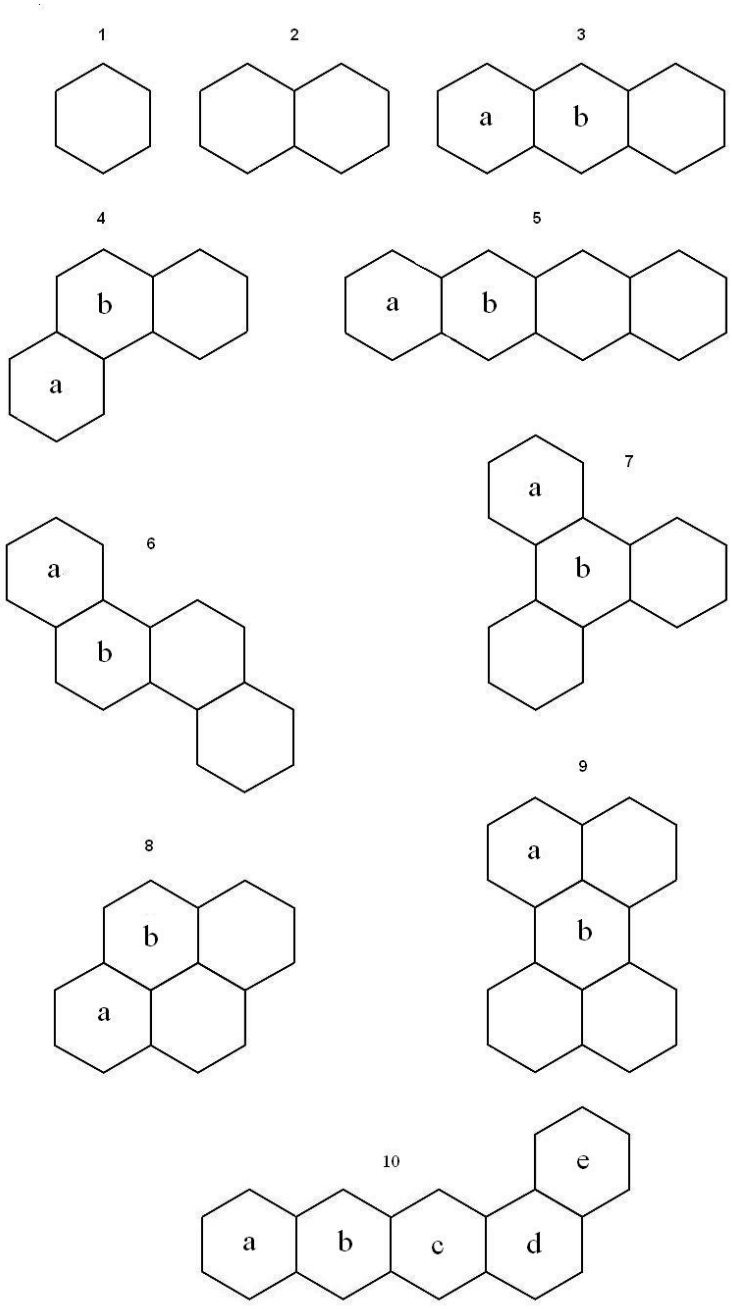

Figure 8.3: Some common PAH, included in this study. Only the σ-framework is shown.

Table 8.1: The R^2 and q^2 values between the different NICS-values and the NICS predicted by the models with FCI-a and FCI-b contributions separately and together (FCI). FRO indicates that the values have been calculated on frozen geometries, OPT that they have been calculated on optimised geometries.

R^2 (q^2)	FCI-a and FCI-b	FCI
NICS(0)/FRO	0.862 (0.860)	0.847 (0.845)
NICS(1)/FRO	0.857 (0.854)	0.839 (0.837)
$NICS_{zz}$(0)/FRO	0.862 (0.859)	0.836 (0.834)
$NICS_{zz}$(1)/FRO	0.857 (0.855)	0.837 (0.835)
PP-NICS/FRO	0.906 (0.905)	0.891 (0.890)
PP-$NICS_{zz}$/FRO	0.902 (0.900)	0.885 (0.884)
PP-NICS/OPT	**0.922 (0.921)**	**0.896 (0.894)**
PP-$NICS_{zz}$/OPT	**0.916 (0.915)**	**0.887 (0.886)**

Table 8.2: The PP-NICS$_{zz}$ value predicted by the model, the different contributions (SCC=Six Centre Contribution, TCC=Ten Centre Contribution and FCC=Fourteen Centre Contribution) to this value and its actual value for the model with FCI-a and FCI-b contributions separate (St-E is the standard error on the Model-PP-NICS$_{zz}$).

Molecule	Ring	PP-NICS$_{zz}$	SCC	TCC	FCC-a	FCC-b	Model-PP-NICS$_{zz}$	St-E
1		-41.21	-70.28	-	-	-	-47.60	± 1.38
2		-40.34	-38.43	-26.91	-	-	-42.66	± 1.79
3	a	-36.90	-29.59	-17.46	-18.49	-	-42.86	± 2.05
	b	-46.99	-26.90	-34.91	-18.49	-	-57.62	± 2.59
4	a	-41.07	-46.10	-12.41	-	-10.95	-46.78	± 1.94
	b	-29.11	-17.56	-24.82	-	-10.95	-30.66	± 1.92
5	a	-34.16	-26.12	-14.21	-13.34	-	-30.99	± 1.69
	b	-46.83	-22.67	-27.18	-26.68	-	-53.86	± 2.59
6	a	-40.82	-43.78	-15.73	-	-5.35	-42.18	± 1.75
	b	-32.47	-22.10	-21.85	-	-10.71	-31.98	± 1.88
7	a	-38.94	-51.08	-5.34	-	-9.11	-42.85	± 1.70
	b	-15.10	-7.90	-16.01	-	-13.67	-14.90	± 1.61
8	a	-49.27	-36.75	-19.29	-	-18.52	-51.88	± 2.39
	b	-20.98	-17.41	-21.56	-	-9.26	-25.55	± 1.73
9	a	-33.41	-34.73	-22.56	-0.87	-0.73	-36.21	± 1.66
	b	20.64	-5.39	-7.23	-1.74	-1.46	6.85	± 0.76
10	a	-35.55	-27.62	-15.42	-14.43	-	-34.80	± 1.80
	b	-47.28	-24.17	-29.23	-19.94	-	-50.65	± 2.42
	c	-43.17	-23.70	-19.66	-19.94	-5.14	-45.76	± 2.33
	d	-18.43	-11.44	-13.58	-5.51	-5.14	-12.99	± 1.39
	e	-39.87	-49.31	-7.72	-	-5.14	-39.50	± 1.56
Average			49.90%	31.30%	8.10%	10.70%		± 1.69

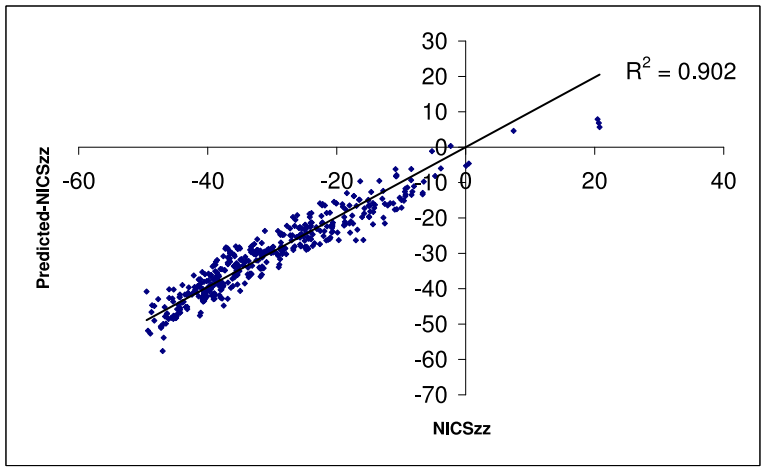

Figure 8.4: The regression between the ab initio computed PP-NICS$_{zz}$ and the PP-NICS$_{zz}$-values obtained by regression, treating the FCI-a and FCI-b separate. The correlation depicted is based on frozen geometries. The correlation with optimised geometries has $R^2 = 0.916$.

From these values it is clear that the trend and magnitude of the NICS are predicted quite well by the models. The mean absolute difference between the actual PP-NICS$_{zz}$ values and the ones given by the models for all 496 symmetry unique rings is around 2.9 ppm. The comparison of these 496 PP-NICS$_{zz}$ values with the ones obtained by both models are shown graphically in figures 8.4 and 8.5.

The very favourable correlation is manifest if compared to the predicted PP-NICS based on only the SCI (Figure 8.2).

Using the linear model one can assess the magnitude of the different contributions to the NICS. One might expect the six-centre contribution (SCC) to the NICS to be the largest, followed by the ten-centre contribution (TCC) and the fourteen-centre contribution (FCC). The different contributions to the PP-NICS$_{zz}$ values within the models are also given in Table 8.2 and 8.3. When examining the different contributions to the NICS one has to bear in mind that the model-NICS is not just the sum of the six-, ten-, and fourteen-centre contributions (SCC, TCC, FCC), but that there is still the constant in equation 7 which is around 23 ppm. By looking at the contributions for the different members of the NICS-family it was found that, as expected, the SCC is the largest, with an average of about 50% of the total sum of the SCC, TCC and FCC, followed by the TCC with about 32% and finally the FCC with about 18% of the total. In those models where the FCI-a and the FCI-b circuit are treated separately an average of about 9% was found for both circuits. As it seems that larger

Table 8.3: The PP-NICS$_{zz}$ value predicted by the model, the different contributions (SCC=Six Centre Contribution, TCC=Ten Centre Contribution and FCC=Fourteen Centre Contribution) to this value and its actual value for the model with FCI-a and FCI-b contributions together (FCC) (St-E is the standard error on the Model-PP-NICS$_{zz}$).

Molecule	Ring	PP-NICS$_{zz}$	SCC	TCC	FCC	Model-PP-NICS$_{zz}$	St-E
1		-41.21	-68.96	-	-	-45.80	± 1.98
2		-40.34	-37.70	-28.75	-	-43.29	± 2.40
3	a	-36.90	-29.03	-18.65	-14.29	-38.81	± 2.66
	b	-46.99	-26.39	-37.31	-14.29	-54.83	± 3.20
4	a	-41.07	-45.23	-13.26	-12.66	-47.99	± 2.55
	b	-29.11	-17.23	-26.52	-12.66	-33.25	± 2.53
5	a	-34.16	-25.62	-15.18	-10.31	-27.96	± 2.30
	b	-46.83	-22.25	-29.04	-20.62	-48.75	± 3.19
6	a	-40.82	-42.95	-16.80	-6.19	-42.79	± 2.36
	b	-32.47	-21.69	-23.35	-12.38	-34.25	± 2.49
7	a	-38.94	-50.12	-5.70	-10.53	-43.20	± 2.30
	b	-15.10	-7.75	-17.10	-15.80	-17.50	± 2.21
8	a	-49.27	-36.06	-20.62	-21.41	-54.92	± 3.00
	b	-20.98	-17.08	-23.04	-10.70	-27.66	± 2.34
9	a	-33.41	-34.07	-24.10	-1.52	-36.53	± 2.26
	b	20.64	-5.29	-7.73	-3.03	7.11	± 1.37
10	a	-35.55	-27.11	-16.47	-11.15	-31.57	± 2.40
	b	-47.28	-23.71	-31.23	-15.41	-47.19	± 3.02
	c	-43.17	-23.25	-21.01	-21.35	-42.45	± 2.94
	d	-18.43	-11.23	-14.51	-10.20	-12.77	± 1.99
	e	-39.87	-48.39	-8.25	-5.94	-39.42	± 2.17
Average			48.50%	33.10%	18.40%		± 2.30

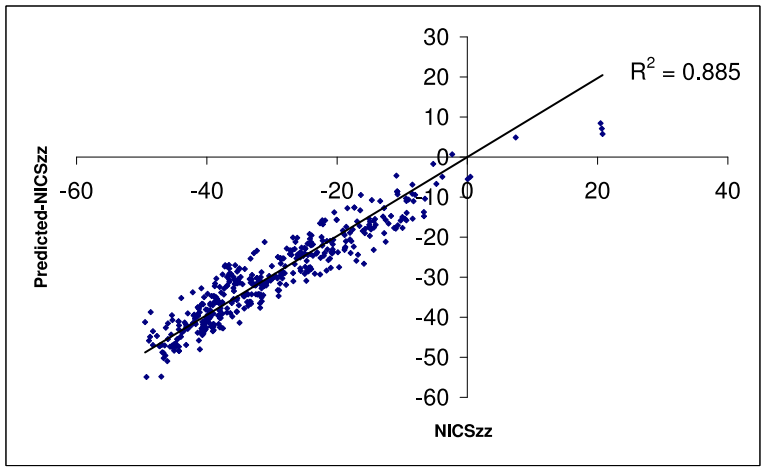

Figure 8.5: The regression between the ab initio computed PP-NICS$_{zz}$ and the PP-NICS$_{zz}$-values obtained by regression, treating the FCI-a and FCI-b together. The correlation depicted is based on frozen geometries. The correlation with optimised geometries has R^2 = 0.887.

circuits have a continuously lowering impact on the predicted NICS, one can expect that higher order circuits have even smaller contributions to the NICS. This is coherent with the fact that for larger polyacenes, the NICS values seem to converge to a limit value rather than to increase continuously.

Of course, statistical models should be substantiated by more than just correlation coefficients. A t-test reveals that all regression coefficients are indeed relevant, as their values are outside the range]-2;+2[. The F-test at the 0.95 confidence level for the significance of the total number of coefficients used is quite high, showing that the correlation reported is causal rather than fortuitous. As an internal validation, the leave-many-out procedure was carried out. In this procedure 40 points where left out from the derivation of the model. The coefficients of equation 8.6 were determined with the remaining molecules. Using these coefficients, the value of the 40 points was predicted and the R^2 between the predicted and the actual NICS value was determined. This was done 100.000 times and the leave-many-out q^2 is computed. This value was found to be virtually equal to the R^2 indicating again a very meaningful correlation. It is gratifying that both for frozen geometries and optimised geometries the R^2 and q^2 are very similar, even with slightly higher values when using optimised geometries. As an alternative internal validation, the NICS values of all rings were randomly permuted 1000 times and a statistical model, including the determination of the q^2, was developed after every permutation. The R^2 and q^2 for all permutations

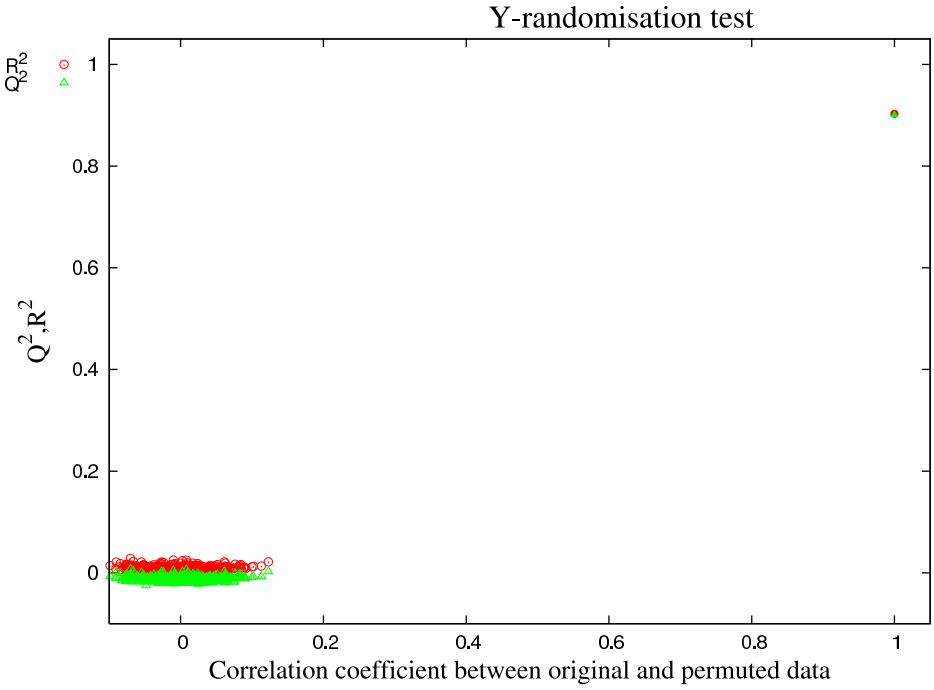

Figure 8.6: The q^2 (green) and R^2 (red) values for the PP-$NICS_{zz}$ after random permutation the NICS of all rings, compared to the q^2 and R^2 value of the original model.

of the PP-NICS$_{zz}$ is reported in figure 8.6. This figure clearly shows again that the model reported above stands out of the other 1000 models. These figures are almost identical for all investigated NICS-values.

8.3.3 Meaning of the local aromaticity concept

The question naturally arises on what information is conceptually contained in the value of multicentre indices and NICS. The local aromaticity concept was previously discussed in detail[18–21,151] and the present findings confirm that some of the multidimensionality arises not *per se* from multidimensionality but may also arise from the diffuseness of the definition of aromaticity and local aromaticity a fortiori.

NICS as a local aromaticity index may be seen to reflect at a chosen point all ring currents in the molecule. So when there are several circuits in a molecule, all of these will contribute to the NICS computed in some chosen point. NICS can not be used to assess a degree of benzenoid character for a specific ring in a PAH, as they not solely contain the ring current of the benzenoid circuit.

On the other hand, multicentre indices allow to reveal the degree of aromaticity in a certain circuit. Depending on the size of the circuit, an index can be computed allowing to compare its degree of aromaticity to another ring of the same size. Optionally, a normalization can be performed which allows even comparing rings of different sizes[152].

So both indices reflect inherently different views of local aromaticity. It is very interesting to mention again that, indeed, if only one circuit is present, there are good correlations between both indices[137]. Obviously, it would be very interesting if NICS could be dissected in the different circuit contributions schematically introduced in equation 8.6. No such procedure exists at the *ab initio* level, unfortunately. Aihara and co-workers[139,144], as well as Anusooya et al.[140] did derive such a graph theoretical procedure and independently from us characterised the strength of different circuits in PAH via circuit specific ring currents or circuit resonance energies. Bultinck et al. have recently shown how extremely tight correlations are found between these dissected NICS and ring current intensities on the one hand and multicentre indices on the other hand[20]. This provides strong arguments to show how the above regression may be considered chemically very meaningful.

Still, there may obviously appear cases where NICS show no correlation with the set of multicentre indices. In such cases, it will again proof very interesting to investigate the grounds for such a lack of adherence to the model. Such cases can be anticipated whenever the NICS approach is likely to produce results not in line with ring current maps. This is the case in e.g., bifurcated circuits[113,114]. By the fact that NICS concentrate all ring current information in a single number at an arbitrarily

chosen point, one is bound to lose quite a lot of information[153]. It is not possible to extract from NICS again the ring current information. As a consequence, ring current maps are far superior to the NICS, this is why the correlation between ring current maps and multicentre indices is being discussed in the next section.

8.4 Correlation of delocalisation indices and current-density maps

In order to establish whether RCM and multicentre indices can also be reconciled, in the present work we develop a method for extracting approximate maps from the multicentre indices and compare them to the *ab initio* maps for a very large set of PAH. The main aim of the present study is thus to assess whether RCM and multicentre indices lead to the same chemical conclusions, thereby reducing the need for a "multidimensional character" of aromaticity.

8.4.1 Method

In the present section, using the constants a, b and c of equation 8.7, approximate RCM have been derived from the Multi Centre Bond Indices. Such approximate maps will be denoted as MCBI-RCM in what follows. To obtain the maps, the values of the SCI were projected as vectors on the bonds of the benzenoid ring in a diatropic manner. In this method, the SCI-vectors of two neighbouring benzenoid rings partially cancel (or strengthen) each other on their common bond. The same was done for the ten-, and fourteen-centre indices (TCI, FCI). For the fourteen-centre indices, anthracene- and phenanthrene-like circuits (F and F$'$ in figure 8.1 respectively) were calculated and used with equal weight to construct one fourteen-centre vector set. The parameters obtained from the regression in equation 8.7[118] were used as weighting factors to scale and then sum the SCI-, TCI- and FCI-vector maps to construct the final MCBI-RCM. Both the MCBI-current maps and full ring current maps were calculated and compared for 394 PAH, constructed from one to seven benzenoid rings. The molecules were taken to be in ideal geometries, with a uniform C-C bond length of 1.4 Å. As many of the PAH are quite large molecules, the pseudo-π technique was used.

8.4.2 Results and discussion

Using the methods described above, RCMs and MCBI-RCMs were computed for the entire range of PAH. In order to study the relation between both types of RCMs and to document the good agreement between them, this section presents a detailed discussion of several specific cases, including some known to be difficult in terms of correlation between aromaticity indices.

Linear polyacenes

Local aromaticity within linear polyacenes is a major point of interest in recent literature[19,111,139–143]. According to some indices, such as NICS, the central rings of linear polyacenes are the most aromatic, whereas other indices, such as SCI, predict the reverse[18,19]. From chemical reactivity, one would also conclude that the central ring is the least aromatic. As there is divergence in views already for a simple molecule like anthracene, reconciliation of NICS and MCBI data might seem a hopeless task. Nevertheless, in the previous section it was shown that the main reason for this apparent disagreement between indices arises from different views of local aromaticity[118]. A NICS value computed for a single point does not reflect solely the current in the six-centre ring encircling this point, but contains significant contributions from other encircling circuits. The MCBI for a specific circuit is by definition related to that circuit alone, and influenced only indirectly by other circuits via the charge and bond order matrix.

Figure 8.7 shows how the MCBI-RCM for a linear polyacene can be constructed in a step-wise fashion for anthracene. Figure 8.7a shows the MCBI-RCM obtained from only the SCI of all three rings. As the SCI is slightly smaller for the central ring than for the outer rings, the MCBI-RC is slightly stronger in the outer rings, but already correctly shows the concentration of ring current on the perimeter. Introduction of TCI and then FCI, gives maps 8.7b-8.7c, which show significant changes with respect to 8.7a. Finally, figure 8.7d shows the *ab initio* computed RCM. Clearly, this directly computed map is in very good agreement with that constructed from 6,10 and 14-centre indices (8.7c).

This indicates that SCI results and RCM do not contradict, but rather reflect two different factors. When RCM are inspected or NICS data examined, one is inclined to attach a degree of local aromaticity to a specific ring by applying a 3-D condensation scheme to “cut” the entire map into pieces. This decomposition is spatially, rather than graph-theoretically based, and the connection is with rings rather than circuits. MCBI, on the other hand, directly reflect individual graph circuits. It is gratifying that both approaches can be reconciled. It is not so much that local aromaticity has multidimensional character as that it can be viewed in two different ways. The

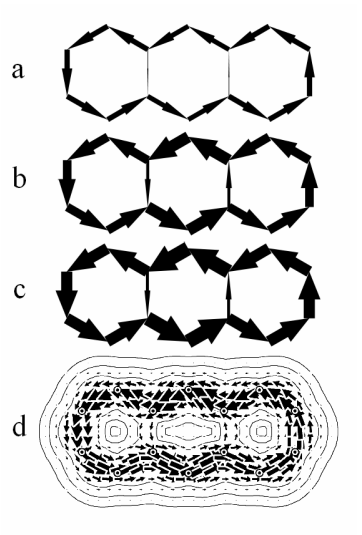

Figure 8.7: The step-wise build-up of the MCBI-RCM for anthracene

spatial decomposition picture has the advantage of "what you see is what you get" approaches, but the circuit picture is also well defined. Choice between the different pictures is more a matter of taste than an objective question.

The RCMs and MCBI-RCMs for the linear acenes are shown in figure 8.8. In all cases, in both the RCM and MCBI-RCM the current increases towards the central rings, implying a higher NICS value, but not because of an intrinsically larger SCI value for the middle ring, but because of the higher number of circuits.

In both RCM and MCBI-RCM the maximum current on the inner rings appears to converge to a limit with system size. This trend is also found in the NICS values of these systems, and gives support to the conclusion drawn by the author above[118] and to the observations of Randić[154] that the influence of higher order circuits becomes less important in the energetics and other properties for increasingly larger circuits. This implies that both NICS and ring currents can be modelled accurately using the MCBI with circuits of sizes up to fourteen.

Kinked polyacenes

Figure 8.9 shows maps for phenanthrene and triphenylene as typical examples of nonlinear PAH. In these molecules there is a larger difference in SCI between inner and outer rings, but TCI and FCI are smaller than in anthracene, which causes a

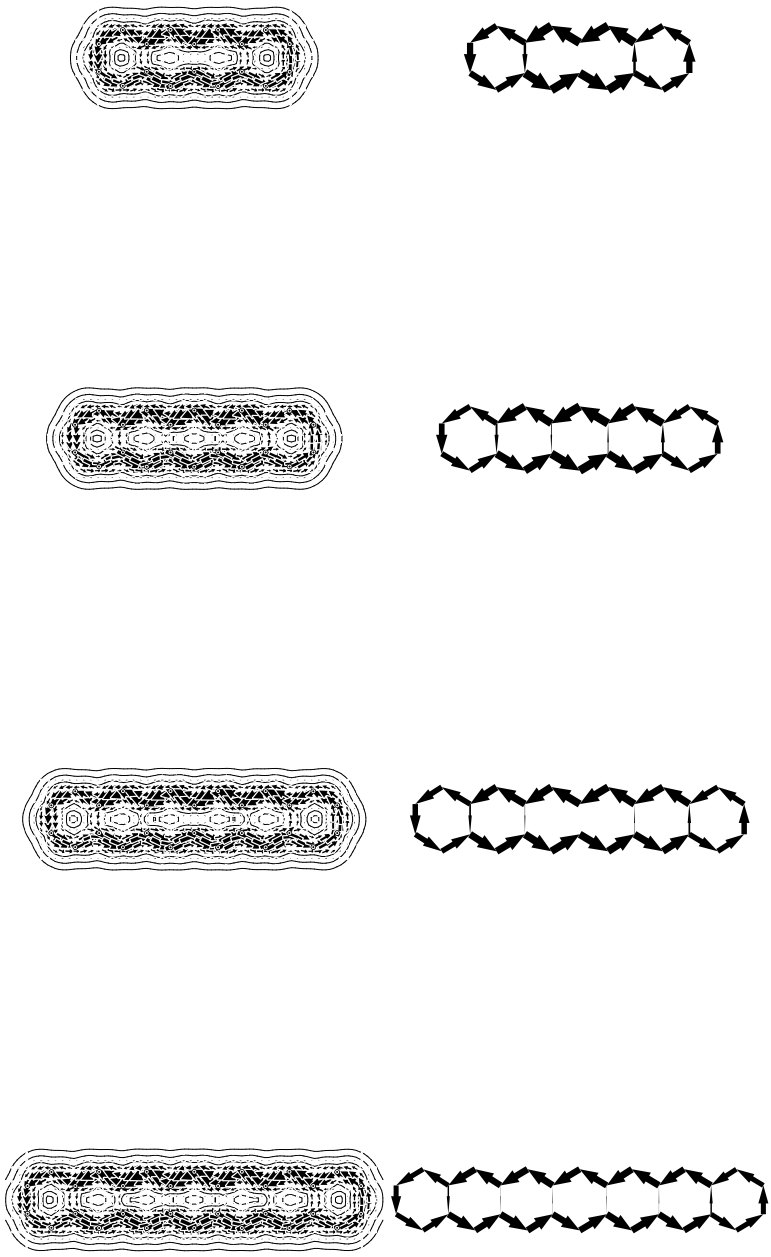

Figure 8.8: RCM and MCBI-RCM for the linear acenes tetracene to heptacene.

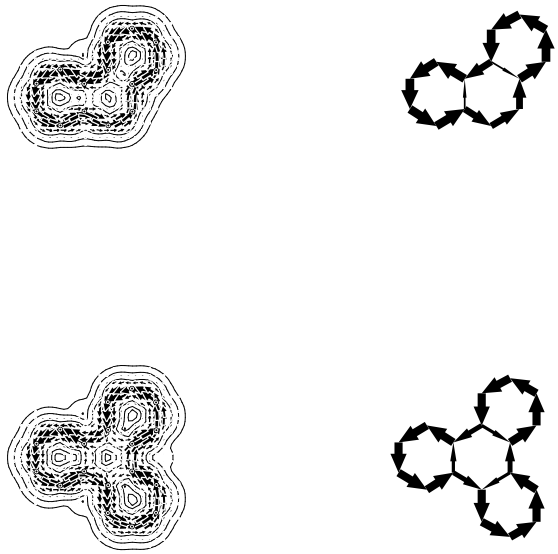

Figure 8.9: RCM and MCBI-RCM for the kinked acenes phenanthrene and triphenylene.

change in the balance of currents. Although the dominant current is on the central ring in anthracene, it is on the outer rings of phenanthrene and triphenylene. This change leads to a distinct pattern of current on the inner ring, with an alternation of para- and diatropic senses. These cases illustrate that reduction of RCM information to a single number can lose the subtleties of the physical phenomenon. NICS would characterise the middle rings of these polyacenes as aromatic, whereas the full current pattern will only be revealed by the full RCM or in the MCBI-RCM.

Pyrene

Figure 8.10 shows maps for pyrene. The main current runs on the periphery and only two outer rings have closed circulations. The RCM shows how to interpret the NICS values for the four rings: NISC(0) is -11.65 ppm for the outer and -4.65 ppm for the inner rings. The ‘aromatic’ value for the outer ring and non-aromatic value for the

Figure 8.10: RCM and MCBI-RCM for pyrene.

inner ring reflect the respective closed and open nature of the currents. Most of the current in pyrene is running along the periphery, and NICS exaggerates the difference between the two rings. It is not clear that the inner rings can be termed aromatic in any significant sense.

Perylene and Dibenzo[cd,lm]perylene

The ring current pattern of perylene shows two distinct naphthalene-like circuits and the current on the bonds connecting the two naphthalene substructures is essentially zero (figure 8.11). The same pattern is seen in the MCBI-RCM. The NICS of the inner ring is positive (NICS(0)=8,19 ppm), induced by the naphthalene-like circuits above and below the central ring. The inner ring can hardly be seen as anti-aromatic, as its positive NICS value (8,19 ppm) would indicate, it is essentially an empty ring, flanked by two diatropic naphthalene circuits (NICS(0)=-5,10 ppm) .

With two more hexagonal rings fused to the naphthalene-like rings, the structure is that of dibenzo[cd,lm]perylene or peropyrene. This molecule shows a completely different ring current pattern. The two strong naphthalene circuits are lost, and replaced by a strong current on the periphery, which runs through the outer bonds of the middle hexagon. The three non-naphtalenoid hexagons all support diatropic ring currents, in addition to the strong perimeter current. The MCBI-RCM accurately reproduces this same ring current pattern.

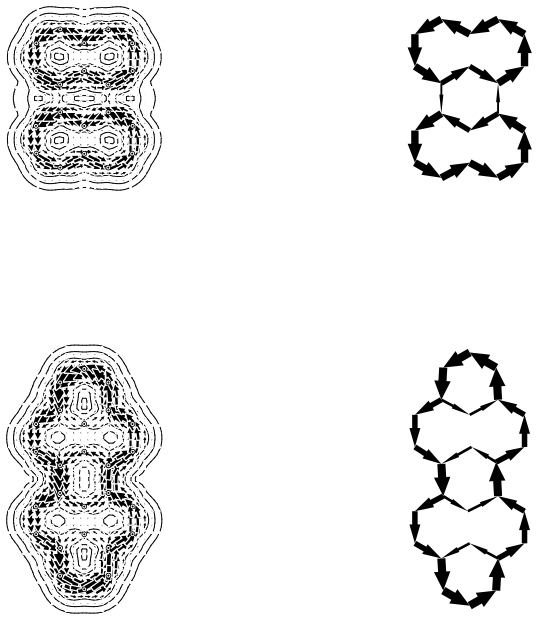

Figure 8.11: RCM and MCBI-RCM for perylene and dibenzo[cd,lm]perylene.

Figure 8.12: RCM and MCBI-RCM for anthanthrene.

Anthanthrene

Typical "hard cases" for which NICS and other aromaticity indices fail are those of molecules which contain bifurcated rings[112–114]. An example of such a molecule is anthanthrene, which has two bifurcated corner-rings, as seen in the maps of figure 8.12 (the upper right and lower left corners). These corner rings are neither aromatic nor anti-aromatic, but the NICS(0) value of -1,81 ppm for these rings assign a questionable quantitative measure of aromaticity, whose sign is determined only by the side on which the strongest current happens to run. A correct physical picture is given only by the RCM and MCBI-RCM, which shows the bifurcation.

Periphery-only currents

Ring-current maps for some PAH show no current in the centre of the molecules, but an entirely peripheral current. This is the case for the benzo[cd]pyrene anion and triangulene, shown in figure 8.13. It is gratifying to see that, although the SCI values of the benzenoid rings vary (figure 8.14), upon addition of the different circuits the MCBI-RCM is able to recover the emptiness of the interior of these molecules. Once again, the NICS reduction of the RCM to a single value for each ring does not lead to the conclusion of the single peripheral current, exhibited in both RCM and MCBI-RCM.

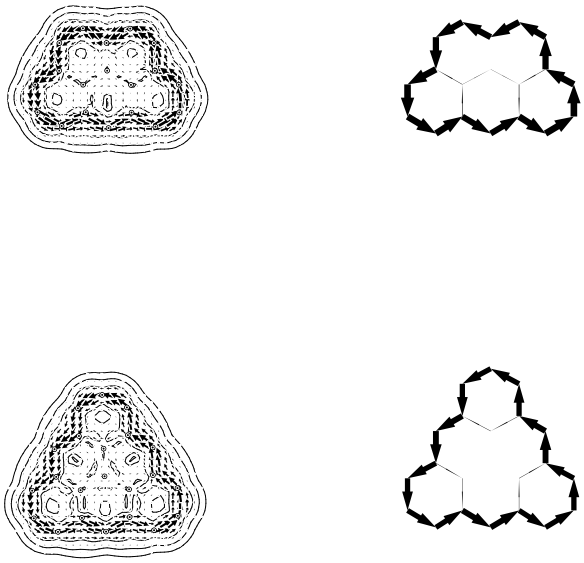

Figure 8.13: RCM and MCBI-RCM for benzo[cd]pyrene anion and triangulene.

Figure 8.14: SCI values for benzo[cd]pyrene anion and triangulene, expressed in terms of the percentages of benzene value.

Benzo[ghi]perylene and coronene

Benzo[ghi]perylene (figure 8.15) is a molecule that is closely related to coronene, but lacks one hexagonal ring. Because of this gap, the central ring of the molecule does not have a closed paratropic current as in coronene. Only five of the six bonds have a current in the paratropic sense. The inner ring is not classifiable as purely anti-aromatic, as only the (RC or MCBI-RC) maps show. Only three rings, in meta positions on the middle ring, have a full diatropic current. These are the sites of the sextets in the Clar electronic structure of this molecule. This distribution is consistent with the SCI, which has larger values on these positions (figure 8.16), favouring a diatropic current. The ring current on the middle ring also alternates in intensity, showing a larger current in the bonds fused to the Clar rings.

For coronene, the MCBI-RCM reproduces the well known current map with a large diatropic current on the edge of the molecule and a small paratropic current around the middle ring. The genesis of this current pattern is already seen in the SCI map, where the outer benzenoid rings have larger delocalisation than the inner (figure 8.16).

Applicability of the MCBI-method

As the above examples show, Multi Centre Bond Indices contain the information necessary for the prediction of current density maps in PAH. Formally, the Multi Centre Bond Indices quantify the delocalisation of the π-electron cloud within a chosen circuit, whereas the RCM refers to the response of the molecule to a magnetic field. The agreement of MCBI-RCM and RCM suggests that the forces in the electrons for the different circuits are at least approximately proportional to the respective Multi Centre Bond Indices .

Having established that the RCM and MCBI-RCM give similar results, it is appropriate to comment on the range of applicability of MCBI as an aromaticity index. As noted earlier, the MCBI reflects delocalisation. All the circuits in the PAH are aromatic in nature, and the MCBI relates to the aromaticity, but it is possible to imagine cases where such simple reasoning could conceivably fail, e.g. rings of other sizes or heterocyclic systems. There are difficulties in applying the pseudo-π model to heterocyclic systems[155] and it would be necessary to make further checks on the agreement between MCBI-RCMs and RCMs.

The Ring Current model allows quantitative comparison of currents by calculation of the flux of the current through planes cutting bonds, although this is quantity is not immediately evident in the usual pictorial presentation. Relative sizes of the longest arrows in ring current maps can also be used to compare to a standard, e.g. the benzene π-current at a hight of one Bohr. The MCBI-RCM essentially assigns a

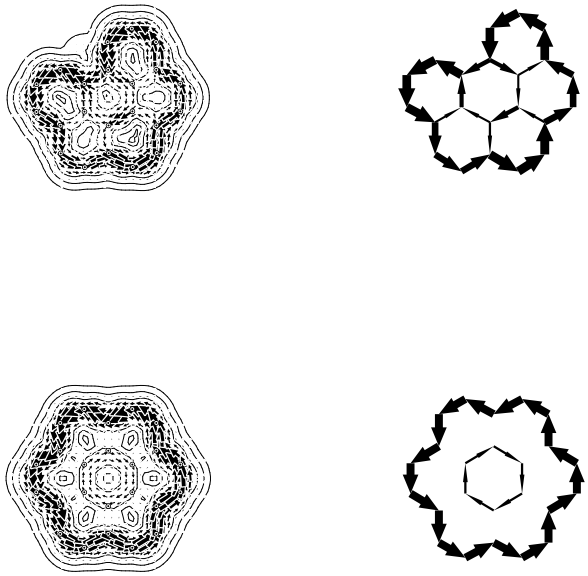

Figure 8.15: RCM and MCBI-RCM for benzo[ghi]perylene and coronene.

Figure 8.16: SCI maps for benzo[ghi]perylene and coronene, expressed in terms of the percentages of benzene value.

numerical value to each bond, which can easily be used for comparison and provides a useful link between RCM, NICS and delocalisation.

The Multidimensional character of aromaticity

The present results show that the MCBI and RCM can be reconciled in a chemically intuitive way. In the previous section it has been shown that using the same reasoning can be used to explain the discrepancies between NICS and the MCBI. Since there is a good correlation between the MCBI and some other local aromaticity indices like the Polansky index[121,123] (*vide supra*), the same correlations will be true for these indices, and in general it is expected that the above reasoning can be used to reconcile any delocalisation index with the magnetic indices. The claimed multidimensionality of aromaticity is in these cases a product of the multidimensional view on aromaticity, without any intrinsic discrepancies between these views. The multidimensionality is just a product of looking at different things, without trying to find the commonalities between the different descriptors. In this work, the RCM reflect all circuits and MCBI reflect local circuits. By making the proper combination of the delocalisation indices for different circuits, the RCM picture can easily be found.

Since all aromaticity indices should represent the same physical reality and are all derived from its same mathematical formulation, the wave function, these indices, as judges of aromaticity, should always come to concurring opinions, the same conclusions using a different reasoning, but never to dissenting opinions, which is the rationale behind the multidimensionality. In the present work we have shown that the MCBI and the RCM do come to such a concurring opinion on aromaticity for a large set of PAHs.

8.5 Multidimensionality of Delocalisation Indices and Nucleus Independent Chemical Shifts II: Proof of Further Non-Locality.

The previous sections have shown that the lack of correlation between especially MCBI and NICS is not due to the multidimensional character, but rather due to the fact that they reflect different phenomena. Through statistical analysis it was shown that for a large set of PAH, the NICS values can be derived from MCBI, refuting the need to invoke a local analogue of the multidimensionality of aromaticity. It was

also shown that ring current maps derived from MCBI, agree very well with *ab initio* computed ring current maps[118,156,157] and thus that MCBI delocalisation indices and Ring Current Maps (RCM) can also be reconciled using a similar reasoning. Approximate Ring Current maps have been constructed from the MCBI and these MCBI-current maps and the *ab initio* ring current maps were calculated and compared for 394 PAH and they were visually confirmed to be the same for all molecules. The results prove that the MCBI contain the necessary information for the prediction of current density maps in PAH.

In the present section we further study the non-local contributions to the NICS by testing the correlation between the MCBI and the NICS using the method in equation 8.7[158]. In the previous section the correlation was derived using 108 PAH, containing 493 symmetry unique rings. In this study a much larger set of 286 PAH, containing 2640 symmetry unique rings is used. This larger test set reveals that the results of NICS and the MCBI for some specific rings can not be reconciled using this method. We show that the problem lies in the non-local character of the NICS. Furthermore the results prove that including this non-local character of the NICS in the model, using the MCBI-vector maps mentioned above, explains the difference between the NICS and MCBI for the problematic rings. The significance of including circuits other than the benzene, naphthalene, anthracene- and phenanthrene-like is also examined.

8.5.1 Results and discussion

Using the constants a to d in equation 8.7, obtained from a set of 108 PAH, the $NICS_{zz}$ of the test set of 286 PAH were predicted using the same equation. The $NICS_{zz}$ versus the Predicted-$NICS_{zz}$ for all 394 molecules of the fitting and test set together are shown in Figure 8.17.

The majority of the rings is well predicted and the R^2 is 0.884. However, the method fails to predict some rings with positive NICS values. The NICS of the cluster of points in the upper right corner (green) in figure 8.17 is predicted too low. These points correspond to the central ring of perylene-like fragments in the PAH (figure 8.18(a)). The points in the lower right quadrant (orange) are predicted with the wrong sign. These points correspond to the central rings of benzo[ghi]perylene fragments in the molecules (figure 8.18(b)). The red point corresponds to the central ring of coronene (figure 8.18(c)) whose NICS is dramatically underestimated using the method. The poor prediction of the NICS for these rings using this model is in contrast to the fact that the MCBI-ring current maps of these molecules are indistinguishable from the *ab initio* Ring Current calculations on these molecules[156]. The SCI values of the individual rings reveal the reason for the poor agreement with the

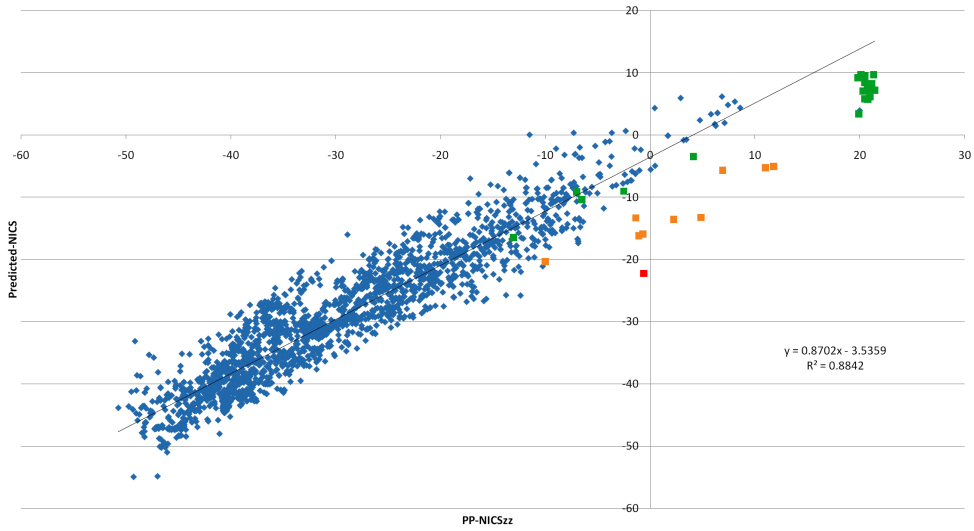

Figure 8.17: The $NICS_{zz}$ versus the Predicted-$NICS_{zz}$ for 394 PAH using equation 8.7

NICS. In all these cases the central ring is surrounded by benzenoid rings with a much higher six centre delocalisation (Figure 8.18). In perylene the delocalisation in the central ring is very small, whereas the two top and bottom rings have higher delocalisation values. In the RCM and MCBI-RCM this results two distinct naphthalene-like circuits and the current on the bonds connecting these two naphthalene substructures is essentially zero[156]. The NICS of the inner ring is positive, not because of the delocalisation in this central ring, but because of the higher delocalisation in the neighbouring rings. The NICS of the inner ring is induced by the naphthalene-like circuits above and below the central ring, but it is essentially an empty ring, flanked by two diatropic naphthalene circuits. Similarly in benzo[ghi]perylene and coronene the paratropic current in the central ring is a consequence of the difference in benzenoid delocalisation between the central and the outer rings, where the outer rings overpower the inner one.

With this observation in mind, one can attempt to prove the existence of these non-local effects on the NICS statistically by changing the model in such a way that it takes these effects into account. This can be done by constructing the SCI, TCI and FCI vector maps as described before (Figure 8.19a and 8.19b) and by taking the average of the values of the vectors around the benzenoid ring to a new SCI, TCI or FCI value for each ring . This is done by summing the SCI,TCI of FCI values of the vectors which run in a diatropic manner around the benzenoid ring and by subtracting the values of the paratropic vectors of the ring (and dividing by 6)(Figure 8.19c). In

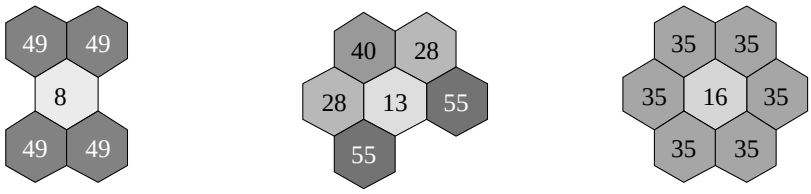

(a) (b) (c)

Figure 8.18: SCI values for perylene(a), benzo[ghi]perylene(b) and coronene(c), expressed in percentages of the benzene value

the example of triphenylene (Figure 8.19), the SCI value of the outer rings is 73% of the value of benzene. The SCI of the inner ring is 11%, so the value of the vector on the common bond becomes 73-11=62%, running diatropic as seen from the outer ring. The average of the vectors is taken, which gives 71.2% $((5 \times 73 + 62)/6)$ for the outer ring and -25.5 $((3 \times 11 - 3 \times 62)/6)$ for the inner ring. These new SCI, TCI and FCI values are now corrected for the effect of (partial) cancellation that the delocalisations in the neighbouring rings have on the current density. Introducing these 'corrected' SCI, TCI and FCI in equation 8.7 should result in a closer correlation with the NICS values. The constants a to d where again obtained using the fitting set of 108 PAH and subsequently tested on the test set of 286 PAH. The $NICS_{zz}$ versus the predicted-$NICS_{zz}$ using this method for all 394 molecules are shown in Figure 8.20.

Using this method, which will be called the vector method from here on, the R^2 increases from 0.88 to 0.94. Moreover the central rings of benzo-[ghi]perylene fragments (orange) have the right sign and the central ring of perylene-like fragments (green) are better predicted (Figure 8.20). These findings show that the vector-model predicts the NICS better than the much simpler model of equation 8.7. This proves that the NICS value is not only influenced by the higher-order circuits encircling the ring, but also by the local aromaticity of the surrounding rings. The NICS for the central ring of coronene however changes from underestimated to overestimated, with a predicted value of 16.60 ppm instead of the *ab initio* -0.60 ppm.

To get a better agreement between the MCBI-predicted NICS and the *ab initio* NICS, one possibly needs to consider more delocalisation circuits. The current model only uses benzene-, naphthalene, anthracene- and phenanthrene-like indices. However many of the PAH also contain phenalene-like twelve-centre circuits and pyrene-like fourteen-centre circuits which are not accounted for in the models de-

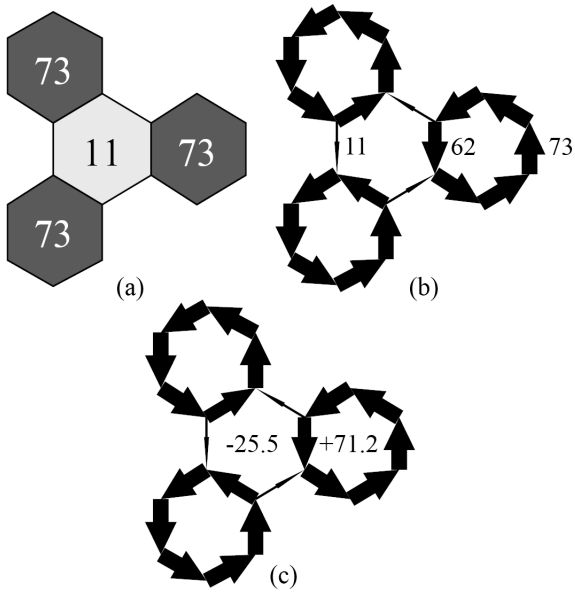

Figure 8.19: The construction of the new SCI values using the vector method of triphenylene. (a) The values of the SCI of the rings, expressed in terms of the percentages of benzene value. (b) The SCI projected as vectors on the bonds of the benzenoid ring in a diatropic manner. The SCI values of the neighbouring rings partially cancel each other on the common bonds (c) The values of the vectors running in a diatropic manner around the benzenoid ring are summed, the paratropic vectors are subtracted and the value is divided by six to form the new SCI.

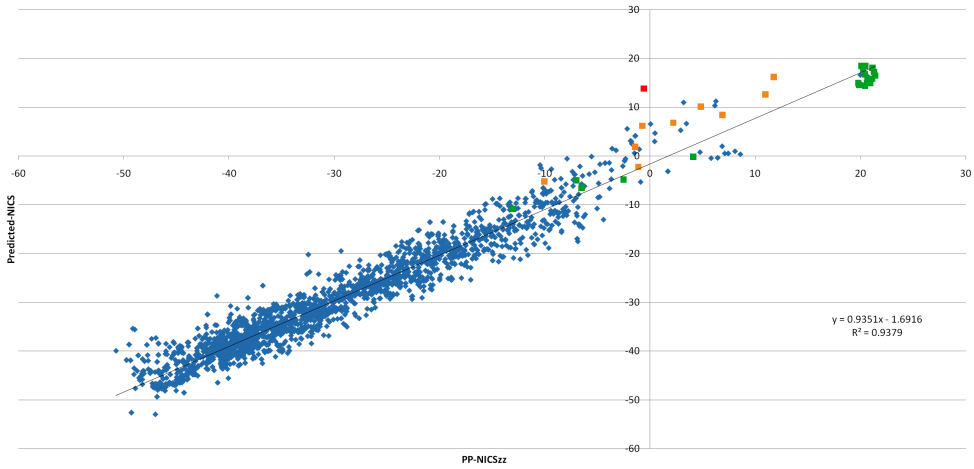

Figure 8.20: The $NICS_{zz}$ versus the Predicted-$NICS_{zz}$ for 394 PAH using the vector method

scribed above, but might contribute to the NICS in a similar fashion. To see whether these twelve- and fourteen-centre circuits have an effect on the NICS, the indices were calculated on all molecules and the above vector-model was reconstructed using a six, ten-, twelve-, and fourteen-centre vector map, where the pyrene-like circuit was summed together with the anthracene- and phenanthrene-circuits to one fourteen-centre vector map. This summation to one map is based on the previous finding that separating the anthracene- and phenanthrene-circuits does not improve the model significantly[118]. We wish to avoid introducing too many variables, resulting in more flexibility in the model than can physically be justified. Inclusion of even higher-order circuits could also be considered, however, since it has been shown that the influence of the circuit becomes smaller with increasing number of centres[118] and keeping the increasing computational cost in mind, only circuits up to fourteen centres were considered in this study.

The results for the vector-method including the phenalene-like twelve- and pyrene-like fourteen-centre circuits are shown in Figure 8.21. These results are again obtained by fitting the model 108 PAH and subsequently using the model for the set of 286 PAH. The immediate observation is that the introduction of the two extra circuits does not change the previous findings. There is no drastic change in the correlation or in the appearance of the graph. The NICS for the central ring of coronene remains overestimated, although there is a small correction in the right direction from 16.60 ppm to 12.03 ppm. The introduction of the twelve-centre vector map is however statistically verified as significant. The t-test reveals a 99.95 % certainty that the

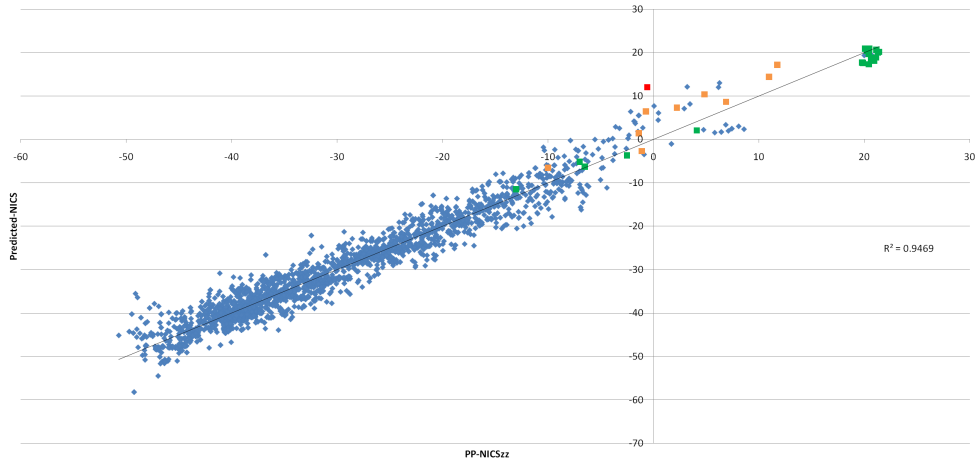

Figure 8.21: The $NICS_{zz}$ versus the Predicted-$NICS_{zz}$ for 394 PAH using the vector method, including the phenalene-like twelve-centre and pyrene-like fourteen-centre circuits

twelve-centre vector map has a significant contribution. The small effect on the results is primarily due to the absence of a twelve-centre circuit in many of the PAH and the small effect the circuit has on the total NICS. The average weight of the twelve-centre circuit for the total NICS value is only 2.1% . An interesting observation is that the twelve-centre delocalisation contributes in a paratropic fashion to the NICS, whereas all other circuits give diatropic contributions. This suggests that the 4N+2 rule is also applicable to the delocalisation indices, where (4N+2)- and 4N-membered circuits contribute in a diatropic and paratropic manner, respectively.

Turning back to coronene, the current adaptations to the model fail to describe the NICS of the central ring, although it has already been shown that the MCBI-ring current map of this molecule is indistinguishable from the full Ring Current calculation[156]. The MCBI-ring current map of coronene (Figure 8.22) reveals the possible problem. The paratropic current on the central ring is rather small compared to the outer diatropic current. In the vector-method used until now, only the vectors on the benzenoid ring at which the NICS is evaluated are used, while other vectors farther from the ring are neglected. Using the continuous set of gauge transformations[37,159,160], the effect of the ring current ($\boldsymbol{J}(\boldsymbol{r})$) to the zz-component of the shielding tensor ($\sigma_{zz}(\boldsymbol{r}_X)$) is proportional to $\times \boldsymbol{r}_X/|\boldsymbol{r}-\boldsymbol{r}_X|^3$ (see equations 5.45 and 5.46):

$$\sigma_{zz}(\boldsymbol{r}_X) = -\frac{1}{Bc}\int \left\{(\boldsymbol{r}-\boldsymbol{r}_X)\times \boldsymbol{J}_Z^{(1)}(\boldsymbol{r})\right\}_z /|\boldsymbol{r}-\boldsymbol{r}_X|^3 d\boldsymbol{r} \qquad (8.8)$$

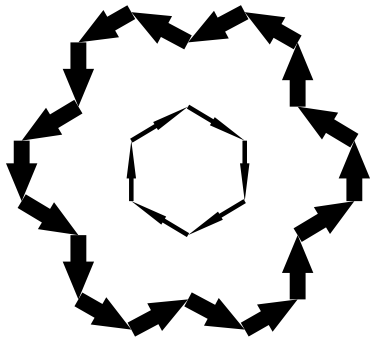

Figure 8.22: The MCBI-ring current map of coronene.

Where $\boldsymbol{J}_Z^{(1)}(\boldsymbol{r})$ the first-order electronic current density induced by a magnetic field along the Z axis. The z-subscript after the brackets surrounding the vector product means that only the z-component of this product is taken. The effect of vectors farther from the ring thus diminishes roughly by $1/|\boldsymbol{r} - \boldsymbol{r}_X|^2$, which justifies neglecting the vectors farther from the ring. In the case of coronene however, the outer current is so strong it can not be neglected for calculating the NICS of the central ring. The fact that only the vectors on the central ring were used is responsible for overestimating the NICS value. The answer to the correct prediction of the central ring of coronene might thus lie in including all vectors of the molecule into the model.

Since the total ring current can be considered as composed of contributions from different circuits[139,144,161] (equation 8.1) and as the contribution from a given N-centre circuit (NC) to the current density ($\boldsymbol{J}_Z(\boldsymbol{r}; NC)$) is proportional to the MCBI for the circuit NC , $\boldsymbol{J}_Z(\boldsymbol{AB}; NC)$ can be approximated by the MCBI projected as a vector in a diatropic manner on the bond between atoms A and B ($\boldsymbol{MCBI}(\boldsymbol{AB}; NC)$), thus:

$$\boldsymbol{J}_Z(\boldsymbol{AB}; NC) \sim \boldsymbol{MCBI}(\boldsymbol{AB}; NC) \tag{8.9}$$

The total ring current can be written in terms of the MCBI-vectors as:

$$\begin{aligned} \boldsymbol{J}_Z^{(1)}(AB) = a & \sum_{NSCI} \boldsymbol{SCI}(\boldsymbol{AB}; NSCI) \\ & + b \sum_{NTCI} \boldsymbol{TCI}(\boldsymbol{AB}; NTCI) \\ & + c \sum_{N12CI} \boldsymbol{12CI}(\boldsymbol{AB}; N12CI) \\ & + d \sum_{NFCI} \boldsymbol{FCI}(\boldsymbol{AB}; NFCI) \\ & + e \end{aligned} \tag{8.10}$$

Similarly the expression for the NICS can be rewritten in terms of shielding tensors associated to the vector map of a certain delocalisation order ($\sigma_{zz}(\boldsymbol{r}_X;MCBI)$):

$$\begin{aligned} \text{NICS}zz(\boldsymbol{r}_\text{x}) = -(a\sigma_{zz}(\boldsymbol{r}_X; SCI) + b\sigma_{zz}(\boldsymbol{r}_X; TCI) + c\sigma_{zz}(\boldsymbol{r}_X; 12CI) \\ + d\sigma_{zz}(\boldsymbol{r}_X; FCI) + e) \end{aligned} \tag{8.11}$$

Where the component of the shielding tensor associated to a certain delocalisation order ($\sigma_{zz}(\boldsymbol{r}_X;MCBI)$) can be written as[158]:

$$\sigma_{zz}^X(\boldsymbol{r}_X; MCBI) = -\frac{1}{Bc} \frac{\sum_{AB=1}^{N} \left\{ (\boldsymbol{r}_{\bar{AB}} - \boldsymbol{r}_X) \times \sum_{NC=1}^{M} \boldsymbol{MCBI}(\boldsymbol{AB}; NC) \right\}_z}{|\boldsymbol{r}_{\bar{AB}} - \boldsymbol{r}_X|^3} \tag{8.12}$$

The summations run over all the bonds (AB) and all the different circuits with a given number of centres (NC) respectivly and $\boldsymbol{r}_{\bar{AB}}$ is the vector pointing to the middle of bond AB.

Constants a, b, c, and d from equation 8.11 can now be obtained by calculating the shielding tensors from the vector maps of the different delocalisation circuits (Equation 8.12). This slightly more complex procedure should correctly describe the NICS of the inner ring of coronene. The results for this method are represented in Figure 8.23. Once again the model was fitted for the 108 PAH and subsequently used for the large set of 286 PAH.

The figure shows that this model indeed closely predicts the NICS of the inner ring of coronene, which is now predicted as 3.26 ppm (the *ab initio* value is -0.60). The R^2 does not increase significantly (0.947 to 0.950) and the root mean square error decreases only a little, from 2.55 to 2.45. The model is not necessarily better in

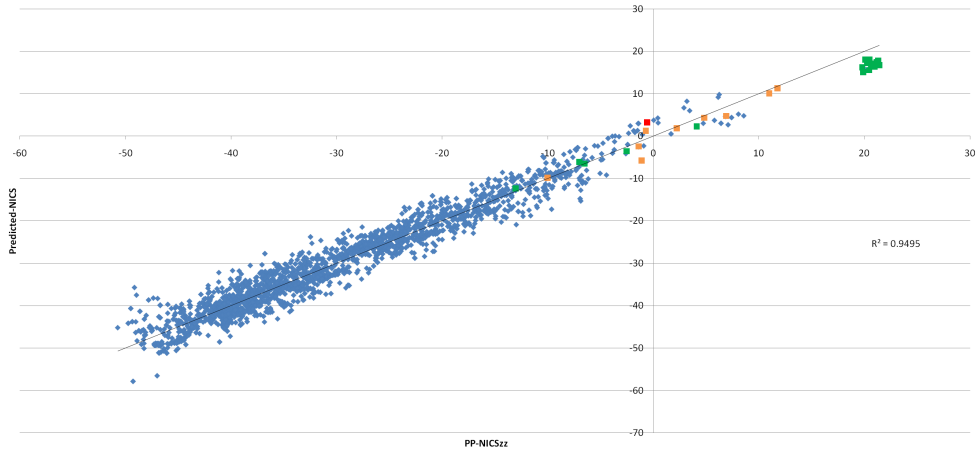

Figure 8.23: The $NICS_{zz}$ versus the Predicted-$NICS_{zz}$ for 394 PAH using equation 8.11

describing the NICS for the whole set of molecules, compared to the simpler vector-model. This is because the $\times \boldsymbol{r}_X/|\boldsymbol{r}_{\bar{AB}} - \boldsymbol{r}_X|^3$ dependence ensures that the effect of other vectors than the ones encircling the ring at which the NICS is evaluated can be neglected in the majority of the PAH. The model is, however, necessary to correctly understand the NICS in coronene. The example of coronene nicely demonstrates that the NICS computed at a benzenoid ring centre should not be used to compare the local aromaticity of benzenoid circuits. In this molecule not only do the different circuits contribute to the NICS value, but the NICS of the central ring is the result of the more aromatic benzene circuits surrounding the inner ring. The effect is subsequently reduced by the large diatropic current running around the edge of the molecule.

The apparent multidimensional character is thus not required to explain disagreements between different indices. Multicentre indices, used to assess benzenoid character, are strictly related to the benzenoid ring and no direct effect of the neighbouring rings is considered. This allows considering local benzenoid aromaticity as the retention of similarity of a benzenoid ring to isolated benzene[121]. NICS take an entirely different approach and reflect in a single point all the currents in a molecule. In the case of PAH, local aromaticity is not multidimensional, it simply follows a different definition. The lack of need for multidimensionality is clearly illustrated by the fact that both can be reconciled as shown above.

8.6 Conclusions

It has been shown that the NICS index in its different versions and the General Population Analysis based SCI do not show any meaningful correlation. The correlation found is so poor that it could easily be attributed to the multidimensional nature of aromaticity. As NICS are related to ring currents and the global ring current can be considered as built from the different currents of all individual circuits in a molecule the hypothesis was put forward that the set of multicentre indices for all different circuits could correlate with the computed NICS values. Indeed, it was shown through thorough statistical analysis that the NICS values and combined multicentre indices for all individual circuits correlate very favourably. The correlation improvement amounts approximately 50%. The observed lack of correlation between NICS computed at a benzenoid ring centre and the multicentre index for the benzenoid circuit infers that NICS should not be used to assess the degree of local aromaticity of a benzenoid circuit. Therefore, it should be avoided to report correlations between aromaticity indices reflecting strictly only a specific circuit and NICS values, even if computed at the centre of that circuit as other circuits can strongly influence the NICS value.

In the course of this study we have shown that the pseudo-π-method is a trustworthy and computationally advantageous alternative to the 'complete' NICS calculation on PAH's. It might even be speculated that these values are a better tool to examine the properties of the π-electron cloud since there is no influence on these values from a σ-framework.

The present results also show that the MCBI and RCM can be reconciled in a chemically intuitive way. By making the proper combination of the delocalisation indices for different circuits, both NICS and the RCM picture can be reconstructed. As there is a good correlation between the MCBI and other local aromaticity indices such as the Polansky index[121,123] (*vide supra*), the same correlations will hold for these indices, and in general it is expected that the above reasoning can be used to reconcile delocalisation based and magnetic indices. The claimed evidence for multidimensionality of aromaticity vanishes in these cases, as it is apparently only a consequence of a choice of description, in terms of rings or graph circuits. By making a suitable combination of the delocalisation indices for different circuits, the NICS and RCM picture is recovered.

There are clearly some advantages to using the MCBI-RCM, it has the advantage of having a numerical value for the current on each bond, while it doesn't lose information contained in the RCM. Surely a single number for the aromaticity in a molecular ring might in many cases be a practical and very powerful method, but some caution is recommend since in some cases it might fail to describe the physical reality. The power of a pictorial representation rather than just a number for the

aromaticity in each ring is demonstrated by a number of special cases like bifurcated rings, 'empty' rings or periphere-only currents, these molecules can hardly be called aromatic, a misconception that might arise when using just a number for the aromaticity of a benzenoid ring. Of course the NICS can also be found from this data when taking the summation of all vectors of a benzenoid ring, equivalent to integrating all current density into one point.

In this chapter the non-local effects on the NICS were studied using the MCBI for a large set of 394 PAH. This revealed that for perylene-like and benzo[ghi]-perylene-like fragments and for the central ring of coronene, the NICS value can not be explained using the six-, ten- and fourteen-centre circuits alone. It was shown that the problem lies in the non-local character of the NICS. This non-local character could be proven using the MCBI-vector maps. Furthermore, it was shown that phenalene like twelve-centre circuits and pyrene-like fourteen-centre circuits at first glance do not lead to a better correlation between the NICS and the MCBI, but statistics show the effect on the NICS is meaningful. The models presented here do not serve as an alternative way to calculate the NICS using the MCBI, but were constructed to fully examine and understand the difference between the NICS and delocalisation indices. In this way, these results have demonstrated that NICS should not be used to assess the degree of local aromaticity of a benzenoid circuit as MCBI do. Three different non-local effects on the NICS were found:

- the influence of the higher-order circuits encircling the ring. Not only the six-, ten- and fourteen-centre circuits have an effect on the NICS, the present study show that also the twelve-centre circuits have a meaningful influence.

- the influence of local aromaticity of the surrounding, neighbouring, rings which can dramatically change the current on the common bonds of neighbouring rings, influencing the NICS of these rings.

- the influence of currents even farther away from the ring at which the NICS is evaluated, like the effect of the outer current in coronene on the NICS in the central ring.

While examining the non-local contributions to the NICS, the results of this study also raised the suggestion that there is a 4N+2 rule applicable to the delocalisation indices, where (4N+2)- and 4N-membered circuits contribute in a diatropic and paratropic manner, respectively. However, further investigation of this 4N+2 rule for delocalisation indices is necessary.

These results show it is possible to find a very tight correlation between the MCBI and the NICS, when taking suitable combination of the delocalisation indices for different circuits. These results confirm once more that the claimed multidimensionality of aromaticity must not be involved in this case. Scrutiny must be used when

reporting correlations between aromaticity indices reflecting only a specific circuit and NICS values.

8.6.1 Supplementary Material Available:

Cartesian coordinates of the PAHs used in this study as well as their total SCF energy, charge and multiplicity, together with a graphical representation of their σ-framework are available as supplementary material at:

http://www.quantum.ugent.be/stijn/SICHAPTER08a.pdf

The the explicit values of constants a to d for reconstructing different members of the NICS family using equation 8.7 , together with the PP-NICS, SCI, summed TCI and FCI for some PAH are given in:

http://www.quantum.ugent.be/stijn/SICHAPTER08b.pdf

Chapter 9

Correlation between delocalisation indices and energy effects

The main problem, which makes the concept of aromaticity so inspiring and at the same time controversial, is that predictions of various aromaticity criteria often contradict each other. The existence of such contradictions is usually attributed to the multidimensional character of aromaticity, exemplified in what is called the orthogonality between classical (structural and energetic) and magnetic criteria of aromaticity[14–16]. Although such an explanation has received wide acceptance, the detailed insights provided by recent theoretical analyses clearly demonstrated that no inconsistencies between the classical and magnetic aromaticity measures are observed provided the comparison involves inherently local aromaticity indices associated with individual rings within polycyclic aromatic hydrocarbons (PAH)[20,118,144,151,156]. This is, e.g., the case of the Polansky similarity index and its recent generalization[121,123], circuit-specific magnetic indices of Aihara and Anusooya[140,144] and the so-called Multi Centre Bond Indices[18,99,100], which all were found to correlate with each other.

Our aim in this study is to follow up with the results of the above recent theoretical analyses and to demonstrate that a similar close parallel also involves the indices characterizing the energetic benefits associated with cyclic arrangement of mobile π-electrons. An example of such an index, specifically focused on the evaluation of energetic effects of the cyclic conjugation in PAH, is represented by the so-called *ef*-values[162–164]. The main goal of this study is to demonstrate the close link between

this particular type of local index and the extent of cyclic delocalisation of mobile π-electrons in individual rings of the PAH, quantitatively gauged by the values of the Multi Centre Bond Indices.

9.1 Theoretical

9.1.1 Energy Effects of Cycles

The dependence of the total π-electron energy E on the structure of the PAH (as computed within the Hückel Molecular Orbital (HMO) approximation, and expressed in the units of the HMO carbon carbon resonance integral β) was much studied in the past and is relatively well understood; for details see the book[165] and reviews[166,167] and the references cited therein. Applying the Sachs theorem[168] to the Coulson integral formula[169] for E, one can envisage the dependence of E on the cycles present in the underlying polycyclic conjugated molecule[170,171]. By means of appropriate mathematical arguments, it was possible to express the energy effect (on the total π-electron energy) caused by an individual cycle Z. The formula reads[163,164]

$$ef(G,Z) = \frac{2}{\pi}\int_0^\infty ln\left|\frac{\phi(G,ix)}{\phi(G,ix)+2\phi(G-Z,ix)}\right| d\boldsymbol{x} \qquad (9.1)$$

where π = 3, 14. . ., i = $\sqrt{-1}$, G is the underlying molecular graph[170,171], $G - Z$ is the subgraph obtained by deleting the cycle Z from G, and where $\phi(H,x)$ is the characteristic polynomial of the graph H[172,173]. Details of the theory on which equation 9.1 is based, as well as numerous examples of its applications can be found in a recent review[162].

9.2 Computational methods

The calculations of Multi Centre Bond Indices and *ef*-values were performed for the set of the PAHs specified in Table I. Based on the numbering of individual symmetry unique benzene rings specified in the Table, the following types of indices were calculated

1) 6-Centre Bond Indices (SCI) and the corresponding *ef*-values for all symmetry unique benzene circuits in PAHs

2) 10-Centre Bond Indices (TCI) and the corresponding *ef*-values for all symmetry-unique naphthalene circuits in the PAHs

3) 14-Centre Bond Indices (FCI) and the corresponding *ef*-values for all symmetry-unique 14-membered circuits in the PAHs. There are three different types of such circuits, corresponding to anthracene, phenanthrene and pyrene fragments.

Table 9.1: Molecules contained in the studied set of PAHs. Roman numbers refer to the different symmetry-unique rings in the molecules.

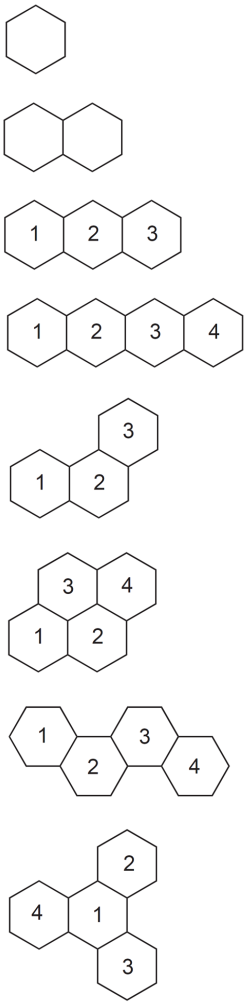

1 benzene

2 naphthalene

3 anthracene

4 tetracene

5 pentacene

6 pyrene

7 chrysene

8 triphenylene

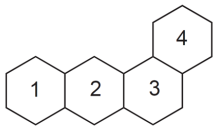

9 benzo$[a]$anthracene

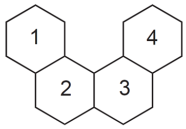

10 benzo$[a]$phenanthrene

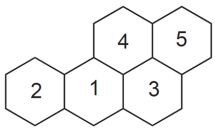

11 benzo$[a]$pyrene

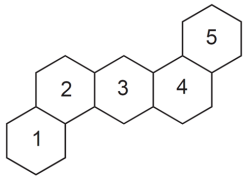

12 dibenzo$[a,h]$anthracene

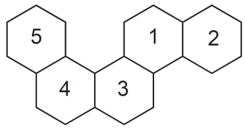

13 benzo$[c]$chrysene

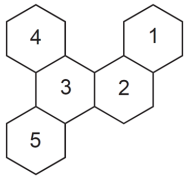

14 dibenzo$[a,c]$phenanthrene

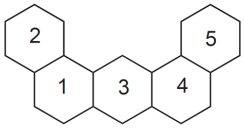

15 dibenzo$[a,j]$anthracene

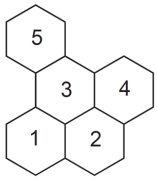

16 benzo$[e]$pyrene

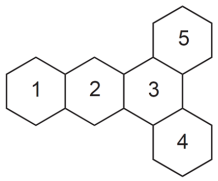

17 dibenzo$[a, c]$anthracene

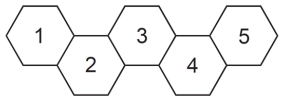

18 picene

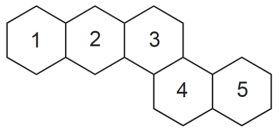

19 dibenzo$[a, h]$phenanthrene

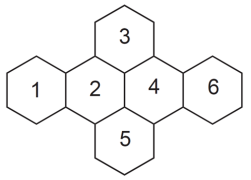

20 dibenzo$[e, l]$pyrene

For the sake of straightforward comparability with the *ef*-values, the Multi Centre Bond Indices were calculated using the so-called pseudo-π approach[12,13,115–117] for the idealised geometries formed in each particular case by formal fusion of clamped benzene rings with the CC bond length 140 pm. Within this approach each of the carbon atoms is represented just by one singly occupied orbital like in the Hückel method, and the only difference compared to HMO theory is that the bond indices are calculated using the formula 4.17 that takes into account actual overlap matrix **S** which in HMO theory is set to unit matrix. The calculated values of the above Multi Centre Delocalisation Indices and the corresponding *ef*-values for 6-, 10- and 14-centre rings are summarised in Tables 9.2-9.4. For the sake of comparison of both approaches we also present the values of HMO 6-centre indices in the Table 9.2.

Table 9.2: Calculated 6-Centre Bond Indices (SCI) and 6-centre *ef*-values (*ef*-(6)) for individual symmetry-unique benzene circuits in the studied PAHs

Molecule	Ring	*ef*-(6) (β-units)	SCI (pseudo-π)	SCI (HMO)
1	1	0.2729	1.5808	1.5802
2	1	0.1211	0.8640	0.8660
3	1	0.0951	0.6656	0.7449
	2	0.0653	0.6048	0.5294
4	1	0.0900	0.5888	0.7124
	2	0.0535	0.5088	0.4679
5	1	0.1586	1.0368	0.9862
	2	0.0534	0.3936	0.4312
6	1	0.1063	0.8256	0.7367
	2	0.0528	0.3904	0.4564
7	1	0.1465	0.9856	0.9534
	2	0.0689	0.4960	0.5034
8	1	0.0242	0.1760	0.2083
	2	0.1910	1.1488	1.0830
9	1	0.1048	0.7360	0.7852
	2	0.0796	0.6592	0.5778
	3	0.0431	0.2944	0.3626
	4	0.1717	1.0880	1.0084
10	1	0.1449	0.9728	0.9430
	2	0.0693	0.4992	0.5043
11	1	0.0504	0.4480	0.3975
	2	0.1294	0.8736	0.8839
	3	0.0455	0.3040	0.4019
	4	0.0686	0.4992	0.5345
	5	0.1050	0.8192	0.7257
12	1	0.1665	1.0688	0.9989
	2	0.0469	0.3264	0.3872

Molecule	Ring	ef-(6) (β-units)	SCI (pseudo-π)	SCI (HMO)
	3	0.1001	0.7488	0.6408
13	1	0.0633	0.4576	0.4833
	2	0.1506	0.9984	0.9531
	3	0.0907	0.6208	0.5851
	4	0.0643	0.4640	0.4771
	5	0.1489	0.9920	0.9627
14	1	0.1369	0.9440	0.9213
	2	0.0829	0.5728	0.5656
	3	0.0304	0.2240	0.2445
	4	0.1790	1.1136	1.0459
	5	0.1813	1.1040	1.0606
15	1	0.0469	0.3264	0.3873
	2	0.1660	1.0656	0.9969
	3	0.1002	0.7488	0.6416
16	1	0.1243	0.8896	0.7995
	2	0.0537	0.3904	0.4545
	3	0.0245	0.1824	0.2244
	5	0.1945	1.1584	1.0843
17	1	0.1116	0.7744	0.8124
	2	0.0908	0.6912	0.6270
	3	0.0206	0.1344	0.1773
	4	0.2003	1.1776	1.0962
18	1	0.1505	0.9984	0.9633
	2	0.0640	0.4640	0.4825
	3	0.0903	0.6176	0.5840
19	1	0.1020	0.7136	0.7738
	2	0.0753	0.6432	0.5656
	3	0.0542	0.3712	0.4276
	4	0.0741	0.5344	0.5195

Molecule	Ring	*ef*-(6) (β-units)	SCI (pseudo-π)	SCI (HMO)
	5	0.1427	0.9600	0.9420
20	1	0.1928	1.1584	1.0832
	2	0.0247	0.1792	0.2221
	3	0.1472	0.9664	0.8720

Table 9.3: Calculated 10-Centre Bond Indices (TCI) and 10-centre *ef*-values (*ef*-(10)) for individual symmetry-unique naphthalene circuits in the studied PAHs

Molecule	*ef*-(10) (β-units)	TCI (pseudo-π)	Circuit
2	0.0709	0.5567	
3	0.0369	0.3612	
4	0.0275	0.294	1+2
	0.0206	0.2684	2+3
5	0.0275	0.2568	
6	0.0198	0.1996	1+2
	0.0056	0.0469	2+3
7	0.0387	0.3254	1+2
	0.0118	0.1267	2+3
8	0.0102	0.1104	
9	0.0471	0.4086	1+2
	0.0139	0.153	2+3
	0.0193	0.1858	3+4
10	0.0389	0.3244	1+2
	0.0118	0.127	2+3
11	0.0281	0.2868	1+2
	0.0091	0.1073	1+3
	0.0091	0.1085	1+4
	0.0068	0.049	3+4

Molecule	*ef*-(10) (β-units)	TCI (pseudo-π)	Circuit
	0.0139	0.1421	3+5
	0.0294	0.2595	4+5
12	0.0223	0.2102	1+2
	0.0178	0.1788	2+3
13	0.0344	0.3	1+2
	0.016	0.1573	1+3
	0.016	0.1578	3+4
	0.0349	0.321	4+5
14	0.0488	0.3737	1+2
	0.0047	0.0553	2+3
	0.0144	0.142	3+4
15	0.0224	0.2102	1+2
	0.0179	0.1788	1+3
16	0.0229	0.2148	1+2
	0.0074	0.087	1+3
	0.0025	0.0262	2+3
	0.0095	0.1105	3+5
17	0.0549	0.4361	1+2
	0.0051	0.0655	2+3
	0.0073	0.0805	3+4
18	0.0348	0.3033	1+2
	0.0159	0.1576	2+3
19	0.0437	0.3955	1+2
	0.0198	0.1978	2+3
	0.0087	0.0933	3+4
	0.0431	0.3498	4+5
20	0.0099	0.1096	1+2
	0.0085	0.0931	2+3
	0.0012	0.0148	2+4

Molecule	*ef*-(10) (β-units)	TCI (pseudo-π)	Circuit

Table 9.4: Calculated 14-Centre Bond Indices (FCI) and 14-centre *ef*-values (*ef*-(14)) for individual symmetry-unique anthracene, phenanthrene and pyrene circuits in the studied PAHs

Molecule	*ef*-(14) (β-units)	FCI (pseudo-π)	Circuit
3	0.0279	0.17808	
4	0.0158	0.12852	
5	0.0198	0.15778	
6	0.0128	0.13342	1+2+4
	0.0128	0.08456	1+2+3+4
7	0.0081	0.07714	
8	0.0068	0.06566	
9	0.0099	0.07686	1+2+3
	0.0099	0.09422	2+3+4
10	0.0081	0.07728	
11	0.0062	0.05600	1+2+3
	0.0062	0.06230	1+2+4
	0.0057	0.07070	1+3+5
	0.0057	0.07252	1+4+5
	0.0057	0.04648	1+3+4+5
12	0.0037	0.03416	2+3+4
	0.0130	0.11046	1+2+3
13	0.0115	0.09618	1+2+3
	0.0033	0.03696	1+3+4
	0.0115	0.09688	3+4+5
14	0.0030	0.03332	1+2+3
	0.0030	0.03304	2+3+4

Molecule	*ef*-(14) (β-units)	FCI (pseudo-π)	Circuit
	0.0102	0.08554	3+4+5
	0.0030	0.03304	2+3+5
15	0.0037	0.03416	1+3+4
	0.0130	0.11046	1+2+3
16	0.0011	0.01218	2+3+5
	0.0153	0.13650	1+2+4
	0.0043	0.05614	1+3+4
	0.0048	0.05236	1+3+5
	0.0043	0.04102	1+2+3+4
17	0.0033	0.03290	1+2+3
	0.0033	0.03822	2+3+4
	0.0044	0.04606	3+4+5
18	0.0114	0.09646	1+2+3
	0.0033	0.03696	2+3+4
19	0.0147	0.09912	1+2+3
	0.0042	0.04732	2+3+4
	0.0055	0.05642	3+4+5
20	0.0005	0.00686	1+2+4
	0.0056	0.05586	1+2+3
	0.0052	0.05726	2+3+5
	0.0015	0.01988	2+3+4+5

9.3 Results and Discussion

The existence of the link between the energetic benefits resulting from the cyclic conjugation of mobile π-electrons and the extent of the cyclic delocalisation in individual conjugated circuits can most straightforwardly be demonstrated by looking for the possible relation between the *ef*-values and Multi Centre Bond Indices for

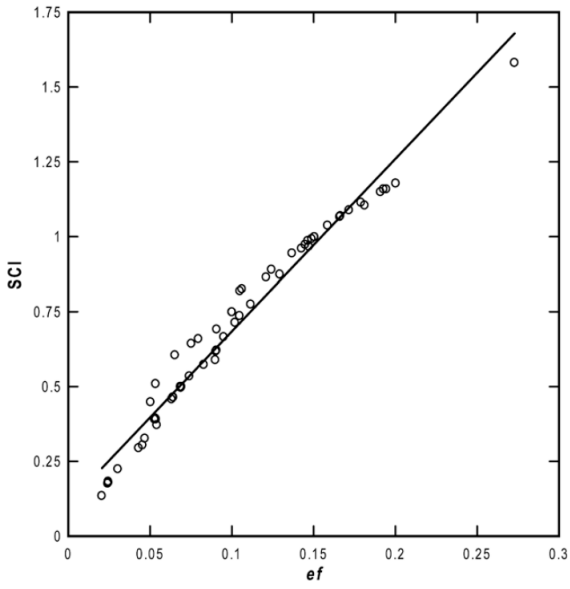

Figure 9.1: Correlation of 6-Centre Bond Indices (SCI) with the *ef*-values for individual symmetry-unique benzenoid rings in the studied set of molecules (correlation coefficient R = 0.986)

individual types of the conjugated circuits. Because of the fact that the stabilising energy contributions due to the cyclic delocalisation rapidly decrease with the size of the cycle, we first focus on the relation between the *ef*-values and the 6-Centre Bond Index (SCI). This dependence is displayed in Fig. 9.1, from which the tight correlation of both indices is straightforwardly evident.

The close parallel between the *ef*-values and Multi Centre Bond Indices is not, however, restricted only to 6-centre contributions of the benzene rings, but similar correlations are observed also for 10- and 14-centre rings and it is interesting that the indices even for these more extended delocalised systems fit the same correlation line as in the case of benzene (Fig. 11.3).

Both indices, of which one reflects the local energetic contribution of an individual conjugated circuit and the other reflects the extent of cyclic conjugation in the same circuit, are seen to correlate very well thereby showing that both approaches to the concept of aromaticity yield the same conclusions. Moreover, the Multi Centre Bond Indices were recently successfully shown to allow the reconstruction of ring current density maps in PAHs[156]. The presently shown correlation in Figure 11.3

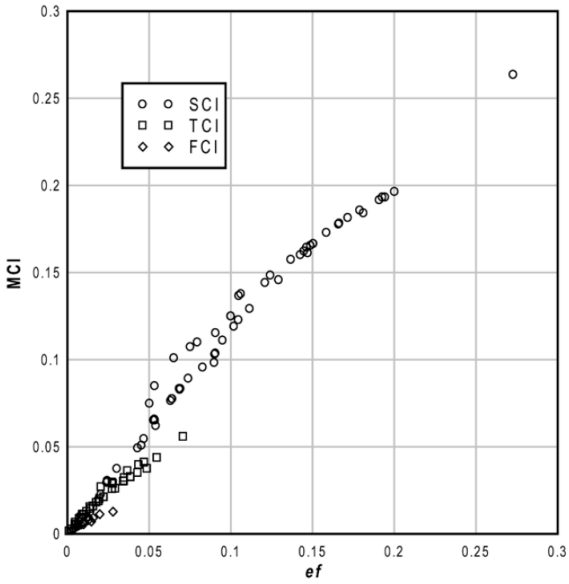

Figure 9.2: Joint correlation of Multi Centre (6-, 10- and 14-centre) Delocalisation Indices (MCBI) with *ef*-values for the studied set of molecules

and the latter fact imply that energetic and magnetic manifestations of aromaticity are also closely related and, moreover, that no discrepancies between both types of indices exist provided the comparison involves strictly local contributions of individual rings. This result is very interesting because of its possible implications for the often observed inconsistencies between the classical and magnetic aromaticity measures. It implies, namely, that such inconsistencies, if observed, do not in fact reflect the "orthogonality" of the corresponding measures, but they stem from the fact that comparison is made between indices that are inherently incomparable. The importance of the requirement of comparability can be best demonstrated by the example of the widely used magnetic aromaticity index NICS[10,107,108,110]. Although this index is calculated in a fixed point associated with a particular ring, and as such seems to represent a local aromaticity measure of a given ring, its correlations with other inherently local aromaticity measures like the Polansky index[123], Aihara's circuit resonance energy[144], Multi Centre Bond Indices[18], etc., dramatically fail. However, the traditional interpretation of such discrepancies in terms of multidimensionality of the aromaticity phenomenon was seriously questioned in recent theoretical studies[18,20,118,174], in which it was demonstrated that the observed lack of correlations is due to the fact that the values of NICS are in fact contaminated by the contributions of the ring currents of all conjugated circuits in the molecule. Provided proper account is taken of the contributions of the contaminating circuits, no inconsistencies between NICS and local aromaticity measures exists. Another example demonstrating the importance of the interference of contaminating conjugated circuits can be found in a recent graph theoretical study[175], in which the correlation of the topological resonance energy (TRE), as global aromaticity measure, with the local energy contributions (*ef*-values) of individual rings was reported. Based on that study, and in view of the correlation between the *ef*-values and Multi Centre Bond Indices, it can be expected that similar correlations will also exist between TRE and the Multi Centre Bond Indices. Because of the dominance of the contributions from 6-centre benzenoid cycles, the correlation of TRE with Multi Centre Bond Indices can, in a first approximation, be written in the form of the following equation 9.2

$$\mathrm{TRE} = a \sum_i \mathrm{SCI}_i + b \tag{9.2}$$

which can also be regarded as the counterpart of a similar relationship between TRE and magnetic resonance energy (MRE) reported in the graph theoretical study of Aihara[144]. In order to demonstrate the difference between the delocalisation indices calculated at the pseudo-π and HMO level of the theory, the parameters of the correlation equation 9.2 were calculated for both types of indices. The resulting values, together with the corresponding correlation coefficients are given bellow (Equation 9.3).

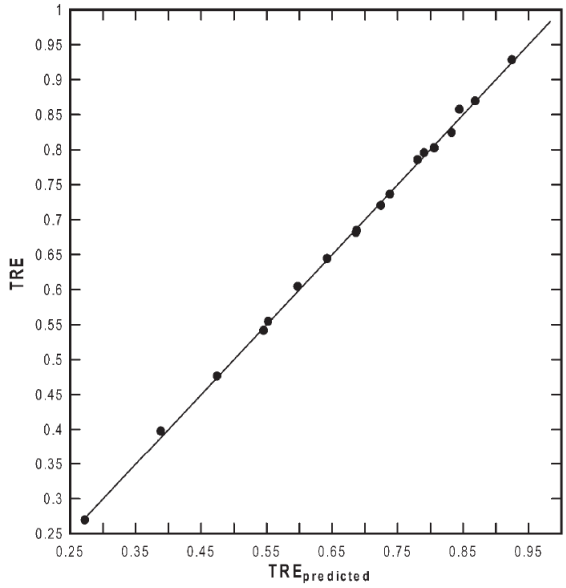

Figure 9.3: Correlation between the topological resonance energy (TRE) and TRE predicted from the correlation equation 9.4 (slope 1.00, intercept 0.00, correlation coefficient R = 0.999)

$$\begin{array}{cccc} \text{Psuedo}-\pi & a=0.2264, & b=0.0029, & R=0.973 \quad (a) \\ \text{HMO} & a=0.2304, & b=0.0250, & R=0.915 \quad (b) \end{array} \tag{9.3}$$

As it is possible to see, the description based on the indices calculated using pseudo-π approach is noticeably better than the one based on the correlation with HMO 6-centre indices. This clearly implies the superiority of the pseudo-π approach used in this study and this is why only this particular approach was considered in the extension of the model based on taking into account the contributions of other contaminating conjugated circuits. The inclusion of these circuits resulted for the studied set of 20 PAHs, in the multilinear correlation equation

$$\text{TRE} = 0.1946 \sum_{\alpha} \text{SCI}_{\alpha} + 0.1784 \sum_{\beta} \text{TCI}_{\beta} + 0.049 \sum_{\gamma} \text{FCI}_{\gamma} - 0.038 \tag{9.4}$$

$$R = 0.999$$

whose statistical analysis[176] confirms that inclusion of additional parameters does

indeed increase the statistical importance of the correlation (Equation 9.4) compared to equation 9.3(a). The internal predictability of the equation 9.4 was tested using the leave-10%-out procedure which resulted in a q^2 of 0.9985. The excellent quality of the correlation equation can also be demonstrated by the simple correlation of theoretical versus predicted TRE values whose plot is displayed in Fig. 9.3. The slope of the correlation line is 1.00, the intercept is 0.00 and the correlation coefficient R = 0.999.

This result is very important because the form of the correlation equation (Equation 9.4) closely resembles the relations recently used to reveal the interfering contributions of contaminating conjugated circuits to the traditional magnetic aromaticity index NICS[118]. The close similarity of both types of the correlation equations thus implies that the parallels between energetic and magnetic criteria of aromaticity are not restricted only to the comparison of the measures of strictly local nature (*ef*-values *vs* MCBI) but, provided proper care is taken of the interfering contribution of all participating conjugated circuits, there is also no inconsistency between the local and global aromaticity measures.

9.4 Conclusions

The results show new evidence questioning the often invoked phenomenon of multidimensionality of the aromaticity exemplified in what is called the orthogonality between the classical (structural and energetic) and magnetic aromaticity measures. The reported approach, that is based on the quantitative comparison of energy benefits associated with the cyclic arrangement of mobile π-electrons in polycyclic aromatic hydrocarbons and the extent of cyclic delocalisation in the corresponding conjugated circuits shows that no discrepancy between both types of indices exists provided the comparison involves local contributions of individual rings and conjugated circuits. In addition we also show that provided the interfering contributions of contaminating conjugated circuits are properly taken into account, the same close parallel can be observed also for global aromaticity measures like TRE and NICS.

Part III

The Aromaticity of Other Aromatic Systems

Introduction

Kekulé, in his earlier works on aromaticity[25,177,178] clearly stated that aromatic compounds are composed "atomistically" of C_6 units and also implicitly gave rise to a system to quantify aromaticity by similarity to benzene although he admitted that he did to know how to express this similarity.

Since Kekulé, many other workers in the field have contributed to the insight in what makes benzene special, but also the concept of aromaticity was broadened to include other molecules that to some extent are similar, or even opposite to the behaviour of benzene. This gave rise to terms like homo-aromaticity, σ-aromaticity, 3D-aromaticity, anti-aromaticity and many more[2]. Virtually all similarity connection to benzene is lost then, except that one can say that broadly they have properties somewhat similar to those of benzene. However, the problem then is what properties to consider key properties that should be retained in order to call a molecule aromatic and to what extent they should be retained. Clearly, from the Kekulé point of view, containing one or more C_6 unit(s) would be needed to speak of an aromatic compound but this view has been abandoned as one also speaks of the aromaticity in systems like hexaiodobenzene, metallic systems or hydroporphyrins, as will be done in this Part. Some other properties have stood the test of time and it now seems that one identifies an aromatic molecule as one that shares at least to some extent the properties of bond length equalisation, electron delocalisation, remarkable reactivity reminiscent of benzene, energetic stabilisation compared to e.g., non-cyclic molecules or non-delocalised molecules and special magnetic properties such as sustaining a ring current similar as in benzene[3,4]. If a molecule has all these properties, it can safely be considered aromatic but naturally the problem arises what to do when a molecule has only a limited number of such properties or when some property is simply not applicable to a certain class of molecules. This is for instance the case in many metallic systems where the typical organic reactivity of benzene is largely inapplicable.

One of the next major steps in the study of aromaticity came with the attempts

to quantify aromaticity. Different indices were introduced that express quantitatively the degree in which some archetypical property of those mentioned above is retained in some molecule. A very important point concerning these different indices is that when applied to some set of molecules, not all indices agree on the classification of the molecules. According to some index a molecule can be highly aromatic whereas another index may classify it as non-aromatic. Clearly this is a major problem, and this observation has resulted in claims that aromaticity is multidimensional[14–16]. However, in Part II it was pointed out that when one sticks to aromatic compounds as they were considered by Kekulé (i.e. benzenoid ring containing molecules only), the multidimensional character must be reconsidered somewhat[118,156]. In those cases it may arise that apparent multidimensionality is rather due to the fact that comparisons are made between indices that inherently reflect different properties. This was found *e.g.*, when studying the correlation between multicentre indices on the one hand and NICS data[118] or ring current maps on the other[156].

Although this shows that multidimensionality must not be invoked too lightly, it remains true that when extending aromaticity to include also other types of molecules, not all indices agree and not all can be brought to meaningful correlation. This is a serious complication as the very goal of aromaticity indices is to measure aromaticity quantitatively but there is no well established rule of the weight that should be attributed to the different indices. For example, how aromatic should one consider a molecule that has equalised bond lengths, has a significant degree of delocalisation but does not show any ring current at all under an external magnetic field? One author might consider geometry and delocalisation as very important properties and ring currents as less important and thus classify the molecule as aromatic. A different author might focus on ring currents and hence conclude that the molecule is non-aromatic. One could say that aromaticity is in the eye of the beholder.

It is obvious that this very strongly undermines the entire issue of quantifying aromaticity. In the spirit of Kekulé one might opt not to rely on manifestations of similarity to benzene in a range of properties but rather to express similarity to benzene directly via some fundamental property such as the electron density. This has been done before but only for molecules consisting of benzenoid rings[20,21,121]. There is, at the moment, not yet any clue on how to properly compare a molecule that differs so much from benzene as for instance a square planar four membered all metal ring as will be considered here.

One might then consider all hope lost, and in fact some authors have suggested banning the word aromaticity from chemistry[179]. Banning a word so popular as aromaticity is probably impossible but it remains that the so-called multidimensionality needs to be examined further and we feel one must be sufficiently critical in using the word aromaticity and especially be careful when extending it to molecules that

deviate strongly from benzene related ones.

In the following chapters, the concurrence and contradictions in describing the degree of aromaticity in hexaiodobenzene (chapter 10), metallic systems (chapter 11) and hydroporphyrins (chapter 12 is examined by mainly by making use of the multicentre indices and the ring current maps, supplemented with some other indices.

Chapter 10

Evidence for σ-delocalisation in the aromatic hexaiodobenzene cation

10.1 Introduction

Notions of π-delocalisation and π-aromaticity are well established in the organic chemistry of planar unsaturated molecules, although the underlying σ bonding in these molecules is almost always described in terms of localised orbitals.[1,2] It has been suggested, however, that a delocalised picture of the σ electronic structure will give a better account of the properties of species containing cyclic arrays of hypervalent main-group atoms.[180,181] A particular example is the dication $C_6I_6^{2+}$ (**2**) formed by the oxidation of hexaiodobenzene, C_6I_6 (**1**).

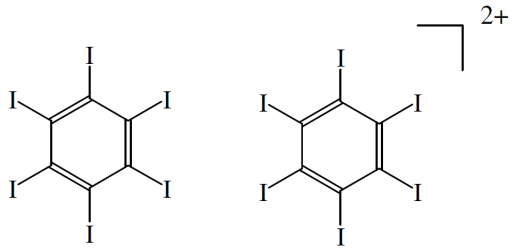

1 **2**

Overlap of in-plane iodine 5p orbitals gives rise to six molecular orbitals (see Scheme below), all occupied in the neutral C_6I_6 (**1**), of which the least bonding combination, corresponding to head-to-tail anti-bonding overlap between tangential p orbitals on all I neighbours, is the calculated[180–182] HOMO.

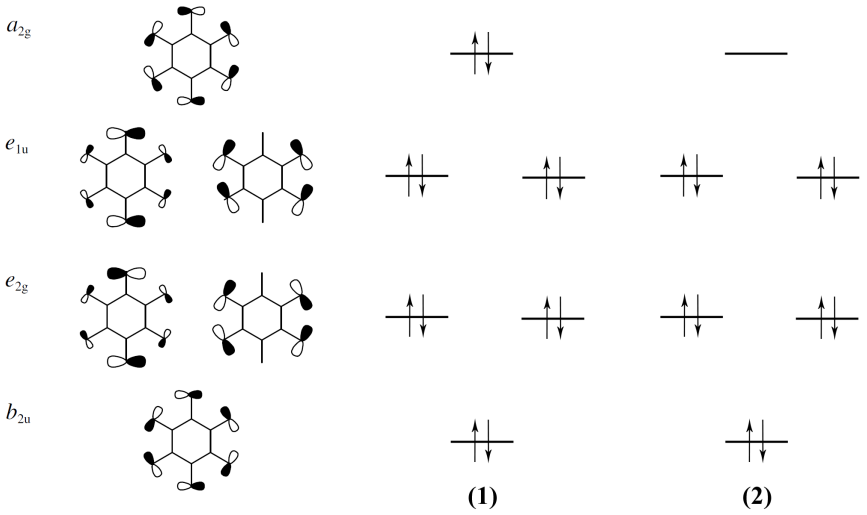

On the magnetic criterion of aromaticity, and using the experimental evidence available from NMR spectroscopy, Sagl and Martin[181] argued that an upfield shift of 42.6 ppm in the position of the ^{13}C NMR singlet on the oxidation of hexaiodobenzene to the dication indicates the presence of an extra ring current in the charged species, and they attributed this to σ-delocalisation within the array of iodine atoms. The carbon nuclei would then lie *inside* a diatropic circulation, and hence would be shifted upfield.

Recent *ab initio* calculations by Ciofini *et al.*[182] yielded a value of 37.2 ppm at the GIAO/PBE0/6-311G(d,p)//PBE0/ LANL2-DZ level for the upfield shift, in good agreement with the experimental value. In the same study, as evidence for the ring-

current explanation of this shift, the authors computed a height profile of the difference in NICS (nucleus-independent chemical shift) values[10] between neutral and cationic species, and deduced an increase in aromaticity in the dication. The fact that the height profile has a maximum in the molecular plane also points to an origin within the σ distribution for the additional ring current.

In this chapter, two complementary theoretical techniques to study σ-delocalisation and σ-aromaticity are used. The first is capable of displaying the ring current directly and also of disentangling σ and π contributions to it. Current-density maps and the orbital contributions to them, as computed in the ipsocentric approach,[12,39,41,160] show that there is indeed a separately identifiable σ ring current in the iodine array of the cation (**2**), in addition to the benzenoid π current sustained by the central ring in both the neutral and cationic species. We provide an orbital model for the sense of the current, and couple these calculations with a second quantitative measure, the multi-centre index,[18,19,21] which characterises the underlying cyclic electron delocalisation in both carbon and iodine circuits. Both criteria support the attribution of σ-aromaticity to the iodine array in $C_6I_6^{2+}$.

10.2 Computational Methods

Geometries of neutral **1** and cationic **2** were optimised at the RHF level in the 6-311G* basis. The D_{6h}-symmetric optimum geometry of **1** lies in a local minimum at this level of theory (R_{CC}(**1**) = 1.401 Å, R_{CI}(**1**) = 2.131 Å), albeit with some low vibrational frequencies (9 cm^{-1} (e_{2u}), 18 cm^{-1} (b_{2g})). However, at the RHF level, the D_{6h} geometry of **2** is a higher-order stationary point, with a doubly degenerate imaginary frequency (R_{CC}(**2**) = 1.383 Å, R_{CI}(**2**) = 2.086 Å; 57i cm^{-1} (e_{1u})). At the DFT level, both are local minima, with bond lengths slightly different from the RHF values ((R_{CC}(**1**) = 1.410 Å, (R_{CI}(**1**) = 2.138 Å, (R_{CC}(**2**) = 1.395 Å, (R_{CI}(**2**) = 2.106 Å). Soft modes for out-of-plane distortion are to be expected for C_6I_6. In the crystal structure,[183,184] this molecule adopts a crown-like structure with a small (0.04 Å) difference between the planes defined by triplets of iodine atoms.

Current-density maps were calculated for **1** and **2** in the ipsocentric approach, at the D_{6h} RHF geometries in the same 6-311G* basis, using the SYSMO program.[146] This involves calculation of the coupled Hartree-Fock response of the system to an external magnetic field, under the imposition of a special choice of origin for current density, where each point is its own origin. The ipsocentric approach leads to the partition of total current density into physically nonredundant occupied-orbital contributions, and also has advantages of economy and accuracy of the computed results.[12] The calculated currents can be rationalised using symmetry and node-counting se-

Table 10.1: Multi Centre Bond Indices calculated at the RHF/6-311G* level, each quoted as a percentage of the reference $\sigma + \pi$ benzene value calculated in the same approach.

		C_6I_6 **1**	$C_6I_6^{2+}$ **2**	C_6H_6
C	σ	0.9	1.0	2.0
	π	76.0	72.1	98.0
I	σ	0.0	50.8	-
	π	0.0	0.0	-

lection rules.[12,41] Plotting conventions are that the current density is determined in a plotting plane at a fixed height from the molecular plane (either $1a_0$ or zero). Contours represent the magnitude, and arrows the 2D-projection, of the current density per unit inducing magnetic field. Anticlockwise circulation represents diatropic current, and clockwise circulation represents paratropic current.

Multi-centre indices are calculated in the Mulliken approach from the charge and bond-order matrix, and the basis function overlap matrix.[18,19,21] In these calculations, carried out at the RHF/6-311G* geometries and using the same 6-311G* basis, separate indices are calculated for the C_6 and I_6 cycles, and separate σ and π contributions are obtained for each.

10.3 Results and discussion

The calculated Multi Centre Bond Indices at the RHF/6-311G* level are shown in Table 10.1. In the neutral system, π-delocalisation is significant for the carbon cycle, whereas σ-delocalisation is small, and for the set of iodine atoms, both σ- and π-delocalisation measures are small. In the dication, the indices for the carbon cycle remain more or less unchanged, but for the set of iodine atoms σ delocalisation becomes significant. These trends are compatible with expectations from the normal aromaticity properties of the central benzene ring (large C_6 π-delocalisation) and the proposed σ-aromaticity of the iodine array (large I_6 σ-delocalisation, but in the cation only).

Within the ipsocentric framework for magnetic response, delocalisation plays an interesting role. It is to be expected that an aromatic system (in the sense of one supporting a ring current) will be delocalised, but the existence of ring current requires more than delocalisation, in that there must be available virtual transitions of appropriate symmetry (translational in the case of diatropic, aromatic current).

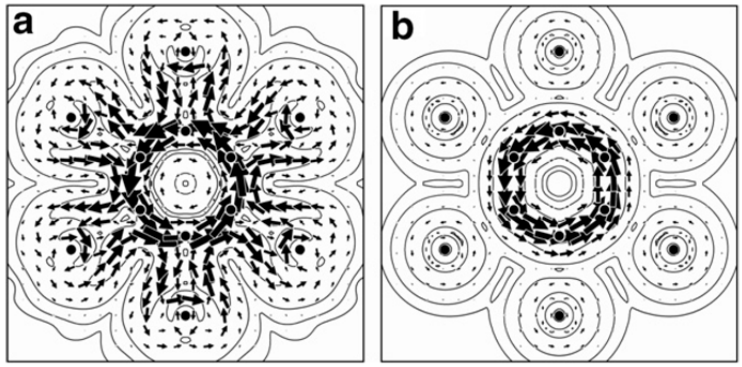

Figure 10.1: Map of the current density induced in C_6I_6 (**1**) by a perpendicular magnetic field, as calculated at the ipsocentric CTOCD-DZ/6-311 G*//RHF/6-311G* level. Contributions of (a) all (σ + π) electrons and (b) the four electrons of the π HOMO are shown, plotted at a height of 1 Bohr from the molecular plane. Arrows indicate the projection of current density in the plotting plane, and anticlockwise circulation corresponds to a diatropic current.

Delocalisation therefore emerges as a necessary rather than a sufficient condition for magnetic aromaticity.

Direct insight into the induced currents is provided by the computed maps (Figs. 10.1 and 10.2). Both molecules show a global diatropic response (Figs. 10.1a and 10.2a). Neutral C_6I_6 supports a diatropic π ring current (Fig. 10.1b). As in benzene itself, this current is dominated by the contribution of the top occupied π orbital, an orbital which has one angular node and hence has a translationally allowed transition to the lowest unoccupied π orbital, which has two angular nodes. Thus, C_6I_6 is a conventional 4π aromatic.[12,41] The σ response of C_6I_6 consists only of localised bond currents and so, on the magnetic criterion, does not constitute an indication of aromaticity.

Dicationic $C_6I_6^{2+}$ shows a similar central 4π ring current (Fig. 10.2b), but also a pronounced current associated with the iodine perimeter. This current is significant in the $1a_0$ plotting plane (Fig. 10.2c), but stronger in the plane of the molecule (Fig. 10.2d), indicating its σ character. This too is a 4-electron current, arising in this case from the contribution of the e_{1u} HOMO of $C_6I_6^{2+}$.

This evidence for the σ-aromaticity of **2** is readily understood within the ipsocentric approach. The ipsocentric formulation is a frontier-orbital, spectroscopic account of ring current, in that contributions to induced current density arise from occupied-to-virtual excitations governed by symmetry selection rules (*vide supra*), and moder-

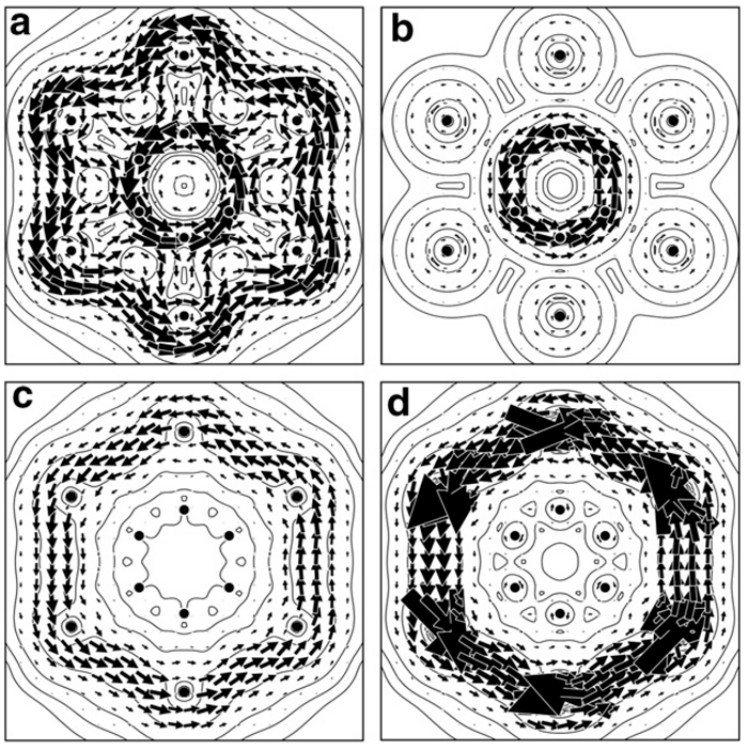

Figure 10.2: Map of the current density induced in $C_6I_6^{2+}$ (**2**) by a perpendicular magnetic field, as calculated at the ipsocentric CTOCD-DZ/6-311 G*//RHF/6-311G* level. Contributions of (a) all (σ + π) electrons, (b) the four electrons of the highest-lying π orbital, and (c) the four electrons of the σ HOMO ($21e_{1u}$) are shown, plotted at a height of one Bohr from the molecular plane. Panel (d) again shows the contribution from the four electrons of the σ HOMO ($21e_{1u}$), but plotted in the molecular plane itself. Arrows indicate the projection of current density in the plotting plane, and anticlockwise circulation corresponds to a diatropic current.

ated by energy denominators that depend on differences between orbital energies.[12]

The symmetry selection rule a for diatropic ring current is that a virtual excitation from an occupied orbital ϕ_1 to an empty orbital ϕ_2 will contribute a diatropic current if there is a totally symmetric component in the product of representations $\Gamma(\phi_1) \otimes \Gamma(T_{x,y}) \otimes \Gamma(\phi_2)$, where $T_{x,y}$ is the pair of translations in the molecular plane. For the π system of a monocyclic molecule, this rule reduces to an angular- momentum requirement: a transition is translationally allowed if and only if ϕ_1 and ϕ_2 differ by one unit of angular momentum. For the σ system formed by tangential in-plane p orbitals, the orbital symmetries are in one-to-one correspondence with those of the conventional π system, each being multiplied by a one-dimensional irreducible representation (Γ_ϵ, the representation of a concerted rotation at all sites). Specifically, therefore, the symmetry products of π orbitals ϕ_1 and ϕ_2 and their σ counterparts are equal, and the selection rules are preserved: in both out-of-plane-p π and tangential-p σ ladders of energy levels, diatropic currents arise from one-step transitions from occupied to empty orbitals.

This formal analogy allows a precise prediction about the perimeter aromaticity of **1** and **2**. In neutral **1**, the whole set of six tangential-π orbitals is occupied, leaving no occupied-to-unoccupied excitations to give rise to a perimeter ring current. In cationic **2**, however, the most anti-bonding tangential-p orbital is empty, allowing a transition from e_{1u} HOMO to a_{2g} LUMO to give rise to a diatropic σ current on the iodine perimeter, an exact analogue of the HOMO-LUMO transition that would be expected to give rise to a conventional π current in a planar 6-centre, 10-electron π system. Therefore, **2** should support a perimeter ring current, whereas **1** should not. As the current-density maps show, this extra σ ring current predicted by basic symmetry arguments is exactly what is found in the computations.

The existence of current is also compatible with the interpretation of reported experimental ^{13}C chemical shifts. In principle, calculations that predict induced current density also predict nuclear magnetic shieldings, and the ipsocentric method and its variants have been tested in this respect for many small molecules.[40] However, quantitative calculation of the ^{13}C nuclear shieldings and chemical shifts in these heavy halocarbons is known to be a difficult problem, requiring explicit consideration of spin-orbit effects.[185] Conventional calculations that neglect such extra terms reproduce the sign and order of magnitude of the difference in chemical shift between **2** and **1**, but give poor and highly method-dependent values for the individual shifts. With the present basis set, the difference chemical shift (experimental value 42.6 ppm[181]) is variously predicted as: 54.8 ppm (coupled HartreeFock (CHF) calculation with the DZ2 variant[40] of the ipsocentric approach); 63.1 ppm (CHF calculation with the PZ2 variant,[40] normally more reliable for the calculation of shieldings); 53.8 ppm (CHF calculation employing gauge-including atomic orbitals

(GIAO)); 38.1 ppm (GIAO/PBE0/6- 311 G*//RHF/6-311G* calculation); and 39.2 ppm (GIAO/ PBE0/6-311 G(d,p)//PBE0/LANL2-DZ calculation[182]). In all cases, even those of the density-functional calculations where the difference shift is close to the measured value, the individual ^{13}C chemical shifts are in poor agreement with experiment, apparently overestimating the shift for **1** (experiment: 121.7 ppm[181]) by 30-40 ppm and for **2** (experiment: 79.1 ppm[181]) by 15-40 ppm. Inclusion of spin-orbit effects has been predicted to cause increases of $\sim$30 ppm in calculated ^{13}C shieldings for centres bonded directly to iodine.[185] Interestingly, these results underline for this difficult case the delicate nature of the deduction of ring current from chemical shift; ring currents are predicted to be present, and the direction of the shift is compatible with their presence, but other effects apparently also make a large contribution both to the separate shieldings and their difference. Quantitative calculation of shieldings is difficult in this case, though the detection of substantial ring current in the calculations has proved to be more straightforward.

Chapter 11

Correlation between electron delocalisation and ring currents in all metallic "aromatic" compounds

In the present work our main interest lies in quantifying two main properties of so-called all metal aromatic compounds, namely delocalisation and ring currents. Is there some quantitative agreement between them as there was in polyaromatic hydrocarbons[118,156] or not? The relation between both is subtle, as electron delocalisation is a necessary but not sufficient condition for a ring current. If no quantitative agreement is found, one is again left with the ambiguity typical for aromaticity. As will become clear further below, there is in the case of one of the best known classes of all metal aromatic compounds, namely the molecules $Li_nAl_4^{n-2}$, no clear connection between both properties. We will therefore refrain from using the word aromaticity and simply discuss separately the extent of electron delocalisation and ring currents and leave it to the reader to conclude whether these molecules must be labelled aromatic or not. We prefer to rather speak of respectively "similar to benzene in electronic delocalisation" and "similar to benzene in the existence of a diatropic ring current".

Before reporting the results of the study, the following sections introduce previous results for the class of compounds studied here, the theoretical tools to establish electron delocalisation and ring currents and later the computational methods.

11.1 Aromaticity in Al_4^{2-} based compounds

Since the discovery of Al_4^{2-} units containing bimetallic clusters[47,186], the interest in these compounds has grown enormously[48,49], not in the least because of claims that the concept of aromaticity could be extended to metallic systems. Together with their discovery also the first theoretical studies were performed[47,186], classifying them as both σ and π aromatic. Since then, the aromaticity of Al_4^{2-} has been studied using different criteria; maps of ring currents[187–190], aromatic ring current shieldings (ARCS)[191,192], nuclear independent chemical shifts (NICS)[193], induced magnetic field analysis[194], valence bond calculations (VB)[195], bifurcation analysis of the electron localisation function (ELF)[196], resonance energy estimations (RE)[197,198], conceptual DFT descriptors[199,200] and the first applications of multicentre indices to establish the electronic delocalisation in these compounds[199,200]. One of main issues fueling this plethora of studies has been the near endless discussions on whether the molecules are either σ, π or σ and π aromatic. Originally, the molecule was claimed to be π aromatic as the HOMO of the free anion is a double occupied π orbital and hence this fitted well the Hückel rule. It is immediately clear from the introduction that there is always the risk that different workers use the same word (aromatic) to describe different effects, e.g. electron delocalisation, diatropic ring currents, and hence come to different conclusions. However, when using only magnetic response as a criterion, again not all studies reached the same conclusions. Now it seemed to depend on whether one uses NICS evaluated at some (set of) point(s) or ring currents. Already in 2001 Fowler and co-workers, using ring current maps and their orbital contributions, built a strong case to show that only the σ system gives rise to a ring current and the π system does not give rise to any sort of ring current[187–190]. However, up to recently, other studies make other claims based mainly on NICS calculations. We show below that the use of NICS, even if computed at specially chosen points and even if only certain components of the tensor are used, is debatable. Many workers consider that if at some point above the molecular plane of an aromatic system (here the Al_4^{2-} plane) the NICS is sufficiently negative, this reflects π aromaticity. This is naturally not true. The π system has a nodal plane in the plane of the Al_4^{2-} system and hence if a ring current is found there, it can only be of σ nature. The alternative reasoning is not true as there is no reason why a σ ring current could not extend to planes above or below the aromatic ring. Hence, the σ system can lead to a ring current in planes parallel to but displaced from the aromatic plane. The degree of discussion on the origin of the ring currents is also clear from so-called Gauge-Including Magnetically Induced Current (GIMIC) calculations leading Lin et al.[192] to conclude that both σ and π electrons are responsible for the magnetically induced ring currents. Juselius et al. using aromatic ring current shielding calculations (ARCS) reached the same conclusion[191].

All the above shows that this class of molecules merits further attention with emphasis on the discussion of any possible link or lack thereof between electron delocalisation and induced ring currents. In the present work we continue pursuing this goal after the first study revealed that within the present set of molecules electron delocalisation and ring current can lead to contradictory claims.

11.2 Computational methods

As tools for measuring electron delocalisation, we opt for the visual inspection of the occupied orbitals and especially the so-called domain averaged Fermi-hole analysis (DAFH) and multicentre indices. Both of these require availability of atomic overlap matrices, where the overlap between two molecular orbitals is obtained in atom condensed form. This requires the definition of an atom in the molecule and in the present study we choose the Hirshfeld-I method. These measures of delocalisation are compared with the ring current maps in the ipsocentric approach.

All molecules considered were studied at the Hartree-Fock level of theory using the 6-311G* basis set. The choice for this modest level of theory is based on the fact that this level of theory is the only one at which (multicentre) delocalisation indices of higher orders can be computed theoretically correct and relatively routinely. Often multicentre indices are computed using Kohn-Sham density functional theory in the same way as on the Hartree- Fock level, using the Kohn-Sham Slater determinant. This is, however, theoretically not entirely justifiable. Moreover, the program used to calculate the ipsocentric ring currents was designed to be used at the Hartree- Fock level. For all molecules different starting geometries were constructed by systematically combining the planar Al_4^{2-} ring with the number of Li ions desired in the different coordination locations (for instance, apical positions, in plane with a triangular coordination to two Al atoms,). These geometries were optimised and for the resulting structures the Hessian was computed to establish whether they correspond to minima. The resulting molecular orbitals were written to a wfn file used in the Hirshfeld-I scheme method to give atomic overlap matrices that in turn are used for computing DAFH eigenvectors and eigenvalues and for computing multicentre indices. The ring current maps at the Hartree-Fock level were computed in the ipsocentric fashion.

All geometry optimizations were performed using the Gaussian03 program[120]. All calculations of Hirshfeld-I data, DAFH, MCBI and ring current maps were carried out using own codes.

11.3 Results and discussion: delocalisation and magnetic response in Al_4^{2-} based compounds

In this section we discuss the extent of electron delocalisation gauged by visual inspection of the Fermi holes and associated eigenvalues and multicentre indices as well as magnetic response such as NICS values and ring current patterns in these compounds.

The compounds studied include the systems Al_4^{2-} , $LiAl_4^-$ and Li_2Al_4 . All these compounds have been the subject of many previous studies, although in the present study we also located some geometries that have not yet been reported previously. Table 11.1 shows the different structures discussed below with the symmetry point group for each structure located. Also included is the number of negative eigenvalues of the Hessian. Most structures are minima except for the D_{4h} Li_2Al_4 structure which was included as it is a minimum in the related Na_2Ga_4 compounds[48,201]. All structures are considered as a closed shell singlet. For highly charged anionic compounds such as Al_4^{2-} , HF/6-311G* can hardly be expected to give the best description of the electronic state but in the interest of comparison with the same unit in the Li coordinated compounds, we stick to this modest level. Moreover, the use of larger basis sets including diffuse functions may easily cause the compound to be described with, at least the second electron essentially as a free electron. This may seriously hamper any comparative study of the type considered here.

Table 11.1: Structures located for the different compounds with symmetry, number of negative Hessian eigenvalues (#Neg. EV), relative energy (RE, in kJ/mol) where relevant, a qualitative structural representation of the compound and the Multi Centre Bond Index (MCBI) over the 4 Al atoms.

	Al_4^{2-}	$LiAl_4^-$	$LiAl_4^-$	Li_2Al_4	Li_2Al_4
Symmetry	D_{4h}	C_{4v}	C_{2v}	C_s	D_{4h}
# Neg. EV	0	0	0	0	4
RE		0.00	15.5	0.00	29.81
	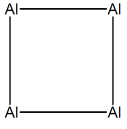	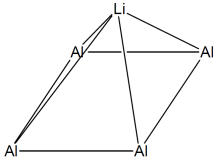	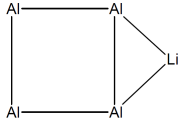	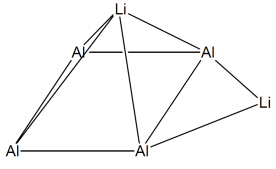	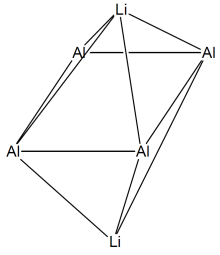
MCBI	0.371	0.248	0.314	0.297	0.265

Table 11.2: MCBI contributions per occupied orbital with the irreducible representation associated with it.

	Al_4^{2-}	$LiAl_4^-$	$LiAl_4^-$	Li_2Al_4	Li_2Al_4
Symmetry	D_{4h}	C_{4v}	C_{2v}	C_s	D_{4h}
HOMO	0.187 (A_{2u})	0.097 (A_1)	0.162 (B_1)	0.098 (A)	0.106 (A_{1g})
HOMO-1	0.117 (A_{1g})	0.069 (B_1)	0.098 (A_1)	0.107 (A)	0.071 (B_{2g})
HOMO-2	0.074 (B_{2g})	0.095 (A_1)	0.045 (A_1)	0.054 (A)	-0.013 (B_{1g})
HOMO-3	-0.014 (B_{1g})	-0.013 (B_2)	-0.008 (B_2)	-0.008 (A)	0.128 (A_{2u})
HOMO-4	-0.025 (E_u)	-0.037 (E)	-0.020 (B_2)	-0.019 (A)	-0.024 (E_u)
HOMO-5	-0.038 (E_u)	-0.025 (E)	-0.020 (A_1)	-0.021 (A)	-0.036 (E_u)
HOMO-6	0.070 (A_{1g})	0.062 (A_1)	0.058 (A_1)	0.054 (A)	0.064 (A_{1g})

Table 11.1 also shows the multicentre indices computed over the four Al atoms using Hirshfeld-I atomic overlap matrices. All MCBI values point out a significant degree of delocalisation over the 4 centres with clearly the highest degree of delocalisation for the non Li coordinated compound. MCBI can be broken down in orbital contributions and table 11.2 shows for each molecule the MCBI contribution per orbital for the higher lying orbitals. Lower lying orbitals have much smaller MCBI contributions and are therefore not shown in detail. Also included is the symmetry of each of the orbitals to allow assessing whether it is a σ or π delocalised orbital. Note that in some cases such a distinction cannot be made rigorously and hence in those cases the data are to be considered approximate.

Table 11.2 very clearly shows that the highest lying orbitals play the most important role. There is a remarkable similarity in how especially the highest 3 orbitals and the HOMO-6 have a large MCBI. The only exception is the D_{2h} Li_2Al_4 structure where the HOMO-2 and HOMO-3 are apparently switched. All this suggests that the electronic structure of the molecule remains quite comparable, especially with respect to the delocalisation in the Al_4^{2-} unit. Based on the symmetries of the orbitals involved, one also sees immediately that there are both important σ and π contributions to the delocalisation index. To check whether the use of MO resolved MCBI is appropriate we also checked the shape of the orbitals to see whether delocalisation over all 4 centres is indeed expected. In case of Al_4^{2-} this is easily seen to be the case as is shown in figure 11.1a-b.

The nature of both these orbitals is quite comparable amongst all molecules. It should be noted that the other orbitals have lower MCBI contributions which in gen-

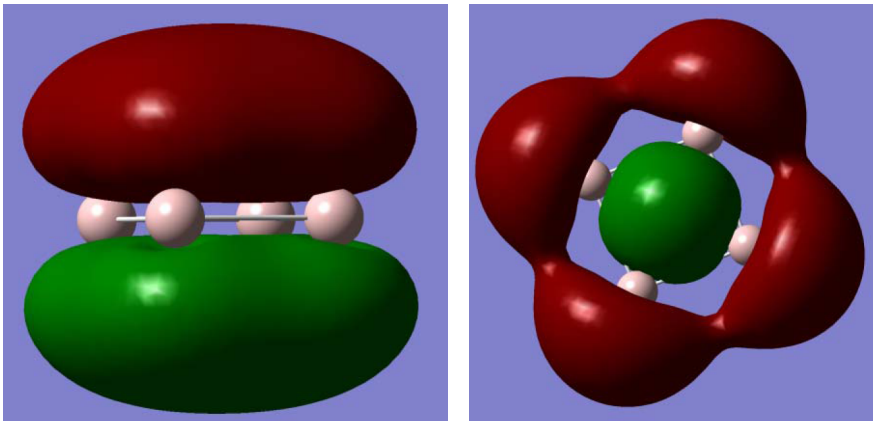

(a) (b)

Figure 11.1: The HOMO (a) and HOMO-1 (b) in Al_4^{2-}

eral agrees with their shape. For orbitals with a less clearly delocalised shape, it is much harder to extract any feeling on their contribution to the MCBI, but as table 11.2 shows, they usually have a significantly lower contribution.

Since the MCBI established that both σ and π delocalisation plays a role, it is worth examining whether the DAFH analysis comes to the same conclusion. The results for Al_4^{2-} with the domain chosen as one single Al atom are straightforward to interpret. The two eigenvectors with an eigenvalue 0.5 are shown in figure 11.3a-b.

Although somewhat less clearly interpretable in the complexes, in almost all cases the DAFH analysis remains very similar. As an example of a non-planar complex, the DAFH eigenvectors for a single Al atom are plotted for $LiAl_4^-$ in the C_{4v} geometry in figure 9.3.

Not only the general shapes remain similar, also the eigenvalues stay relatively close to 0.5 although obviously some small deviations are possible as not all Al atoms and domains are symmetry equivalent in all molecules. All this suggests that the Li ions do not strongly influence the electronic structure of the Al_4^{2-} unit.

In conclusion, in all structures there is clear σ and π delocalisation. However, as delocalisation is only a necessary and not sufficient condition for an induced ring current, one cannot always conclude that the molecule will also show a ring current. In the previous chapter it was shown to be possible in polyaromatic hydrocarbons via statistical analysis of NICS or ring current maps and MCBI data[118,156] but this does not need to be so in general. In order to examine whether there is a ring current in the compounds considered here, ring currents were computed in the Al_4^{2-} plane and one atomic unit above and below. A warning should be issued that a simple plot of

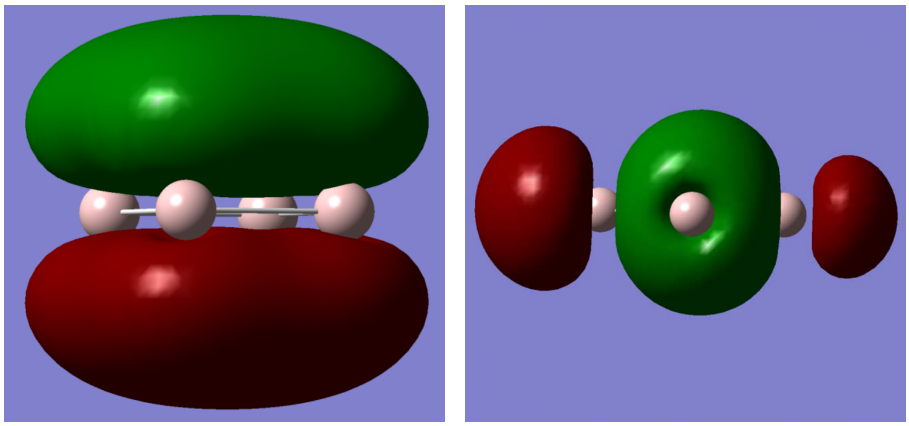

(a) (b)

Figure 11.2: The two eigenvectors with eigenvalue 0.5 in Al_4^{2-}

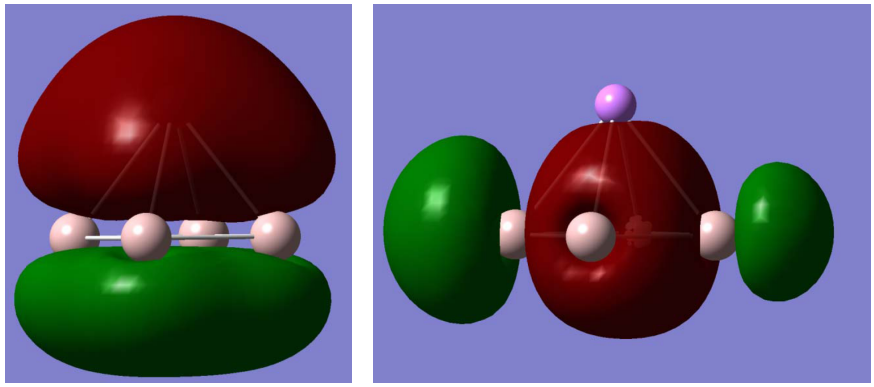

(a) (b)

Figure 11.3: The two eigenvectors with eigenvalue near 0.5 in C_{4v} $LiAl_4^-$

Table 11.3: NICS data computed at ring centres (NICS(0)), one Å above (NICS(1)) and below (NICS(1)) where different from NICS(1) . Both the isotropic value and the zz tensor component are shown.

	Al_4^{2-}	$LiAl_4^-$	$LiAl_4^-$	Li_2Al_4	Li_2Al_4
Symmetry	D_{4h}	C_{4v}	C_{2v}	C_s	D_{4h}
NICS(0)	-51.63	-27.30	-56.44	-32.68	+4.49
$NICS(0)_{zz}$	-66.40	-66.41	-62.28	-22.37	-67.10
NICS(1)	-37.33	-31.78	-39.17	-34.74	-18.69
$NICS(1)_{zz}$	-55.70	-59.49	-33.32	-23.96	-58.78
NICS(-1)		-24.22		-26.46	
$NICS(-1)_{zz}$		-53.84		-14.79	

ring currents cannot distinguish completely between σ and π ring currents. If there is a ring current in the plane it must be of σ nature. If there is one above or below the plane, it can be of both σ and π nature as there is no symmetry reason why the σ current would disappear there. Before proceeding to the ring current plots, it is useful to consider NICS as a simple indication of the existence of a ring current. It is often assumed that a negative NICS reflects the existence of a diatropic ("aromatic") ring current, although this is not necessarily always so. Table 11.3 shows the NICS values evaluated at the centre of the Al_4^{2-} ring or at some point displaced from the ring centre along the z-axis. Where relevant, the positive direction always corresponds to the direction of the sole Li ion coordinated above the Al_4^{2-} cycle.

Table 11.3 reveals that the NICS data point out a strong diatropic ring current in all compounds, although D_{4h} Li_2Al_4 very clearly stands out. There a positive NICS(0) is found, which is questionable given that there is a high degree of similarity between the delocalisation and (occupied) orbitals between all molecules. The use of NICS for the present molecules has been debated previously[190] and so instead of an in depth study of the NICS data, we opt for the calculation of ring currents in the Al_4^{2-} plane and the planes 1 atomic unit above and below. The total ring currents are shown in tables 11.4-11.6. The ring currents in all cases were calculated with a magnetic field along the axis perpendicular to the molecular plane. The length of the arrow is related to the strength of the current and diatropic currents are shown counter-clockwise. Dalton symbols[202] show the location of the atoms.

The ring current maps very clearly show that in the Al_4^{2-} unit there is always a diatropic ring current and that it remains in all complexes considered. The ring currents

Table 11.4: HF/6-311G* ring current $\boldsymbol{J}(\boldsymbol{r})$ maps computed in the Al_4^{2-} plane in Al_4^{2-} and one atomic unit above.

$\boldsymbol{J}(\boldsymbol{r})(0)$	$\boldsymbol{J}(\boldsymbol{r})(1)$
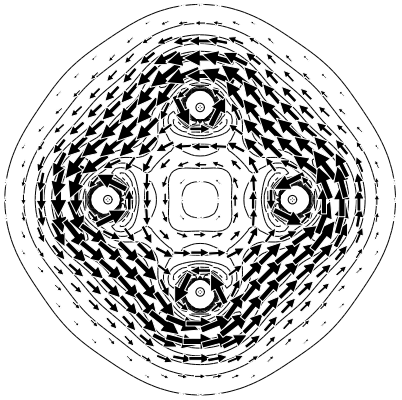	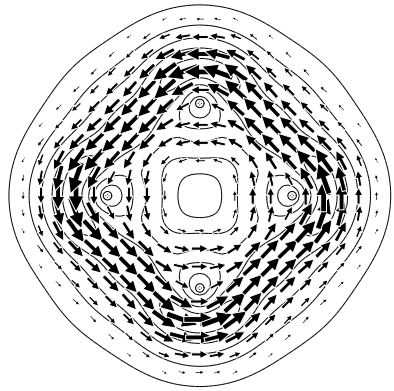

are also retained in planes above and below the Al_4^{2-} unit. As a consequence one cannot simply conclude whether the ring current is of σ or π type. In order to reveal the nature of the ring current, one can compute the different orbital contributions[43,44]. As has been shown above, an occupied orbital can only give a significant current density if a virtual orbital of appropriate symmetry is available and at the same time is energetically not too far separated from the occupied orbital. In practice, the latter requirement means that the ring current mainly originates from high energy orbitals. As an example, we consider Al_4^{2-} . The HOMO was clearly delocalised and of π type. There is however no ring current associated to this orbital. On the other hand, the HOMO-1 orbital contributes clearly to a σ ring current. The ring currents for the orbitals HOMO up to HOMO-5 are shown in table 11.7.

As is clear from table 11.7, the ring current in Al_4^{2-} is clearly of σ type rather than of π type. Apparently, no symmetry allowed virtual orbital is energetically close enough to the HOMO to result in a meaningful current density. The HOMO-1 current density is still quite small and so still other orbitals must yield significant current densities in order to lead to the total current density as shown in table 11.4. This is indeed the case. The HOMO-2 and HOMO-3 both contribute strongly to the current density and to much larger extent than the HOMO-1 orbital. As a consequence, one must conclude that one cannot judge from mere MCBI contributions which orbitals will have significant contributions to the ring current. There is clearly no π current in Al_4^{2-} although a naïve look at the NICS data might have suggested this. This agrees

Table 11.5: HF/6-311G* ring current maps computed in the Al_4^{2-} plane and 1 atomic unit above and below (where different from that 1 atomic unit above) in $LiAl_4^-$.

Symmetry	C_{4v}	C_{2v}
$\boldsymbol{J}(\boldsymbol{r})(0)$	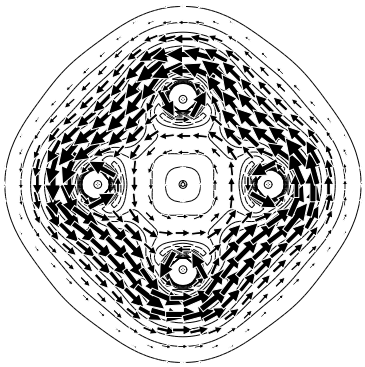	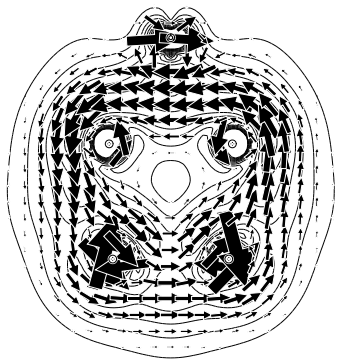
$\boldsymbol{J}(\boldsymbol{r})(1)$	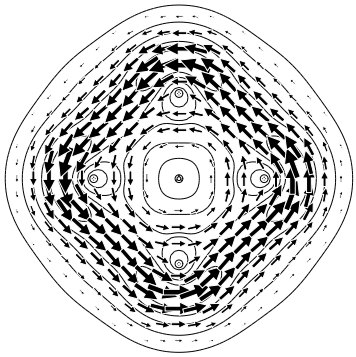	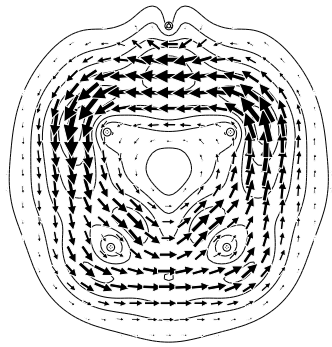
$\boldsymbol{J}(\boldsymbol{r})(-1)$	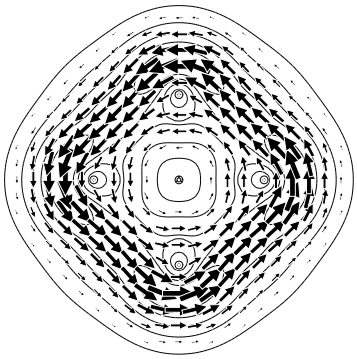	

Table 11.6: HF/6-311G* ring current maps computed in the Al_4^{2-} plane and 1 atomic unit above and below (where different from that 1 atomic unit above) in Li_2Al_4 .

Symmetry	C_s	D_{4h}
$\boldsymbol{J}(\boldsymbol{r})$(0)	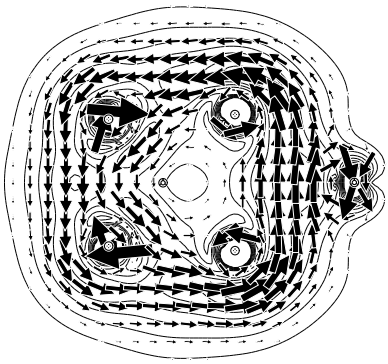	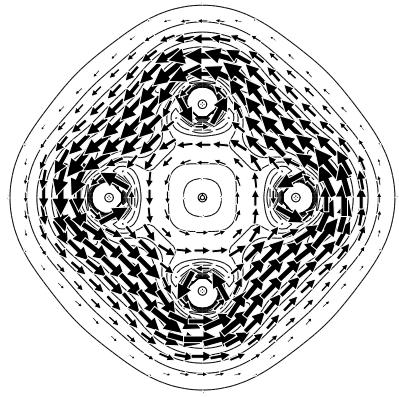
$\boldsymbol{J}(\boldsymbol{r})$(1)	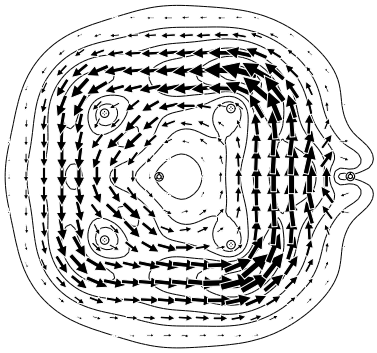	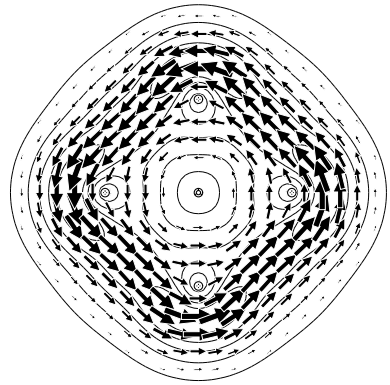
$\boldsymbol{J}(\boldsymbol{r})$(-1)	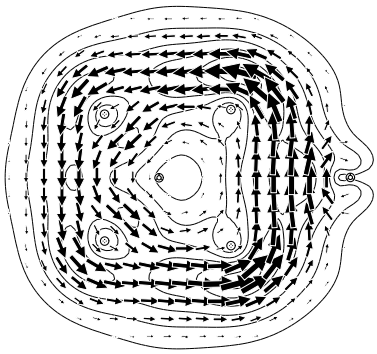	

with previous findings of Fowler and co-workers[187–190] and shows that NICS(1) data cannot automatically be considered to reflect the existence of π diatropic ring current.

Table 11.7: Orbital resolved ring current maps in the Al_4^{2-} plane in Al_4^{2-} except for the HOMO where it is evaluated at 1 au above the plane.

MO	HOMO	HOMO-1
Symmetry	A_{2u}	A_{1g}
Eigenvalue	0.081	0.073
$\boldsymbol{J}(\boldsymbol{r})$	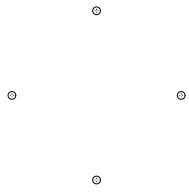	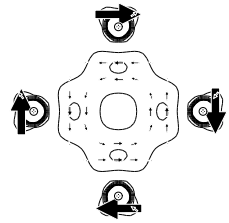

MO	HOMO-2	HOMO-3
Symmetry	B_{2g}	B_{1g}
Eigenvalue	0.064	0.035
$\boldsymbol{J}(\boldsymbol{r})$	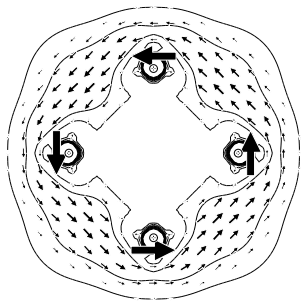	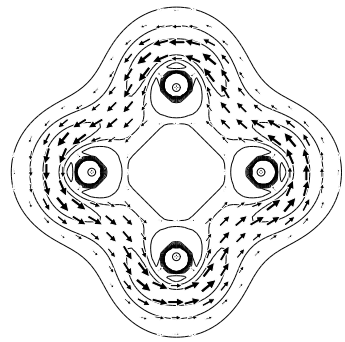

MO	HOMO-4	HOMO-5
Symmetry	E_u	E_u
Eigenvalue	-0.121	-0.121
$\boldsymbol{J}(\boldsymbol{r})$	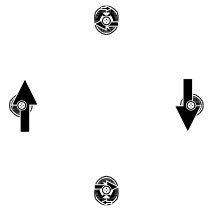	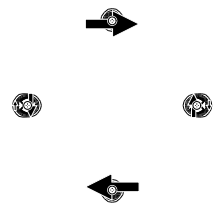

Staying within the same point group, we also examined D_{4h} Li_2 Al_4 , finding again no significant ring current from the π orbital despite the large delocalisation index associated with it. Again the fact that the orbital is delocalised does not allow concluding that there will also be a ring current. In agreement with earlier findings of Havenith et al.[189], the ring currents are qualitatively very similar between the different molecules; suggesting that the Li ions have, as mentioned above, only a modest effect on the electronic structure of the Al_4^{2-} unit. In some compounds, such as the C_s Li_2 Al_4 the ring currents comes from orbitals as low as HOMO-4. There is no relation between the degree of delocalisation of an orbital and the ring current intensity of it, nor can NICS be used to conclude the extent of σ or π contributions to the ring current. A σ ring current survives out of the plane of the Al_4^{2-} unit, whereas a negative NICS computed at a point elevated from the ring centre is often considered testimonial of a π ring current. Such a simple approach is clearly inappropriate.

Another approach to orbital resolved magnetic response is the use of Canonic Molecular Orbitals(CMO)-NICS[203]. In this approach, NICS are dissected in orbital contributions, although in a different way to that performed for computing the ring currents. NICS are computed using the GIAO method[204] and as a consequence the NICS dissected in this way do not have to bear a direct relation or even similarity to the chemical shift that could be computed using the law of Biot-Savart and using the orbital resolved ring currents. As an example, table 11.8 shows the CMO-NICS data for $NICS(1)_{zz}$ for Al_4^{2-}.

Clearly, a different picture arises with CMO-NICS. However, CMO-NICS do not

Table 11.8: CMO-NICS(1)$_{zz}$ for Al_4^{2-}.

	CMO-NICS(1)$_{zz}$		CMO-NICS(1)$_{zz}$
HOMO	-7.96	HOMO-3	-4.14
HOMO-1	-7.39	HOMO-4	-8.04
HOMO-2	-9.41	HOMO-5	-8.04

have the nice conceptual interpretability as orbital resolved ring currents. The latter, in the ipsocentric formulation, arise purely from occupied-virtual transitions whereas in CMO-NICS many other terms are involved too, including occupied-occupied interactions[205]. This may lead to the, according to us wrong conclusion, that the strong diatropic currents in the compounds studied here are also in part due to the π system.

The problem naturally remains as to what one should think of the use of the word aromaticity in this context. Here the lack of a proper definition becomes most apparent. When considering a molecule aromatic based on the presence of electron delocalisation, one can consider all molecules both σ and π aromatic. If one adds as a requirement that the molecule must also sustain a (diatropic) ring current, the molecules here are to be considered σ aromatic. The present example clearly shows that the degree of aromaticity or even any statement on the aromaticity of a molecule depends on the property considered and on whether one is willing to involve only occupied orbitals or also transitions to virtual orbitals. In the case of polyaromatic hydrocarbons, both approaches can be reconciled quite well but this is no longer the case in the present types of molecules.

All the above is based on the question what is the source of aromaticity in the compounds studied here. MCBI data not only for the Al_4^{2-} unit but also for other molecular fragments have been reported, showing that the delocalisation is not restricted to this unit but that also other units show important delocalisation. This then raises the question whether the present molecules should not be considered simply metallic[206].

11.4 Conclusions

It has been shown that there is no direct relation between electron delocalisation and the presence of a ring current, other than that a delocalised system is a necessary but not sufficient condition to lead to a ring current. In the case of Al_4^{2-} derived compounds, there is clearly both σ and π electron delocalisation although only the

σ system gives rise to a ring current. The analysis of CMO-NICS data is shown to lead to a different conclusion although this method also contains occupied-occupied terms and is not so easily interpretable as ipsocentric ring current maps.

Fermi hole analysis and multicentre indices agree very well among each other in describing electron delocalisation.

Concerning the use of the term aromaticity in the present context, one faces the problem of the lack of definition of aromaticity outside the range of benzenoid ring containing molecules. There is no clear cut reason what "benzene like" properties should be conserved most in other molecules to describe them as aromatic. If electron delocalisation suffices, the compounds studied here could be described as both σ and π aromatic. If the presence of a ring current is a requirement for aromaticity, the present molecules are only σ aromatic. We therefore suggest to always narrow down what exactly is meant when using the notion aromaticity. In this context Al_4^{2-} is σ and π aromatic on the account of electron delocalisation but only σ aromatic on the account of presence of a ring current.

Chapter 12

Does aromaticity rule the thermodynamic stability of hydroporphyrins?

12.1 Introduction

Porphyrins are a unique class of compounds that are ubiquitous in nature and perform a wide variety of functions ranging from oxygen transport, electron transfer, and oxidation catalysis to photosynthesis.[207] They are among the most widely distributed and important cofactors found in nature and are crucial regulatory effectors in many biochemical processes. Hydroporphyrins are partly reduced derivatives of the porphyrin ring system in which one or more double bonds have been saturated by the formal addition of hydrogen atoms or alkyl groups across a double bond.[208] Several chemical differences between hydroporphyrins and porphyrins have been observed. For instance, hydroporphyrins have intrinsically larger core sizes and exhibit both a larger tendency to adopt nonplanar conformations and bigger displacements from planarity than the corresponding porphyrin complexes that have similar peripheral substitution.[209–211] Standard reduction potentials of ligand-centred redox processes generally decrease with increasing macrocycle saturation.[212–216] Thus, hydroporphyrin macrocycles are easier to oxidise and more difficult to reduce than porphyrins.

The resistance of the macrocycle to reduction and the larger core size are reasons of why hydroporphyrins can stabilise metal ions in less common, low-valent oxidation states such as Cu(I) and Ni(I),[217–219] which are not readily accessible in porphyrins.

The most common naturally occurring hydroporphyrins are the dihydroporphyrins (Chlorins) and the tetrahydroporphyrins (bacteriochlorins and isobacteriochlorins).[220,221] Depending on the hydrogenation sites one can distinguish different isomers of chlorin (**2a** and **2b** in Figure12.1) and bacteriochlorin (**3a** and **3c**). However, only one isomer of isobacteriochlorin (**3c**) is possible. Representative examples of these hydroporphyrins include chlorophyll, the ubiquitous chlorin that regulates photosynthesis in green plants, algae, and cyanobacteria; bonellin, the sex-differentiating chlorin of the marine worm *Bonella viridis*;[222] bacteriochlorophyll and siroheme, the isobacteriochlorin prosthetic group of numerous sulphite and nitrite reductases.[223,224] Due to their favorable photophysical properties some members of the chlorin and bacteriochlorin families are also of medical interest. For instance, they have been shown to reverse tumor multidrug resistance and may find use in cancer chemotherapy.[225]

On the other hand, in the wake of the investigation of the biosynthesis of vitamin B12 different forms of hexahydroporphyrins (derivatives of molecule **4a**) have also been synthesised.[221] The discovery, structural elucidation and chemistry of factor F430, a dodecahydroporphyrin, has given an additional drive for the study of the chemistry of highly reduced porphyrins.[221] However, the missing links in the series of hydroporphinoid structures, octahydroporphin (**5**) and decahydroporphin have not been found yet.

There is no doubt that most of the physical and chemical properties of porphyrins and hydroporphyrins are intrinsically related to their aromatic character. Thus, two striking properties of the porphin ring (**1**), its visible electronic spectrum and NMR chemical shifts, are due to the delocalised π-electron system and its associated ring currents. Indirect evidence of currents in the porphin ring comes from experimental proton chemical shifts[226] and from calculations of the magnetic shielding at chosen points within the molecule.[227,228] Although the aromaticity of porphin has been extensively confirmed using different aromaticity criteria, the role played by all the possible aromatic pathways in the total aromaticity of porphin is still a controversial issue. Whereas the results obtained by some authors support the presence of a 18π-[16] annulene inner cross aromatic pathway with the C_2H_2 groups of the pyrrolic rings functioning only as exocylic bridges,[227] other results support the existence of a bridged 18π-[18] annulene with the inner NH groups acting as inert bridges.[229–232]

A much smaller number of studies has been devoted to the study of the aromaticity in hydroporphyrins. Only a few addressed the topic in chlorin and bacteriochlorin using magnetic criteria[113,228,233] and bond resonance energy, BRE.[234] Special attention deserve the study of Aihara and co-workers using $BREs$,[234] who quantified

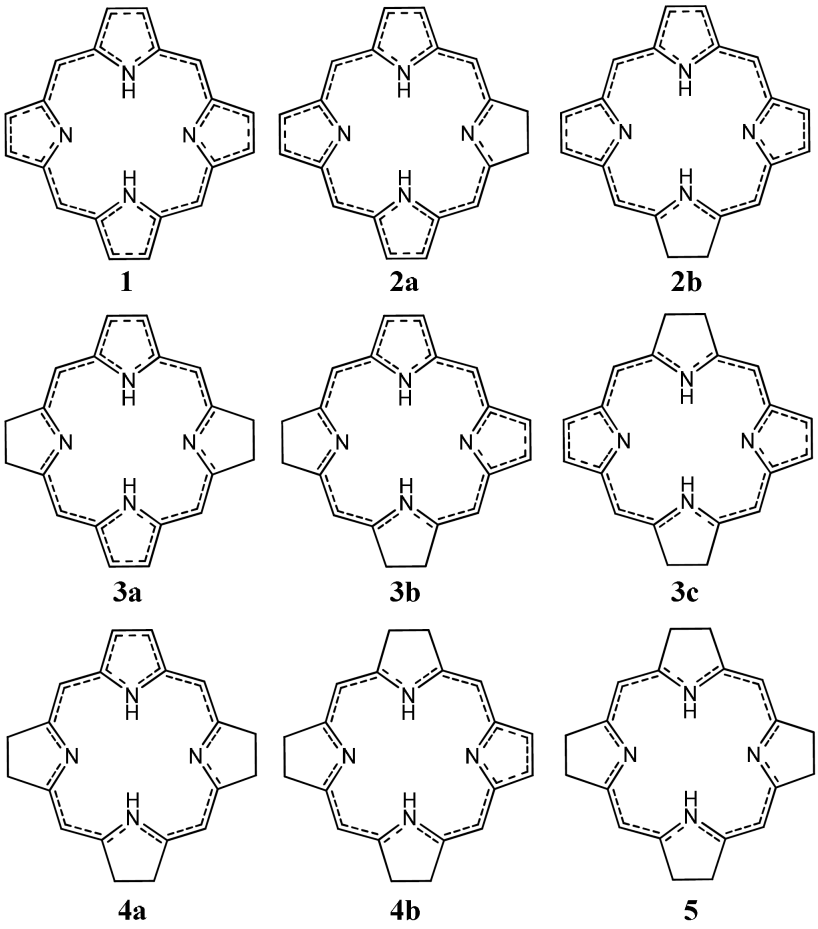

Figure 12.1: Porphin (**1**) and the series of hydroporphirins (**2**-**5**).

at the Hückel molecular orbital level the relative weight of different aromatic pathways on the total aromaticity. Steiner, Fowler and co-workers have previously computed ring current maps for porphyrins, including bacteriochlorin[113,233] and ring current maps obtained in the present study will be compared to theirs. Although several works by these authors did explore several porphyrin derivatives,[114,235,236] they did not consider the complete hydrogenation series as discussed in the present study.

Hydrogenation of porphyrins mostly produces modifications of the electronic structure of the π system, which in turn changes the aromatic stabilisation of the molecules. Then, it is expected that aromaticity plays a key role in the thermodynamic stability of hydroporphyrins. In this work we analyze in detail the aromatic character along the series of molecules represented in Figure 12.1, paying special attention to the local aromaticity and its changes upon hydrogenation. Two main questions, essential for the understanding of the relative abundance of porphyrins in nature, are addressed in this paper; the relative stabilisation of different isomers of hydroporphyrins **2**, **3** and **4** and the apparent thermodynamic instability of octahydroporphin (**5**). Several methodologies comprising magnetic, energetic and electron density based aromaticity criteria are employed in this chapter, putting the different indices calculated in a common scale using recently developed approaches[118,156,158,237,238]. The large set of methods employed here supports the reliability of the results obtained.

12.2 Methodology

12.2.1 Energy Effects of Cycles and Bond Resonance Energies

The extent of conjugation in a given circuit Z of a polycyclic conjugated π-electron system can be measured by the respective *energy effect* of the circuit, *ef(Z)*.[163,164] The *ef(Z)*-quantity is defined as the difference between the total π-electron energy and an appropriate reference energy in which the contributions coming from the given circuit are neglected, whereas contributions coming from any other structural feature are taken into account. Using chemical-graph-theory tools within the Hückel molecular orbital (HMO) theory it can be shown that (see also equation 9.1)

$$ef(G,Z) = \frac{2}{\pi}\int_0^\infty ln\left|\frac{\phi(G,ix)}{\phi(G,ix)+2\phi(G-Z,ix)}\right| d\boldsymbol{x} \qquad (12.1)$$

where G is the molecular graph representing the π-electron system considered, $\phi(G)$ is its characteristic polynomial and $G-Z$ is the subgraph obtained by deleting the circuit Z from G. Details of the underlying theory, as well as an exhaus-

tive bibliography can be found in the review by Gutman[162] and in some recent papers.[175,239,240] On the other hand, the topological resonance energy, TRE,[241,242] is obtained by deleting from G all the possible circuits and measures the total aromatic stabilisation of the system.

Bond resonance energy (BRE)[243,244] is another energetic quantity aimed at measuring the extent of π-electron conjugation in polycyclic systems. Let β the resonance integral between two adjacent p_z orbitals of two atoms P and Q in the Hückel MO theory. By setting $\beta_{PQ} = i\beta$ and $\beta_{QP} = -i\beta$ the cyclic conjugation through the P-Q-bond is blocked. In this modified π-system, no circulation is expected in the circuits that pass along the P-Q-bond. The BRE for the P-Q-bond is calculated as the as the destabilisation energy between the hypothetical, modified, π-system and the unmodified system. Calculated in this way, BRE represents a measure of stabilisation or destabilisation of the system considered due to π-electron conjugation along the circuits that share the given π-bond. The BRE-concept was elaborated and applied in numerous articles (see, for instance references[234,245–247]).

In the present chapter, the parametrisation scheme for the heteroatoms proposed by Van Catladge[248] is used, and calculated *ef*- and BRE-values are expressed in units of the HMO carbon-carbon resonance integral β_{CC}. Because β_{CC} is a negative quantity, positive *ef*- and BRE-values imply thermodynamic stabilisation, whereas negative *ef*- and BRE-values imply thermodynamic destabilisation of the given conjugated π-electron system.

12.2.2 Multi Centre Bond Indices

Given an atomic partitioning of the molecular electron density, the Multi Centre Bond Indices,[18,152] MCBIs, represent the extent to which the electrons are delocalised among a set of n atoms (*vide supra*, Part I). Using the Mulliken partitioning scheme,[66–69] the MCBI for a cycle of n atoms, Δ_n, adopts the following form (*cf.* equation 4.17),

$$\Delta_n = \sum_i \Gamma_i \left[\sum_{\nu\in A} \sum_{\mu\in B} \ldots \sum_{\xi\in F} \left(\mathbf{P}^\alpha\mathbf{S}\right)_{\nu\mu} \left(\mathbf{P}^\alpha\mathbf{S}\right)_{\mu\lambda} \ldots \left(\mathbf{P}^\alpha\mathbf{S}\right)_{\psi\xi} \left(\mathbf{P}^\alpha\mathbf{S}\right)_{\xi\nu} + \right. \tag{12.2}$$

$$\left. \sum_{\nu\in A} \sum_{\mu\in B} \ldots \sum_{\xi\in F} \left(\mathbf{P}^\beta\mathbf{S}\right)_{\nu\mu} \left(\mathbf{P}^\beta\mathbf{S}\right)_{\mu\lambda} \ldots \left(\mathbf{P}^\beta\mathbf{S}\right)_{\psi\xi} \left(\mathbf{P}^\beta\mathbf{S}\right)_{\xi\nu} \right] \tag{12.3}$$

Here $\mathbf{P}^\alpha$ and $\mathbf{P}^\beta$ is the so-called alpha and beta charge and bond order density matrix and $\mathbf{S}$ is the overlap matrix of the basis functions, Greek symbols refer to the

basis functions, and Γ_i is a permutation operator that generates (n-1)! terms by interchanging the Greek basis function labels μ to ξ. The remaining summations run over the basis functions centred on the atoms A, B, *etc.* Since the number of permutations increases rapidly with the number of atoms, the calculation of the multicentre index using equation 12.2 turns out to be unfeasible for large circuits such as the 16 to 20 centre circuits in the hydroporphyrins (*vide infra*). So, in these cases the use of the Giambiagi's ring index, I_n,[122,249]

$$I_n = \left[\sum_{\nu \in A} \sum_{\mu \in B} \ldots \sum_{\xi \in F} \left(\mathbf{P}^{\alpha}\mathbf{S}\right)_{\nu\mu} \left(\mathbf{P}^{\alpha}\mathbf{S}\right)_{\mu\lambda} \ldots \left(\mathbf{P}^{\alpha}\mathbf{S}\right)_{\psi\xi} \left(\mathbf{P}^{\alpha}\mathbf{S}\right)_{\xi\nu} + \right. \tag{12.4}$$

$$\left. \sum_{\nu \in A} \sum_{\mu \in B} \ldots \sum_{\xi \in F} \left(\mathbf{P}^{\beta}\mathbf{S}\right)_{\nu\mu} \left(\mathbf{P}^{\beta}\mathbf{S}\right)_{\mu\lambda} \ldots \left(\mathbf{P}^{\beta}\mathbf{S}\right)_{\psi\xi} \left(\mathbf{P}^{\beta}\mathbf{S}\right)_{\xi\nu} \right] \tag{12.5}$$

where just the consecutive cyclic array of the atoms forming the ring is considered, is a good alternative for the determination of the multicentre electron delocalisation.[121,237] In addition, the value of the multicentre index shows a strong dependence on the number of centres and decreases dramatically as n increases.[152] This makes multicentre indices difficult to compare with other aromaticity measures such as ring currents or *ef(Z)* or even among themselves if rings of different size are involved. The problem can be partially solved using a recently proposed approach,[237] where I_n is first normalised and then transformed to provide estimates of Aiharas circuit resonance energy, CRE,[144] given by,

$$\text{CRE-MCBI} = \frac{1.332}{n} \frac{\left(I_n\right)^{n+1/n}}{\left(I_{n^0}\right)^{n+1/n^0}} \tag{12.6}$$

in which I_{n^0} refers to Giambiagi's ring index of benzene (n^0 = 6), which is employed as reference.

In this chapter the values of CRE-MCBI will be discussed as they contain similar chemical information as the MCBI and can be compared directly to the *ef(Z)*. Using the Biot-Savar law and a reasoning similar to the one that led to equation 8.12, the zz-component of the chemical shielding calculated at the centre of a planar ring with n_b bonds can be approximated by the following expression,

$$\sigma_{zz}(\mathbf{r}_x) \approx A \left[\sum_{i=1}^{n_b} \frac{I_i}{\left|\mathbf{r}_i - \mathbf{r}_x\right|^2} sin(\theta_1) \right] \tag{12.7}$$

where I_i represents the current intensity (positive or negative for diatropic or paratropic sense, respectively) circulating through a given bond i, $\mathbf{r}_i$ is the position vector

of the centre of the bond and θ_i is the angle formed by the current vector at $\mathbf{r}_i$ and $(\mathbf{r}_i - \mathbf{r}_x)$. A is a parameter that mainly depends on the magnetic field strength. As shown in Chapter 8, replacing the values of I_i by the multicentre indices, Δ_n, in equation 12.7 one can estimate the value of the zz component of the nuclear independent chemical shift NICS$_{zz}$, which is defined as -σ_{zz}.

12.3 Computational Details

Geometries and energies of the series of molecules **1**-**5** were obtained at the B3LYP/6-31++G(d,p) level using the Gaussian 03 program.[120] Energies and molecular symmetries can be seen in Table 12.1, whereas geometries have been incorporated in atomic Cartesian coordinates in the Supporting Information[1]. As a remarkable feature we have found that hydrogenation of non-protonated pyrrol rings preserves the planar structure of the C-N skeleton of porphin, where hydrogenation of protonated pyrrol rings results in a distortion from planarity. However, the energy difference between planar and non-planar geometries is very small (between 0.1 and 0.5 kcal mol^{-1}). In the planar structures the molecular orbitals can be univocally classified as σ and π, so that ring currents and multicentre indices can be split up into σ and π contributions, the latter being related to the π-aromaticity of the system. For that reason we will only discuss the planar structures. NICS$_{zz}$ obtained at different points within the molecules and the zz-component of the magnetic susceptibility, χ_{zz}, were also calculated at the B3LYP/6-31++G(d,p) level.

Calculations of ring currents and multicentre indices were performed using a minimal basis set (STO-3G) and own Fortran routines requiring as only input formatted checkpoint files from Gaussian 03. The required two-electron integrals for the ring currents are obtained from locally modified codes from the BRABO ab initio package.[250] The reason for such reduction of the basis set in these calculations is merely computational. It has been proven for the calculation of ring currents[116,251] and multicentre indices[97,117,118,156,158,237,238] that a minimal basis set provides essentially the same information as other larger basis sets with a much lower computational effort. This is because the main important factors here are the symmetry and the shape of the molecular orbitals. Symmetry does not depend on the basis set and the shape of the orbitals is not significantly altered by the number of basis functions employed. Even using the pseudo-π method[116,251], where carbons are replaced by hydrogens and the STO-3G basis set is employed, one captures the same essential information about the ring currents and multicentre electron delocalisation in polycyclic aromatic hydrocarbons. Unfortunately, the pseudo-π method is not applicable

[1] http://www.quantum.ugent.be/stijn/SICHAPTER12.pdf

Table 12.1: B3LYP/6-31++G(d,p) molecular electronic energies, E, topological resonance energies, TRE, and molecular symmetries. E is given in au and TRE in β units (see text).

Mol	**Symmetry**	**E** (Hartree)	**TRE**
1	D_{2h}	-989.61198	0.4322
2a	C_{2v}	-990.82771	0.3955
2b	C_2	-990.81659	—
	$C_{2v}^{[a]}$	-990.81643	0.3319
3a	D_{2h}	-992.03853	0.3172
3b	C_1	-992.03173	—
	$C_s^{[a]}$	-992.03150	0.3087
3c	C_{2h}	-992.01061	—
	$D_{2h}^{[a]}$	-992.01031	0.2280
4a	C_2	-993.24051	—
	$C_{2v}^{[a]}$	-993.24006	0.2407
4b	C_2	-993.22223	—
	$C_{2v}^{[a]}$	-993.22165	0.2140
5	C_{2h}	-994.41895	—
	$D_{2h}^{[a]}$	-994.41816	0.0770

[a] Structures with the C-N skeleton in planar conformation

to porphyrins because we have to distinguish between nitrogen and carbon atoms. The magnetic field is always considered perpendicular to the plane formed by the C-N skeleton and the perturbed orbitals are computed using the first order coupled Hartree-Fock approach (FO-CHF). Ring currents are plotted on a grid in or one Bohr above the molecular plane with a diatropic current represented by a counterclockwise circulation.

Multicentre indices and energy effects of cycles were calculated for all the circuits represented in Figure 12.2. Then, CRE-MCBI values were obtained using equation 12.6, current intensities and magnetic susceptibilities were estimated from the MCBI values following the procedure described in reference[237] and NICS$_{zz}$ values were estimated from equation 12.7. Ring current maps as well as MCBI were both separated into σ and π contributions, and the results obtained for the latter are presented in the next section. Orbital resolved ring current maps were also calculated for all molecules.

12.4 Results and Discussion

Thermodynamic Stability of Hydroporphyrins Taking into account that the isomerisation of the hydroporphyrins of Figure 12.1 does not entail a significant change of entropy, we will employ the molecular electronic energy to establish the relative thermodynamic stability of different isomers. Thus, the molecular electronic energies collected in Table 12.1 clearly reflect that the most stable isomers correspond to the molecules labelled by "**a**". This means that the hydrogenation of non-protonated pyrrol rings is thermodynamically favoured over the hydrogenation of protonated pyrrol rings throughout the series. This is not a new finding but just confirms the experimental observations. One of the main goals of this work is to elucidate whether or not aromaticity responsible for this thermodynamically favoured hydrogenation of non-protonated pyrrol. A first proof of the important role played by the aromatic stabilisation in hydroporphyrins can be found in the values of the TRE collected in Table 12.1. They reflect the same stability sequence as the *ab initio* energies, even the TRE is able to predict the small destabilisation of the isomer **3b** with respect to **3a** and a much larger destabilisation of the isomer **3c**.

There are many ways of accounting for the relative aromatic stabilisation of isomers. However, the difference between the isomers considered in this work is just the hydrogenation site. The most suitable quantity thus seems to be the BRE of the C-C bond involved in the process. All hydrogenation paths linking the hydroporphyrins of Figure 12.1 are summarised in Figure 12.3 and confronted with the $BREs$ and the *ab initio* hydrogenation energies involved. The hydrogenation energies were calcu-

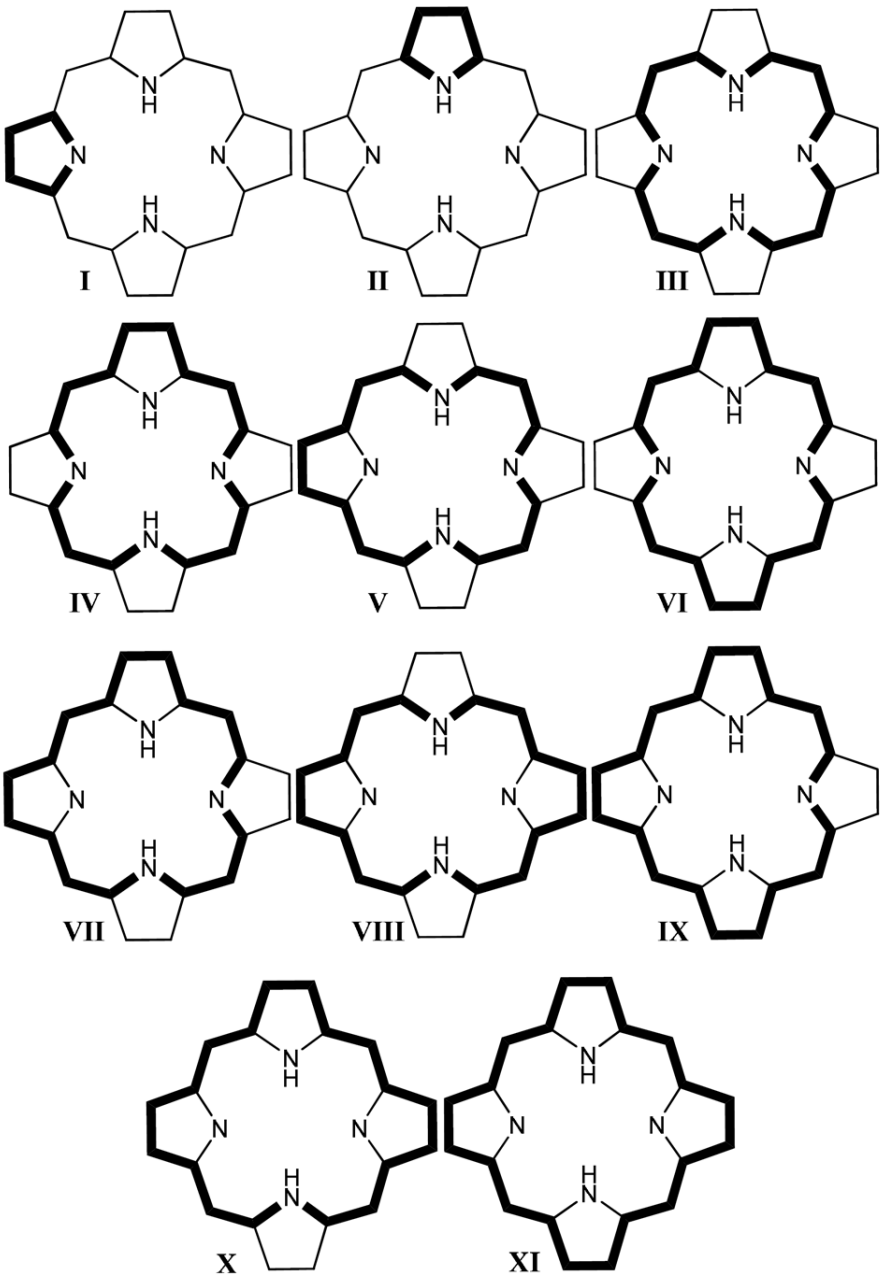

Figure 12.2: Ring circuits in porphin.

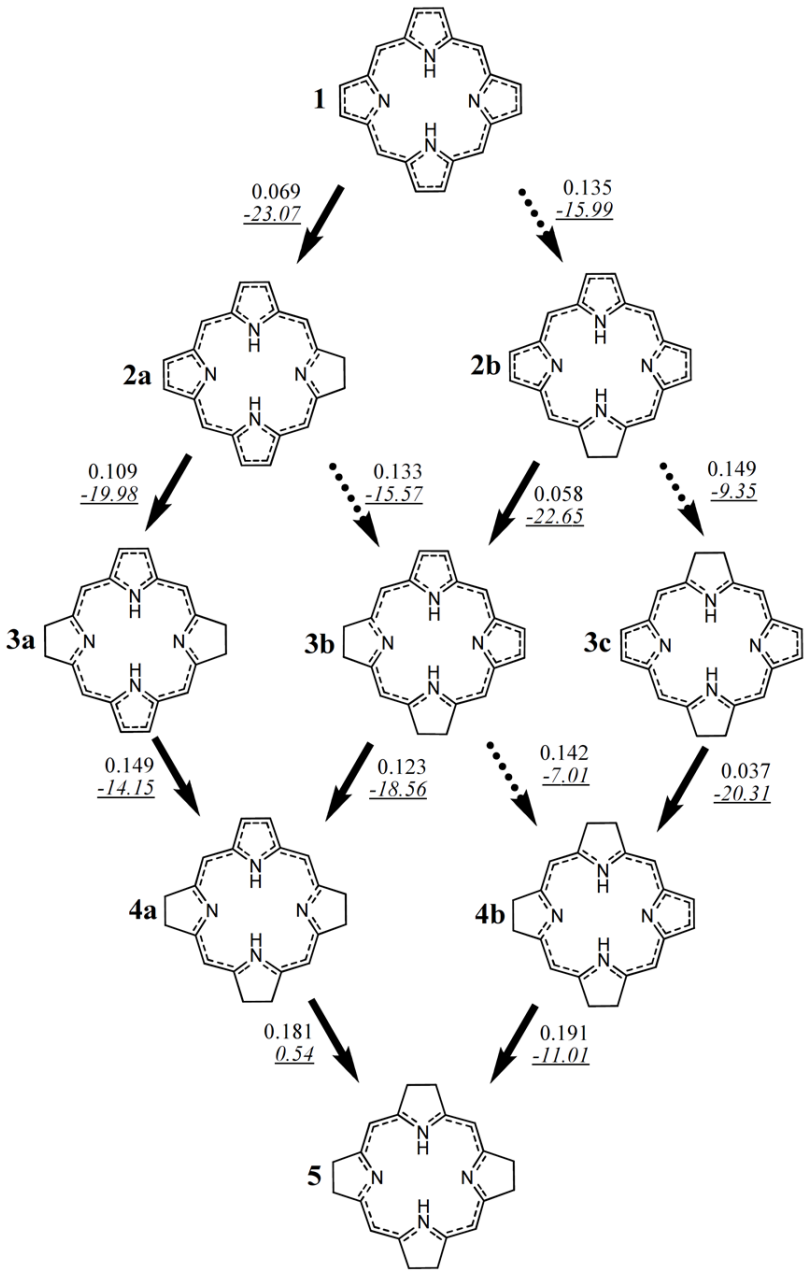

Figure 12.3: Hydrogenation paths linking porphin (**1**) with octahydroporphin (**5**), $BREs$ for the C-C bonds involved in the hydrogenation (in β units, see text) and B3LYP/6-31++G(d,p) hydrogenation energies (underlined, in kcal.mol^{-1}). Solid arrow indicates the thermodynamically favoured path whereas the unfavoured one is indicated with a dashed arrow.

lated as the difference between the electronic energy of the hydrogenated product and the sum of the electronic energy of the non-hydrogenated reactant plus the electronic energy of the isolated hydrogen molecule. As mentioned in the "Computational Details" section only the planar structures were employed in the calculations. In the figure the thermodynamically favoured paths are denoted by solid arrows whereas the unfavoured ones are denoted by dashed arrows. In all cases the favoured hydrogenation coincides with the smallest BRE value, which means that the hydrogenation occurs on the C-C bond where the entailing aromatic destabilisation is smaller. Figure 12.3 shows that the most stable products resulting from the progressive hydrogenation of porphin correspond to the series **2a**-**3a**-**4a**. The hydrogenation of **4a** to give **5** is energetically unfavoured with a positive hydrogenation energy and a quite large value of the BRE. Moreover, the entropic contribution to the Gibbs free energy is expected to disfavour even more the hydrogenation process, at least within the ideal gas phase model. On the contrary, the hydrogenation of **4b** to give **5** is energetically feasible, but the previous formation of **4b** is unlikely according to the energies presented in Figure 12.3.

Table 12.2: *ef(Z)* and CRE-MCBI values calculated for the ring circuits depicted in Figure 12.2. All values are given in β units (see text). Values for circuits with no π-conjugation are not included because of being zero or close to zero (in the case of CRE-MCBI).

	Mol/Ring	I	II	III	IV	V	VI	VII	VIII	IX	X	XI
1	*ef(Z)*	0.0450	0.0799	0.0075	0.0100	0.0034	0.0130	0.0042	0.0013	0.0052	0.0015	0.0017
	CRE-MCBI	0.0713	0.0764	0.0062	0.0069	0.0029	0.0076	0.0032	0.0014	0.0036	0.0015	0.0017
2a	*ef(Z)*	0.0808	0.0806	0.0064	0.0086	0.0033	0.0114	0.0041	—	0.0051	—	—
	CRE-MCBI	0.0796	0.0767	0.0069	0.0080	0.0036	0.0093	0.0048	—	0.0042	—	—
2b	*ef(Z)*	0.0392	0.1016	0.0102	0.0134	0.0047	—	0.0059	0.0019	—	0.0023	—
	CRE-MCBI	0.0718	0.0966	0.0063	0.0078	0.0031	—	0.0038	0.0015	—	0.0019	—
3a	*ef(Z)*	—	0.0894	0.0099	0.0138	—	0.0188	—	—	—	—	—
	CRE-MCBI	—	0.0812	0.0081	0.0099	—	0.0122	—	—	—	—	—
3b	*ef(Z)*	0.1013	0.1022	0.0116	0.0162	0.0063	—	0.0081	—	—	—	—
	CRE-MCBI	0.0815	0.0995	0.0066	0.0085	0.0036	—	0.0048	—	—	—	—
3c	*ef(Z)*	0.0196	—	0.0292	—	0.0129	—	—	0.0052	—	—	—
	CRE-MCBI	0.0858	—	0.0104	—	0.0055	—	—	0.0029	—	—	—
4a	*ef(Z)*	—	0.1319	0.0187	0.0276	—	—	—	—	—	—	—
	CRE-MCBI	—	0.1110	0.0065	0.0094	—	—	—	—	—	—	—
4b	*ef(Z)*	0.1532	—	0.0204	—	0.0067	—	—	—	—	—	—
	CRE-MCBI	0.1082	—	0.0111	—	0.0072	—	—	—	—	—	—
5	*ef(Z)*	—	—	0.0770	—	—	—	—	—	—	—	—
	CRE-MCBI	—	—	0.0156	—	—	—	—	—	—	—	—

The BRE of a given bond can be analysed in detail with the energy effects of the circuits that share the bond. All the possible circuits are shown in Figure 12.2 for the porphin molecule, but depending on the hydrogenation sites some of them may not appear in the corresponding hydroporphyrin. The *ef(Z)* and CRE-MCBI values calculated for these circuits are collected in Table 12.2. First, we must mention that there are important discrepancies between both quantities. Thus, according to the *ef(Z)* values the aromatic stabilisation of protonated pyrrol rings is larger than that of non-protonated pyrrol rings except for molecules **2a** and **3b**. On the contrary, the CRE-MCBI values do not reflect important differences between both, being in general larger for the protonated pyrrol. The *ef(Z)* values associated to the macrocycles are in general larger than the CRE-MCBI values, with the exception of porphin and the naturally occurring hydroporphyrins (chlorin (**2a**) and bacteriochlorin (**3a**)) where the values are quite similar. In spite of these differences, a similar explanation for the relative stabilisation of the isomers is extracted from the *ef(Z)* and CRE-MCBI values. Thus, in both cases the aromatic stabilisation of macrocycles **IV** (17 centres), **VI** (18 centres) and **IX** (19 centres) is significantly larger than that of the corresponding macrocycles **V** (17 centres), **VII** and **VIII** (18 centres) and **X** (19 centres) for all the isomeric series. Macrocycles **IV**, **VI** and **IX** encircle the protonated pyrrol rings and leave out the non-protonated ones, contributing to the resonance energy of the C_β-C_β bonds in the former. On the contrary, macrocycles **V**, **VII** and **X** encircle the non-protonated pyrrol rings and leave out the protonated ones, contributing to the resonance energy of the C_β-C_β bonds in the former. The result is that hydrogenation of protonated pyrrol rings breaks the cyclic electron delocalisation in macrocycles with stronger π-electron conjugation, which entails a larger aromatic destabilisation. This is in fact in agreement with qualitative information obtained from traditional non-polar Kekulé structures in combination with the conjugated circuits model.[154,252,253] According to the conjugated circuits model, only rings supporting conjugated circuits are expected to contribute significantly to the aromatic stabilisation. In our case, due to the small values for the conjugated circuits encircling the rings **V**, **VII**, **VIII** and **X** (Table 12.2) these rings are expected to provide a smaller aromatic stabilisation. In recent contributions some of the authors showed the connection existing between conjugated circuits and measures of aromaticity such as MCBI[254] and ring currents[255] in polycyclic aromatic hydrocarbons.

The most remarkable difference between *ef(Z)* and CRE-MCBI values is found in the macrocycle **III**, the central 16-centre ring, in molecule **5**. The CRE-MCBI predicts a much lower aromatic stabilisation associated to this macrocycle than the *ef(Z)*. This seems to reflect a divorce between aromatic stabilisation and electron delocalisation. In principle the absence of conjugated circuits in this macrocycle should be reflected by a relatively small electron delocalisation. This is true for molecules **1**, **2a**,

2b, **3a**, **3b** and **4a**, where the *ef(Z)* and CRE-MCBI values of cycle **III** are lower than those of cycles **IV** and **VI**. The fact that these cycles contain a larger number of centres than cycle **III**, so decreasing their relative aromatic stabilisation, reinforces the result. However, the *ef(Z)* of molecule **5** is remarkably large and does not come with a parallel increase of the π-electron delocalisation. The aromatic stabilisation due to the π-conjugation in this circuit is significantly large but the electron delocalisation is still small in agreement with the qualitative predictions. It must be mentioned here that results obtained by Jusélius *et al.* using the aromatic ring current shielding (ARCS) method[228] also pointed out to that an aromatic pathway corresponding to cycle **III** (a 18π-[16]annulene inner cross) only exists in the octahydroporphin **5**.

The Ring Current Maps of Hydroporphyrins Measures of the magnetic response of the system can shed light on the contradictions between aromatic stabilisation and electron delocalisation in these systems. *Ab initio* π-ring currents are represented in Figure 12.4 and the translational and rotational transitions (*vide supra*, section 5.3), are depicted in Figure 12.5. The π-ring current map of porphin (**1**) shows a ring current that is bifurcated around the protonated pyrrol rings, the current being somewhat stronger at the outer side of the ring. In the non-protonated pyrrol rings, however, the current remains at the inside of the ring, with virtually no π-current running through the outer side of the ring. The ring current mainly originates from the translational transitions from the HOMO and HOMO-1 to the LUMO and LUMO+1 (see Figure 12.5). Apart from these, there is a relatively small rotational transition from the HOMO-2 to the LUMO, corresponding to a paratropic current encircling the two non-protonated pyrrol rings. The observed bifurcation is in agreement with the findings by Steiner and Fowler.[113,233] Their interpretation of the ring current in terms of only four active electrons is also in good agreement with the diagram presented in Figure 12.5. Steiner and Fowler did not mention the small rotational transition although our diagram also shows that this contribution is likely very small due to the larger energy difference between the two molecular orbitals involved. Figure 12.7 indeed also confirms that the HOMO-2 contribution to the ring current is very small.

When hydrogenating a non-protonated pyrrol ring of porphin (to form dihydroporphin (**2a**)), the π-ring current pattern remains unchanged. Examining the diamagnetic and paramagnetic contributions shows that the HOMO-2 to the LUMO rotational transition has disappeared. Instead, two small rotational transitions from the HOMO and HOMO-1 are present (HOMO to LUMO and HOMO-1 to LUMO+1). Hydrogenating a protonated pyrrol ring on the other hand largely annihilates the ring current of the molecule **2b**. Besides becoming smaller, the bifurcation around the non-protonated pyrrol ring is lost, the ring current running over the outer side of the ring. The HOMO-LUMO gaps of molecules **2a** and **2b** are more or less the same and

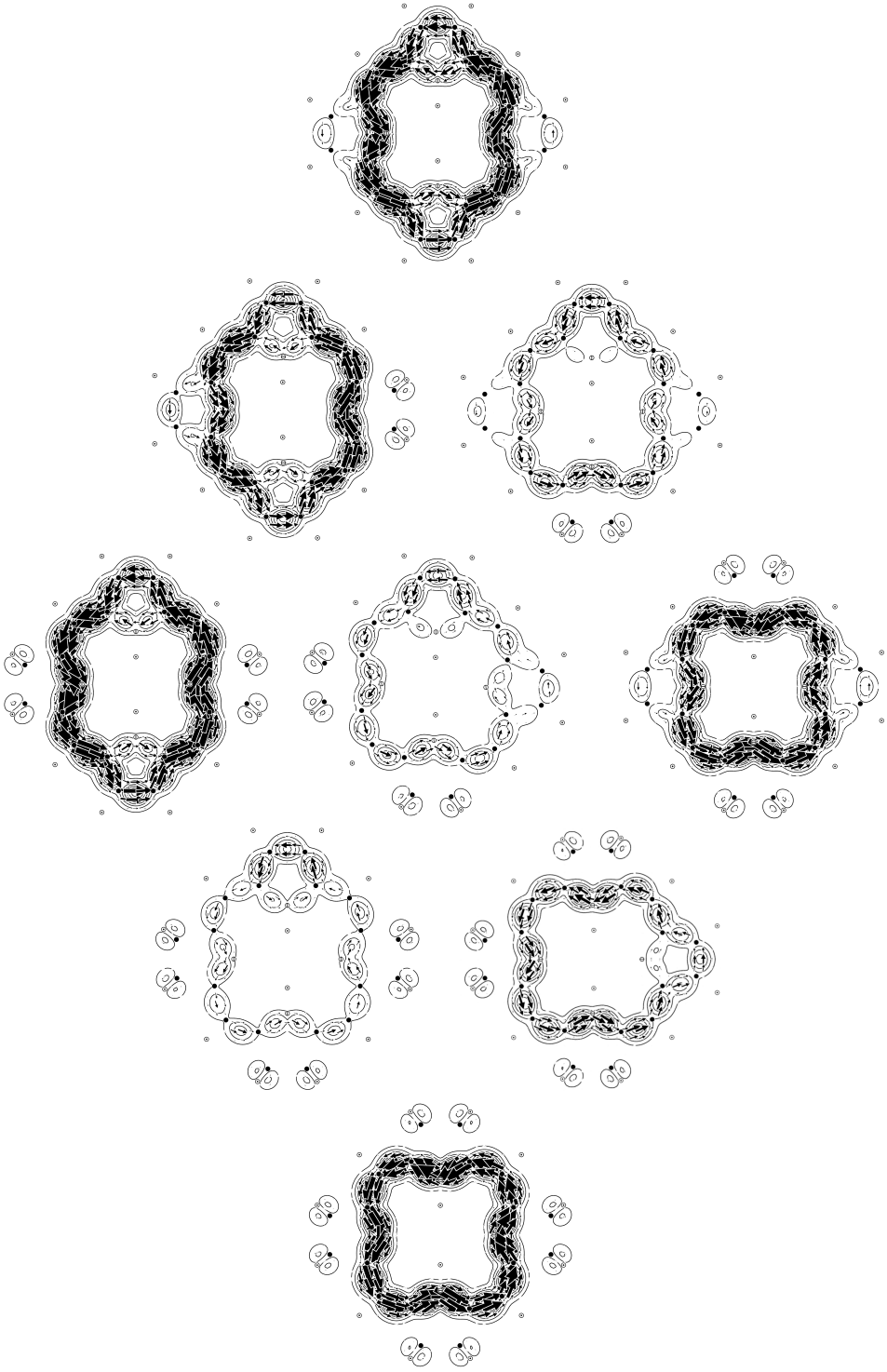

Figure 12.4: CPHF/STO-3G π ring current plots obtained at 1 Å above the molecule

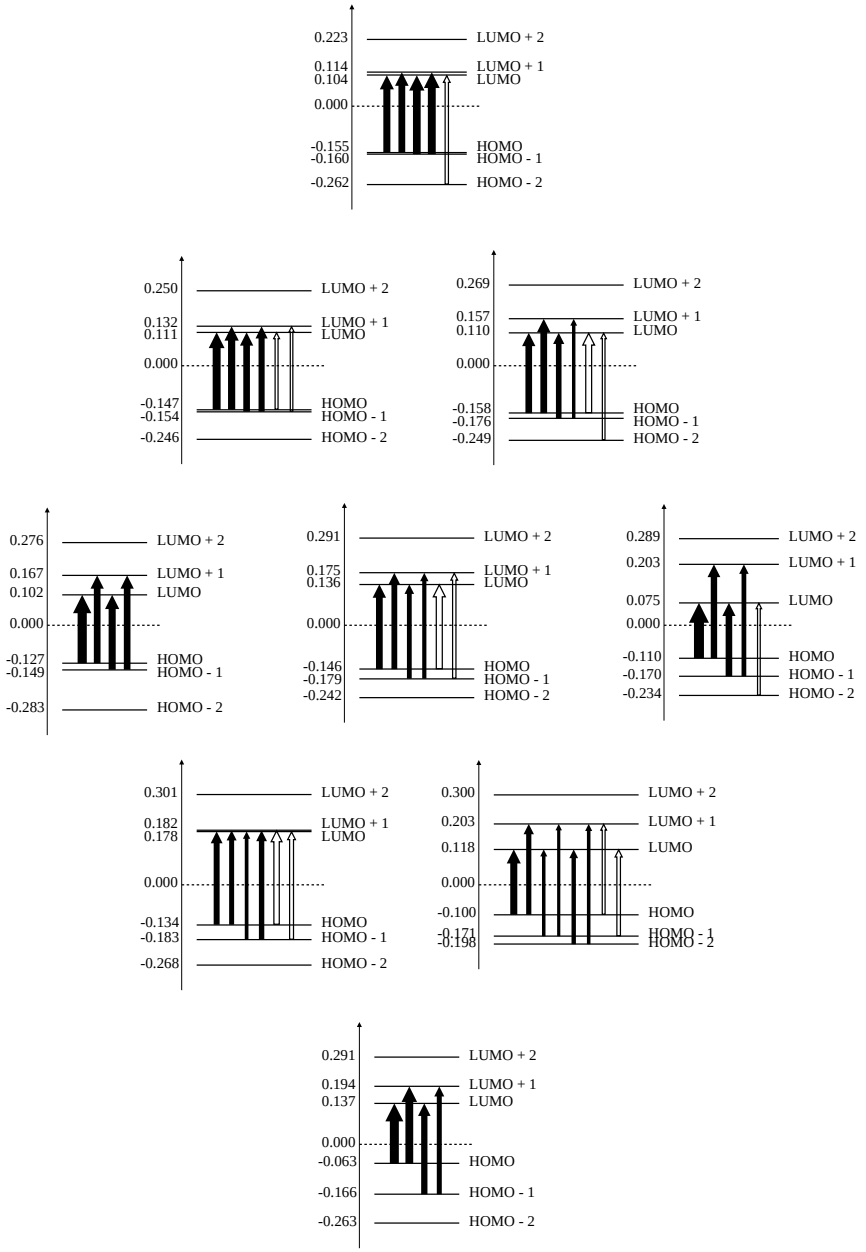

Figure 12.5: Translational (diatropic, black arrows) and rotational (paratropic, arrows without filling) transitions between individual pairs of an occupied and virtual orbital for all molecules. Only significant contributions are shown and the width of the arrow reflects the magnitude of the contribution to the total current. The vertical axis denotes orbital energies (in au)

thus do not explain the change in the ring current. The reason for the dramatic change can be seen in the transition-diagram, which shows how the translational transitions become smaller compared to molecule **2a** and how the HOMO to LUMO rotational transition becomes stronger. Moreover, there is the same small rotational transition from the HOMO-2 to the LUMO as in porphin, diatropically encircling the two non-protonated pyrrol rings.

Hydrogenating the second non-protonated pyrrol ring of **2a** (to form tetrahydroporphin (**3a**)), once again has no impact on the form of the π-ring current pattern. The HOMO-LUMO gap is smaller than that of molecule **2a**, the translational transitions are larger (possibly due to the smaller HOMO-LUMO gap) and the rotational transitions are gone. This explains the somewhat larger ring current compared to molecule **2a**.

Tetrahydroporphin (**3b**), like dihydroporphin (**2b**), has smaller translational transitions and a large HOMO to LUMO rotational transition, explaining the small ring current of the molecule. The HOMO-2 to the LUMO rotational transition is no longer present, but a small HOMO-1 to LUMO+1 rotational transition can be seen. Molecule **3b** also has the largest HOMO-LUMO gap of the molecules **3a-c**.

Tetrahydroporphin (**3c**) has a strong diamagnetic ring current pattern, following macrocycle **III**. The molecule has a much smaller HOMO-LUMO gap than molecules **3a** and **3b**. It has strong translational transitions from the HOMO and HOMO-1 to the LUMO and LUMO+1 (possibly due to the smaller HOMO-LUMO gap) and the same small rotational transition from the HOMO-2 to the LUMO as in porphin and molecule **2b**, encircling the two non-protonated pyrrol rings.

Hexahydroporphins **4a** and **4b** both have a relatively weak ring current, the one of **4b** being somewhat larger than that of **4a**. Both molecules have small translational transitions compared to the other molecules and both have two rotational transitions from HOMO to LUMO+1 and from HOMO-1 to LUMO. Molecule **4b** has the smallest HOMO-LUMO gap and two important extra HOMO-2 to LUMO and LUMO+1 translational transitions, explaining the larger ring current.

Octahydroporphin (**5**), like tetrahydroporphin (**3c**), has a strong diamagnetic ring current pattern, following macrocycle **III**. The molecule only has large translational transitions from the HOMO and HOMO-1 to the LUMO and LUMO+1.

The *ab initio* ring current plots can be compared with the pictorial representation of the ring currents obtained from multicentre indices (represented in Figure 12.6). In this figure the arrows represent both the sense and the relative strength of the current intensity circulating through each bond. The intensity for a given bond is obtained by summation of the I_i values, estimated using multicentre indices, of all circuits containing the bond.

As one can see comparing Figure 12.4 and Figure 12.6, there is a good correspon-

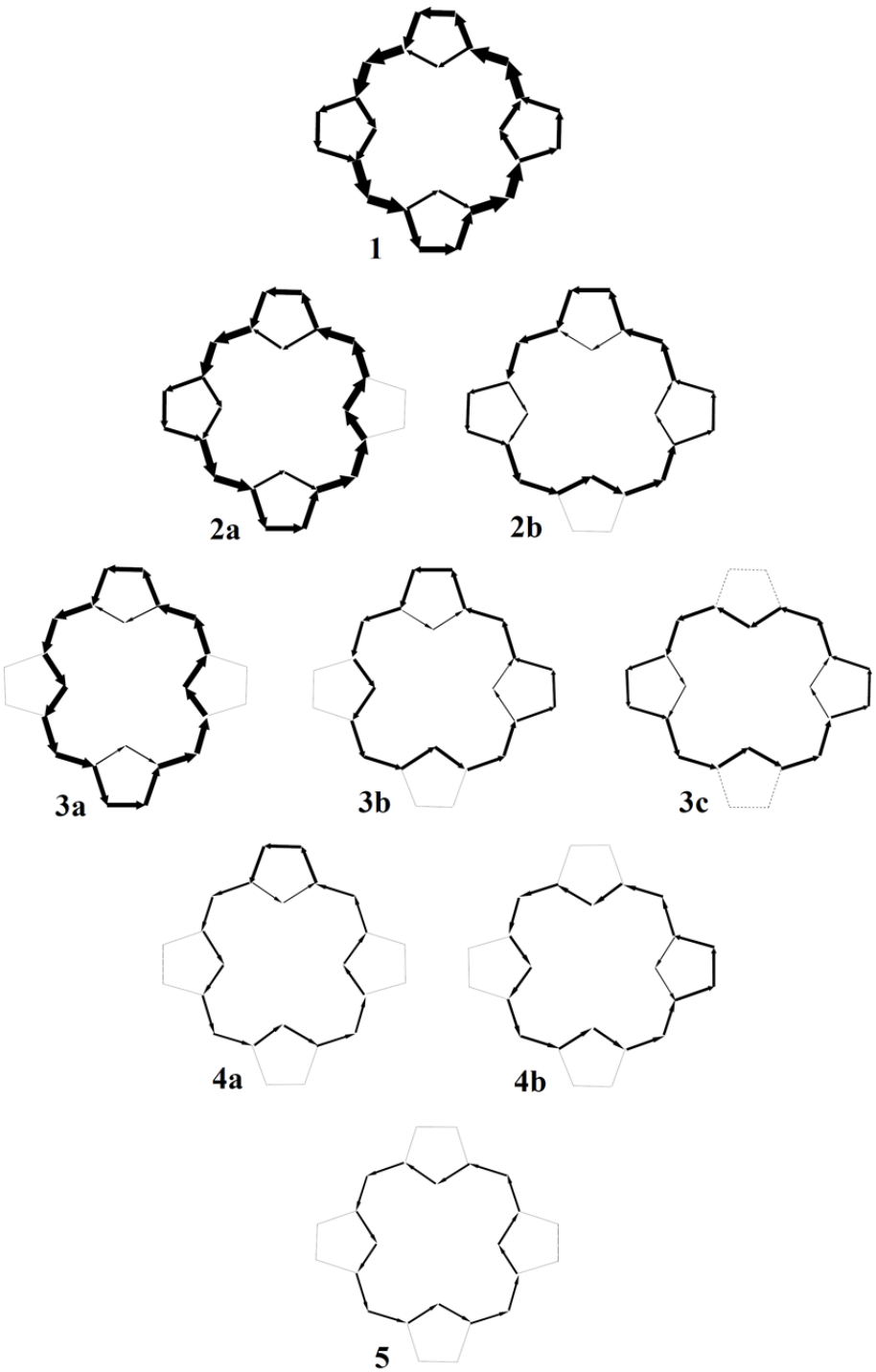

Figure 12.6: Pictorial representation of the ring currents obtained from multicentre indices.

dence between MCBIs and ring currents for most of molecules. However, multicentre indices predict a remarkably smaller current intensity in octahydroporphin **5**, similar to that of hexahydroporphin **4a**. As one can see in the figure, the same happens for tetrahydroporphin **3b**. An explanation for this disagreement can be found in the analysis of the orbital interactions. As mentioned before there are three necessary conditions for a strong ring current; large values for a translational (or rotational) transition, a favourable spatial distribution of the occupied and virtual orbitals and a small energy gap between these orbitals (see 5.3). The latter of these condition causes the ring current to be mainly produced by interactions between the highest occupied orbitals and the lowest virtual orbitals. The MCBI depends only on the first order density matrix, which does not contain explicitly information on the virtual orbitals. Hence, the MCBI and derived quantities cannot reflect all subtleties that differentiate among molecules.

We have depicted the orbital contributions to the ring current from the four highest occupied orbitals of molecules **1**, **4a** and **5** in Figure 12.7 (the complete orbital resolved ring currents for all molecules can be found in the Supporting Information[2]). As one can see, only two orbitals (HOMO and HOMO-1) have a significant contribution to the ring current. These orbitals yield a strong current density along the central ring for molecules **1** and **5**, whereas the current density is significantly smaller for molecule **4a**. We are now able to state that, even when two hydroporphyrins present similar ring electron delocalisation, they can display significantly different ring current densities if their occupied-virtual orbital interactions differ substantially.

On the other hand, we have replaced the values of the CRE-MCBI by the *ef(Z)* to represent the current intensity in molecules **4a** and **5** and to check if discrepancies also appear using energy effects. This is not however completely supported by theory as the mathematical relation between electron current intensity and energy stabilisation due to cyclic electron conjugation was established by Aihara[144] using the circuit resonance energy, CRE, which differs from Gutman's definition of *ef(Z)*. However, both quantities usually correlate and are expected to provide very similar information. As one can see in Figure 12.8, the *ef(Z)* values predict the stronger current in molecule **5**. There is, however, a discrepancy with the ring current maps that is corrected using multicentre indices. Thus, the paratropic sense of the current circulating by the C-N(H)-C unit in the non-hydrogenated Pyrrol ring of **4a** is wrongly represented using the *ef(Z)* values but correctly represented with multicentre indices.

Additional proof of the differences in the magnetic response of molecules **4a** and **5** can be obtained from the values presented in Table 12.3 for the magnetic susceptibility and $\mathrm{NICS}_{zz}(1)$ calculated one Å above the centre of the molecule. The centre of the molecule was chosen as the position of the ring critical point of the electron

[2] http://www.quantum.ugent.be/stijn/SICHAPTER12.pdf

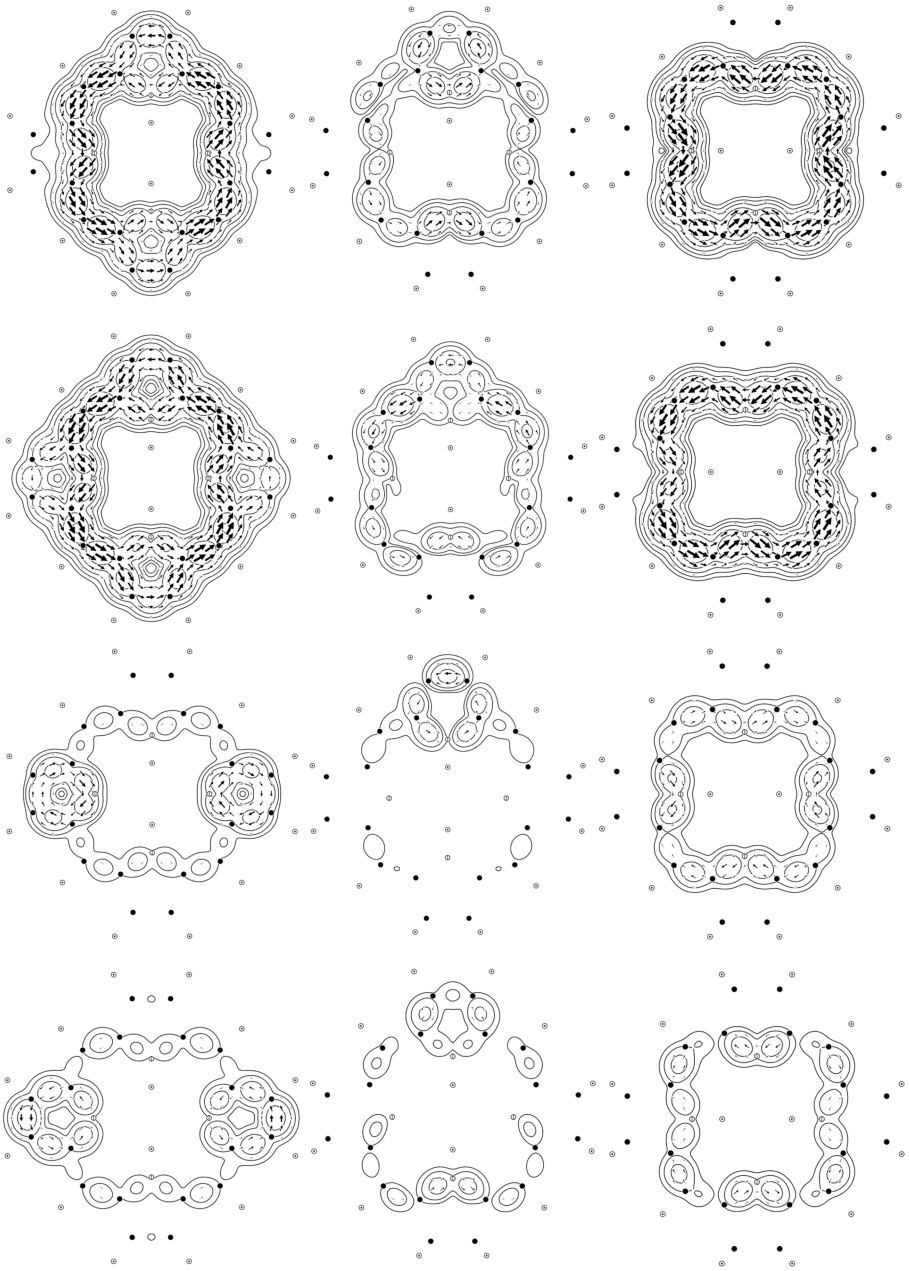

Figure 12.7: Orbital resolved ring currents for molecules **1**, **4a** and **5** (from left to right). In the figure are represented the contributions from the HOMO, HOMO-1, HOMO-2 and HOMO-3 (from up to down).

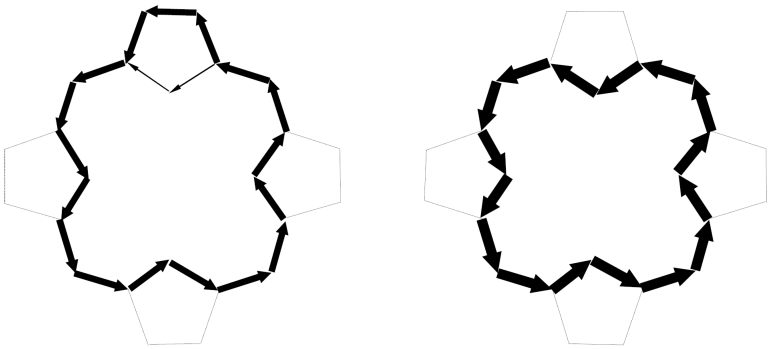

Figure 12.8: Pictorial representation of the ring currents obtained from *ef(Z)* values for molecules **4a** (left) and **5** (right).

Table 12.3: zz component of the magnetic susceptibility tensor, χ_{zz}, and NICS$_{zz}$(1) values calculated at the B3LYP/6-31++G(d,p) level. Values for the hydrogenated pyrrol rings are not included because of being non-aromatic rings. Values of χ_{zz} are given relative to the value of isolated benzene, NICS$_{zz}$(1) values are in ppm.

Mol	$\chi_{\mathbf{zz}}$	**NICS$_{zz}$(1)**$^{[a]}$	**NICS$_{zz}$(1)**$^{[b]}$	**NICS$_{zz}$(1)**$^{[c]}$
1	8.33	-37.4	-32.2	-12.9
2a	7.26	-32.6	-32.1	-16.8
2b	6.10	-24.1	-30.6	-14.7
3a	6.68	-33.0	-35.3	—
3b	4.67	-16.7	-29.3	-18.2
3c	5.81	-28.2	—	-19.1
4a	3.83	-13.5	-31.1	—
4b	4.29	-19.9	—	-25.2
5	4.27	-24.5	—	—

[a] Calculated at the centre of ring circuits of type III (see Figure 12.2)

[b] Calculated at the centre of ring circuits of type II (see Figure 12.2)

[c] Calculated at the centre of ring circuits of type I (see Figure 12.2)

density corresponding to the central ring.

The zz component of the magnetic susceptibility tensor is slightly larger for **5** than for **4a**, even though the large differences in the ring currents are not reflected on the magnetic susceptibilities. On the other hand, the $NICS_{zz}(1)$ calculated at the central ring is significantly larger for **5** than for **4a**. However, both the magnetic susceptibility and the $NICS_{zz}(1)$ are significantly smaller for molecule **5** than for molecules **1**, **2a** and **3a**, differences that do not match well the ring current plots. It must be also mentioned that the $NICS_{zz}(1)$ values calculated at the centre of the non-hydrogenated Pyrrol rings increases when going from **1** to **5** (see values in Table 12.3), which is in agreement with the parallel increase of the CRE-MCBI and *ef(Z)* values for these rings.

Turning back to Figure 12.4, one can glimpse that differences between magnetic and electron density criteria of aromaticity for the series of hydroporphyrins only affect molecules **5** and **3c**. Comparing magnitudes such as magnetic susceptibilities and NICS can help to confirm this observation. Thus, the magnetic susceptibility exaltations obtained from multicentre indices, χ-MCBI, correlate perfectly with the *ab initio* zz component of the magnetic susceptibility tensor. It can be seen in Figure 12.9 that only molecules **3c** and **5** display a noticeable deviation. In spite of the worse regression coefficient, the correlation found between *ab initio* $NICS_{zz}(1)$ and NICS estimated from multicentre indices is even more remarkable. Taking into account the rough approximations introduced in equation 12.7 for the calculation of the magnetic shielding, the correlation shown in Figure 12.9 can be considered quite satisfactory. Once again, molecules **3c** and **5** are the ones displaying important deviations.

It must be mentioned that we have also replaced the CRE-MCBI values by the *ef(Z)* to get similar representations to those of Figure 12.9. The correlations obtained using *ef(Z)* were significantly worse than those obtained with CRE-MCBI, which indicates that even though the circuit energy effects account for the different magnetic response of molecules **4a** and **5**, multicentre indices correlate in general better with magnetic indices. The fact that energy effects lead to a worse representation of the magnetic response of the systems investigated here could be related to the level of calculation. In porphyrins and hydroporphyrins the presence of heteroatoms and hydrogenated rings is difficult to account for with the limitations of the HMO level.

12.5 Conclusions

The relative stability of different hydroporphyrin isomers as well as the naturally and synthetically inaccessibility of octahydroporphin (**5**) have been explained in terms of total and local aromaticity by using a large variety of methods, including energetic,

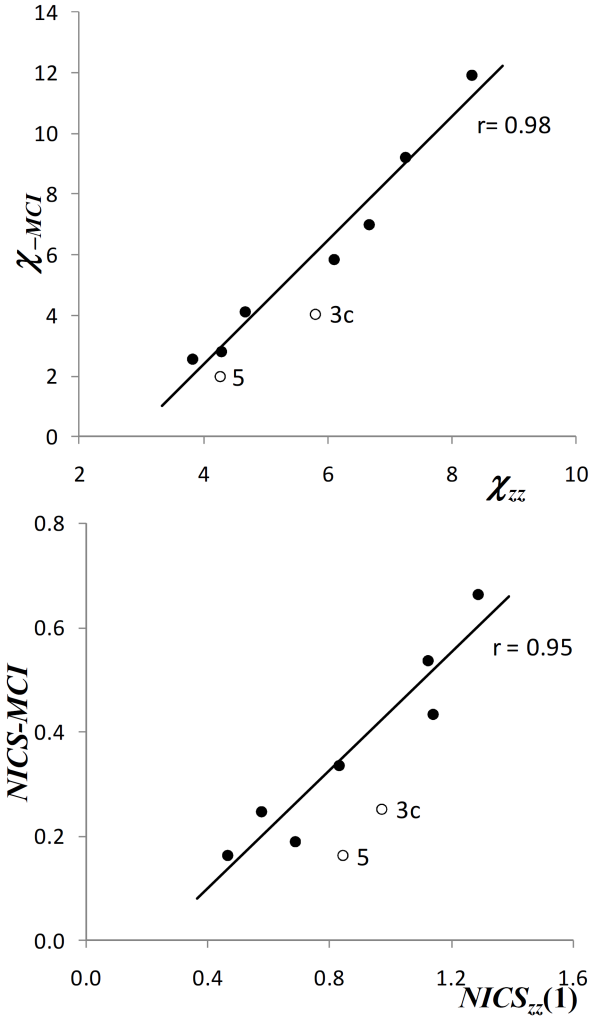

Figure 12.9: Correlation between the magnetic susceptibility exaltation estimated from multicentre indices and the zz component of the magnetic susceptibility tensor calculated at the B3LYP/6-31++G(d,p) level (upper plot), and correlation between the NICS estimated from multicentre indices and the NICS$_{zz}$(1) calculated at the B3LYP/6-31++G(d,p) level at the centre of ring circuits of type III in Figure 12.2 (lower plot). All values are given relative to the corresponding value for isolated benzene.

magnetic and electron density criteria.

By partitioning the total aromaticity into individual circuit contributions it was concluded that aromaticity alone can explain why the hydrogenation of non-protonated pyrrol rings is always favoured over that of protonated pyrrol rings in porphyrins and hydroporphyrins. Although the local contribution to the aromaticity of pyrrol cycles is significantly larger than that of the macrocycles that connect the pyrrol units, the latter play a crucial role in the relative stability of the different isomers.

The hydrogenation energies along the different hydrogenation paths connecting porphin with octahydroporphin (**5**) have been analysed. The conclusion is that formation of (**5**) is energetically unfavoured, and that the energy destabilisation associated to the disruption of the electron conjugation upon hydrogenation can perfectly explain this fact.

Analysis of the electron delocalisation and different magnetic response properties lead to the same conclusions as the measures of aromatic stabilisation energy. In order to compare the different methods we have put their information in the same scale by using some recently proposed approaches. Only for molecules (**3c**) and (**5**) do the different methods employed differ substantially, although this fact does not affect the general conclusions obtained.

Part IV

Conclusions

General Conclusions

Although derived and introduced as a measure of delocalisation, comparison with the Polansky and the NOEL index has shown that, in the case of Polycyclic Aromatic Hydrocarbons, the Multi Centre Bond Index can be used to measure the similarity between an individual C_6-ring and benzene. Keeping Kekulé's definition of aromaticity as the similarity to benzene in mind, the multicentre index has proven to be a quantum chemical descriptor for this earliest definition of Aromaticity.

The, at first glance disagreeing, results between the Multi Centre Bond Index and magnetic criteria as the NICS and Ring Current Maps could easily have been discarded as being the result of the multidimensional character of Aromaticity. By studying a large set of Polycyclic Aromatic Hydrocarbons and using a thorough statistical analysis, however, the present results show that the MCBI and both NICS and the RCM can be reconciled in a chemically intuitive way. This elaborate study on 394 PAH has shown the heart of the differences between local indices as the MCBI and global properties as current density and the NICS, and the findings have shown how to reconcile both. By making the proper combination of the delocalisation indices for different circuits, both NICS and the RCM picture can be reconstructed. As there is a good correlation between the MCBI and other local aromaticity indices such as the Polansky index, NOEL, *ef*-value, *etc.* the same correlations hold for these indices. The method used can thus be transposed to other local and global properties as we have shown for the topological resonance energy. In general it can expected that taking the proper combination of any local aromaticity index can be used to reconcile this index with the magnetic indices or an other global aromaticity index. The claimed evidence for multidimensionality of aromaticity vanishes in these cases, as it is apparently only a consequence of a choice of description, in terms of rings or graph circuits.

This work has also revealed the non-local effects on the NICS. The NICS of the central ring of perylene-like and benzo[ghi]-perylene-like fragments and the NICS of the central ring of coronene can not be explained using the six-, ten- and fourteen-

centre circuits encircling the central ring alone. It was shown that the problem lies in the non-local character of the NICS. This non-local character could be proven using the MCBI-vector maps. Three different non-local effects on the NICS were found:

- the influence of the higher-order circuits encircling the ring. Not only the six-, ten- and fourteen-centre circuits have an effect on the NICS, the present study shows that also the twelve-centre circuits have a meaningful influence.

- the influence of local aromaticity of the surrounding, neighbouring, rings that can dramatically change the current on the common bonds of neighbouring rings, influencing the NICS of these rings.

- the influence of currents even farther away from the ring at which the NICS is evaluated, like the effect of the outer current in coronene on the NICS in the central ring.

In this way, these results have demonstrated that NICS should not be used to assess the degree of local aromaticity of a benzenoid circuit as MCBI do. It should be clear, however, that the models presented in this work do not serve as an alternative way to calculate the NICS using the MCBI, but were constructed only to fully examine and understand the difference between the NICS and delocalisation indices.

While examining the non-local contributions to the NICS, the results of this study also raised the interesting suggestion that there could be a 4N+2 rule applicable to the delocalisation indices, where(4N+2)- and 4N-membered circuits contribute in a diatropic and paratropic manner, respectively. It would be interesting to further investigate this 4N+2 rule for delocalisation indices in the near future.

The question naturally arises on what information is conceptually contained in the value of Multi Centre Bond Indices and NICS. NICS as an aromaticity index may be seen to reflect, at a chosen point, all ring currents in the molecule. So when there are several circuits in a molecule, all of these will contribute to the NICS computed in some chosen point. NICS can not be used to assess a degree of benzenoid character for a specific ring in a PAH, as they not solely contain the ring current of the benzenoid circuit. There are also cases where the NICS approach produces results not in line with ring current maps. This is the case in e.g., bifurcated circuits. Because of the fact that NICS concentrate all ring current information in a single number at an arbitrarily chosen point, one is bound to lose quite a lot of information. It is not possible to extract from NICS again the ring current information. As a consequence, ring current maps are far superior to the NICS, this is why the correlation between ring current maps and Multi Centre Bond Indices is being discussed in the next section.

On the other hand, multicentre indices allow to reveal the degree of aromaticity in a certain circuit. Depending on the size of the circuit, an index can be computed

allowing to compare its degree of aromaticity to another ring of the same size. Optionally, a normalization can be performed which allows even comparing rings of different sizes. So both indices reflect inherently different views of aromaticity.

Not only the magnetic criteria show a correlation with the Multi Centre Bond Index, also energy based criteria like the *ef* value correlate with the MCBI. Using the proper combination of the delocalisation indices for different circuits also the topological resonance energy can be shown to correlate with the MCBI. This show that the same close parallel can be observed also for global aromaticity measures like TRE and NICS.

When turning to aromatic systems other than Polycyclic Aromatic Hydrocarbons, the close relation between the Multi Centre Bond Index and the current density is partially lost. For a simple molecule such as hexaiodobenzene and its cation, the relation still holds, but turning to more complicated molecules such as the metallic Al_4^{2-} and hydroporphyrins, things become more complicated. In the case of the metallic $Li_nAl_4^{n-2}$ systems it has been shown that there is no direct relation between electron delocalisation and the presence of a ring current, other than that a delocalised system is a necessary but not sufficient condition to lead to a ring current. In the case of Al_4^{2-} derived compounds, there is clearly both σ and π electron delocalisation although only the σ system gives rise to a ring current. The reason for this disagreement may lie in the fact that the presence of a ring current, besides a delocalised system, requires suitable occupied to virtual transitions. These transitions depend on the symmetry of the occupied and virtual orbital, a favourable spatial distribution of the occupied and virtual orbitals and a small energy gap between these orbitals. The Multi Centre Bond Index, however, is only calculated using occupied orbitals and does not depend on the form of the virtual orbitals or the energy gap between occupied and virtual orbitals. The analysis of CMO-NICS data for Al_4^{2-} is shown to lead to yet different conclusions, although this method also contains occupied-occupied terms and is not so easily interpretable as ipsocentric ring current maps. The Fermi hole analysis and multicentre indices on the other hand agree very well among each other in describing electron delocalisation. This is no surprise since both are founded on the same theoretical background.

Concerning the use of the term aromaticity in the context of the all metallic $Li_nAl_4^{n-2}$ systems, one faces the problem of the lack of definition of aromaticity outside the range of benzenoid ring containing molecules. There is no clear cut reason what "benzene like" properties should be conserved most in other molecules to describe them as aromatic. If electron delocalisation suffices, the compounds studied here could be described as both σ and π aromatic. If the presence of a ring current is a requirement for aromaticity, the present molecules are only σ aromatic. We therefore suggest to always narrow down what exactly is meant when using the no-

tion aromaticity. In this context Al_4^{2-} is σ and π aromatic on the account of electron delocalisation but only σ aromatic on the account of presence of a ring current.

In the last chapter, the relative stability of different hydroporphyrin isomers as well as the naturally and synthetic inaccessibility of octahydroporphin have been explained in terms of total and local aromaticity using a large variety of methods, including energetic, magnetic and electron density criteria.

By partitioning the total aromaticity into individual circuit contributions it was concluded that aromaticity alone can explain why the hydrogenation of non-protonated pyrrol rings is always favoured over that of protonated pyrrol rings in porphyrins and hydroporphyrins. Although the local contribution to the aromaticity of pyrrol cycles is significantly larger than that of the macrocycles that connect the pyrrol units, the latter play a crucial role in the relative stability of the different isomers.

The hydrogenation energies along the different hydrogenation paths connecting porphin with octahydroporphin have been analysed. The conclusion is that formation of octahydroporphin is energetically unfavoured, and that the energy destabilisation associated to the disruption of the electron conjugation upon hydrogenation can perfectly explain this fact.

Analysis of the electron delocalisation and different magnetic response properties lead to the same conclusions as the measures of aromatic stabilisation energy. In order to compare the different methods we have put their information in the same scale by using some recently proposed approaches. Only for molecules (**3c**) and (**5**) the different methods employed differ substantially, even though this fact does not affect the general conclusions obtained.

In general, the results show that the MCBI is a useful measure for the delocalisation in both organic and inorganic molecules. For the PAH, the MCBI correlates well with the similarity of the rings to benzene and with other local aromaticity indices. A good correlation can also be found with global aromaticity indices when the proper combination of conjugated circuits is taken. For molecules which show little or no relation to benzene, the correlation between different aromaticity measures is partially lost. There is no clear cut reason to say which "benzene like" properties should be conserved most in other molecules to describe them as aromatic. This leads to different interpretations of the aromaticity in these molecules, depending on the "benzene like" property used to describe the aromaticity of the molecule. Concerning the use of the term aromaticity in these molecules it is therefore suggested always to narrow down what is meant exactly when using the notion aromaticity.

Afterword

I would like to take a moment to write a more personal reflection on my work of the last six years. Thanks to Prof. Bultinck, I learned quite a bit of Fortran and learned to enjoy writing the programs to calculate a wide variety of molecular properties. Over the last few years, I programmed the Multi Centre Index, in all possible varieties, the Becke integration scheme, the Iterative Hirshfeld method and the code for calculating the Ring Current Maps. Although it lacks some computational efficiency, I'm proud to have programmed the Ring Current code, which turned out to be a challenging mix of integral transformation, Coupled Perturbed Hartree-Fock, calculation of the Ring Currents themselves and plotting them in PostScript. From the different topics in this thesis, I am especially proud of the work done in comparing the MCBI, NICS and RCM for the PAHs. This work has shown that the differences between these indices are not as dramatic as they might have seemed when I started my work.

During the course of this thesis a wide variety of aromaticity indices have been mentioned and studied. One can ask himself which index is the best to describe aromaticity. As mentioned before every scientist has a different view on what characteristic is defining for the concept of aromaticity. Some, like me, prefer electron delocalisation, some the energetic stability, others the magnetic properties, *etc*. This is more a matter of taste than a matter of science. And as we know, *De gustibus non est disputandum*. This is why I advocated to narrow down what is meant exactly when referring to the concept of aromaticity.

Apart from the question of what defines aromaticity, all indices have some strengths and some weaknesses. The DAFH-analysis is a nice and visual method of describing the bonding in a molecule. The visual character of the method is both its strength and its weakness. It is easy to interpret the bonding in a molecule by visualising the bonds, but for small changes it is harder to say which bond is stronger or weaker and which one is more or less delocalised. MCBI is on the other hand is a single number, but to understand the aromaticity in polycyclic aromatic molecules, one needs to calculate the index for each circuit and comparing the value between circuits with a

different number of centres is not easy. The MCBI also depends on the population analysis chosen and this might in some cases influence the value and the conclusions drawn from of the index. Similar problems arise with the PDI and FLU index. The Ring Current Map is a nice visual tool to understand the magnetic response of a molecule, but like the DAFH analysis, it is not always easy to see small changes in the ring current between two molecules. For some molecules, different plots on different heights might be needed to understand the complete Ring Current picture. The NICS has the elegance of a single number, but integrating all ring current information to a single number remains questionable, as completely different RCM could give rise to nearly indistinguishable NICS values.

Every scientist, however, seems to easily accept the down-side of an index when he/she is convinced that the index is the right measure for this benzene-like property which he/she defines as aromaticity. It thus seems there are as many indices available as there are researchers active in calculating the aromaticity of molecules. This reminds me of a Tibetan proverb:

ཞི། །ལུང་པ་རེ་རེར་སྐད་ལུགས་རེ་རེ།

བླ་མ་རེ་རེར་ཆོས་ལུགས་རེ་རེ། །

"Every valley (or land) has its own dialect Every lama (Tibetan priest) has his own religion."

In our case we could easily adapt the proverb to:

"Every valley has its own dialect Every chemist has his own measure of aromaticity."

Appendix A

The Electromagnetic Field

A.1 Vector Functions

The magnetic field is described by making use of a vector function. A vector function is a function that attaches a vector of a certain magnitude and direction to each point in space, in contrast to the scalar function which associates a single number to each point in space. Vector functions can in general be written in the following form:

$$\boldsymbol{V} = f_x\boldsymbol{i} + f_y\boldsymbol{j} + f_z\boldsymbol{k} \tag{A.1}$$

with $\boldsymbol{i}$, $\boldsymbol{j}$ and $\boldsymbol{k}$ the orthogonal unit vectors. As an example two important vector functions are shown in figures A.1 and A.2. Their vector function is described by:

$$\boldsymbol{C} = -y\boldsymbol{i} + x\boldsymbol{j} \tag{A.2}$$

$$\boldsymbol{C'} = x\boldsymbol{i} + y\boldsymbol{j} \tag{A.3}$$

For the description of the electric and magnetic field, the divergence and curl of the vector functions are used. The divergence of a vector-field is defined as:

$$\nabla \cdot \boldsymbol{V} = \frac{\partial f_x}{\partial x}\boldsymbol{i} + \frac{\partial f_y}{\partial y}\boldsymbol{j} + \frac{\partial f_z}{\partial z}\boldsymbol{k} \tag{A.4}$$

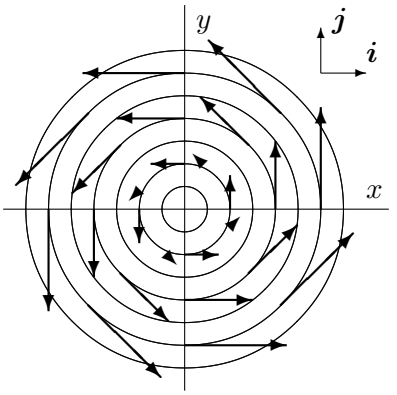

Figure A.1: $\boldsymbol{C} = -y\boldsymbol{i} + x\boldsymbol{j}$

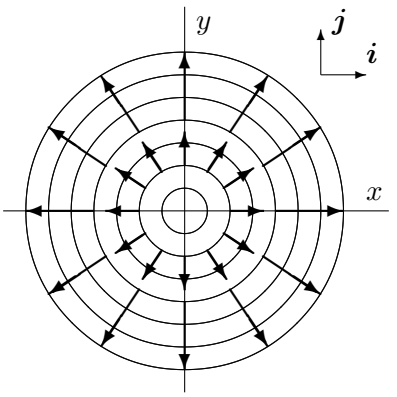

Figure A.2: $\boldsymbol{C'} = x\boldsymbol{i} + y\boldsymbol{j}$

(note the difference with the gradient of a scalar function $\nabla\psi$). This means that the divergence for the vector functions $\boldsymbol{C}$ and $\boldsymbol{C'}$ is:

$$\nabla \cdot \boldsymbol{C} = 0 \qquad \nabla \cdot \boldsymbol{C'} = 2$$

illustrating the origin of the name 'divergence'. The curl of a vector field is defined as:

$$\nabla \times \boldsymbol{V} = \begin{vmatrix} \boldsymbol{i} & \boldsymbol{j} & \boldsymbol{k} \\ \partial/\partial x & \partial/\partial y & \partial/\partial z \\ f_x & f_y & f_z \end{vmatrix} \tag{A.5}$$

Once again, evaluating the value of the curl for $\boldsymbol{C}$ and $\boldsymbol{C'}$ illustrates the origin of the name:

$$\nabla \times \boldsymbol{C} = 2\boldsymbol{k} \qquad \nabla \times \boldsymbol{C'} = 0$$

Since $\boldsymbol{C}$, has a curl but zero divergence, this function is commonly used to describe the magnetic field in the Coulomb gauge (*vide supra*).

From the definitions it follows that the divergence of the curl of any vector function is zero:

$$\nabla \cdot (\nabla \times \boldsymbol{V}) = 0 \tag{A.6}$$

As a consequence one can say that if the divergence of a vector function $\boldsymbol{V}$ is zero, there is some vector function $\boldsymbol{W}$ such that $\boldsymbol{V}$ is the curl of that vector fuction $\boldsymbol{W}$:

$$\begin{array}{ll} \text{If} & \nabla \cdot \boldsymbol{V} = 0 \\ \text{there is a} & \boldsymbol{W} \\ \text{such that} & \boldsymbol{V} = \nabla \times \boldsymbol{W} \end{array} \tag{A.7}$$

A.2 The Maxwell Equations

The Maxwell equations are a set of four partial differential equations that describe the properties of the electromagnetic field:

$$\begin{array}{llll} \text{(I)} & \nabla \cdot \boldsymbol{E} = 4\pi\rho & \text{(II)} & \nabla \cdot \boldsymbol{B} = 0 \\ \text{(III)} & \nabla \times \boldsymbol{E} = -\frac{1}{c}\frac{\partial \boldsymbol{B}}{\partial t} & \text{(IV)} & \nabla \times \boldsymbol{B} = \frac{4\pi}{c}\boldsymbol{J} + \frac{1}{c}\frac{\partial \boldsymbol{E}}{\partial t} \end{array} \tag{A.8}$$

where

$\boldsymbol{E}$	electric field strength
ρ	charge (electron) density
$\boldsymbol{B}$	magnetic field strength
$\boldsymbol{J}$	current density

Because the divergence of a curl is zero, using the second Maxwell equation, the magnetic flux density can be written in terms of a suitable vector function $\boldsymbol{A}$ (see A.7):

$$\boldsymbol{B} = \nabla \times \boldsymbol{A} \tag{A.9}$$

The third Maxwell equation can then be written as:

$$\nabla \times \left(\boldsymbol{E} + \frac{1}{c} \frac{\partial \boldsymbol{A}}{\partial t} \right) = 0$$

or

$$\boldsymbol{E} = -\frac{1}{c} \frac{\partial \boldsymbol{A}}{\partial t} + \boldsymbol{f}$$

where $\boldsymbol{f}$ is a vector function with zero curl. By analogy with A.6, the curl of the gradient of a scalar function is zero, so $\boldsymbol{f}$ can be written as minus the gradient of a scalar function ξ ($\boldsymbol{f} = -\nabla\xi$):

$$\boldsymbol{E} = -\frac{1}{c} \frac{\partial \boldsymbol{A}}{\partial t} - \nabla\xi \tag{A.10}$$

Or when $\boldsymbol{A}$ is independant of time:

$$\boldsymbol{E} = -\nabla\xi \tag{A.11}$$

Using these expressions from classical physics, the Hamiltonian for a charged particle in the presence of a magnetic field can be found. This Hamiltonian can in turn be used to calculate the current density induced in the molecule by a magnetic field.

A.3 The Hamiltonian

In classical Physics, the force on a point charge due to an electromagnetic field is given by the Lorenz force:

$$\boldsymbol{F} = q(\boldsymbol{E} + \frac{1}{c} \dot{\boldsymbol{r}} \times \boldsymbol{B}) \tag{A.12}$$

or in terms of the vector potential $\boldsymbol{A}$ and scalar potential ϕ:

$$\boldsymbol{F} = q \left(-\frac{\partial \boldsymbol{A}}{\partial t} - \nabla\xi + \frac{1}{c} \dot{\boldsymbol{r}} \times (\nabla \times \boldsymbol{A}) \right) \tag{A.13}$$

For the electron and for $\boldsymbol{A}$ independant of time, this equation becomes:

$$m_e \ddot{\boldsymbol{r}} = e \left(\nabla\xi - \frac{1}{c} \dot{\boldsymbol{r}} \times (\nabla \times \boldsymbol{A}) \right) \tag{A.14}$$

Using the Lagrange or Euler-Lagrange equation[256],

$$\left(\frac{\partial L}{\partial r}\right) - \frac{d}{dt}\left(\frac{\partial L}{\partial \dot{\boldsymbol{r}}}\right) = 0 \tag{A.15}$$

the form of the Lagrangian can be found which satisfies the Euler-Lagrange equation:

$$L = \frac{1}{2} m_e \dot{\boldsymbol{r}}^2 + e\xi - \frac{e}{c}\dot{\boldsymbol{r}}.\boldsymbol{A} \tag{A.16}$$

From this Lagrangian the momentum can be calculated ($\boldsymbol{p} = \frac{\partial_L}{\partial \dot{\boldsymbol{r}}}$) as:

$$\boldsymbol{p} = m_e \dot{\boldsymbol{r}} - \frac{e}{c}\boldsymbol{A} \tag{A.17}$$

And the Hamiltonian ($H = \sum_i \boldsymbol{p}_i.\dot{\boldsymbol{r}}_i - L$)[257] as:

$$H = \frac{1}{2m_e}\left(\boldsymbol{p} + \frac{e}{c}\boldsymbol{A}\right)^2 - e\xi \tag{A.18}$$

where $-e\xi$ is nothing else than the potential energy V. This Hamiltonian is the 'classical' Hamiltonian for a charged particle in the presence of a magnetic field. By replacing the momentum $\boldsymbol{p}$ by $\frac{\hbar}{i}\nabla$, this Hamiltonian can be used to calculate the effect of the magnetic field on a charged particle in quantum mechanics. This Hamiltonian can thus be used to calculate the current density induced in a molecule by a magnetic field and this via the perturbation theory and the Hartree-Fock method.

List of Publications

Articles

- De Proft, F ; Fias, S. ; Van Alsenoy, C ; Geerlings, P., "Spin-polarised Conceptual DFT Study of the Regioselectivity in the [2+2] Photocycloaddition of Substituted Alkenes to Enones.", *Journal of Physical Chemistry A* **2005** (109): 6335-6343.

- Bultinck P.; Fias S.; Ponec R., "Local Aromaticity in Polycyclic Aromatic Hydrocarbons: Electron Delocalization versus Magnetic Indices.", *Chemistry-A European Journal* **2006** (12): 8813-8818.

- Bultinck, P.; Ponec, R.; Gallegos, A.; Fias, S.; Van Damme, S.; Carbó-Dorca, R., "Generalized Polansky Index as a New Means for the Quantitative Characterization of Aromaticity in Polycyclic Aromatic Hydrocarbons.", *Croatica Chemica Acta* **2006** (79): 363-371.

- De Proft, F.; Ayers, P.W.; Fias, S.; Geerlings, P., "Woodward-Hoffman rules in Density Functional Theory: Initial Hardness Response." *Journal of Chemical Physics* **2006** (125): Art. No. 214101.

- Fias, S.; Bultinck, P., Comment on "Current-density maps as probes of aromaticity: Global and Clar ring currents in totally resonant polycyclic aromatic hydrocarbons." by Steiner E., Fowler P.W., Soncini A., Jenneskens L.W. , *Faraday Discussions* **2007** (135): 381-384.

- Bultinck, P.; Ayers, P. W.; Fias, S.; Tiels, K.; Van Alsenoy, C., "Uniqueness and basis set dependence of iterative Hirshfeld charges.", *Chemical Physics Letters* **2007** (444): 205-208.

- Bultinck, P; Fias, S.; Van Alsenoy, C.; Ayers, P.W.; Carbó-Dorca, R. "Critical thoughts on computing atom condensed Fukui functions.", *Journal of Chemical Physics*, **2007** (127): Art. No. 034102.

- Fias, S.; Van Damme, S.; Bultinck, P., "Multidimentionallity of Delocalization Indices and Nucleus Independant Chemical Shifts in Polycyclic Aromatic Hydrocarbons.", *Journal of Computational Chemistry* **2008** (29): 358-366.

- Havenith, R.W.A.; Fowler, P.W.; Fias, S.; Bultinck, P., "Evidence from current-density mapping for σ-delocalisation in the aromatic hexaiodobenzene cation.", *Tetrahedron Letters* **2008** (49): 1421-1424.

- Fias, S.; Fowler, P.W.; Delgado, J.L.; Hahn, U; Bultinck, P., "Correlation of Delocalization Indices and Current-Density Maps in Polycyclic Aromatic Hydrocarbons.", *Chemistry-A European Journal* **2008** (14): 3093-3099.

- Ponec, R.; Fias, S.; Bultinck, P.; Gutman, I; Stankovic, S. "Benzoid szénhidrogének aromas és lokális aromás tulajdonságairól", *Magyar kémiai folyóirat (HUNGARIAN JOURNAL OF CHEMISTRY), Kémiai k¨ozlemények (CHEMICAL COMMUNICATIONS) (Nyomtatott)* **2008** (114): 177-182.

- Ponec, R.; Fias, S.; Van Damme, S.; Bultinck, P.; Gutman, I; Stankovic, S. "The close relation between cyclic delocalization, energy effects of cycles and aromaticity.", *Collection of Czechoslovak Chemical Communications* **2009** (74): 147-166.

- Van Damme, S.; Bultinck, P.; Fias, S.; "Electrostatic Potentials from Self-Consistent Hirshfeld Atomic Charges.", *Journal of Chemical Theory and Computation* **2009** (5): 334-340.

- Fias, S.; Van Damme, S.; Bultinck, P., "Multidimensionality of Delocalization Indices and Nucleus-Independent Chemical Shifts in Polycyclic Aromatic Hydrocarbons II: Proof of Further Nonlocality.", *Journal of Computational Chemistry* **2010** (29): 2286-2293.

Book Chapter

P. Bultinck, S. Fias, M. Mandado, and R. Ponec; *Correlation between Electron Delocalization and Ring Currents in All Metallic "Aromatic" Compounds* in: *Aromaticity and Metal Clusters*, Chattaraj, P. K., Ed., CRC press, 2010, pp.245-270

Presentations

Poster Presentations

- S. Fias and P. Bultinck, "The Hirshfeld Atom in the Molecule Revisited", DFT 2007, August 26-30, 2007, Amsterdam (NL).
- Stijn Fias, Sofie Van Damme, Patrick W. Fowler, Patrick Bultinck."Is aromaticity a multidimensional concept or not?" Quantum Chemistry in Belgium (QCB-8), 8 February 2008, Hasselt (B).

Oral Presentations

- Comment to P.W. Fowler et al. Faraday Discussions 135: Chemical Concepts for Quantum Mechanics, 4-6 sept 2006, University of Manchester, UK:
- PRINCIPLES AND APPLICATION OF THE SELF-CONSISTENT HIRSHFELD ATOMS-IN-MOLECULES METHOD. VIII Girona conference on aromaticity: basics and applications, 07-10 July 2008, Girona, Spain.
- IS AROMATICITY A MULTIDIMENSIONAL CONCEPT OR NOT? Vlaams Jongerencongres van de chemie (Flemish Youth Congress of Chemistry) (jongKVCV), 1 -2 Match 2010, Blankenberge, Belgium.

Bibliography

[1] Smith, M. B.; March, J. *March's Advanced Organic Chemistry: Reactions, Mechanisms and Structure, 5th ed.;* John Wiley and Sons, New York, 2001.

[2] Minkin, V.; Glukhovtsev, M.; Simkin, B. *Aromaticity and Antiaromaticity;* Wiley Interscience, New York, 1994.

[3] Schleyer, P. *Chem. Rev.* **2001**, *101*, 1115–1566.

[4] Schleyer, P. *Chem. Rev.* **2005**, *105*, 3433–3947.

[5] Kekulé, A. *Lehrbuch der Organischen Chemie, Zweiter Band;* Ferdinand Enke Verlag, Erlangen, 1866.

[6] Cyrañski, M.; Krygowski, T. M.; Katritzky, A. R.; Schleyer, P. v. R. *J. Org. Chem.* **2002**, *67*, 1333–1338.

[7] Krygowski, T.; Cyrañski, M. *Chem. Rev.* **2001**, *101*, 1385–1419.

[8] Poater, J.; Duran, M.; Solà, M.; Silvi, B. *Chem. Rev.* **2005**, *105*, 3911–3947.

[9] Elser, V.; Haddon, R. *Nature* **1987**, *325*, 792–794.

[10] Schleyer, P.; Maerker, C.; Dransfeld, A.; Jiao, H.; Hommes, N. *J. Am. Chem. Soc* **1996**, *118*, 6317–6318.

[11] Lazzeretti, P. *Phys. Chem. Chem. Phys.* **2004**, *6*, 217–223.

[12] Steiner, E.; Fowler, P. W. *J. Phys. Chem. A* **2001**, *105*, 9553–9562.

[13] Steiner, E.; Fowler, P.; Jenneskens, L. *Angew. Chem. Int. Ed.* **2001**, *40*, 362–366.

[14] Jug, K.; Koster, A. M. *J. Phys. Org. Chem.* **1991**, *4*, 163–169.

[15] Katritzky, A. R.; Karelson, M.; Sild, S.; Krygowski, T. M.; Jug, K. *J. Org. Chem.* **1998**, *63*, 5228–5231.

[16] Katritzky, A. R.; Barczynski, P.; Musumarra, G.; Pisano, D.; Szafran, M. *J. Am. Chem. Soc.* **1989**, *111*, 7–15.

[17] Poater, J.; García-Cruz, I.; Illas, F.; Solà, M. *Phys. Chem. Chem. Phys.* **2004**, *6*, 314–318.

[18] Bultinck, P.; Ponec, R.; Van Damme, S. *J. Phys. Org. Chem.* **2005**, *18*, 706–718.

[19] Bultinck, P.; Rafat, M.; Ponec, R.; Carbó-Dorca, R.; Popelier, P. *J. Phys. Chem. A* **2006**, *110*(24), 7642–7648.

[20] Bultinck, P.; Fias, S.; Ponec, R. *Chem.-Eur. J.* **2006**, *12*, 8813–8818.

[21] Bultinck, P.; Ponec, R.; Carbó-Dorca, R. *J. Comput. Chem.* **2007**, *28*, 152–160.

[22] Feixas, F.; Matito, E.; Poater, J.; Solà, M. *J. Comput. Chem.* **2008**, *29*(10), 1543–1554.

[23] Faraday, M. *Philos. Trans. R. Soc. London* **1825**, *115*, 440–466.

[24] Hofmann, A. *Proc. Roy. Soc. (London)* **1855**, *8*, 1–3.

[25] Kekulé, A. *Bulletin de la Societe Chimique de Paris* **1865**, *3*, 98–110.

[26] Dewar, J. *Proc. Roy. Soc. Edinburgh* **1967**, *6*, 82–86.

[27] Baker, W.; Rouvray, D. H. *J. Chem. Ed.* **1978**, *55*(10), 645.

[28] Lonsdale, K. *Proc. Roy. Soc. (London) A* **1929**, *123*, 494–515.

[29] Hückel, E. *Z. Physik* **1930**, *60*, 423–456.

[30] Hückel, E. *Z. Physik.* **1931**, *70*, 204–286.

[31] Hückel. *Z. Physik.* **1931**, *72*, 310–337.

[32] Hückel. *Z. Physik.* **1932**, *76*, 628–648.

[33] Kruszewski, J.; Krygowski, T. M. *Bull. Acad. Pol. Sci., Ser. Sci. Chim.* **1972**, *20*, 907–915.

[34] Kruszewski, J.; Krygowski, T. M. *Tetrahedron Lett.* **1972**, *36*, 3839–3842.

[35] Solomons, G.; Fryhle, C. *Organic Chemistry, 7th Ed.;* John Wiley and Sons, New York, 1998.

[36] Iupac compendium of chemical terminology – the gold book.

[37] Keith, T. A.; Bader, R. F. W. *Chem. Phys. Lett.* **1993**, *210*, 223–231.

[38] Coriani, S.; Lazzeretti, P.; Malagoli, M.; Zanasi, R. *Theor. Chim. Acta* **1994**, *89*, 181–192.

[39] Lazzeretti, P.; Malagoli, M.; Zanasi, R. *Chem. Phys. Lett.* **1994**, *220*, 299–304.

[40] Zanasi, R. *J. Chem. Phys.* **1996**, *105*, 1460–1469.

[41] Steiner, E.; Fowler, P. W. *Chem. Commun.* **2001**, pages 2220–2221.

[42] Steiner, E.; Fowler, P. W.; Havenith, R. W. A. *J. Phys. Chem. A* **2002**, *106*, 7048–7056.

[43] Steiner, E.; Fowler, P. *Phys. Chem. Chem. Phys.* **2004**, *6*, 261–272.

[44] Fowler, P.; Lillington, M.; Olson, L. *Pure Appl. Chem.* **2007**, *79*, 969–979.

[45] Poater, J.; Fradera, X.; Duran, M.; Solà, M. *Chem.-Eur. J.* **2003**, *9*, 400–406.

[46] Matito, E.; Duran, M.; Solà, M. *J. Chem. Phys.* **2005**, *122*, 014109.

[47] Li, X.; Kuznetsov, A.; Zhang, H.-F.; Boldyrev, A. I.; Wang, L. *Science* **2001**, *291*, 859–861.

[48] Boldyrev, A.; Wang, L.-S. *Chem. Rev.* **2005**, *249*, 3716–3757.

[49] Tsipis, C. *Coord. Chem. Rev.* **2005**, *249*, 2740–2762.

[50] Zubarev, D.; Averkiev, B.; H.J., Z.; L.S., W.; Boldyrev, A. *Phys. Chem. Chem. Phys.* **2008**, *10*, 257–267.

[51] Zhai, H.; B.B., A.; Zubarev, D.; L.S., W.; A.I., B. *Angew. Chem. Int. Ed.* **2007**, *46*, 4277–4280.

[52] Muller, P. *Pure & Appl. Chem.* **1994**, *66*(5), 1077–1184.

[53] Schleyer, P. v. R.; Jiao, H. *Pure & Appl. Chem.* **1996**, *68*(2), 209–218.

[54] Born, M.; Oppenheimer, J. R. *Ann. Physik.* **1927**, *84*, 457–484.

[55] Born, M.; Huang, K. *Dynamical theory of crystal lattices;* Oxford, Clarendon Press, 1954.

[56] Roothaan, C. *Rev. Mod. Phys.* **1951**, *23*(2), 69–89.

[57] Szabo, A.; Ostlund, N. S. *Modern Quantum Chemistry: Introduction to Advanced Electronic Structure Theory;* McGraw-Hill, New York, 1989.

[58] Hall, G. *Proc. Roy. Soc. (London) A* **1951**, *205*, 541–552.

[59] Löwdin, P. *Adv. Chem. Phys* **1959**, *2*, 207–322.

[60] Stevens, R. M.; Pitzer, R.; Lipscomb, W. N. *J. Chem. Phys.* **1963**, *38*(2), 550–560.

[61] McWeeny, R.and Sutcliffe, B. *Methods of Molecular Quantum Mechanics;* Academic Press: London, New York, 1969.

[62] Parr, R. G.; Yang, W. *Density-functional Theory of Atoms and Molecules;* Oxforf University Press: London and New York, 1989.

[63] Slater, J. *Phys. Rev.* **1951**, *81*, 385–390.

[64] Koch, W.; Holthausen, M. *A Chemists Guide to Density Functional Theory, 2ed.;* Wiley-VCH Verlag GmbH, 2001.

[65] Baerends, E.; Gritsenko, O. *J. Phys. Chem. A, 101, 5390 (1997))* **1997**, *101*, 5383–5403.

[66] Mulliken, R. S. *J. Chem. Phys.* **1955**, *23*(10), 1833–1840.

[67] Mulliken, R. S. *J. Chem. Phys.* **1955**, *23*(10), 1841–1846.

[68] Mulliken, R. S. *J. Chem. Phys.* **1955**, *23*(12), 2338–2342.

[69] Mulliken, R. S. *J. Chem. Phys.* **1955**, *23*(12), 2343–2346.

[70] Bachrach, S. M.; *Reviews in Computational Chemistry volume 5*, Lipkowitz, K. B., Boyd, D. B., Eds.; VCH, New York, 1995.

[71] Hirshfeld, F. L. *Theor. Chim. Acta.* **1977**, *44*, 129–138.

[72] Bultinck, P.; Ayers, P.; Fias, S.; Tiels, K.; Van Alsenoy, C. *Chem. Phys. Lett.* **2007**, *444*, 205–208.

[73] Davidson, E.; Chakravorty, S. *Theor. Chim. Acta* **1992**, *83*, 319–330.

[74] Bultinck, P.; Van Alsenoy, C.; Ayers, P.; Carbó-Dorca, R. *J. Chem. Phys.* **2007**, *126*, 144111.

[75] Ayers, P. *J. Chem. Phys.* **2000**, *113*, 10886–10898.

[76] Ayers, P.; Morrison, R.; Roy, R. *J. Chem. Phys.* **2002**, *116*, 8721–8744.

[77] Parr, R.; Ayers, P.; Nalewajski, R. *J. Phys. Chem. A* **2005**, *109*, 3957–3959.

[78] Nalewajski, R. F.; Parr, R. G. *Proc. Natl. Acad. Sci. U.S.A.* **2000**, *97*, 8879–8882.

[79] Nalewajski, R. F.; Switka, E.; Michalak, A. *Int. J. Quant. Chem.* **2002**, *87*, 198–213.

[80] Nalewajski, R. F. *Chem. Phys. Lett.* **2003**, *372*, 28–34.

[81] Nalewajski, R. F.; Broniatowska, E. *Int. J. Quant. Chem* **2005**, *101*, 349–362.

[82] Perdew, J.; Parr, R.; Levy, M.; Balduz Jr., J. *Phys. Rev. Lett.* **1982**, *49*, 1691–1694.

[83] Yang, W.; Zhang, Y.; Ayers, P. *Phys. Rev. Lett.* **2000**, *84*, 5172–5175.

[84] Bultinck, P.; Cooper, D. L.; Van Neck, D. *Phys. Chem. Chem. Phys.* **2009**, *11*, 3424–3429.

[85] Bader, R. *Atoms in Molecules: A Quantum Theory;* Clarendon Press, Oxford, 1990.

[86] Bader, R. *Chem. Rev.* **1991**, *91*, 893–928.

[87] Popelier, P. *Atoms in Molecules. An introduction;* Pearson Educ, London, 2000.

[88] Bader, R.; Streitwieser, A.; Neuhaus, A.; Laidig, K.; Speers, P. *J. Am. Chem. Soc.* **1996**, *118*, 4959–4965.

[89] Ponec, R. *J. Math. Chem.* **1997**, *21*, 323–333.

[90] Ponec, R. *J. Math. Chem.* **1998**, *23*, 85–103.

[91] Ponec, R.; Duben, A. *J. Comput. Chem.* **1999**, *20*, 760–771.

[92] Bultinck, P.; Cooper, D.; Ponec, R. *J. Phys. Chem. A* **2010**, *114*, 8754–8763.

[93] Cioslowski, J. *Int. J. Quant. Chem. Symp.* **1990**, *24*, 15–28.

[94] Wiberg, K. *Tetrahedron* **1968**, *24*, 1083–1096.

[95] Giambiagi, M.; de Giambiagi, M.; Grempel, D.; Heymann, C. *J. Chim. Phys.* **1975**, *72*, 15–22.

[96] Mayer, I. *Chem. Phys. Lett.* **1983**, *97*, 270–274.

[97] Mandado, M.; Mosquera, R. *Chem. Phys. Lett.* **2009**, *470*, 140–146.

[98] Bochicchio, R.; Ponec, R.; Torre, A.; Lain, L. *Theor. Chim. Acc.* **2001**, *105*, 292–298.

[99] Ponec, R.; Uhlk, F. *Croat. Chem. Acta* **1996**, *69*(3), 941–954.

[100] Ponec, R.; I. Mayer, I. *J. Phys. Chem. A* **1997**, *101*, 1738–1741.

[101] Ponec, R.; Cooper, D. *Int. J. Quant. Chem.* **2004**, *97*, 1002–1011.

[102] Güell, M.; Matito, E.; Luis, J. M.; Poater, J.; Solà, M. *J. Phys. Chem. A.* **2006**, *110*, 11569–11574.

[103] Mayer, I. *Int. J. Quant. Chem* **1986**, *29*, 73–84.

[104] Van Vleck, J. *The Theory of Electric and Magnetic Susceptibilities;* Oxford University Press: London and New York, 1932.

[105] Bishop, D. M. *Group Theory and Chemistry;* Clarendon Press, Oxford, 1973.

[106] Atkins, P.; Friedman, R. *Molecular Quantum Mechanics;* Oxford University Press: London and New York, 1997.

[107] Schleyer, P. v. R.; Jiao, H.; Hommes, N. J. R. v. E.; Malkin, V. G.; Malkina, O. *J. Am. Chem. Soc.* **1997**, *119*, 12669–12670.

[108] Fallah-Bagher-Shaidaei, H.; Wannere, C.; Corminboeuf, C.; Puchta, R.; Schleyer, P. *Org. Lett.* **2006**, *8*, 863–866.

[109] Fowler, P.; Steiner, E. *Mol. Phys.* **2000**, *98*, 945–953.

[110] Corminboeuf, C.; Heine, T.; Seifert, G.; Schleyer, P. v. R. *Phys. Chem. Chem. Phys.* **2004**, *6*, 273–276.

[111] Stanger, A. *J. Org. Chem.* **2006**, *71*, 883–893.

[112] Steiner, E. *Faraday Discuss.* **2007**, *135*, 394–395.

[113] Steiner, E.; Fowler, P. W. *ChemPhysChem* **2002**, *3*, 114–116.

[114] Steiner, E.; Soncini, A.; Fowler, P. W. *Org. Biomol. Chem.* **2005**, *3*, 4053–4059.

[115] London, F. *J. Phys. Radium* **1937**, *8*, 397–409.

[116] Fowler, P. W.; Steiner, E. *Chem. Phys. Lett.* **2002**, *364*, 259–266.

[117] Bultinck, P.; Mandado, M.; Mosquera, R. *J. Math. Chem.* **2008**, *43*, 111–118.

[118] Fias, S.; Van Damme, S.; Bultinck, P. *J. Comput. Chem.* **2008**, *29*, 358–366.

[119] Fias, S.; Bultinck, P. *Faraday Discuss.* **2007**, *135*, 381–384.

[120] Gaussian 03, revision b.03. Frisch, M. J.; Trucks, G. W.; Schlegel, H. B.; Scuseria, G. E.; Robb, M. A.; Cheeseman, J. R.; Montgomery, J. A.; Vreven, T.; Kudin, K. N.; Burant, J. C.; Millam, J. M.; Iyengar, S. S.; Tomasi, J.; Barone, V.; Mennucci, B.; Cossi, M.; Scalmani, G.; Rega, N.; Petersson, G. A.; Nakatsuji, H.; Hada, M.; Ehara, M.; Toyota, K.; Fukuda, R.; Hasegawa, J.; Ishida, M.; Nakajima, T.; Honda, Y.; Kitao, O.; Nakai, H.; Klene, M.; Li, X.; Knox, J. E.; Hratchian, H. P.; Cross, J. B.; Adamo, C.; Jaramillo, J.; Gomperts, R.; Stratmann, R. E.; Yazyev, O.; Austin, A. J.; Cammi, R.; Pomelli, C.; Ochterski, J. W.; Ayala, P. Y.; Morokuma, K.; Voth, G. A.; Salvador, P.; Dannenberg, J. J.; Zakrzewski, V. G.; Dapprich, S.; Daniels, A. D.; Strain, M. C.; Farkas, O.; Malick, D. K.; Rabuck, A. D.; Raghavachari, K.; Foresman, J. B.; Ortiz, J. V.; Cui, Q.; Baboul, A. G.; Clifford, S.; Cioslowski, J.; Stefanov, B. B.; Liu, G.; Liashenko, A.; Piskorz, P.; Komaromi, I.; Martin, R. L.; Fox, D. J.; Keith, T.; Al-Laham, M. A.; Peng, C. Y.; Nanayakkara, A.; Challacombe, M.; Gill, P. M. W.; Johnson, B.; Chen, W.; Wong, M. W.; Gonzalez, C.; Pople, J. A. **2003**.

[121] Bultinck, P.; Ponec, R.; Gallegos, A.; Fias, S.; Van Damme, S.; Carbó-Dorca, R. *Croat. Chem. Acta* **2006**, *79*(3), 363–371.

[122] Giambiagi, M.; de Giambiagi, M.; dos Santos, C.; de Figueiredo, A. P. *Phys. Chem. Chem. Phys.* **2000**, *2*, 3381–3392.

[123] Polansky, O.; Derflinger, G. *Int. J. Quant. Chem.* **1967**, *1*, 379–401.

[124] Clar, E. *Aromatische Kohlenwasserstoffe;* Springer-Verlag, Berlin, 1952.

[125] Carbó-Dorca, R.; Gironés, X.; *Computational Medicinal Chemistry for Drug Discovery*, Bultinck, P., De Winter, H., Langenaeker, W., Tollenaere, J. P., Eds.; Dekker, Inc., New York., 2003, pages 364–386.

[126] Bultinck, P.; Carbó-Dorca, R.; Gironés, X.; *Reviews in Computational Chemistry Vol. 21*, Lipkowitz, K., Larter, R., Cundari, T., Eds.; JohnWiley, Hoboken (USA), 2005, pages 127–207.

[127] Cioslowski, J.; Fleischmann, E. *J. Am. Chem. Soc.* **1991**, *113*, 64–67.

[128] Davidson, E. *Reduced density matrices in quantum chemistry;* Academic Press, New York, 1976.

[129] Cioslowski, J.; Fleischmann, E. *Croat. Chem. Acta* **1993**, *66*, 113–121.

[130] Carbó-Dorca, R.; Bultinck, P. *J. Math. Chem.* **2004**, *36*, 201–210.

[131] Carbó-Dorca, R.; Bultinck, P. *J. Math. Chem.* **2004**, *36*, 231–239.

[132] Becke, A. D. *J. Chem. Phys.* **1993**, *98*, 5648–5652.

[133] Lee, C.; Yang, W.; Parr, R. *Phys. Rev. B - Condens. Matter.* **1988**, *37*, 785–789.

[134] Stephens, P.; Devlin, J.; Chabalowski, C. *J. Phys. Chem.* **1994**, *98*, 11623–11627.

[135] Hariharan, P.; Pople, J. *Theor. Chim. Acta.* **1973**, *28*, 213–222.

[136] Francl, M.; Petro, W. J.; Hehre, W.; Binkley, J.; Gordon, M.; DeFrees, D.; Pople, J. *J. Chem. Phys.* **1982**, *77*, 3654–3665.

[137] Ponec, R.; Bultinck, P.; Gallegos, A. *J. Phys. Chem. A* **2005**, *109*, 6606–6609.

[138] Fowler, P. W. *Faraday Discuss.* **2007**, *135*, 384–385.

[139] Aihara, J.; Kanno, H. *J. Phys. Chem. A* **2005**, *109*, 3717–3721.

[140] Anusooya, Y.; Chakrabarti, A.; Pati, S. K.; Ramasesha, S. *Int. J. Quant. Chem.* **1998**, *70*, 503–513.

[141] Portella, G.; Poater, J.; Bofill, J.; Alemany, P.; Solà, M. *J. Org. Chem.* **2005**, *70*, 2509–2521.

[142] Poater, J.; Bofill, J.; Alemany, P.; Solà, M. *J. Phys. Chem. A* **2005**, *109*, 10629–10632.

[143] Schleyer, P. v. R.; Manoharan, M.; Wang, Z.-X.; Kiran, B.; Jiao, H.; Puchta, R.; Hommes, N. E. *Org. Lett.* **2001**, *3*, 2465–2468.

[144] Aihara, J. *J. Am. Chem. Soc.* **2006**, *128*, 2873–2879.

[145] Van Damme, S.; Bultinck, P. *J. Comput. Chem.* **2007**, *28*(11), 1924–1928.

[146] Sysmo Package, University of Modena. Lazzeretti, P.; Zanas, R.; with additional routines by Steiner, E.; Fowler, P. W.; Havenith, R. W. A.; Soncini, A. **1980**.

[147] Poater, J.; Solà, M.; Viglione, R. G.; Zanasi, R. *J. Org. Chem.* **2004**, *69*, 7537–7542.

[148] Osuna, S.; Poater, J.; Bofill, J. M.; Alemany, P.; Solà, M. *Chem. Phys. Lett.* **2006**, *428*, 191–195.

[149] Topliss, J.; Edwards, R. *J. Med. Chem.* **1979**, *22*, 1238–1244.

[150] Worth, A.; Bassan, A.; Gallegos, A.; Netzeva, T.; Patlewicz, G.; Pavan, M.; Tsakovska, I.; Vracko, M. *The Characterisation of (Quantitative) Structure-Activity Relationships: Preliminary Guidance;* European Chemicals Bureau, Report EUR 21866 EN, 2005.

[151] Bultinck, P. A. *Faraday Discuss.* **2007**, *135*, 347–365.

[152] Mandado, M.; González-Moa, M.; Mosquera, R. A. *J. Comput. Chem.* **2007**, *28*, 127–136.

[153] Soncini, A.; Steiner, E.; Fowler, P. W.; Havenith, R. W. A.; Jenneskens, L. W. *Chem.-Eur. J.* **2003**, *9*, 2974–2981.

[154] Randić, M. *Chem. Rev.* **2003**, *103*, 3449–3605.

[155] Soncini, A.; Domene, C.; Engelberts, J. J.; Fowler, P. W.; Rassat, A.; van Lenthe, J. H.; Havenith, R. W. A.; Jenneskens, L. W. *Chem.-Eur. J.* **2005**, *11*, 1257–1266.

[156] Fias, S.; Fowler, P. W.; Delgado, J. L.; Hahn, U.; Bultinck, P. *Chem.-Eur. J.* **2008**, *14*, 3093–3099.

[157] Havenith, R. W. A.; Fowler, P. W.; Fias, S.; Bultinck, P. *Tet. Lett.* **2008**, *49*, 1421–1424.

[158] Fias, S.; Van Damme, S.; Bultinck, P. *J. Comput. Chem.* **2010**, *29*, 2286–2293.

[159] Keith, T. A.; Bader, R. F. W. *Chem. Phys. Lett.* **1992**, *194*, 1–8.

[160] Keith, T. A.; Bader, R. F. W. *J. Chem. Phys.* **1993**, *99*, 3669–3682.

[161] Aihara, J. *Chem. Phys. Lett.* **2004**, *393*, 7–11.

[162] Gutman, I. *Monatsh. Chem.* **2005**, *136*, 1055–1069.

[163] Gutman, I.; Bosanac, S. *Tetrahedron* **1977**, *33*, 1809–1812.

[164] Bosanac, S.; Gutman, I. *Z. Naturforsch., A* **1977**, *32*, 10–12.

[165] Graovac, A.; Gutman, I.; Trinajstić, N. *Topological Approach to the Chemistry of Conjugated Molecules.;* Springer-Verlag, Berlin, 1977.

[166] Gutman, I. *Top. Curr. Chem.* **1992**, *162*, 29–63.

[167] Gutman, I. *J. Serb. Chem. Soc.* **2005**, *70*, 441–456.

[168] Graovac, A.; Gutman, I.; Trinajstić, N.; Zivković, T. *Theor. Chim. Acta* **1972**, *26*, 67–78.

[169] Coulson, C. A. *Proc. Cambridge Philos. Soc.* **1940**, *36*, 201–203.

[170] Gutman, I.; Trinajstić, N. *J. Chem. Phys.* **1976**, *64*, 4921–4925.

[171] Gutman, I. *Chem. Phys. Lett.* **1977**, *46*, 169–171.

[172] Trinajstić, N. *Chemical Graph Theory.;* CRC Press, Boca Raton, 1983.

[173] Gutman, I.; Polansky, O. E. *Mathematical Concepts in Organic Chemistry.;* Springer-Verlag, Berlin, 1986.

[174] Aihara, J.; Oe, S. *Bull. Chem. Soc. Jpn.* **2003**, *76*, 1363–1364.

[175] Gutman, I.; Stanković, S.; Đurđević, J.; Furtula, B. *J. Chem. Inf. Model.* **2007**, *47*, 776–781.

[176] Pecka, J.; Ponec, R. *J. Math. Chem.* **2000**, *27*, 13–22.

[177] Kekulé, A. *Bull. Acad. Roy. Belg.* **1865**, *19*, 551.

[178] Kekulé, A. *Liebigs Ann. Chem* **1865**, *137*, 129–136.

[179] Binsch, G. *Naturwissenschaften* **1973**, *60*, 369–374.

[180] Martin, J.; Schaad, L. *Pure Appl. Chem.* **1990**, *62*, 547–550.

[181] Sagl, D.; Martin, J. *J. Am. Chem. Soc.* **1988**, *110*, 5827–5832.

[182] Ciofini, I.; Lainé, P.; Adamo, C. *Chem. Phys. Lett.* **2007**, *435*, 171–175.

[183] Steer, R.; Watkins, S.; Woodward, P. *J. Chem. Soc. (C)* **1970**, pages 403–404.

[184] Nakayama, A.; Fujihisa, H.; Aoki, K. *Phys. Rev. B* **2000**, *62*, 8759–8765.

[185] Kaupp, M.; Malkina, O. L.; Malkin, V. G.; Pyykko, P. *Chem.-Eur. J.* **1998**, *4*, 118–126.

[186] Kuznetsov, A.; Birch, K.; Boldyrev, A.; Li, X.; Zhai, H.-J.; L.-S., W. *Science* **2003**, *300*, 622–625.

[187] Fowler, P. W.; Havenith, R. W. A.; Steiner, E. *Chem. Phys. Lett.* **2001**, *342*, 85–90.

[188] Fowler, P. W.; Havenith, R. W. A.; Steiner, E. *Chem. Phys. Lett.* **2002**, *359*, 530–536.

[189] Havenith, R. W. A.; Fowler, P. W.; Steiner, E.; Shetty, S.; Kanhere, D.; Pal, S. *Phys. Chem. Chem. Phys.* **2004**, *6*, 285–288.

[190] Havenith, R. W. A.; Fowler, P. W. *Phys. Chem. Chem. Phys.* **2006**, *8*, 3383–3386.

[191] Juselius, J.; Straka, M.; Sundholm, D. *J. Phys. Chem. A* **2001**, *105*, 9939–9944.

[192] Lin, Y.-C.; Juselius, J.; Sundholm, D.; Gauss, J. *J. Chem. Phys.* **2005**, *122*, 214308.

[193] Chen, Z.; Corminboeuf, C.; Bohmann, J.; Schleyer, P. v. R. *J. Am. Chem. Soc.* **2003**, *125*, 13930–13931.

[194] Islas, R.; Heine, T.; Merino, G. *J. Chem. Theory Comput.* **2007**, *3*, 775–781.

[195] Havenith, R. W. A.; van Lenthe, J. H. *Chem. Phys. Lett.* **2004**, *385*, 198–201.

[196] Santos, J. C.; Tiznado, W.; Contreras, R.; Fuentealba, P. *J. Chem. Phys.* **2004**, *120*, 1670–1673.

[197] Zhan, C.-G.; Zheng, F.; Dixon, D. A. *J. Am. Chem. Soc.* **2002**, *124*, 14795–14803.

[198] Boldyrev, A. I.; Kuznetsov, A. E. *Inorg. Chem.* **2002**, *41*, 532–537.

[199] Chattaraj, P. K.; Roy, D. R.; Elango, M.; Subramanian, V. *J. Mol. Struct. (THEOCHEM)* **2006**, *759*, 109–110.

[200] Roy, D.; Bultinck, P.; Subramanian, V.; Chattaraj, P. *J. Mol. Struct. (THEOCHEM)* **2008**, *854*, 35–39.

[201] Kuznetsov, A. E.; Boldyrev, A. I.; Li, X.; S., W. L. *J. Am. Chem. Soc.* **2001**, *123*, 8825–8831.

[202] Dalton, J. *A New System of Chemical Philosophy;* R. Bickerstaff, Stand: London, 1808.

[203] Heine, T.; Schleyer, P.; Corminboeuf, C.; Seifert, G.; Reviakine, R.; Weber, J. *J. Phys. Chem. A* **2003**, *107*, 6470–6475.

[204] Ditchfield, R. *Mol. Phys.* **1974**, *27*, 789–807.

[205] Pérez-Juste, I.; Mandado, M.; Carballeira, L. *Chem. Phys. Lett.* **2010**, *491*, 224–229.

[206] Mandado, M.; Krishtal, A.; Van Alsenoy, C.; Bultinck, P.; Hermida-Ramn, J. *J. Phys. Chem. A* **2007**, *111*, 11885–11893.

[207] Kadish, K., Smith, K., Guilard, R., Eds. *The Porphyrin Handbook;* Academic Press: San Diego, 2000.

[208] Sheer, H.; *The Porphyrins*, Dolphin, D., Ed.; Academic Press: New York, 1978, pages Vol.2, pp1–44.

[209] Scheidt, W.; Lee, Y. *Struct. Bonding (Berlin)* **1987**, *64*, 1–7.

[210] Stolzenberg, A.; Schussel, L.; Summers, J.; Foxman, B.; Petersen, J. *Inorg. Chem.* **1992**, *31*, 1678–1686.

[211] Stolzenberg, A.; Haymond, G. *Inorg. Chem.* **2002**, *41*, 300–308.

[212] Richardson, P.; Chang, C.; Spaulding, L. D.; Fajer, J. *J. Am. Chem. Soc.* **1979**, *101*, 7736–7738.

[213] Stolzenberg, A.; Spreer, L.; Holm, R. *J. Am. Chem. Soc.* **1980**, *102*, 364–370.

[214] Chang, C.; Fajer, J. *J. Am. Chem. Soc.* **1980**, *102*, 848–851.

[215] Stolzenberg, A.; Strauss, S.; Holm, R. *J. Am. Chem. Soc.* **1981**, *103*, 4763–4778.

[216] Chang, C.; Hanson, L.; Richardson, P.; Young, R.; Fajer, J. *Proc. Natl. Acad. Sci. U.S.A.* **1981**, *78*, 2652–2656.

[217] Stolzenberg, A.; Stershic, M. *Inorg. Chem.* **1987**, *26*, 3082–3083.

[218] Stolzenberg, A.; Stershic, M. *J. Am. Chem. Soc.* **1988**, *110*, 6391–6402.

[219] Stolzenberg, A.; Schussel, L. *Inorg. Chem.* **1991**, *30*, 3205–3213.

[220] Battersby, A. *Nat. Prod. Rep.* **2000**, *17*, 507–526.

[221] Montforts, F.-P.; Gerlach, B.; Höper, F. *Chem. Rev.* **1994**, *94*, 327–347.

[222] Agius, L.; Ballantine, J.; Ferrito, V.; Jaccarini, V.; Murray-Rust, P.; Pelter, A.; Psaila, A.; Schembri, P. *Pure Appl. Chem.* **1979**, *51*, 1847–1864.

[223] Murphy, M.; Siegel, L. *J. Biol. Chem.* **1973**, *248*, 6911–6919.

[224] Murphy, M.; Siegel, L.; Tove, S.; Kamin, H. *Proc. Natl. Acad. Sci. U.S.A.* **1974**, *71*, 612–616.

[225] Prinsep, M.; Caplan, F.; Moore, R.; Patterson, G.; Smith, C. *J. Am. Chem. Soc.* **1992**, *114*, 385–387.

[226] Scheer, H.; Katz, J.; *Porphyrins and Metalloporphyrins*, Smith, K., Ed.; Elsevier, Amsterdam, 1975, page 399.

[227] Cyrañski, M.; Krygowski, M.; Wisiorowski, M.; van Eikema Hommes, N.; Schleyer, P. v. R. *Angew. Chem. Int. Ed.* **1998**, *37*, 177–180.

[228] Jusélius, J.; Sundholm, D. *Phys. Chem. Chem. Phys.* **2000**, *2*, 2145–2151.

[229] Vogel, E.; Haas, W.; Knipp, B.; Lex, J.; Schmickler, H. *Angew. Chem. Int. Ed.* **1988**, *27*, 406–410.

[230] Vogel, E. *J. Heterocycl. Chem.* **1996**, *33*, 1461–1487.

[231] Lash, T.; Chaney, S. *Chem.-Eur. J.* **1996**, *2*, 944–948.

[232] Lash, T.; Romanic, J.; Hayes, J.; Spence, J. *Chem. Commun.* **1999**, pages 819–820.

[233] Steiner, E.; Fowler, P.; *Chlorophylls and Bacteriochlorophylls: Biochemistry, Biophysics, Functions and Applications (Advances in Photosynthesis and Respiration)*, Grimm, B., Porra, R., Rüdiger, W., Scheer, H., Eds.; Springer, Dordrecht, 2005, pages Vol 25, pp. 337–347.

[234] J., A.; Makino, M. *Org. Bio. Chem.* **2010**, *8*, 261–266.

[235] Steiner, E.; Fowler, P. W. *Org. Biomol. Chem.* **2004**, *2*, 34–37.

[236] Steiner, E.; Fowler, P. W. *Org. Biomol. Chem.* **2006**, *4*, 2473–2476.

[237] Mandado, M. *Theor. Chem. Acc.* **2010**, *126*, 339.

[238] Ponec, R.; Fias, S.; Van Damme, S.; Bultinck, P.; Gutman, I.; Stanković, S. *Collec. Czech. Chem. Comm.* **2009**, *74*, 147–166.

[239] Balaban, A.; Durđević, J.; Gutman, I.; Jeremić, S.; Radenković, S. *J. Phys. Chem. A.* **2010**, *114*, 5870–5877.

[240] Radenković, S.; Durđević, J.; Gutman, I. *Chem. Phys. Lett.* **2009**, *475*, 289–292.

[241] Aihara, J. *J. Am. Chem. Soc.* **1976**, *98*, 2750–2758.

[242] Gutman, I.; Milun, M.; Trinajstic, N. *J. Am. Chem. Soc.* **1977**, *99*, 1692–1704.

[243] Aihara, J. *J. Am. Chem. Soc.* **1995**, *117*, 4130.–4136.

[244] Aihara, J. *J. Chem. Soc. Perkin Trans.* **1996**, *2*, 2185–2195.

[245] Aihara, J. *J. Phys. Chem.* **1995**, *99*, 12739–12742.

[246] Aihara, J.; Ishida, T.; Kanno, H. *Bull. Chem. Soc. Jap.* **2007**, *80*, 1518–1521.

[247] Aihara, J. *J. Phys. Chem. A* **2008**, *112*, 4382–4385.

[248] Van-Catledge, F. *J. Org. Chem.* **1980**, *45*, 4801–4802.

[249] Bollini, C.; Giambiagi, M.; de Giambiagi, M.; Figueiredo, A. *J. Math. Chem.* **2000**, *28*, 71–81.

[250] Van Alsenoy, C.; Peeters, A. *J. Mol. Struct. (Theochem)* **1993**, *286*, 19–34.

[251] Monaco, G.; Viglione, R.; Zanasi, R.; Fowler, P. *J. Phys. Chem. A* **2006**, *110*, 7447–7452.

[252] Randić, M. *Chem. Phys. Lett.* **1976**, *38*, 3839–3842.

[253] Gomes, J.; Mallion, R. *Rev. Port. Quim.* **1979**, *21*, 82.

[254] Mandado, M.; González-Moa, M.; Mosquera, R. A. *J. Comput. Chem.* **2007**, *27*, 1625–1633.

[255] Mandado, M. *J. Chem. Theory Comput.* **2009**, *5*, 2694–2701.

[256] Landau, L. D.; Lifshitz, E. M.; *Mechanics, Third Edition: Volume 1;* Butterworth-Heinemann: Oxford, 1976, pages 1–12.

[257] Landau, L. D.; Lifshitz, E. M.; *Mechanics, Third Edition: Volume 1;* Butterworth-Heinemann: Oxford, 1976, pages 131–133.